ANAEROBIC HEME DEGRADATION IN *VIBRIO CHOLERAE*

by

MARLEY ANN BRIMBERRY

(Under the Direction of William Lanzilotta)

ABSTRACT

Iron is a necessary micronutrient for organisms, it is incorporated into proteins as a biocatalyst or into electron carrier proteins vital for many biological processes. The importance of iron for bacterial survival and pathogenesis is evident by the variety of highly conserved and broadly employed iron acquisition strategies among bacterial pathogens including siderophore production, heme uptake systems, and hemophore-receptor systems. Humans and other mammals even coordinate an immune response specifically limiting iron availability to invading microorganisms through nutritional immunity. In environments where iron or heme levels are low, the ability to express high-affinity receptors specific for heme and heme degrading enzymes provide a significant advantage to the pathogen. Bacterial pathogens liberate iron from heme through heme-degrading enzymes, and the ability to utilize heme as an iron source is essential for virulence and pathogenesis. *Vibrio cholerae* and *Escherichia coli* O157:H7 are common hemolytic enteric pathogens that infect the lower intestine and have been shown to use heme as an iron source; however, the catabolic fate of heme and how iron is scavenged in an anaerobic environment remained unknown. Herein, we demonstrate that like *E. coli* O157:H7, *V. cholerae* encodes a radical *S*-adenosylmethionine (SAM) methyl transferase (HutW) involved in the anaerobic

opening of the porphyring ring of heme. However, in contrast to the *E. coli* O157:H7 enzyme, there are notable differences in the genetic cluster, mechanism and products, including the ability to utilize reduced nicotinamide adenine dinucleotide phosphate (NADPH) as an electron source. The ability of HutW to use NADPH directly is unique in the radical SAM (RS) field, where most RS enzymes require either a chemical reductant or a redox partner protein to reduce the catalytic [4Fe-4S] cluster. Therefore, we subsequently pursued elucidation for this electron transfer mechanism where we showed that either the heme porphyrin ring and/or subsequent tetrapyrrole intermediates facilitate electron transfer from NADPH to the [4Fe-4S] cluster. This work not only expands the RS field, but also rationalizes the genetic cluster arrangement for enteric bacteria lacking an anaerobilin reductase.

INDEX WORDS: Iron, bioinorganic chemistry, heme degradation, radical *S*-adenosylmethionine enzymes, metal clusters, redox reactions, anaerobes, tetrapyrroles

ANAEROBIC HEME DEGRADATION IN *VIBRIO CHOLERAE*

by

MARLEY ANN BRIMBERRY

B.S., Indiana University Bloomington, 2014

A Dissertation Submitted to the Graduate Faculty of The University of Georgia in Partial Fulfillment of the Requirements for the Degree

DOCTOR OF PHILOSOPHY

ATHENS, GEORGIA

2022

ANAEROBIC HEME DEGRADATION IN *VIBRIO CHOLERAE*

by

MARLEY ANN BRIMBERRY

Major Professor:	William Lanzilotta
Committee:	Michael W. W. Adams
	Amy Medlock
	M. Stephen Trent

Electronic Version Approved:

Ron Walcott
Vice Provost for Graduate Education and Dean of the Graduate School
The University of Georgia
August 2022

DEDICATION

This dissertation is dedicated to all of the women scientists and women before me who forged the path I now walk.

ACKNOWLEDGEMENTS

Thank you to everyone who is wondering if I'm thanking them. I am.

I would like to thank Dr. William Lanzilotta first of all, for mentorship and believing in me and my science. He taught me how to "think like a PhD student" and how to prepare and write manuscripts. I would also like to thank my committee members Dr. Amy Medlock, Dr. M. Stephen Trent for helpful suggestions and encouragement throughout the years. Not to be left out of these acknowledgments is Dr. Zac Wood for whom I would be remiss if I did not mention and thank him taking time to mentor me and respond to any ridiculous crystallization question I had. I would like to thank my friends within the department and outside who not only listened to me complain about experiments, but were empathetic and supportive in my struggles. I would like to thank my family, who encouraged their daughter to pursue this path in life

TABLE OF CONTENTS

Page

LIST OF TABLES

Page

LIST OF FIGURES

Page

LIST OF SCHEMES

Page

CHAPTER 1

INTRODUCTION AND LITERURE REVIEW

Relevance

Methylation reactions are prevalent across biology with methyl groups being added to a variety of biological molecules. This includes small-molecule metabolites as well as natural products, macromolecules including proteins, DNA, RNA, carbohydrates and lipids. Methylation is important to a variety of cellular processes including transcription, translation, gene regulation, signal transduction, and the biosynthesis of numerous essential metabolites.[1–4] Near universally, the source of the methyl group is *S*-adenosylmethionine (SAM). This cofactor consists of a central sulfur atom bound to three carbon atoms. The electrophilic nature of each of the three carbon atoms bound to the sulfur of SAM allows for facile transfer of the substituents to nucleophilic acceptors.[5] In 2001, the radical SAM (RS) superfamily was identified, which uses SAM as a cofactor to initiate radical rearrangements.[6] A class within the RS superfamily, the radical SAM methyltransferases (RSMT) have been shown to use a variety of cofactors in addition to the catalytically-required SAM to methylate inert carbon or phosphorous. One of the identified pathways that utilizes a radical SAM methyltransferase is within anaerobic heme degradation in enteric pathogens.[7–14] Therefore, understanding how these poorly characterized class of RS enzymes function will inform not only related methylases involved in antibiotic biosynthesis, but also provide a potential target for antibiotic development themselves.

Gram negative Bacterial Iron Acquisition

Iron is central to all life, being an important constituent in a diverse array of essential biochemical reactions including energy production, biosynthesis, metabolism, replication, regulation of gene expression, and locomotion. Iron exists as two forms, Fe^{2+}, ferrous iron, and Fe^{3+}, ferric iron. Ferrous iron is the more soluble form but oxidizes to the less bioavailable ferric iron at physiological pH.[15] Iron can also be complexed with protoporphyrin IX, or heme, which similarly carries out many essential biological functions. It is the cofactor in cytochromes, peroxidases and catalases as well as the ligand for molecular oxygen in hemoglobin. However, due to the redox activity of both of these species, their storage and utilization is tightly regulated.[16]

Pathogenic bacteria must similarly obtain iron within the host for vital cellular processes during the course of an infection. This is complicated because not only is the concentration of available iron too low for bacterial growth, but it is further sequestered during infection.[17] Therefore, both Gram-positive (*Cornebacterium diptheria, Staphylococcus aureus, Bacillus*) and Gram-negative (*Vibrio cholera, Pseudomonas aeruginosa, Escherichia coli, Shigella, Neisseria, Acinetobacter, Klebsiella, Serratia marcescens*) bacteria have evolved multiple uptake systems for the various forms of iron, including ferric iron (Fe^{3+}), ferrous iron, (Fe^{2+}) as well as heme and heme intercalated within hemoproteins. The methods for obtaining each type of iron can be divided into categories, siderophore based systems for obtaining Fe^{2+} or Fe^{3+}, heme acquisition systems for iron acquisition from heme, and receptors for iron and hemoproteins.[18,19] Because iron is restricted as part of the innate immune system, bacteria enter a period of iron starvation during infection and have evolved a number of sensing mechanisms that are often markers of infection. Additionally, iron has further been shown to regulate a multiplicity of virulence factors including toxins, secretion systems, siderophores, quorum sensing molecules and biofilm formation.[20–22]

This sensing is typically through the master iron-dependent repressor Fur (ferric uptake regulator).[23–26]

Fur-mediated iron uptake

In bacteria, iron is regulated through the Fur protein which utilizes Fe^{2+} as a corepressor to repress transcription of iron storage and sequestration proteins as well as de-repressing transcription of genes associated with iron acquisition.[25,27] Therefore, in low iron conditions, such as when bacterial pathogens enter the host, Fe^{2+} does not bind Fur and Fur is not bound to DNA, allowing for transcription of iron regulated genes. Conversely, when iron levels are high, Fe^{2+} is bound and Fur binds to the promoter DNA regions, known as "Fur boxes," to block the RNA polymerases and repress transcription. However, the role of Fur is likely much more complex than in its role as a transcriptional repressor of metal acquisition as it has been further shown to be involved in activating virulence genes.[28]

Ferrous iron uptake

In anaerobic host environments, such as the enteric gut, where dioxygen levels are < 1 mm Hg, ferrous iron is the more abundant form of iron.[29,30] In Gram-negative bacteria, ferrous iron is taken up via the Feo system once the Fe^{2+} has diffused through the outer membrane porins to the periplasm.[29,31] The Feo transporter consists of three proteins expressed as an operon, *feoABC*. The *feoA* and *feoB* genes are widely distributed across bacteria, while the *feoC* gene is only present within γ-proteobacteria.[29,31–33] Regardless of operon organization or bacterial organism, the Feo systems have been shown to be regulated by either Fur or the fumarate and nitrate reductase transcriptional regulator (Fnr). As previously mentioned, Fur acts as a repressor in replete iron conditions while Fnr acts as an oxygen sensor to upregulate the Feo system under anaerobic conditions. [31,34,35] In *E. coli*, FeoA encodes a hydrophilic protein thought to facilitate Fe^{2+} binding

to the cytoplasmic domain of FeoB, FeoB a polytopic transmembrane protein capable of GTP hydrolysis, which is required for Fe^{2+} uptake.[36,37] FeoC is a small cytosolic protein predicted to possess a LysR-like winged-helix motif, known to interact with DNA by inserting a helix into the major groove to regulate transcription.[31,38] Annotation of the sequence indicated the presence of four cysteines which are perfectly conserved, suggesting that they could be involved in iron sensing.[29] Further evidence to support this role is the structural characterization of *Klebsiella pneumoniae* FeoC, where the cysteines form iron-sulfur clusters.[39] *V. cholerae* encodes *feoABC*, with FeoA and FeoB each having 40% amino acid identity with FeoA and FeoB from *E. coli*. The *feoC* gene initiates with a codon that overlaps the stop codon of *feoB*, and while predicted to be of similar size, the proteins only share 11% amino acid identity.[40] Moreover, biochemical analysis of the *V. cholerae feoABC* operon indicated that these genes were indeed responsible for transport of ferrous iron.[40,41]

Ferric iron uptake

Many bacteria, including *V. cholerae*, import Fe^{2+} with the ferrous transporter Feo, an advantage crucial for colonization and/or virulence across pathogenic gram-negative bacteria.[29] However, because Fe^{2+} is largely restricted as part of the innate immune response as well as the chemical properties of Fe under physiological conditions, iron is predominantly in the ferric (Fe^{3+}) form. Additionally, all Fe^{3+} in serum is bound to various host proteins including transferrin, ferritin, or lactoferrin.[42] One approach that pathogens use to overcome iron limitation in any environment, including within hosts, are through siderophores. Siderophores are low molecular weight, high-affinity Fe^{3+}-binding compounds secreted and imported by bacteria for iron acquisition. Most of these compounds bind Fe^{3+} with a high affinity ($K_D < 1 \times 10^{-30}$), enough to outcompete transferrin chelation.[43,44] It is therefore not surprising that siderophore production is linked to bacterial

infection in various pathogens including *Pseudomonas aeruginosa* (pyochelin and pyoverdine),[45,46] *Klebsiella pneumoniae* (yersiniabactin, enterobactin, salmochelin, and aerobactin),[47–50] and *V. cholerae* (vibriobactin).[51,52] In addition to producing its own siderophore, vibriobactin, *V. cholerae* can use several receptors for xenosiderophores, including two enterobactin receptors as well as agrobactin and fluvibactin.[41,53–55] It is unknown if xenosiderophore utilization provides a selective advantage to *V. cholerae*, but since enterobactin is secreted by bacteria in the colon, it could be an important iron source during pathogenesis. In Gram-negative bacteria, siderophores are transported across the outer membrane by a TonB-dependent system then trafficked through the periplasm and imported into the cytoplasm by ATP-binding cassette transporters.[44]

V. cholerae has two periplasmic binding ABC transport systems for siderophore intake: *viuPDGC*, identified within the vibriobactin biosynthetic gene cluster, and *vctPDGC*, part of the enterobactin intake cluster. Mutants of either the *vctPDGC* or *viuPDGC* used both vibriobactin and enterobactin, but a double mutant transported neither, indicating that ViuPDGC and VctPDGC transport both siderophores.[55,56] In addition to ABC transporters, each operon encodes additional proteins for siderophore transport and utilization. Within the *viu* genetic cluster is *viuA*, which encodes the outer membrane receptor for vibriobactin and *viuB*, a gene hypothesized to encode a protein required for removal of iron from ferri-vibriobacin following its internalization.[57–59] Xenosiderophores agrobactin and fluvibactin have similar structures to vibriobactin and transported using the *vui* system.[60] However, as enterobactin is a catechol siderophore, it is instead transported by VctA, part of *vct* cluster. VctA has similarity to the enterobactin receptor FetA of *N. gonorrhoeae*, and is therefore hypothesized to be responsible for transport of enterobactin in *V. cholerae*.[61,62] Alternatively, an additional enterobactin receptor, *irgA* encodes a homologous

protein to *E. coli* CirA, which could also transport enterobactin.[63,64] Additionally, *V. cholerae* encodes a receptor gene, *fhuA* in addition to genes for transport of ferrichrome, *fhuBCD*.[65] The sideophore synthesized by *V. cholerae*, vibriobactin, is derived from chorismite, requiring the activity of VibABC to append three 2,3-dihydroxybenzoly residues to a norspermide backbone either directly or via L-threonine.[66–68] The genes required for vibiobactin both map to chromosome 1, which contains most of the genes required for growth and pathogenicity, which may reflect the central role of vibriobactin in the growth and survival of *V. cholerae*.[69]

While ferric iron is limited in the host, *V. cholerae* encodes genes necessary to support the cycle of environmental survival, transmission, and dissemination. *V. cholerae* is considered an environmental pathogen and its inhabitance in the aquatic environment requires it to adapt to fluctuating environmental conditions.[70] Therefore, in the context of iron acquisition, the *V. cholerae* genome contains annotated genes for ferric iron transporters. One of systems, FbpABC, shares sequence identity with the Fbp system in *Mannheimia haemolytica*, and consists of a periplasmic binding protein, a permease protein, and an ATPase.[71–73] The remaining sets of genes annotated as potential ferric iron transporters are not regulated by iron or Fur, and evidence suggests that they do not function in iron transport.[40,74] Intriguingly, when a triple mutant of *vibB, feoB, fbpA* was tested for iron acquisition, the strain still formed colonies in the presence of an iron chelator. This indicated that there is at least one unknown additional functional iron transport system; however, no genes have been identified in the *V. cholerae* genome with similarity to known iron transporters.[40,41] As with the ferrous iron uptake system in *V. cholerae*, the ferric iron transporters as well as the genes for siderophore synthesis are under the control of the master iron regulator Fur.27

Gram-negative bacterial heme uptake

Gram-negative bacteria, including *V. cholerae, E. coli, P. aeruginosa, S. dysenteriae, Y. pestis,* and *S. marcescens* have a cell envelop which is composed of a peptidoglycan cell wall between an inner and outer cell membrane. Therefore, metabolite transport into the bacterium is complicated, and outer membrane (OM) receptors must couple the cytoplasmic proton-motive force to the movement of molecules through the interstitial periplasm. The ion electrochemical gradient used to import complexes outside the diffusion limit of the OM is harvested by the heteromultimeric complexes of ExbB and ExbD proteins of TonB. This includes iron-siderophore complexes, vitamin B12, and heme.[75] The OM siderophore and heme receptors are similar in overall fold, and require the complete TonB-ExbB-ExbD complex for active transport. *V. cholera* contains two *tonB* systems. The *tonB1* genes are divergently cotranscribed with the genes for transport of heme across the inner membrane, *hutWXZ*.[13,59] This system has further been shown to facilitate the uptake of ferrichrome.[76] The *tonB2* system is redundant for the transport of ferrichrome, heme, and the *V. cholerae* siderophore vibriobactin, but is required for the use of enterobactin and heme transport through the OM receptor HasR.[41,74,77]

The heme receptors HutA and HutR function with either TonB1 or TonB2. All three OM receptors have overlapping and unique roles. *V. cholerae* can use both heme and hemoglobin as a source of iron.[78–80] The deletion of *hutA, hutR* and *hasR* completely abolished heme uptake, while hemoglobin utilization was dramatically reduced with a *hutA* deletion, indicating that all three receptors function to bind heme while HutA is more specific for hemoglobin.[41,74,77] While the OM receptor HasR was so named for its similarity to the *hasR* hemophore receptor genes of *P. aeruginosa* and *S. marcescens,* no gene with similarity to known hemophores has been identified in *V. cholerae*.[41,81] However, extracellular hemophores have been structurally characterized in

several other bacteria including *Y. pestis*[82], *S. marcescens*[83], and *P. aeruginosa*[84] and these proteins scavenge heme from the extracellular environment including from hemopexin, methemoglobin, and complexes of haptoglobin-methemogobin.[85,86] Although *V. cholerae* does not appear to encode a hemophore, either the *hasA* gene was lost, or the *hasR* gene was acquired independently of *hasA*. Alternatively, *V. cholerae* could encode a structurally and functionally distinct HasA hemophore, or simply have evolved to take advantage of hemophores produced by other organisms in the same environment.

Following receptor binding and TonB-dependent transport into the periplasm, heme is sequestered by a putative heme-specific periplasmic binding protein, HutB as well as cytoplasmic membrane permeases HutC and HutD.[59] Once internalized, heme is likely sequestered by a cytoplasmic heme binding chaperone, HutX. HutX has been shown to bind heme, however, it is unresolved if HutX chaperones heme to the aerobic heme oxygenase HutZ, or, alternatively, functions to deliver heme to the anaerobic heme-degrading enzyme HutW or bind the breakdown product of anaerobic heme degradation, a hydrophobic tetrapyrrole chemically reactive and toxic similar to biliverdin.[8–10,87,88] Under aerobic conditions, iron is released through the action of the heme oxygenase HutZ and under anaerobic conditions, delivered to HutW for anaerobic heme degradation, *vide infra*.

Heme degradation

To utilize iron as a micronutrient, pathogenic bacteria must release the intercalated metal from within the heme macrocycle. Therefore, enzymes that catalyze the opening of the heme porphyrin ring play a role in pathogenesis, and this class of enzymes can be further divided based on mechanism. Canonical heme degradation by heme oxygenases (HOs) result in release of Fe^{2+}, CO and conversion of heme to biliverdin (BVIX).[89–91] Non-canonical heme oxygenases convert heme

to mycobilin (*M. tuberculosis*)[92] or staphylobilin (*S. aureus*)[93,94]. In addition to oxygen-dependent heme degrading enzymes, enteric pathogens inhabiting the anaerobic and micro-aerobic environments have been shown to encode enzymes for oxygen-independent cleavage of heme where a radical-SAM mediated cleavage of the porphyrin releases iron and a linear tetrapyrrole.[9–11] The metabolites have also been shown to be important in infectivity and virulence.

Canonical heme degradation

All heme oxygenases (HO) share the same mechanism, a heme-dependent activation of O_2 to ferric hydroperoxide followed by stabilization of the ferric hydroperoxide which promotes hydroxylation at the *meso* carbon. This mechanism is well established to occur through three steps (1) hydroxylation of heme to *meso*-hydroxyheme, (2) oxidation of *meso*-hydroxyheme to verdoheme with release of CO, and (3) ring opening of verdoheme to biliverdin with Fe^{2+} release.[95–97] The reaction requires three molecules of oxygen and seven electrons. HOs from pathogenic bacteria have been identified, and several have been shown to share the same reaction mechanism as eukaryotic HOs including those from *C. diptheriae*[89], *N. meningitidis*[90], *A baumanii*, and *P. aeruginosa*[91]. Many of the intermediates have been characterized spectroscopically in a number of different enzymes. In the first oxidation, heme iron binds oxygen forming the oxy-ferrous species (Fe^{2+}-O_2) and is reduced to Fe^{2+}.[98] Further reduction of the iron atom yields an Fe^{3+} hydroperoxide (Fe^{3+}-OOH).[99] The oxygen then attacks the *meso*-carbon to give α-*meso*-hydroxyheme.[100] The *meso*-hydroxyheme intermediate was determined to be formed through single electron reduction of a Fe^{3+} hydroperoxide intermediate via ENDOR and EPR.[101] Further mutagenesis implicated both the hydrogen bonding network surrounding the active site as well as a Gly-Gly motif as required to drive attack at the *meso* position.[102] The electronic structure of the Fe^{3+}-OOH species

obtained through NMR and indicated that the hydrogen bond network bends Fe^{3+}-OOH toward the activated *meso*-carbon favoring homolytic O-O bond cleavage and radical attack.[103]

The second step, oxidation of the α-*meso*-hydroxyheme intermediate and decay to verdoheme mechanism relies on three resonance states of the Fe^{3+}-*meso*-hydroxyheme, oxophlorin, phenolate, and a neutral Fe^{2+} radical.[104–106] Either the neutral Fe^{2+} radical resonance structure or the oxophlorin resonance structure reacts with oxygen forming a Fe^{2+} peroxy radical. The Fe^{3+} peroxy decays to a ferryl intermediate with release of CO.[107] Following protonation and release of water, the Fe^{3+} *meso*-carbocation forms Fe^{3+} verdoheme, an unstable intermediate that spontaneously converts in the presence of oxygen to biliverdin. Recent crystal structures of HO-1 (human heme oxygenase) with Fe^{2+}-N_3-verdoheme supported a mechanism whereby the Fe^{3+}-OOH species electrophilically adds to produce biliverdin.[108,109] This mechanism was initially proposed based on substitution of O_2 and two reducing equivalents with H_2O_2 and alkyl-peroxide respectively.[110,111]

V. cholerae can utilize heme as an iron source, and this activity is dependent upon the *hutWXZ* gene cluster. Initial research into this operon identified HutZ, encoded by the gene *hutZ* in the heme uptake operon, as the putative heme oxygenase. However, HutZ did not exhibit any heme oxygenase activity with ascorbate or the NADPH cytochrome P450 reductase system. More striking was the elimination of activity in the presence of catalase, included to prevent nonspecific reaction of hydrogen peroxide, and resulted in no formation of either biliverdin or a verdoheme intermediate.[13] In contrast, later spectroscopic analysis by Uchida *et al* of the HutZ heme degradation reaction with ascorbate indicated formation of verdoheme.[112] Further studies using time-resolved UV-visible absorption and resonance Raman spectroscopy of the HutZ reaction using either reductant H_2O_2 or ascorbate identified oxyferrous heme, *meso*-hydroxyheme and

verdoheme as intermediates. This was based solely on spectroscopic data, specifically, identical vibrational modes of the porphyrin macrocycle, $^{V}Fe\text{-}O_2$ for HutZ and HO-1. Furthermore, when supplied H_2O_2, HutZ converted ferric heme into *meso*-hydroxyheme.[113] It was found that the heme degradation reaction of HutZ using ascorbate as a reductant was accelerated at lower pH which was attributed to the change in heme spin state from a low spin to high spin. [112–114] Therefore, despite low sequence and structural similarity, it appears that HutZ is a heme oxygenase in *V. cholerae* that uses a mechanism similar to that of canonical HOs.

Non-canonical heme degradation

The alternative proteins for degrading heme aerobically exploit changes in structure of the heme macrocycle when bound to the enzyme to yield unique products. The first of these non-canonical HOs to be identified was IsdG and IsdI, which share 78% sequence identity. These enzymes degrade heme to staphylobilins (5-oxo-δ-bilirubin and 15-oxo-β-bilirubin) with concurrent release of formaldehyde and Fe^{3+} using either ascorbic acid or NADPH and the native reductase IruO.[93,94,115,116] From NMR, resonance Raman (RR), and EPR of IsdG/I bound heme, the normally planar heme was judged to be significantly distorted, and this heme ruffling was essential for the catalytic activity.[117–119] Specifically, ^{1}H NMR experiments suggested up field *meso*-H shifts and downfield methyl shifts indicative of a ruffled electronic configuration.[119] Resonance Raman and EPR further supported this electronic assignment and further demonstrated mixing of planar heme and ruffled heme spin configurations.[118] Mutation of a conserved heme pocket residue, Trp66 (IsdI) and Trp67 (IsdG) implicated in heme ruffling further confirmed the necessity of heme ruffling for the reaction mechanism of IsdG/I.[120] Similar spectroscopic analysis of MhuD indicates that heme ruffling is critical for non-canonical heme degradation in *M. tuberculosis.* H NMR, magnetic circular dichroism (MCD), and crystallographic analysis for MhuD suggest a more

ruffled heme compared to canonical HOs but less ruffled compared to IsdI/G.[121,122] NMR and MCD experiments showed a mixed population of planar and ruffled heme, similar to what was seen with IsdG/I. Furthermore, heme ruffling was validated by the crystal structure and mutation of Trp66, where mixed electronic heme states was seen in UV-visible absorbance spectroscopy that decreased for mutants of Trp66.[121,122]

Unlike canonical HOs, the non-canonical heme oxygenases do not have a conserved hydrogen bonding network which has been shown to be integral for proton donation in the heme oxygenase mechanism.[117,123] The first oxidation step has been proposed to occur through a Fe^{3+}-OOH hydroperoxyl intermediate which forms an oxygen bridge transition state with a proton of a terminal amide of Asp7. This hydrogen bonding puts the oxygen bridge over the β/δ *meso*-carbon, which allows for hydroxylation of either the β– or δ– *meso*-carbons.[124] Alternatively, a Fe^{3+}-OO• hydroperoxo species could be possible, as IsdI contains no known proton donor. A ferryl species was ruled out in IsdI, and the current mechanism supports the Fe^{3+} peroxo species as the intermediate during β/δ *meso*-carbon hydroxylation.[125] Similar experiments with MhuD showed that MhuD primarily hydroxylates the β– or δ– *meso* carbon atoms, due to their deviation from the heme plane, and to dioxygenase the α-*meso* position. This mechanism was proposed from UV-visible absorbance bands at 540 and 615 nm characteristic of hydroxyheme intermediate when MhuD was given excess H_2O_2, supporting a Fe^{3+}-OOH or Fe^{3+}-OO• intermediate similar to what was seen with IsdI. Non-canonical heme oxygenases then diverge after forming this shared intermediate. In MhuD, dioxygenation proceeds from the hydroxyheme intermediate through a porphyrin radical where the oxygen adds to the *meso*- and pyrrole carbons. A O-O bond was further proposed, which breaks open to a Fe^{3+} mycobilin product, without the release of CO or formation of verdoheme.[126] This study has been further supported by subsequent QM/MM analysis which

developed a model for the reaction by predicting energy changes associated with addition of molecular oxygen to ruffled α-*meso* hydroxyheme.[127] Detailed kinetic analysis of the reaction using both ESI-MS and UV-visible absorbance spectroscopy confirmed all oxygenations of meso-hydroxyheme occur at the -meso carbon position; however, this intermediate must adopt a planar conformation prior to further oxygenation.[128] The IsdG/I mechanism is proposed to undergo similar hydroxylation followed by deoxygenation, but without the release of formaldehyde containing the *meso* carbon.[129] The source of the oxygen atoms for both staphylobilins and mycobilins have been shown to come from O_2 through $^{18}O_2$-labeling studies. However, it was noted that the oxygen containing functional group only occurred with both $^{18}O_2$ and $H_2{}^{18}O_2$, indicating that it must exchange with water.[130] The evolution of the non-canonical heme oxygenases IsdG/I and MhuD is thought to be a means for the pathogens to avoid activation of CO-dependent dormancy genes and allow for continued survival and virulence as these enzymes do not have the concurrent release of CO like canonical HOs.[131]

Anaerobic heme degradation

While the degradation of heme under aerobic conditions has been well studied; only recently has a mechanism for the anaerobic catabolism of heme been identified.[132] The enzymes ChuW and ChuY have been characterized in at least two pathogenic strains of *Escherichia coli*.[11,12,133] The available evidence indicates that ChuW is a radical *S-adenosylmethionine* (SAM) methyltransferase responsible for opening the porphyrin ring of heme under anaerobic conditions, whereas ChuY is an NADPH-dependent reductase that reduces the tetrapyrrole product of ChuW.[10,11] Interestingly, *Vibrio cholera*, another enteric pathogen that colonizes the tight mucosal layer of the intestine, can also utilize heme as an iron source.[41] Similarly, *V. cholera* also expresses

an enzyme, HutW (39% sequence identity with ChuW), that is capable of opening the porphyrin ring under anaerobic conditions.[9]

Both ChuW and HutW initiate catalysis through reductive cleavage of SAM, yielding the 5′-deoxyadenosyl radical (5′- dA•). The 5′-dA• rapidly abstracts a hydrogen atom from a second SAM molecule to yield a methylene radical that adds to the porphyrin forming a transient SAM-porphyrin adduct. A protonation event, facilitated by an active site amino acid, on the adjacent pyrrole carbon allows for the ring opening step by a β-scission reaction, resulting in an intermediate tetrapyrrole radical. The second SAM molecule also facilitates the methyl transfer step forming the leaving group, *S-adenosyl*-L-homocysteine (SAH). For a related RS enzyme with sequence similarity to ChuW and HutW, CpdH (formerly HemN), the methylene radical functions as part of a "hydrogen relay" and simply serves to abstract a hydrogen atom from the substrate, coproporphyrinogen III. Ji *et al.* demonstrated that this methylene radical could add to the porphyrin substrate through the identification of a SAM−porphyrin adduct.[134] The methylene radical is added to a double bond, resulting in a methyl transfer reaction and, in many cases, further radical catalyzed chemical rearrangements.[135] For both ChuW and HutW, the enzyme has evolved to perform the β-scission of a carbon−carbon bond, resulting in opening of the porphyrin ring along with the liberation of the iron atom. The iron atom does not participate in the reaction, and in fact, several metal-free porphyrins have been shown to be acceptable substrates for ChuW and HutW.[9,10] It is also important to point out that the electron source as well as the tetrapyrrole product produced by ChuW is different from what has been observed for HutW. ChuW utilizes the E. coli flavodoxin (EcFldA)/ferredoxin (flavodoxin):NADP+ oxidoreductase (EcFpr)/NADPH system to reduce the [4Fe−4S] cluster, and the resulting tetrapyrrole still has a high degree of aromaticity, hence the necessity for ChuY. Interestingly, characterization of HutW revealed that NADPH could

be utilized directly as the electron source. All radical SAM enzymes must quench a radical intermediate at some step in their reaction mechanism. In the case of HutW, this could be facilitated by the porphyrin substrate and/or the tetrapyrrole product itself. In fact, direct electron transfer from NADPH to heme has been observed for P450nor.[136–140] Specifically in that system, heme facilitates a hydride transfer reaction in this system. The proposal that HutW utilizes a similar mechanism is consistent with the requirement of two electrons and a proton to get from heme to product. Genes associated with the anaerobic heme degradation pathway appear to be conserved in enteric pathogens and further highlight the diversity of heme utilization in bacterial pathogens.

Radical S-adenosylmethionine Enzyme Superfamily Consensus Features

In 2001, the radical *S*-adenosylmethionine (radical SAM, RS) enzymes were identified as a superfamily.[6] Although enzymes that utilized SAM to initiate radical reactions had been known for decades, the breadth and diversity of chemical transformations these enzymes employ has only now begun to be appreciated.[141–143] The initial work identified approximately 600 members, but this number has since has expanded to nearly 115,000 as of 2017.[144] Initial recognition by Sofia *et al* of the conserved and characteristic CX_3CX_2C motif present across the superfamily, a marker for the catalytic [4Fe-4S]. Although there are variations on the motif, these three cysteine residues typically coordinate three of the four irons of the [4Fe-4S] cluster found within the active site.[145] However, in the active, cofactor bound state of the protein, the unique iron is coordinated by the amino and carboxylate moieties of SAM, forming a chelate ring. This structural feature was found to be unique to radical SAM enzymes, and further characterized using Mössbauer spectroscopy, X-ray crystallography and ENDOR spectroscopy.[146,147] The coordination complex of SAM to the [4Fe-4S] cluster is one of the few unifying structural and catalytic features of radical SAM enzymes. [137] The [4Fe-4S] cluster has been shown to exist in an array of states, especially since

the cluster is highly sensitive to oxygen and can degrade to a [3Fe-4S].[148–150] Additionally, a subset of RS enzymes contain one or more iron sulfur cluster in addition to the catalytic cluster required for SAM cleavage.[151]

The crystal structures of RS enzymes typically exhibit a full or partial triose phosphate isomerase (TIM) barrel. A full TIM barrel consists of eight alpha helices alternating with eight beta strands, which form a barrel-like structure with the beta strands on the interior and the alpha helices surrounding them $(\beta\alpha)_8$. The partial TIM barrels have either $(\beta\alpha)_4$ or $(\beta\alpha)_6$ structures, and the fold likely evolved from $(\beta\alpha)_2$ units.[152,153] Within this structure, the catalytic iron sulfur cluster and active site are occluded from solvent by at least 7Å, while still allowing SAM and the substrate to enter the interior of the protein through the opening of the barrel.[145] Within the active site, the cluster binding motif (CX_3CX_2CX) and the "GGE" motif that forms H-bonds to the amino portion of the methionyl group of SAM are conserved across RS enzymes. However, there is no common substrate binding motif, likely due to the diverse substrates RS enzymes are known to bind.

Common to all members of the RS superfamily is the requirement for reduction of the [4Fe-4S] cluster to the +1 oxidation state from the resting +2 form. In fact, this requirement was recognized prior to the identification of the superfamily itself when Knappe *et al* determined that the activating enzyme for Pyruvate Formate Lyse (PFL-AE) from *E. coli* was reduced by *E. coli* flavodoxin (*Ec*FldA).[154–156] *Ec*FldA has also been shown to activate other RS enzymes in *E. coli* including anaerobic ribonucleotide reductase, biotin synthase, 7-carobxy-7-deazaguanine synthase (QueE), among a variety of radical SAM enzymes from diverse bacterial sources.[157–161] Interestingly, a systematic study in *Bacillus subtilis* with one of these RS enzymes, QueE, was conducted that looked at the redox transfer using *Ec*FldA compared to a chemical reductant, sodium dithionite, and the native flavodoxins (*Bs*YkuN and *Bs*YkuP). Results from this study

showed that both the *B. subtilis* flavodoxins as well as the *Ec*FldA supported QueE turnover; however, both *Bs*YkuN and *Bs*TkuP were more efficient than *Ec*FldA.[162] This indicates that RS enzymes are most efficiently reduced by the homologous flavodoxin from the same organism, even though chemical reductants or a heterologous flavodoxin may support turnover. A subsequent study that compared the crystal structure of QueE from three different organisms, *Bacillus subtilis*, *Burkholderia multivorans*, and *E. coli* examined structural and electrostatic differences in the protein structures. These variations affect binding to their cognate reductant and efficiency of electron transfer.[163] Moreover, dithionite either reduced QueE to a lesser degree than *Ec*FldA or a greater degree, depending on the protein.[164] Therefore, we can hypothesize that specific redox partner proteins have evolved for each RS enzyme and likely share charge-charge complementarity surface complementarity with their cognate reductants, Modern AI tools may be able to help identify the appropriate redox partners. In addition, the ability of chemicals to serve as a reductant for a given radical SAM enzyme likely has to do with their ability to reach the iron-sulfur cluster and transfer an electron through the protein architecture.[165]

Catalysis in RS enzymes is initiated via electron transfer from the reduced $[4Fe\text{-}4S]^{1+}$ cluster to the sulfonium of SAM[166,167], resulting in reductive cleavage of the S-C5′ bond of SAM.[168,169] In early studies, this was determined through isotopically labeled substrate, where H-atom transfer from substrate to deoxyadenosine occurred during catalysis.[170,171] Additional evidence from a synthesized precursor to a stable allylic radical species, *S*-3′,4′-anhydroadenosyl-L-methionine (anSAM), that, when reacted with reduced Lysine Amino Mutase (LAM), gave rise to an allylic radical species anAdo•. [172,173] Results from these studies identified SAM as a precursor of a dAdo• in radical SAM enzymes followed by the dAdo• abstracting a H-atom from substrate during catalysis. Furthermore, this cleavage of SAM to dAdo• was shown to require a catalytically

active [4Fe-4S]$^{+1}$. This was elegantly demonstrated by Henshaw *et al* through spin-quantification of the [4Fe-4S]$^{+1}$ in Pyruvate Formate Lyase Activating Enzyme (PFL-AE), and following addition of the substrate, Pyruvate Formate Lyase (PFL), comparing these data to the amount of glycyl radical generated on PFL. The results conclusively demonstrated that for every [4Fe-4S]$^{+1}$ oxidized in PFL-AE, a glycyl radical was generated on PFL.[174] Although this work showed that the iron-sulfur cluster was the source of the electron required for reductive cleavage of SAM, it was still unclear how this was mediated.

Initial evidence for direct interaction of SAM with the cluster was first indicated by Mössbauer spectroscopy where the [4Fe-4S] cluster was exposed to oxygen to generate a [3Fe-4S] cluster followed by chemical reconstitution with ^{57}Fe. The results from this experiment demonstrated that in the presence of SAM the unique iron site underwent a significant change in isomer shift consistent with direct coordination of SAM.[175] Moreover, orbital overlap of SAM with the [4Fe-4S]$^{+1}$ cluster was demonstrated through ENDOR and utilization of SAM labeled with ^{13}C or ^{2}H at the methyl, ^{15}N at the amino, and ^{17}O and ^{13}C at the carboxyl.[176] Paralleling this earlier work, more recently, an organometallic intermediate, Ω, was identified where the 5′-C of the 5′-deoxyadenosyl fragment is directly bound to the unique iron of the [4Fe-4S] cluster.[177,178] Typically, RS enzymes cleave the S-C(5′) bond. Cleavage of the S-C(methyl) bond is not seen in as this species would likely be very high energy and difficult to direct within the active site. This ability to discriminate the bond for cleavage is likely due to SAM positioning within the active site, where SAM binds such that the S-C(5′) bond is in the trans position.[179] The regioselective cleavage of the S-C bond correlates with SAM ribose conformation as well as active site forces that induce a Jahn-Teller (JT) distortion to localize the odd electron in a single priority S-C antibonding sphere. Thermal conformational changes during catalysis enable electron transfer

from the iron atom of the iron-sulfur cluster then specifically selects the S-C(5′) bond for cleavage.[180] Formation of the Ω species has been observed in a variety of RS enzymes and likely reflects a conserved intermediate within the family. Ω is proposed to be formed from homolytic cleavage of the Fe-C5′ bond, that yields the 5′-dA• which goes on to perform H atom abstraction. This was demonstrated by ENDOR studies and rapid freeze quench (RFQ) EPR, where both SAM and the [4Fe-4S] cluster were isotopically labeled. Additionally, the Ω species was shown to be a reaction intermediate because Ω was converted directly to the PFL glycyl radical when the frozen sample was annealed at increased temperatures, a result that could only occur via homolytic cleavage of the Fe-C(5′) of Ω species to generate a 5′-dA• intermediate that then abstracts a H atom from PFL.[3,178]

The 5′-dA• intermediate, central to RS catalysis, was identified through reductive cleavage of the $[4Fe\text{-}4S]^{1+}$-SAM complex (Ω) induced by cryogenic irradiation via both EPR and ENDOR spectroscopies.[181] This was done by RFQ at varying time points, where initial formation of the organometallic intermediate Ω was identified by EPR with g=2.035 and g=2.004 observed at 500 ms peptide radical was unequivocally identified at approximately 8 s, and over the time course, additional paramagnetic species appeared following thermal annealing and the 5′-dA• was identified through spectral subtraction.[180] A consensus mechanism has been presented whereby a reduced iron-sulfur cluster transfers an inner sphere electron through the p orbitals of the sulfonium sulfur, breaking the sulfur carbon bond and forming an organometallic bond between the unique Fe and the carbon atom (Ω).[182,183] This species then is homolytically cleaved and the 5′-dA• intermediate is generated. The substrate and 5′-dA• are in direct orbital overlap prior to H atom abstraction, and the protein goes through no structural rearrangement following this step, maintaining the substrate radical and methyl group of dAdH within van der Waals contact.[184,185]

Again, where the 5′-dA• is a shared intermediate within the RS superfamily, the substrate that undergoes H atom abstraction is specific for each enzyme.

Alternatively, Donnan *et al* have employed broken-symmetry density functional theory (BS-DFT) to evaluate the experimental characterization of the Ω species. Evaluating several structural models of Ω, their results showed that the calculated hyperfine coupling constants (HFCCs) were inconsistent with the experimental values, and better reflected a near-attack conformer of SAM bound to the catalytic [4Fe-4S] cluster where the distance between the unique iron and the SAM sulfur atom is ~3Å.[186]

Radical SAM Methyltransferases

Radical SAM methyltransferases (RSMTs) can be grouped into distinct classes by their protein architecture, cofactor requirement, and mechanism. [187] RSMTs have also been found in a myriad of metabolic and catabolic pathways. Class A RSMTs have conserved cysteine residues, Class B have a cobalamin (Cbl) cofactor, Class C RSMTs bind two molecules of the prototypical RS cofactor, SAM, and Class D RSMTs are proposed to use methylenetretrahydrofolate as the methyl donor.[188] Although enzymes within each class likely utilize the cofactors and protein architecture differently for each substrate, at least one protein has been structurally characterized, and can be used as a guide for the proposed mechanism.

Class A RS Methylases

Class A RS methyltransferases contain the RS consensus domain, and the most representative enzymes of this subclass of RSMTs are RlmN and Cfr. RlmN catalyzes methylation of C2 of adenosine 2503 in 23S rRNA as well as C2 of adenosine 37 in several tRNAs, this is thought to enhance the translational fidelity and fitness of the organism.[189–191] This action is through two additional strictly conserved cysteine residues that are essential for catalysis. High resolution mass

spectrometry of purified RlmN when grown in a methionine auxotropic *E. coli* culture supplemented with [*methyl*-$^{2}H_3$]methionine, showed a methyl group added to the Cys-355 of the protein.[192,193] Further evidence for this came from the X-ray crystal structure of RlmN with bound SAM, where the structure shows coordination of SAM to the unique iron of the [4Fe-4S] cluster near the catalytic cysteine residue.[193] From the X-ray crystal structure and isotope feeding coupled with high resolution mass spectrometry of purified RlmN and Cfr, the authors proposed a mechanism whereby the methyl group of one molecule of SAM is transferred to one of the conserved cysteine residues. This is followed by a second molecule of SAM binding which is reductively cleaved to 5′-dA•, which abstracts a hydrogen atom from the methylated cysteine. The methylene radical then adds to the adenosine substrate forming a cross-linked protein-RNA radical intermediate. Detailed EPR characterization of an inactive RlmN variant, in concert with strategic isotopic labeling, suggested that a second cysteine residue was involved in relieving the radical species by acting as a base that abstracts a proton from the RNA substrate.[194,195] Although Cfr is proposed to utilize a similar reaction mechanism, there are distinct structural differences between the two proteins. Notably, differences in SAM cleavage between the two active site cysteine residues could indicate differences in the SAM and/or substrate binding mode within the active site that increases Cfr functionality.[195–197]

Class B RSMTs

Similar to Class A RSMTs, Class B RSMTs methylate inactivated carbon or phosphorus atoms.[188] They are found in a variety of biosynthetic pathways including chlorophyll and lipid among other natural products .[198] Also like Class A RSMTs, they share the common radical SAM fold; however, they are differentiated by an N-terminal cobalamin binding domain, where the presence or absence of different axial ligands to the Co-containing macrocycle include adenosyl (Ado)-Cbl, methyl

(Me)-Cbl, and open Cbl, ("base-off") which lacks an upper axial ligand.[199–201] Although the majority of annotated Clb-dependent radical SAM enzymes are proposed to use radical SAM chemistry and MeClb to methylate inert substrates, they diverge in function, and can be divided by their reaction mechanism.

Within Class B RSMTs, the structure of an enzyme, TokK, which falls into the grouping of enzymes that carry out radical-based methylation was recently solved.[202] In this work, Knox *et al* proposed a reaction mechanism where the 5′-dA•, generated through reductive cleavage of SAM and, attacks the methyl group of methylcobalamin(MeCbl), inducing homolytic cleavage of the cobalt-carbon bond to yield cob(II)alamin and the methylated product. Following product dissociation, methionine and 5′-deoxyadenosine (5′-dAH), another molecule of SAM binds in the active site, cob(II)alamin is reduced to cob(I)alamin, which then performs a nucleophilic attack on the second molecule of SAM to regenerate MeCbl.[198,203–205] This proposed mechanism for radical methylation likely covers only a subset of class B RSMTs that, like TokK, catalyze iterative methylation reactions and includes homologs such as ThnK[206], CysS[207] PctJ[208], Swb9[209], BchQ[210] and PoyB[211] among others. Cbl-dependent RS enzymes that, like those previously listed, are implicated in radical-based methylation, but only add one methyl group to substrate include some of the first identified such as Fom3.[212,213] Other enzymes that fall into this category of Class B RSMTs include HpnP/HpnR[214], involved in hopanoid tailoring; GntE[215–217] which is responsible for methylation of gentamicin, and bacteriochlorphyll *c*, BchR[218]. The mechanism for this group of enzymes proceeds similarly to that of the iterative methylases, where the 5′-dA• abstracts a hydrogen atom from substrate. Then, a methyl radical is transferred from methylcobalamin to give product and cob(II)alamin followed by regernation of cob(II)alamin to cob(I)alamin and transfer of a methyl group from SAM to cob(I)alamin.[217]

Class B RSMTs that function as non-methylases include the first Class B RSMT to be structurally characterized, OxsB.[219] The crystal structure of OxsB demonstrated coordination of SAM with the [4Fe-4S] cluster in two orientations, one has SAM poised for reductive homolysis by the $[4Fe\text{-}4S]^{1+}$ cluster while the other has SAM located close enough to Cbl to permit methyl transfer and generation of Me-Cbl and SAH. Subsequent research detailing the mechanism for this enzyme detected formation of the methylated product (2′-dAMP), but the precise structure of the methylated product has yet to be determined. Additionally, Zhong *et al* identified that demethylation of SAM to SAH is catalyzed by OxsB, consistent with its dual positioning in the OxsB structure. These researchers proposed three mechanisms consistent with oxetanocin-A formation: (1) substrate is methylated and the concomitantly formed SAH serves as the precursor to the homocysteine moiety seen in product; (2) methionine generated from reductive cleavage of SAM adds to the protonated aldehyde and the resulting adduct undergoes a Cbl mediated migration of the methyl group to give product and methanol; (3) homocysteine is produced in the enzymatic incubation and condensed non-enzymatically with aldehyde to produce oxetanocin-A.[219–221]

The third Class B RSMT that has been structurally characterized, TsrM, does not perform a radical-based methylation. Instead, this enzyme is involved in the biosynthetic pathway of thiostrepton and uses polar chemistry to methylate L-tryptophan. The crystal structure revealed that SAM binding was not ligating the [4Fe-4S] cluster, this lead the authors to propose that SAM is required to reform MeClb from co(I)alamin at the end of the catalytic cycle.[222] This follows the TsrM mechanism where an active site base removes a proton from L-tryptophan inducing the π electrons to attack the methyl group of MeCbl via a polar nucleophilic mechanism to generate cob(I)alamin and a methylated tryptophan intermediate.[223] Interestingly, the crystal structure showed an essential arginine residue in the proximal coordination sphere of the cobalamin cofactor and a

[4Fe-4S] cluster ligated by a glutamyl residue in addition to the canonical cystines of the RS motif. This suggests that TsrM evolved from a Class B RSMT to carry out non-radical methylation, suggesting that the core fold for this superfamily can be adapted to sequester and protect both their Cbl cofactor as well as the iron sulfur cluster.[224]

Class C RSMTs

The third class of radical SAM methyltransferases have similar amino acid sequences to the oxygen-independent coproporphyrinogen III oxidase, HemN. Class C RS enzymes are methyltransferases, but utilize a different mechanism than the Class A, B or D enzymes. Interestingly, it is thought that many of the currently annotated HemN-like enzymes may actually be Class C radical SAM methyltransferases.[225] Class C RS enzymes will be further detailed in Chapter 1, "Making and Breaking carbon-carbon bonds in class C radical SAM methyltransferases."

Class D RSMTs

Within the classification of RSMTs, the source of the methyl group is what largely differentiates the groups. For Class D RSMTs, the source of the methyl group is methylenetetrahydrofolate.[188] A putative RS enzyme, MJ0619 from *Methanocaldococcus jannaschii*, hypothesized to be involved in the biosynthesis of methanopterin (MPT), a coenzyme used in C1 metabolism in methanotrophic archaea and bacteria.[226] This cofactor contains a pterin ring with methyl groups appended at C7 and C9. Consistent with this assignment, when Allen *et al* heterologously expressed MJ0619 in *E. coli*, methylated pterins were detected including those at C7 and C9. Subsequent metabolic feeding studies showed a labeling pattern of deuterium incorporation indicating that the methyl group was not derived from L-methionine, cobalamin, or methyltetrahydrofolate, but instead from methylenetetrahydroolate (CH_2THF). From this

information, the authors proposed a mechanism whereby the 5′-dA• abstracts a hydrogen atom from C7 of the substrate. This is followed by radical addition of substrate onto CH_2THF, reduction and protonation, and finally elimination of tetrahydrofolate (THF).[226]

Unclassified RSMTs

A recently discovered RSMT that doesn't fall into one of the previously established classes, MA4551, does not share significant amino acid sequence similarity with any of the other RSMTs, and instead belongs to an uncharacterized group. These enzymes, MA4551 and other "methanogenesis marker 10," *mm10,* gene-encoding enzymes contain a CX_3CX_2C motif as well as a second strictly conserved motif, $CX_2CX_{5-6}CX_2C$. Studies into the function of MA4551 indicated that it installed a methyl group on an arginine and glutamine residue within the McrA subunit of methyl-coenzyme M reductase (MCR).226

Iron Sulfur Proteins

Iron-sulfur proteins are characterized by the presence of di- tri- or tetra-iron linked to sulfide in variable oxidation states. These cluster cofactors are likely the most evolutionarily ancient as well as ubiquitous and functionally versatile prosthetic groups and represent extraordinary functional and structural diversity.[228–230] In fact, biological iron-sulfur clusters are the major components of respiratory and photosynthetic electron transport chains, in addition to being involved in redox-active centers in membrane-bound and soluble enzymes, typically forming [2Fe-2S], [3Fe-4S], [4Fe-4S] or [8Fe-7S] units. The Fe atom within these clusters is typically coordinated by cysteine, and occasionally aspartate, histidine, serine or a backbone amide. This type of ligation is what is seen with radical SAM enzymes, where the amino and carboxylate groups of the *S*-adenosylmethionine coordinate the unique iron to facilitate reductive cleavage. This protein superfamily contains at least one catalytically active [4Fe-4S] cluster.[145] The properties of [4Fe-

4S] clusters will therefore be the focus of this discussion, as it is most relevant for this protein superfamily.

Properties of [4Fe-4S] Clusters

Cubane [4Fe-4S] clusters are assembled from two [$Fe_2(\mu_2\text{-}S)_2$] units, through dedicated protein machinery *in vivo*. At least three operons – *nif, suf,* and *isc* have been shown to encode genes in bacterial Fe-S cluster biosynthesis.[231,232] However, [4Fe-4S] clusters can alternatively be assembled synthetically with added iron and sulfide in the presence of reductant.[233–236] Importantly, this process can reconstitute the correct cluster type.[237] It is unknown which genetic cluster is responsible for assembling the iron-sulfur cluster in RS enzymes.

As the iron-sulfur cluster is central to catalysis for RS enzymes, it is necessary to understand the electronic and magnetic properties to recognize redox transfer and reactivity. Iron-sulfur clusters are ideal for electron transfer and redox reactions because they access various redox states, which can be further finely tuned by the coordination environment where electronic properties of the protein site where they are anchored and hydrogen bonding interactions influence the redox potential. The redox potential for Fe-S clusters range from 500 mV to -500 mV, and while the redox potential for SAM is not known, it is estimated to be approximately -1.8 V.[238] Therefore, the electron transfer from the cluster to SAM appears highly energetically unfavorable; however, it is hypothesized that the close proximity of the positively charged sulfonium group and coordination of one iron of the cluster by the hard, charged atoms of the methionine moiety would affect the cluster reduction potential.[239,240] It was proposed, through work on the RS SAM enzyme lysine amino mutase (LAM), that the reduction potential for the cluster is approximately -479 mV and addition of SAM shifts the potential +49 mV. Furthermore, when all substrates are present in the active site, the reduction potential of the cluster was estimated to drop to about -600 mV and

the negative potential of free SAM is elevated to -990 mV. [239] Additionally, as is true for Fe-S clusters in other metalloproteins outside the RS superfamily, the active site environment plays a significant role in turning the redox potential. For RS enzymes, this is important because the reaction barrier has been shown to increase with rising polarity.[241] This is consistent with the observation that low potential Fe-S clusters tend to be sequestered in hydrophobic pockets.

Although the oxidation state, magnetic, and electronic properties can be calculated for the individual Fe atoms within the cluster, the atoms within the cluster do not have clear oxidation states. The observed UV-visible spectra of these proteins typically have a broad and intense absorbance in the visible region, arising from iron-sulfur charge transfer bands. Proteins containing a $[4Fe\text{-}4S]^{2+}$ cluster have a peak near 400 nm. Upon reduction, the absorbance decreases by about 50% the maximum difference point near 420 nm. Upon oxidation of the cluster, there is an increase in absorbance throughout the visible region.[242] The magnetic properties of iron-sulfur clusters exhibit EPR resonances at low temperatures (below 35 K) in the +1 or +3 state, while +2 clusters are silent. An EPR spectrum of a single $[4Fe\text{-}4S]^{1+}$ exhibits either an axial or a rhombic signal with one g near 1.94 and a $g = 2.05$.[242] The reduced or *as isolated* RS enzymes containing at least one [4Fe-4S] cluster show g values within a range of 1.92 to 2.06, as predicted from their cluster assignment.[145] Ground state properties resulting from antiferromagnetic coupling of high-spin Fe^{2+} (S=2) and high-spin Fe^{3+} (S=5/2) result in g values less than 2.0.[243] Spectroscopic characterization from Mössbauer analysis, which measures the isomer shift (δ) and measures the *d* electron population is a good indicator of the oxidation state of the iron sites.[244] The localization-delocalization patterns of Fe_4S_4 clusters in their most common oxidation states contain delocalized $Fe^{2.5+}Fe^{2.5+}$ pairs. Mössbauer spectra of $[4Fe\text{-}4S]^{2+}$ clusters have two equivalent $Fe^{2.5+}Fe^{2.5+}$ pairs with $\delta = 0.45$ mm/s. Reduced $[4Fe\text{-}4S]^{1+}$ clusters have one $Fe^{2.5+}Fe^{2.5+}$ pair with $\delta = 0.49$ mm/s and

one $Fe^{2+}Fe^{2+}$ pair with δ = 0.62 mm/s, and generally have a localized pattern.[230] For the RS enzymes that have been characterized using this spectroscopic technique, the δ isomer shift varies from δ = 0.43 to 0.72 in the $[4Fe\text{-}4S]^{2+}$ form and δ = 0.50 to δ = 0.85, indicate that there is much spin-state variability which depend on the environment surrounding the cluster.[145]

Relevance

Iron-sulfur clusters and the redox reactions or electron transfers that they enable are central to biochemistry.[245] These metallocofactors helped to identify a new class of proteins, the radical *S*-adenosylmethionine superfamily, that employ a radical to initiate diverse types of chemical transformations.[145] Within this superfamily of enzymes are methyltransferases, which are further categorized depending upon the cofactor and domain architecture. The class C RSMTs utilize two molecules of SAM to methylate sp^2 hybridized Carbon centers.[188] Given that class C RSMTs have been shown to be involved in the biosynthesis of numerous natural products with antibiotic properties, understanding how they function is valuable for the development of antimicrobial therapeutics, but also, more broadly, biological methylation reactions.

References

(1) Roje, S. S-Adenosyl-l-Methionine: Beyond the Universal Methyl Group Donor. *Phytochemistry* **2006**, *67* (15), 1686–1698. https://doi.org/10.1016/j.phytochem.2006.04.019.

(2) Sufrin, J.; Finckbeiner, S.; Oliver, C. Marine-Derived Metabolites of S-Adenosylmethionine as Templates for New Anti-Infectives. *Marine Drugs* **2009**, *7* (3), 401–434. https://doi.org/10.3390/md7030401.

(3) Broderick, W. E.; Hoffman, B. M.; Broderick, J. B. Mechanism of Radical Initiation in the Radical *S* -Adenosyl- <scp>l</Scp> -Methionine Superfamily. *Accounts of Chemical Research* **2018**, *51* (11). https://doi.org/10.1021/acs.accounts.8b00356.

(4) Challand, M. R.; Driesener, R. C.; Roach, P. L. Radical S-Adenosylmethionine Enzymes: Mechanism, Control and Function. *Natural Product Reports* **2011**, *28* (10), 1696. https://doi.org/10.1039/c1np00036e.

(5) Fontecave, M.; Atta, M.; Mulliez, E. S-Adenosylmethionine: Nothing Goes to Waste. *Trends in Biochemical Sciences* **2004**, *29* (5), 243–249. https://doi.org/10.1016/j.tibs.2004.03.007.

(6) Sofia, H. J. Radical SAM, a Novel Protein Superfamily Linking Unresolved Steps in Familiar Biosynthetic Pathways with Radical Mechanisms: Functional Characterization Using New Analysis and Information Visualization Methods. *Nucleic Acids Research* **2001**, *29* (5), 1097–1106. https://doi.org/10.1093/nar/29.5.1097.

(7) Brimberry, M. A.; Mathew, L.; Lanzilotta, W. Making and Breaking Carbon-Carbon Bonds in Class C Radical SAM Methyltransferases. *Journal of Inorganic Biochemistry* **2022**, *226*, 111636. https://doi.org/10.1016/j.jinorgbio.2021.111636.

(8) Mathew, L. G.; Brimberry, M.; Lanzilotta, W. N. Class C Radical SAM Methyltransferases Involved in Anaerobic Heme Degradation. *ACS Bio & Med Chem Au* **2021**, acsbiomedchemau.1c00047. https://doi.org/10.1021/acsbiomedchemau.1c00047.

(9) Brimberry, M.; Toma, M. A.; Hines, K. M.; Lanzilotta, W. N. HutW from Vibrio Cholerae Is an Anaerobic Heme-Degrading Enzyme with Unique Functional Properties. *Biochemistry* **2021**, *60* (9). https://doi.org/10.1021/acs.biochem.0c00950.

(10) Mathew, L. G.; Beattie, N. R.; Pritchett, C.; Lanzilotta, W. N. New Insight into the Mechanism of Anaerobic Heme Degradation. *Biochemistry* **2019**, *58* (46). https://doi.org/10.1021/acs.biochem.9b00841.

(11) LaMattina, J. W.; Nix, D. B.; Lanzilotta, W. N. Radical New Paradigm for Heme Degradation in *Escherichia Coli* O157:H7. *Proceedings of the National Academy of Sciences* **2016**, *113* (43). https://doi.org/10.1073/pnas.1603209113.

(12) LaMattina, J. W.; Delrossi, M.; Uy, K. G.; Keul, N. D.; Nix, D. B.; Neelam, A. R.; Lanzilotta, W. N. Anaerobic Heme Degradation: ChuY Is an Anaerobilin Reductase That Exhibits Kinetic Cooperativity. *Biochemistry* **2017**, *56* (6). https://doi.org/10.1021/acs.biochem.6b01099.

(13) Wyckoff, E. E.; Schmitt, M.; Wilks, A.; Payne, S. M. HutZ Is Required for Efficient Heme Utilization in *Vibrio Cholerae*. *Journal of Bacteriology* **2004**, *186* (13), 4142–4151. https://doi.org/10.1128/JB.186.13.4142-4151.2004.

(14) Wyckoff, E. E.; Duncan, D.; Torres, A. G.; Mills, M.; Maase, K.; Payne, S. M. Structure of the Shigella Dysenteriae Haem Transport Locus and Its Phylogenetic Distribution in Enteric Bacteria. *Molecular Microbiology* **1998**, *28* (6), 1139–1152. https://doi.org/10.1046/j.1365-2958.1998.00873.x.

(15) Frey, P. A.; Reed, G. H. The Ubiquity of Iron. *ACS Chemical Biology* **2012**, *7* (9), 1477–1481. https://doi.org/10.1021/cb300323q.

(16) Aisen, P. Chemistry and Biology of Eukaryotic Iron Metabolism. *The International Journal of Biochemistry & Cell Biology* **2001**, *33* (10), 940–959. https://doi.org/10.1016/S1357-2725(01)00063-2.

(17) Bullen, J. J.; Rogers, H. J.; Griffiths, E. Role of Iron in Bacterial Infection; 1978; pp 1–35. https://doi.org/10.1007/978-3-642-66956-9_1.

(18) Richard, K. L.; Kelley, B. R.; Johnson, J. G. Heme Uptake and Utilization by Gram-Negative Bacterial Pathogens. *Frontiers in Cellular and Infection Microbiology* **2019**, *9*. https://doi.org/10.3389/fcimb.2019.00081.

(19) Huang, W.; Wilks, A. Extracellular Heme Uptake and the Challenge of Bacterial Cell Membranes. *Annual Review of Biochemistry* **2017**, *86* (1), 799–823. https://doi.org/10.1146/annurev-biochem-060815-014214.

(20) Pappenheimer, A. M. DIPHTHERIA TOXIN. *Journal of Biological Chemistry* **1947**, *167* (1), 251–259. https://doi.org/10.1016/S0021-9258(17)35162-1.

(21) Melton-Celsa, A. R. Shiga Toxin (Stx) Classification, Structure, and Function. *Microbiology Spectrum* **2014**, *2* (4). https://doi.org/10.1128/microbiolspec.EHEC-0024-2013.

(22) Ochsner, U. A.; Johnson, Z.; Lamont, I. L.; Cunliffe, H. E.; Vasil, M. L. **Exotoxin A Production in *Pseudomonas Aeruginosa* Requires the Iron-regulated *PvdS* Gene Encoding an Alternative Sigma Factor** . *Molecular Microbiology* **1996**, *21* (5), 1019–1028. https://doi.org/10.1046/j.1365-2958.1996.481425.x.

(23) Hantke, K. Regulation of Ferric Iron Transport in Escherichia Coli K12: Isolation of a Constitutive Mutant. *Molecular and General Genetics MGG* **1981**, *182* (2), 288–292. https://doi.org/10.1007/BF00269672.

(24) Skaar, E. P. The Battle for Iron between Bacterial Pathogens and Their Vertebrate Hosts. *PLoS Pathogens* **2010**, *6* (8), e1000949. https://doi.org/10.1371/journal.ppat.1000949.

(25) Bagg, A.; Neilands, J. B. Ferric Uptake Regulation Protein Acts as a Repressor, Employing Iron(II) as a Cofactor to Bind the Operator of an Iron Transport Operon in Escherichia Coli. *Biochemistry* **1987**, *26* (17), 5471–5477. https://doi.org/10.1021/bi00391a039.

(26) Xiong, A.; Singh, V. K.; Cabrera, G.; Jayaswal, R. K. Molecular Characterization of the Ferric-Uptake Regulator, Fur, from Staphylococcus Aureus The GenBank Accession Numbers for the S. Aureus Fur Gene and Fhu Operon Reported in This Paper Are AF118839 and AF132117, Respectively. *Microbiology (N Y)* **2000**, *146* (3), 659–668. https://doi.org/10.1099/00221287-146-3-659.

(27) Hantke, K. Regulation of Ferric Iron Transport in Escherichia Coli K12: Isolation of a Constitutive Mutant. *Molecular and General Genetics MGG* **1981**, *182* (2), 288–292. https://doi.org/10.1007/BF00269672.

(28) Troxell, B.; Hassan, H. M. Transcriptional Regulation by Ferric Uptake Regulator (Fur) in Pathogenic Bacteria. *Frontiers in Cellular and Infection Microbiology* **2013**, *3*. https://doi.org/10.3389/fcimb.2013.00059.

(29) Lau, C. K. Y.; Krewulak, K. D.; Vogel, H. J. Bacterial Ferrous Iron Transport: The Feo System. *FEMS Microbiology Reviews* **2016**, *40* (2), 273–298. https://doi.org/10.1093/femsre/fuv049.

(30) Albenberg, L.; Esipova, T. v.; Judge, C. P.; Bittinger, K.; Chen, J.; Laughlin, A.; Grunberg, S.; Baldassano, R. N.; Lewis, J. D.; Li, H.; Thom, S. R.; Bushman, F. D.; Vinogradov, S. A.; Wu, G. D. Correlation Between Intraluminal Oxygen Gradient and Radial Partitioning of Intestinal Microbiota. *Gastroenterology* **2014**, *147* (5), 1055-1063.e8. https://doi.org/10.1053/j.gastro.2014.07.020.

(31) Cartron, M. L.; Maddocks, S.; Gillingham, P.; Craven, C. J.; Andrews, S. C. Feo – Transport of Ferrous Iron into Bacteria. *BioMetals* **2006**, *19* (2), 143–157. https://doi.org/10.1007/s10534-006-0003-2.

(32) Hantke, K. Ferrous Iron Transport Mutants in *Escherichia Coli* K12. *FEMS Microbiology Letters* **1987**, *44* (1), 53–57. https://doi.org/10.1111/j.1574-6968.1987.tb02241.x.

(33) Kammler, M.; Schön, C.; Hantke, K. Characterization of the Ferrous Iron Uptake System of Escherichia Coli. *Journal of Bacteriology* **1993**, *175* (19), 6212–6219. https://doi.org/10.1128/jb.175.19.6212-6219.1993.

(34) Spiro, S.; Guest, J. R. FNR and Its Role in Oxygen-Regulated Gene Expression in *Escherichia Coli*. *FEMS Microbiology Letters* **1990**, *75* (4), 399–428. https://doi.org/10.1111/j.1574-6968.1990.tb04109.x.

(35) Escolar, L.; Pérez-Martín, J.; de Lorenzo, V. Opening the Iron Box: Transcriptional Metalloregulation by the Fur Protein. *Journal of Bacteriology* **1999**, *181* (20), 6223–6229. https://doi.org/10.1128/JB.181.20.6223-6229.1999.

(36) Lau, C. K. Y.; Ishida, H.; Liu, Z.; Vogel, H. J. Solution Structure of Escherichia Coli FeoA and Its Potential Role in Bacterial Ferrous Iron Transport. *Journal of Bacteriology* **2013**, *195* (1), 46–55. https://doi.org/10.1128/JB.01121-12.

(37) Marlovits, T. C.; Haase, W.; Herrmann, C.; Aller, S. G.; Unger, V. M. The Membrane Protein FeoB Contains an Intramolecular G Protein Essential for Fe(II) Uptake in Bacteria. *Proceedings of the National Academy of Sciences* **2002**, *99* (25), 16243–16248. https://doi.org/10.1073/pnas.242338299.

(38) Maddocks, S. E.; Oyston, P. C. F. Structure and Function of the LysR-Type Transcriptional Regulator (LTTR) Family Proteins. *Microbiology (N Y)* **2008**, *154* (12), 3609–3623. https://doi.org/10.1099/mic.0.2008/022772-0.

(39) Hung, K.-W.; Juan, T.; Hsu, Y.; Huang, T. H. NMR Structure Note: The Ferrous Iron Transport Protein C (FeoC) from Klebsiella Pneumoniae. *Journal of Biomolecular NMR* **2012**, *53* (2), 161–165. https://doi.org/10.1007/s10858-012-9633-6.

(40) Wyckoff, E. E.; Mey, A. R.; Leimbach, A.; Fisher, C. F.; Payne, S. M. Characterization of Ferric and Ferrous Iron Transport Systems in *Vibrio Cholerae*. *Journal of Bacteriology* **2006**, *188* (18), 6515–6523. https://doi.org/10.1128/JB.00626-06.

(41) Wyckoff, E. E.; Mey, A. R.; Payne, S. M. Iron Acquisition in Vibrio Cholerae. *BioMetals* **2007**, *20* (3–4), 405–416. https://doi.org/10.1007/s10534-006-9073-4.

(42) Cassat, J. E.; Skaar, E. P. Iron in Infection and Immunity. *Cell Host & Microbe* **2013**, *13* (5), 509–519. https://doi.org/10.1016/j.chom.2013.04.010.

(43) Saha, R.; Saha, N.; Donofrio, R. S.; Bestervelt, L. L. Microbial Siderophores: A Mini Review. *Journal of Basic Microbiology* **2013**, *53* (4), 303–317. https://doi.org/10.1002/jobm.201100552.

(44) Miethke, M.; Marahiel, M. A. Siderophore-Based Iron Acquisition and Pathogen Control. *Microbiology and Molecular Biology Reviews* **2007**, *71* (3), 413–451. https://doi.org/10.1128/MMBR.00012-07.

(45) Minandri, F.; Imperi, F.; Frangipani, E.; Bonchi, C.; Visaggio, D.; Facchini, M.; Pasquali, P.; Bragonzi, A.; Visca, P. Role of Iron Uptake Systems in Pseudomonas Aeruginosa Virulence and Airway Infection. *Infection and Immunity* **2016**, *84* (8), 2324–2335. https://doi.org/10.1128/IAI.00098-16.

(46) Cornelis, P.; Dingemans, J. Pseudomonas Aeruginosa Adapts Its Iron Uptake Strategies in Function of the Type of Infections. *Frontiers in Cellular and Infection Microbiology* **2013**, *3*. https://doi.org/10.3389/fcimb.2013.00075.

(47) Koczura, R.; Kaznowski, A. Occurrence of the Yersinia High-Pathogenicity Island and Iron Uptake Systems in Clinical Isolates of Klebsiella Pneumoniae. *Microbial Pathogenesis* **2003**, *35* (5), 197–202. https://doi.org/10.1016/S0882-4010(03)00125-6.

(48) Bach, S.; Almeida, A.; Carniel, E. The *Yersinia* High-Pathogenicity Island Is Present in Different Members of the Family *Enterobacteriaceae*. *FEMS Microbiology Letters* **2000**, *183* (2), 289–294. https://doi.org/10.1111/j.1574-6968.2000.tb08973.x.

(49) Tarkkanen, A. M.; Allen, B. L.; Williams, P. H.; Kauppi, M.; Haahtela, K.; Siitonen, A.; Orskov, I.; Orskov, F.; Clegg, S.; Korhonen, T. K. Fimbriation, Capsulation, and Iron-Scavenging Systems of Klebsiella Strains Associated with Human Urinary Tract Infection. *Infection and Immunity* **1992**, *60* (3), 1187–1192. https://doi.org/10.1128/iai.60.3.1187-1192.1992.

(50) Paczosa, M. K.; Mecsas, J. Klebsiella Pneumoniae: Going on the Offense with a Strong Defense. *Microbiology and Molecular Biology Reviews* **2016**, *80* (3), 629–661. https://doi.org/10.1128/MMBR.00078-15.

(51) Sigel, S. P.; Payne, S. M. Effect of Iron Limitation on Growth, Siderophore Production, and Expression of Outer Membrane Proteins of Vibrio Cholerae. *Journal of Bacteriology* **1982**, *150* (1), 148–155. https://doi.org/10.1128/jb.150.1.148-155.1982.

(52) Wyckoff, E. E.; Allred, B. E.; Raymond, K. N.; Payne, S. M. Catechol Siderophore Transport by Vibrio Cholerae. *Journal of Bacteriology* **2015**, *197* (17), 2840–2849. https://doi.org/10.1128/JB.00417-15.

(53) Okujo, N.; Saito, M.; Yamamoto, S.; Yoshida, T.; Miyoshi, S.; Shinoda, S. Structure of Vulnibactin, a New Polyamine-Containing Siderophore from Vibrio Vulnificus. *Biometals* **1994**, *7* (2). https://doi.org/10.1007/BF00140480.

(54) Griffiths GL, S. S. P. S. N. J. Vibriobactin, a Siderophore from Vibrio Cholerae. *J Biol Chem.* **1984**, *10* (259), 383–385.

(55) Mey, A. R.; Wyckoff, E. E.; Oglesby, A. G.; Rab, E.; Taylor, R. K.; Payne, S. M. Identification of the *Vibrio Cholerae* Enterobactin Receptors VctA and IrgA: IrgA Is Not Required for Virulence. *Infection and Immunity* **2002**, *70* (7), 3419–3426. https://doi.org/10.1128/IAI.70.7.3419-3426.2002.

(56) Wyckoff, E. E.; Valle, A.-M.; Smith, S. L.; Payne, S. M. A Multifunctional ATP-Binding Cassette Transporter System from *Vibrio Cholerae* Transports Vibriobactin and Enterobactin. *Journal of Bacteriology* **1999**, *181* (24), 7588–7596. https://doi.org/10.1128/JB.181.24.7588-7596.1999.

(57) Litwin, C. M.; Calderwood, S. B. Analysis of the Complexity of Gene Regulation by Fur in Vibrio Cholerae. *Journal of Bacteriology* **1994**, *176* (1), 240–248. https://doi.org/10.1128/jb.176.1.240-248.1994.

(58) Butterton, J. R.; Stoebner, J. A.; Payne, S. M.; Calderwood, S. B. Cloning, Sequencing, and Transcriptional Regulation of ViuA, the Gene Encoding the Ferric Vibriobactin Receptor of Vibrio Cholerae. *Journal of Bacteriology* **1992**, *174* (11), 3729–3738. https://doi.org/10.1128/jb.174.11.3729-3738.1992.

(59) Occhino, D. A.; Wyckoff, E. E.; Henderson, D. P.; Wrona, T. J.; Payne, S. M. *Vibrio Cholerae* Iron Transport: Haem Transport Genes Are Linked to One of Two Sets of *TonB* , *ExbB*, *ExbD* Genes. *Molecular Microbiology* **1998**, *29* (6), 1493–1507. https://doi.org/10.1046/j.1365-2958.1998.01034.x.

(60) Griffiths, G. L.; Sigel, S. P.; Payne, S. M.; Neilands, J. B. Vibriobactin, a Siderophore from Vibrio Cholerae. *J Biol Chem* **1984**, *259* (1), 383–385.

(61) Carson, S. D. B.; Klebba, P. E.; Newton, S. M. C.; Sparling, P. F. Ferric Enterobactin Binding and Utilization by *Neisseria Gonorrhoeae*. *Journal of Bacteriology* **1999**, *181* (9), 2895–2901. https://doi.org/10.1128/JB.181.9.2895-2901.1999.

(62) Beucher, M.; Sparling, P. F. Cloning, Sequencing, and Characterization of the Gene Encoding FrpB, a Major Iron-Regulated, Outer Membrane Protein of Neisseria Gonorrhoeae. *Journal of Bacteriology* **1995**, *177* (8), 2041–2049. https://doi.org/10.1128/jb.177.8.2041-2049.1995.

(63) Goldberg, M. B.; Boyko, S. A.; Butterton, J. R.; Stoebner, J. A.; Payne, S. M.; Calderwood, S. B. Characterization of a Vibrio Cholerae Virulence Factor Homologous to the Family of TonB-Dependent Proteins. *Molecular Microbiology* **1992**, *6* (16), 2407–2418. https://doi.org/10.1111/j.1365-2958.1992.tb01415.x.

(64) Goldberg, M. B.; DiRita, V. J.; Calderwood, S. B. Identification of an Iron-Regulated Virulence Determinant in Vibrio Cholerae, Using TnphoA Mutagenesis. *Infection and Immunity* **1990**, *58* (1), 55–60. https://doi.org/10.1128/iai.58.1.55-60.1990.

(65) Rogers, M. B.; Sexton, J. A.; DeCastro, G. J.; Calderwood, S. B. Identification of an Operon Required for Ferrichrome Iron Utilization in *Vibrio Cholerae*. *Journal of Bacteriology* **2000**, *182* (8), 2350–2353. https://doi.org/10.1128/JB.182.8.2350-2353.2000.

(66) Crosa, J. H.; Walsh, C. T. Genetics and Assembly Line Enzymology of Siderophore Biosynthesis in Bacteria. *Microbiology and Molecular Biology Reviews* **2002**, *66* (2), 223–249. https://doi.org/10.1128/MMBR.66.2.223-249.2002.

(67) Keating, T. A.; Marshall, C. G.; Walsh, C. T. Reconstitution and Characterization of the *Vibrio Cholerae* Vibriobactin Synthetase from VibB, VibE, VibF, and VibH. *Biochemistry* **2000**, *39* (50), 15522–15530. https://doi.org/10.1021/bi0016523.

(68) Wyckoff, E. E.; Stoebner, J. A.; Reed, K. E.; Payne, S. M. Cloning of a Vibrio Cholerae Vibriobactin Gene Cluster: Identification of Genes Required for Early Steps in Siderophore Biosynthesis. *Journal of Bacteriology* **1997**, *179* (22), 7055–7062. https://doi.org/10.1128/jb.179.22.7055-7062.1997.

(69) Heidelberg, J. F.; Eisen, J. A.; Nelson, W. C.; Clayton, R. A.; Gwinn, M. L.; Dodson, R. J.; Haft, D. H.; Hickey, E. K.; Peterson, J. D.; Umayam, L.; Gill, S. R.; Nelson, K. E.; Read, T. D.; Tettelin, H.; Richardson, D.; Ermolaeva, M. D.; Vamathevan, J.; Bass, S.; Qin, H.; Dragoi, I.; Sellers, P.; McDonald, L.; Utterback, T.; Fleishmann, R. D.; Nierman, W. C.; White, O.; Salzberg, S. L.; Smith, H. O.; Colwell, R. R.; Mekalanos, J. J.; Venter,

J. C.; Fraser, C. M. DNA Sequence of Both Chromosomes of the Cholera Pathogen Vibrio Cholerae. *Nature* **2000**, *406* (6795), 477–483. https://doi.org/10.1038/35020000.

(70) Cadmus, P.; Brinkman, S. F.; May, M. K. Chronic Toxicity of Ferric Iron for North American Aquatic Organisms: Derivation of a Chronic Water Quality Criterion Using Single Species and Mesocosm Data. *Archives of Environmental Contamination and Toxicology* **2018**, *74* (4), 605–615. https://doi.org/10.1007/s00244-018-0505-2.

(71) Stoebner, J. A.; Payne, S. M. Iron-Regulated Hemolysin Production and Utilization of Heme and Hemoglobin by Vibrio Cholerae. *Infection and Immunity* **1988**, *56* (11), 2891–2895. https://doi.org/10.1128/iai.56.11.2891-2895.1988.

(72) Shouldice, S. R.; Skene, R. J.; Dougan, D. R.; Snell, G.; McRee, D. E.; Schryvers, A. B.; Tari, L. W. Structural Basis for Iron Binding and Release by a Novel Class of Periplasmic Iron-Binding Proteins Found in Gram-Negative Pathogens. *Journal of Bacteriology* **2004**, *186* (12), 3903–3910. https://doi.org/10.1128/JB.186.12.3903-3910.2004.

(73) Shouldice, S. R.; Dougan, D. R.; Williams, P. A.; Skene, R. J.; Snell, G.; Scheibe, D.; Kirby, S.; Hosfield, D. J.; McRee, D. E.; Schryvers, A. B.; Tari, L. W. Crystal Structure of Pasteurella Haemolytica Ferric Ion-Binding Protein A Reveals a Novel Class of Bacterial Iron-Binding Proteins. *Journal of Biological Chemistry* **2003**, *278* (42), 41093–41098. https://doi.org/10.1074/jbc.M306821200.

(74) Mey, A. R.; Wyckoff, E. E.; Kanukurthy, V.; Fisher, C. R.; Payne, S. M. Iron and Fur Regulation in *Vibrio Cholerae* and the Role of Fur in Virulence. *Infection and Immunity* **2005**, *73* (12), 8167–8178. https://doi.org/10.1128/IAI.73.12.8167-8178.2005.

(75) Postle, K.; Larsen, R. A. TonB-Dependent Energy Transduction between Outer and Cytoplasmic Membranes. *BioMetals* **2007**, *20* (3–4), 453–465. https://doi.org/10.1007/s10534-006-9071-6.

(76) Rogers, M. B.; Sexton, J. A.; DeCastro, G. J.; Calderwood, S. B. Identification of an Operon Required for Ferrichrome Iron Utilization in *Vibrio Cholerae*. *Journal of Bacteriology* **2000**, *182* (8), 2350–2353. https://doi.org/10.1128/JB.182.8.2350-2353.2000.

(77) Seliger, S.; Mey, A.; Valle, A.-M.; Payne, S. The Two TonB Systems in Vibrio Cholerae Redundant and Specific Functions. *Mol. Microbiol* **2001**, *39*, 801–812.

(78) Stoebner, J. A.; Payne, S. M. Iron-Regulated Hemolysin Production and Utilization of Heme and Hemoglobin by Vibrio Cholerae. *Infection and Immunity* **1988**, *56* (11), 2891–2895. https://doi.org/10.1128/iai.56.11.2891-2895.1988.

(79) Henderson, D. P.; Payne, S. M. Cloning and Characterization of the Vibrio Cholerae Genes Encoding the Utilization of Iron from Haemin and Haemoglobin. *Molecular Microbiology* **1993**, *7* (3), 461–469. https://doi.org/10.1111/j.1365-2958.1993.tb01137.x.

(80) Occhino, D. A.; Wyckoff, E. E.; Henderson, D. P.; Wrona, T. J.; Payne, S. M. *Vibrio Cholerae* Iron Transport: Haem Transport Genes Are Linked to One of Two Sets of *TonB* , *ExbB*, *ExbD* Genes. *Molecular Microbiology* **1998**, *29* (6), 1493–1507. https://doi.org/10.1046/j.1365-2958.1998.01034.x.

(81) Mey, A. R.; Payne, S. M. Haem Utilization in Vibrio Cholerae Involves Multiple TonB-Dependent Haem Receptors. *Molecular Microbiology* **2008**, *42* (3), 835–849. https://doi.org/10.1046/j.1365-2958.2001.02683.x.

(82) Kumar, R.; Lovell, S.; Matsumura, H.; Battaile, K. P.; Moënne-Loccoz, P.; Rivera, M. The Hemophore HasA from *Yersinia Pestis* (HasA $_{yp}$) Coordinates Hemin with a Single Residue, Tyr75, and with Minimal Conformational Change. *Biochemistry* **2013**, *52* (16), 2705–2707. https://doi.org/10.1021/bi400280z.

(83) Létoffé, S.; Ghigo, J. M.; Wandersman, C. Iron Acquisition from Heme and Hemoglobin by a Serratia Marcescens Extracellular Protein. *Proceedings of the National Academy of Sciences* **1994**, *91* (21), 9876–9880. https://doi.org/10.1073/pnas.91.21.9876.

(84) Letoffe, S.; Redeker, V.; Wandersman, C. Isolation and Characterization of an Extracellular Haem-Binding Protein from Pseudomonas Aeruginosa That Shares Function and Sequence Similarities with the Serratia Marcescens HasA Haemophore. *Molecular Microbiology* **1998**, *28* (6), 1223–1234. https://doi.org/10.1046/j.1365-2958.1998.00885.x.

(85) Contreras, H.; Chim, N.; Credali, A.; Goulding, C. W. Heme Uptake in Bacterial Pathogens. *Current Opinion in Chemical Biology* **2014**, *19*, 34–41. https://doi.org/10.1016/j.cbpa.2013.12.014.

(86) Wandersman, C.; Delepelaire, P. Haemophore Functions Revisited. *Molecular Microbiology* **2012**, *85* (4), 618–631. https://doi.org/10.1111/j.1365-2958.2012.08136.x.

(87) Liu, X.; Gong, J.; Wei, T.; Wang, Z.; Du, Q.; Zhu, D.; Huang, Y.; Xu, S.; Gu, L. Crystal Structure of HutZ, a Heme Storage Protein from Vibrio Cholerae: A Structural Mismatch Observed in the Region of High Sequence Conservation. *BMC Structural Biology* **2012**, *12* (1), 23. https://doi.org/10.1186/1472-6807-12-23.

(88) Sekine, Y.; Tanzawa, T.; Tanaka, Y.; Ishimori, K.; Uchida, T. Cytoplasmic Heme-Binding Protein (HutX) from *Vibrio Cholerae* Is an Intracellular Heme Transport Protein for the

Heme-Degrading Enzyme, HutZ. *Biochemistry* **2016**, *55* (6), 884–893. https://doi.org/10.1021/acs.biochem.5b01273.

(89) Wilks, A.; Schmitt, M. P. Expression and Characterization of a Heme Oxygenase (Hmu O) FromCorynebacterium Diphtheriae. *Journal of Biological Chemistry* **1998**, *273* (2), 837–841. https://doi.org/10.1074/jbc.273.2.837.

(90) Zhu, W.; Wilks, A.; Stojiljkovic, I. Degradation of Heme in Gram-Negative Bacteria: The Product of the *HemO* Gene of Neisseriae Is a Heme Oxygenase. *Journal of Bacteriology* **2000**, *182* (23), 6783–6790. https://doi.org/10.1128/JB.182.23.6783-6790.2000.

(91) Ratliff, M.; Zhu, W.; Deshmukh, R.; Wilks, A.; Stojiljkovic, I. Homologues of Neisserial Heme Oxygenase in Gram-Negative Bacteria: Degradation of Heme by the Product of the PigA Gene of Pseudomonas Aeruginosa. *Journal of Bacteriology* **2001**, *183* (21), 6394–6403. https://doi.org/10.1128/JB.183.21.6394-6403.2001.

(92) Nambu, S.; Matsui, T.; Goulding, C. W.; Takahashi, S.; Ikeda-Saito, M. A New Way to Degrade Heme. *Journal of Biological Chemistry* **2013**, *288* (14). https://doi.org/10.1074/jbc.M112.448399.

(93) Reniere, M. L.; Ukpabi, G. N.; Harry, S. R.; Stec, D. F.; Krull, R.; Wright, D. W.; Bachmann, B. O.; Murphy, M. E.; Skaar, E. P. The IsdG-Family of Haem Oxygenases Degrades Haem to a Novel Chromophore. *Molecular Microbiology* **2010**, *75* (6), 1529–1538. https://doi.org/10.1111/j.1365-2958.2010.07076.x.

(94) Matsui, T.; Nambu, S.; Ono, Y.; Goulding, C. W.; Tsumoto, K.; Ikeda-Saito, M. Heme Degradation by *Staphylococcus Aureus* IsdG and IsdI Liberates Formaldehyde Rather Than Carbon Monoxide. *Biochemistry* **2013**, *52* (18), 3025–3027. https://doi.org/10.1021/bi400382p.

(95) Poulos, T. L.; Schuller, D. J.; Wilks, A.; Ortiz de Montellano, P. R. Crystal Structure of Human Heme Oxygenase-1. *Nature Structural Biology* **1999**, *6* (9), 860–867. https://doi.org/10.1038/12319.

(96) Matsui, T.; Unno, M.; Ikeda-Saito, M. Heme Oxygenase Reveals Its Strategy for Catalyzing Three Successive Oxygenation Reactions. *Accounts of Chemical Research* **2010**, *43* (2), 240–247. https://doi.org/10.1021/ar9001685.

(97) Wilks, A.; Heinzl, G. Heme Oxygenation and the Widening Paradigm of Heme Degradation. *Archives of Biochemistry and Biophysics* **2014**, *544*, 87–95. https://doi.org/10.1016/j.abb.2013.10.013.

(98) Unno, M.; Matsui, T.; Chu, G. C.; Couture, M.; Yoshida, T.; Rousseau, D. L.; Olson, John. S.; Ikeda-Saito, M. Crystal Structure of the Dioxygen-Bound Heme Oxygenase from Corynebacterium Diphtheriae. *Journal of Biological Chemistry* **2004**, *279* (20), 21055–21061. https://doi.org/10.1074/jbc.M400491200.

(99) Wilks, A.; Ortiz de Montellano, P. Rat Liver Heme Oxygenase. High Level Expression of a Truncated Soluble Form and Nature of the Meso-Hydroxylating Species. *J Biol Cem* **1993**.

(100) Takahashi, S.; Matera, K. M.; Fujii, H.; Zhou, H.; Ishikawa, K.; Yoshida, T.; Ikeda-Saito, M.; Rousseau, D. L. Resonance Raman Spectroscopic Characterization of α-Hydroxyheme and Verdoheme Complexes of Heme Oxygenase. *Biochemistry* **1997**, *36* (6), 1402–1410. https://doi.org/10.1021/bi962361q.

(101) Garcia-Serres, R.; Davydov, R. M.; Matsui, T.; Ikeda-Saito, M.; Hoffman, B. M.; Huynh, B. H. Distinct Reaction Pathways Followed upon Reduction of Oxy-Heme Oxygenase and

Oxy-Myoglobin as Characterized by Mössbauer Spectroscopy. *J Am Chem Soc* **2007**, *129* (5), 1402–1412. https://doi.org/10.1021/ja067209i.

(102) Matsui, T.; Furukawa, M.; Unno, M.; Tomita, T.; Ikeda-Saito, M. Roles of Distal Asp in Heme Oxygenase from Corynebacterium Diphtheriae, HmuO. *Journal of Biological Chemistry* **2005**, *280* (4), 2981–2989. https://doi.org/10.1074/jbc.M410263200.

(103) Zeng, Y.; Caignan, G. A.; Bunce, R. A.; Rodríguez, J. C.; Wilks, A.; Rivera, M. Azide-Inhibited Bacterial Heme Oxygenases Exhibit an $S = 3/2$ $(d_{xz}, d_{yz})^3 (d_{xy})^1 (d_{z^2})^1$ Spin State: Mechanistic Implications for Heme Oxidation. *J Am Chem Soc* **2005**, *127* (27), 9794–9807. https://doi.org/10.1021/ja0425987.

(104) Wilks, A.; Torpey, J.; Ortiz de Montellano, P. Heme Oxygenase (HO-1). Evidence for Electrophilic Oxygen Addition to the Porphyrin Ring in the Formation of Alpha-Meso-Hydroxyheme. *J Biol Chem* **1994**, *269* (47), 29553–29556.

(105) Liu, Y.; Moënne-Loccoz, P.; Loehr, T. M.; de Montellano, P. R. O. Heme Oxygenase-1, Intermediates in Verdoheme Formation and the Requirement for Reduction Equivalents. *Journal of Biological Chemistry* **1997**, *272* (11), 6909–6917. https://doi.org/10.1074/jbc.272.11.6909.

(106) Ortiz de Montellano, P. The Mechanism of Heme Oxygenase. *Current Opinion in Chemical Biology* **2000**, *4* (2), 221–227. https://doi.org/10.1016/S1367-5931(99)00079-4.

(107) Alavi, F. S.; Gheidi, M.; Zahedi, M.; Safari, N.; Ryde, U. A Novel Mechanism of Heme Degradation to Biliverdin Studied by QM/MM and QM Calculations. *Dalton Transactions* **2018**, *47* (25), 8283–8291. https://doi.org/10.1039/C8DT00064F.

(108) Unno, M.; Matsui, T.; Ikeda-Saito, M. Crystallographic Studies of Heme Oxygenase Complexed with an Unstable Reaction Intermediate, Verdoheme. *Journal of Inorganic Biochemistry* **2012**, *113*, 102–109. https://doi.org/10.1016/j.jinorgbio.2012.04.012.

(109) Sato, H.; Sugishima, M.; Sakamoto, H.; Higashimoto, Y.; Shimokawa, C.; Fukuyama, K.; Palmer, G.; Noguchi, M. Crystal Structure of Rat Haem Oxygenase-1 in Complex with Ferrous Verdohaem: Presence of a Hydrogen-Bond Network on the Distal Side. *Biochemical Journal* **2009**, *419* (2), 339–345. https://doi.org/10.1042/BJ20082279.

(110) Matsui, T.; Omori, K.; Jin, H.; Ikeda-Saito, M. Alkyl Peroxides Reveal the Ring Opening Mechanism of Verdoheme Catalyzed by Heme Oxygenase. *J Am Chem Soc* **2008**, *130* (13), 4220–4221. https://doi.org/10.1021/ja710495z.

(111) Matsui, T.; Nakajima, A.; Fujii, H.; Matera, K. M.; Migita, C. T.; Yoshida, T.; Ikeda-Saito, M. O2- and H2O2-Dependent Verdoheme Degradation by Heme Oxygenase. *Journal of Biological Chemistry* **2005**, *280* (44), 36833–36840. https://doi.org/10.1074/jbc.M503529200.

(112) Uchida, T.; Sekine, Y.; Matsui, T.; Ikeda-Saito, M.; Ishimori, K. A Heme Degradation Enzyme, HutZ, from Vibrio Choleraewz. *Chem. Commun* **2012**, *48*, 6741–6743. https://doi.org/10.1039/c2cc31147j.

(113) Uchida, T.; Sekine, Y.; Dojun, N.; Lewis-Ballester, A.; Ishigami, I.; Matsui, T.; Yeh, S.-R.; Ishimori, K. Reaction Intermediates in the Heme Degradation Reaction by HutZ from Vibrio Cholerae. *Dalton Transactions* **2017**, *46* (25), 8104–8109. https://doi.org/10.1039/C7DT01562C.

(114) Uchida, T.; Dojun, N.; Sekine, Y.; Ishimori, K. Heme Proximal Hydrogen Bonding between His170 and Asp132 Plays an Essential Role in the Heme Degradation Reaction

of HutZ from *Vibrio Cholerae*. *Biochemistry* **2017**, *56* (21), 2723–2734. https://doi.org/10.1021/acs.biochem.7b00152.

(115) Skaar, E. P.; Gaspar, A. H.; Schneewind, O. IsdG and IsdI, Heme-Degrading Enzymes in the Cytoplasm of Staphylococcus Aureus. *Journal of Biological Chemistry* **2004**, *279* (1). https://doi.org/10.1074/jbc.M307952200.

(116) Loutet, S. A.; Kobylarz, M. J.; Chau, C. H. T.; Murphy, M. E. P. IruO Is a Reductase for Heme Degradation by IsdI and IsdG Proteins in Staphylococcus Aureus. *Journal of Biological Chemistry* **2013**, *288* (36), 25749–25759. https://doi.org/10.1074/jbc.M113.470518.

(117) Lee, W. C.; Reniere, M. L.; Skaar, E. P.; Murphy, M. E. P. Ruffling of Metalloporphyrins Bound to IsdG and IsdI, Two Heme-Degrading Enzymes in Staphylococcus Aureus. *Journal of Biological Chemistry* **2008**, *283* (45), 30957–30963. https://doi.org/10.1074/jbc.M709486200.

(118) Takahashi, S.; Nambu, S.; Matsui, T.; Fujii, H.; Ishikawa, H.; Mizutani, Y.; Tsumoto, K.; Ikeda-Saito, M. Unique Electronic Structures of the Highly Ruffled Hemes in Heme-Degrading Enzymes of *Staphylococcus Aureus* , IsdG and IsdI, by Resonance Raman and Electron Paramagnetic Resonance Spectroscopies. *Biochemistry* **2020**, *59* (40), 3918–3928. https://doi.org/10.1021/acs.biochem.0c00731.

(119) Takayama, S. J.; Ukpabi, G.; Murphy, M. E. P.; Mauk, A. G. Electronic Properties of the Highly Ruffled Heme Bound to the Heme Degrading Enzyme IsdI. *Proceedings of the National Academy of Sciences* **2011**, *108* (32), 13071–13076. https://doi.org/10.1073/pnas.1101459108.

(120) Ukpabi, G.; Takayama, S. J.; Mauk, A. G.; Murphy, M. E. P. Inactivation of the Heme Degrading Enzyme IsdI by an Active Site Substitution That Diminishes Heme Ruffling. *Journal of Biological Chemistry* **2012**, *287* (41), 34179–34188. https://doi.org/10.1074/jbc.M112.393249.

(121) Graves, A. B.; Graves, M. T.; Liptak, M. D. Measurement of Heme Ruffling Changes in MhuD Using UV–Vis Spectroscopy. *The Journal of Physical Chemistry B* **2016**, *120* (16), 3844–3853. https://doi.org/10.1021/acs.jpcb.6b01497.

(122) Graves, A. B.; Morse, R. P.; Chao, A.; Iniguez, A.; Goulding, C. W.; Liptak, M. D. Crystallographic and Spectroscopic Insights into Heme Degradation by *Mycobacterium Tuberculosis* MhuD. *Inorganic Chemistry* **2014**, *53* (12), 5931–5940. https://doi.org/10.1021/ic500033b.

(123) Chim, N.; Iniguez, A.; Nguyen, T. Q.; Goulding, C. W. Unusual Diheme Conformation of the Heme-Degrading Protein from Mycobacterium Tuberculosis. *Journal of Molecular Biology* **2010**, *395* (3), 595–608. https://doi.org/10.1016/j.jmb.2009.11.025.

(124) Lockhart, C. L.; Conger, M. A.; Pittman, D. S.; Liptak, M. D. Hydrogen Bond Donation to the Heme Distal Ligand of Staphylococcus Aureus IsdG Tunes the Electronic Structure. *JBIC Journal of Biological Inorganic Chemistry* **2015**, *20* (5), 757–770. https://doi.org/10.1007/s00775-015-1263-5.

(125) Takayama, S. J.; Loutet, S. A.; Mauk, A. G.; Murphy, M. E. P. A Ferric–Peroxo Intermediate in the Oxidation of Heme by IsdI. *Biochemistry* **2015**, *54* (16), 2613–2621. https://doi.org/10.1021/acs.biochem.5b00239.

(126) Matsui, T.; Nambu, S.; Goulding, C. W.; Takahashi, S.; Fujii, H.; Ikeda-Saito, M. Unique Coupling of Mono- and Dioxygenase Chemistries in a Single Active Site Promotes Heme

Degradation. *Proceedings of the National Academy of Sciences* **2016**, *113* (14), 3779–3784. https://doi.org/10.1073/pnas.1523333113.

(127) Yuan, C.; Zhang, Y.; Tan, H.; Li, X.; Chen, G.; Jia, Z. ONIOM Investigations of the Heme Degradation Mechanism by MhuD: The Critical Function of Heme Ruffling. *Physical Chemistry Chemical Physics* **2020**, *22* (16), 8817–8826. https://doi.org/10.1039/C9CP05868K.

(128) Thakuri, B.; O'Rourke, B. D.; Graves, A. B.; Liptak, M. D. A Dynamic Substrate Is Required for MhuD-Catalyzed Degradation of Heme to Mycobilin. *Biochemistry* **2021**, *60* (12), 918–928. https://doi.org/10.1021/acs.biochem.0c00892.

(129) Streit, B. R.; Kant, R.; Tokmina-Lukaszewska, M.; Celis, A. I.; Machovina, M. M.; Skaar, E. P.; Bothner, B.; DuBois, J. L. Time-Resolved Studies of IsdG Protein Identify Molecular Signposts along the Non-Canonical Heme Oxygenase Pathway. *Journal of Biological Chemistry* **2016**, *291* (2), 862–871. https://doi.org/10.1074/jbc.M115.666560.

(130) Chao, A.; Goulding, C. W. A Single Mutation in the *Mycobacterium Tuberculosis* Heme-Degrading Protein, MhuD, Results in Different Products. *Biochemistry* **2019**, *58* (6), 489–492. https://doi.org/10.1021/acs.biochem.8b01198.

(131) Kumar, A.; Deshane, J. S.; Crossman, D. K.; Bolisetty, S.; Yan, B.-S.; Kramnik, I.; Agarwal, A.; Steyn, A. J. C. Heme Oxygenase-1-Derived Carbon Monoxide Induces the Mycobacterium Tuberculosis Dormancy Regulon. *Journal of Biological Chemistry* **2008**, *283* (26), 18032–18039. https://doi.org/10.1074/jbc.M802274200.

(132) Wilks, A.; Ikeda-Saito, M. Heme Utilization by Pathogenic Bacteria: Not All Pathways Lead to Biliverdin. *Accounts of Chemical Research* **2014**, *47* (8), 2291–2298. https://doi.org/10.1021/ar500028n.

(133) Kim, H.; Chaurasia, A. K.; Kim, T.; Choi, J.; Ha, S. C.; Kim, D.; Kim, K. K. Structural and Functional Study of ChuY from Escherichia Coli Strain CFT073. *Biochemical and Biophysical Research Communications* **2017**, *482* (4), 1176–1182. https://doi.org/10.1016/j.bbrc.2016.12.008.

(134) Ji, X.; Mo, T.; Liu, W.; Ding, W.; Deng, Z.; Zhang, Q. Revisiting the Mechanism of the Anaerobic Coproporphyrinogen III Oxidase HemN. *Angewandte Chemie International Edition* **2019**, *58* (19), 6235–6238. https://doi.org/10.1002/anie.201814708.

(135) Jin, W.-B.; Wu, S.; Xu, Y.-F.; Yuan, H.; Tang, G.-L. Recent Advances in HemN-like Radical *S* -Adenosyl- <scp>l</Scp> -Methionine Enzyme-Catalyzed Reactions. *Natural Product Reports* **2020**, *37* (1), 17–28. https://doi.org/10.1039/C9NP00032A.

(136) Krámos, B.; Menyhárd, D. K.; Oláh, J. Direct Hydride Shift Mechanism and Stereoselectivity of P450 $_{nor}$ Confirmed by QM/MM Calculations. *The Journal of Physical Chemistry B* **2012**, *116* (2), 872–885. https://doi.org/10.1021/jp2080918.

(137) Oshima, R.; Fushinobu, S.; Su, F.; Zhang, L.; Takaya, N.; Shoun, H. Structural Evidence for Direct Hydride Transfer from NADH to Cytochrome P450nor. *Journal of Molecular Biology* **2004**, *342* (1), 207–217. https://doi.org/10.1016/j.jmb.2004.07.009.

(138) Shoun, H.; Fushinobu, S.; Jiang, L.; Kim, S.-W.; Wakagi, T. Fungal Denitrification and Nitric Oxide Reductase Cytochrome P450nor. *Philosophical Transactions of the Royal Society B: Biological Sciences* **2012**, *367* (1593). https://doi.org/10.1098/rstb.2011.0335.

(139) Zhang, L.; Kudo, T.; Takaya, N.; Shoun, H. The B′ Helix Determines Cytochrome P450nor Specificity for the Electron Donors NADH and NADPH. *Journal of Biological Chemistry* **2002**, *277* (37), 33842–33847. https://doi.org/10.1074/jbc.M203923200.

(140) Tosha, T.; Nomura, T.; Nishida, T.; Saeki, N.; Okubayashi, K.; Yamagiwa, R.; Sugahara, M.; Nakane, T.; Yamashita, K.; Hirata, K.; Ueno, G.; Kimura, T.; Hisano, T.; Muramoto, K.; Sawai, H.; Takeda, H.; Mizohata, E.; Yamashita, A.; Kanematsu, Y.; Takano, Y.; Nango, E.; Tanaka, R.; Nureki, O.; Shoji, O.; Ikemoto, Y.; Murakami, H.; Owada, S.; Tono, K.; Yabashi, M.; Yamamoto, M.; Ago, H.; Iwata, S.; Sugimoto, H.; Shiro, Y.; Kubo, M. Capturing an Initial Intermediate during the P450nor Enzymatic Reaction Using Time-Resolved XFEL Crystallography and Caged-Substrate. *Nature Communications* **2017**, *8* (1), 1585. https://doi.org/10.1038/s41467-017-01702-1.

(141) Chirpich, T.; Zappia, V.; Costilow, R.; Barker, H. Lysine 2,3-Aminomutase. Purification and Properties of a Pyridoxal Phosphate and S-Adenosylmethionine-Activating Enzyme. *J Biol Chem.* **1970**, *10* (245), 1778–1789.

(142) Ollagnier, S.; Meier, C.; Mulliez, E.; Gaillard, J.; Schuenemann, V.; Trautwein, A.; Mattioli, T.; Lutz, M.; Fontecave, M. Assembly of 2Fe-2S and 4Fe-4S Clusters in the Anaerobic Ribonucleotide Reductase from *Escherichia c Oli*. *J Am Chem Soc* **1999**, *121* (27), 6344–6350. https://doi.org/10.1021/ja990073m.

(143) Knappe, J.; Neugebauer, F. A.; Blaschkowski, H. P.; Gänzler, M. Post-Translational Activation Introduces a Free Radical into Pyruvate Formate-Lyase. *Proceedings of the National Academy of Sciences* **1984**, *81* (5), 1332–1335. https://doi.org/10.1073/pnas.81.5.1332.

(144) Holliday, G. L.; Akiva, E.; Meng, E. C.; Brown, S. D.; Calhoun, S.; Pieper, U.; Sali, A.; Booker, S. J.; Babbitt, P. C. Atlas of the Radical SAM Superfamily: Divergent Evolution of Function Using a “Plug and Play” Domain; 2018. https://doi.org/10.1016/bs.mie.2018.06.004.

(145) Broderick, J. B.; Duffus, B. R.; Duschene, K. S.; Shepard, E. M. Radical *S* -Adenosylmethionine Enzymes. *Chemical Reviews* **2014**, *114* (8). https://doi.org/10.1021/cr4004709.

(146) Walsby, C. J.; Hong, W.; Broderick, W. E.; Cheek, J.; Ortillo, D.; Broderick, J. B.; Hoffman, B. M. Electron-Nuclear Double Resonance Spectroscopic Evidence That *S* -Adenosylmethionine Binds in Contact with the Catalytically Active [4Fe−4S] $^{+}$ Cluster of Pyruvate Formate-Lyase Activating Enzyme. *J Am Chem Soc* **2002**, *124* (12), 3143–3151. https://doi.org/10.1021/ja012034s.

(147) Chen, D.; Walsby, C.; Hoffman, B. M.; Frey, P. A. Coordination and Mechanism of Reversible Cleavage of *S* -Adenosylmethionine by the [4Fe-4S] Center in Lysine 2,3-Aminomutase. *J Am Chem Soc* **2003**, *125* (39), 11788–11789. https://doi.org/10.1021/ja036120z.

(148) Walsby, C. J.; Hong, W.; Broderick, W. E.; Cheek, J.; Ortillo, D.; Broderick, J. B.; Hoffman, B. M. Electron-Nuclear Double Resonance Spectroscopic Evidence That *S* -Adenosylmethionine Binds in Contact with the Catalytically Active [4Fe−4S] $^{+}$ Cluster of Pyruvate Formate-Lyase Activating Enzyme. *J Am Chem Soc* **2002**, *124* (12). https://doi.org/10.1021/ja012034s.

(149) Chen, D.; Walsby, C.; Hoffman, B. M.; Frey, P. A. Coordination and Mechanism of Reversible Cleavage of *S* -Adenosylmethionine by the [4Fe-4S] Center in Lysine 2,3-Aminomutase. *J Am Chem Soc* **2003**, *125* (39). https://doi.org/10.1021/ja036120z.

(150) Zhang, W.; Wong, K. K.; Magliozzo, R. S.; Kozarich, J. W. Inactivation of Pyruvate Formate-Lyase by Dioxygen: Defining the Mechanistic Interplay of Glycine 734 and

Cysteine 419 by Rapid Freeze-Quench EPR. *Biochemistry* **2001**, *40* (13), 4123–4130. https://doi.org/10.1021/bi002589k.

(151) Lanz, N. D.; Booker, S. J. Identification and Function of Auxiliary Iron–Sulfur Clusters in Radical SAM Enzymes. *Biochimica et Biophysica Acta (BBA) - Proteins and Proteomics* **2012**, *1824* (11), 1196–1212. https://doi.org/10.1016/j.bbapap.2012.07.009.

(152) Nicolet, Y. AdoMet Radical Proteins--from Structure to Evolution--Alignment of Divergent Protein Sequences Reveals Strong Secondary Structure Element Conservation. *Nucleic Acids Research* **2004**, *32* (13), 4015–4025. https://doi.org/10.1093/nar/gkh728.

(153) Nagano, N.; Orengo, C. A.; Thornton, J. M. One Fold with Many Functions: The Evolutionary Relationships between TIM Barrel Families Based on Their Sequences, Structures and Functions. *Journal of Molecular Biology* **2002**, *321* (5), 741–765. https://doi.org/10.1016/S0022-2836(02)00649-6.

(154) Chirpich, T.; Zappia, V.; Costilow, R.; Barker, H. Lysine 2,3-Aminomutase. Purification and Properties of a Pyridoxal Phosphate and S-Adenosylmethionine-Activated Enzyme. *J Biol Chem.* **1970**, *10* (245), 1778–17789.

(155) KNAPPE, J.; BLASCHKOWSKI, H. P.; GROBNER, P.; SCHMTTT, T. Pyruvate Formate-Lyase of Escherichia Coli: The Acetyl-Enzyme Intermediate. *European Journal of Biochemistry* **1974**, *50* (1), 253–263. https://doi.org/10.1111/j.1432-1033.1974.tb03894.x.

(156) Knappe, J.; Schacht, J.; Mockel, W.; Hopner, Th.; Vetter, H.; Edenharder, R. Pyruvate Formate-Lyase Reaction in Escherichia Coli. The Enzymatic System Converting and Inactive Form of the Lyase into the Catalytically Active Enzyme. *European Journal of Biochemistry* **1969**, *11* (2), 316–327. https://doi.org/10.1111/j.1432-1033.1969.tb00775.x.

(157) McCarty, R. M.; Krebs, C.; Bandarian, V. Spectroscopic, Steady-State Kinetic, and Mechanistic Characterization of the Radical SAM Enzyme QueE, Which Catalyzes a Complex Cyclization Reaction in the Biosynthesis of 7-Deazapurines. *Biochemistry* **2013**, *52* (1), 188–198. https://doi.org/10.1021/bi301156w.

(158) Dowling, D. P.; Bruender, N. A.; Young, A. P.; McCarty, R. M.; Bandarian, V.; Drennan, C. L. Radical SAM Enzyme QueE Defines a New Minimal Core Fold and Metal-Dependent Mechanism. *Nature Chemical Biology* **2014**, *10* (2), 106–112. https://doi.org/10.1038/nchembio.1426.

(159) McCarty, R. M.; Krebs, C.; Bandarian, V. Spectroscopic, Steady-State Kinetic, and Mechanistic Characterization of the Radical SAM Enzyme QueE, Which Catalyzes a Complex Cyclization Reaction in the Biosynthesis of 7-Deazapurines. *Biochemistry* **2013**, *52* (1), 188–198. https://doi.org/10.1021/bi301156w.

(160) Grove, T. L.; Ahlum, J. H.; Qin, R. M.; Lanz, N. D.; Radle, M. I.; Krebs, C.; Booker, S. J. Further Characterization of Cys-Type and Ser-Type Anaerobic Sulfatase Maturating Enzymes Suggests a Commonality in the Mechanism of Catalysis. *Biochemistry* **2013**, *52* (17), 2874–2887. https://doi.org/10.1021/bi400136u.

(161) Grove, T. L.; Lee, K.-H.; st. Clair, J.; Krebs, C.; Booker, S. J. In Vitro Characterization of AtsB, a Radical SAM Formylglycine-Generating Enzyme That Contains Three [4Fe-4S] Clusters. *Biochemistry* **2008**, *47* (28), 7523–7538. https://doi.org/10.1021/bi8004297.

(162) Bruender, N. A.; Young, A. P.; Bandarian, V. Chemical and Biological Reduction of the Radical SAM Enzyme CPH $_4$ Synthase. *Biochemistry* **2015**, *54* (18), 2903–2910. https://doi.org/10.1021/acs.biochem.5b00210.

(163) Amara, P.; Saragaglia, C.; Mouesca, J.-M.; Martin, L.; Nicolet, Y. L-Tyrosine-Bound ThiH Structure Reveals C–C Bond Break Differences within Radical SAM Aromatic Amino Acid Lyases. *Nature Communications* **2022**, *13* (1), 2284. https://doi.org/10.1038/s41467-022-29980-4.

(164) Grell, T. A. J.; Bell, B. N.; Nguyen, C.; Dowling, D. P.; Bruender, N. A.; Bandarian, V.; Drennan, C. L. Crystal Structure of AdoMet Radical Enzyme 7-carboxy-7-deazaguanine Synthase from <scp> *Escherichia Coli* </Scp> Suggests How Modifications near [4Fe–4S] Cluster Engender Flavodoxin Specificity. *Protein Science* **2019**, *28* (1), 202–215. https://doi.org/10.1002/pro.3529.

(165) Gray, H. B.; Winkler, J. R. Electron Flow through Proteins. *Chemical Physics Letters* **2009**, *483* (1–3), 1–9. https://doi.org/10.1016/j.cplett.2009.10.051.

(166) Lieder, K. W.; Booker, S.; Ruzicka, F. J.; Beinert, H.; Reed, G. H.; Frey, P. A. *S* -Adenosylmethionine-Dependent Reduction of Lysine 2,3-Aminomutase and Observation of the Catalytically Functional Iron−Sulfur Centers by Electron Paramagnetic Resonance. *Biochemistry* **1998**, *37* (8), 2578–2585. https://doi.org/10.1021/bi972417w.

(167) Henshaw, T. F.; Cheek, J.; Broderick, J. B. The [4Fe-4S] $^{1+}$ Cluster of Pyruvate Formate-Lyase Activating Enzyme Generates the Glycyl Radical on Pyruvate Formate-Lyase: EPR-Detected Single Turnover. *J Am Chem Soc* **2000**, *122* (34), 8331–8332. https://doi.org/10.1021/ja002012q.

(168) Moss, M.; Frey, P. A. The Role of S-Adenosylmethionine in the Lysine 2,3-Aminomutase Reaction. *J Biol Chem* **1987**, *262* (31), 14859–14862.

(169) Frey, P. A.; Magnusson, O. Th. *S* -Adenosylmethionine: A Wolf in Sheep's Clothing, or a Rich Man's Adenosylcobalamin? *Chemical Reviews* **2003**, *103* (6), 2129–2148. https://doi.org/10.1021/cr020422m.

(170) Frey, P. A. Lysine 2,3-aminomutase: Is Adenosylmethionine a Poor Man's Adenosylcobalamin? *The FASEB Journal* **1993**, *7* (8), 662–670. https://doi.org/10.1096/fasebj.7.8.8500691.

(171) Jordan, A.; Reichard, P. RIBONUCLEOTIDE REDUCTASES. *Annual Review of Biochemistry* **1998**, *67* (1), 71–98. https://doi.org/10.1146/annurev.biochem.67.1.71.

(172) Magnusson, O. Th.; Reed, G. H.; Frey, P. A. Characterization of an Allylic Analogue of the 5'-Deoxyadenosyl Radical: An Intermediate in the Reaction of Lysine 2,3-Aminomutase. *Biochemistry* **2001**, *40* (26), 7773–7782. https://doi.org/10.1021/bi0104569.

(173) Magnusson, O. Th.; Reed, G. H.; Frey, P. A. Spectroscopic Evidence for the Participation of an Allylic Analogue of the 5'-Deoxyadenosyl Radical in the Reaction of Lysine 2,3-Aminomutase. *J Am Chem Soc* **1999**, *121* (41), 9764–9765. https://doi.org/10.1021/ja9925507.

(174) Henshaw, T. F.; Cheek, J.; Broderick, J. B. The [4Fe-4S] $^{1+}$ Cluster of Pyruvate Formate-Lyase Activating Enzyme Generates the Glycyl Radical on Pyruvate Formate-Lyase: EPR-Detected Single Turnover. *J Am Chem Soc* **2000**, *122* (34), 8331–8332. https://doi.org/10.1021/ja002012q.

(175) Krebs, C.; Henshaw, T. F.; Cheek, J.; Huynh, B. H.; Broderick, J. B. Conversion of 3Fe-4S to 4Fe-4S Clusters in Native Pyruvate Formate-Lyase Activating Enzyme: Mössbauer

Characterization and Implications for Mechanism. *J Am Chem Soc* **2000**, *122* (50), 12497–12506. https://doi.org/10.1021/ja003335p.

(176) Walsby, C. J.; Hong, W.; Broderick, W. E.; Cheek, J.; Ortillo, D.; Broderick, J. B.; Hoffman, B. M. Electron-Nuclear Double Resonance Spectroscopic Evidence That *S* -Adenosylmethionine Binds in Contact with the Catalytically Active [4Fe−4S] $^{+}$ Cluster of Pyruvate Formate-Lyase Activating Enzyme. *J Am Chem Soc* **2002**, *124* (12), 3143–3151. https://doi.org/10.1021/ja012034s.

(177) Horitani, M.; Shisler, K.; Broderick, W. E.; Hutcheson, R. U.; Duschene, K. S.; Marts, A. R.; Hoffman, B. M.; Broderick, J. B. Radical SAM Catalysis via an Organometallic Intermediate with an Fe–[5′-C]-Deoxyadenosyl Bond. *Science (1979)* **2016**, *352* (6287). https://doi.org/10.1126/science.aaf5327.

(178) Byer, A. S.; Yang, H.; McDaniel, E. C.; Kathiresan, V.; Impano, S.; Pagnier, A.; Watts, H.; Denler, C.; Vagstad, A. L.; Piel, J.; Duschene, K. S.; Shepard, E. M.; Shields, T. P.; Scott, L. G.; Lilla, E. A.; Yokoyama, K.; Broderick, W. E.; Hoffman, B. M.; Broderick, J. B. Paradigm Shift for Radical *S* -Adenosyl- <scp>l</Scp> -Methionine Reactions: The Organometallic Intermediate Ω Is Central to Catalysis. *J Am Chem Soc* **2018**, *140* (28). https://doi.org/10.1021/jacs.8b04061.

(179) Vey, J. L.; Drennan, C. L. Structural Insights into Radical Generation by the Radical SAM Superfamily. *Chemical Reviews* **2011**, *111* (4), 2487–2506. https://doi.org/10.1021/cr9002616.

(180) Impano, S.; Yang, H.; Jodts, R. J.; Pagnier, A.; Swimley, R.; McDaniel, E. C.; Shepard, E. M.; Broderick, W. E.; Broderick, J. B.; Hoffman, B. M. Active-Site Controlled, Jahn–Teller Enabled Regioselectivity in Reductive S–C Bond Cleavage of *S* -

Adenosylmethionine in Radical SAM Enzymes. *J Am Chem Soc* **2021**, *143* (1), 335–348. https://doi.org/10.1021/jacs.0c10925.

(181) Yang, H.; McDaniel, E. C.; Impano, S.; Byer, A. S.; Jodts, R. J.; Yokoyama, K.; Broderick, W. E.; Broderick, J. B.; Hoffman, B. M. The Elusive 5′-Deoxyadenosyl Radical: Captured and Characterized by Electron Paramagnetic Resonance and Electron Nuclear Double Resonance Spectroscopies. *J Am Chem Soc* **2019**, *141* (30), 12139–12146. https://doi.org/10.1021/jacs.9b05926.

(182) Dey, A.; Peng, Y.; Broderick, W. E.; Hedman, B.; Hodgson, K. O.; Broderick, J. B.; Solomon, E. I. S K-Edge XAS and DFT Calculations on SAM Dependent Pyruvate Formate-Lyase Activating Enzyme: Nature of Interaction between the Fe_4S_4 Cluster and SAM and Its Role in Reactivity. *J Am Chem Soc* **2011**, *133* (46), 18656–18662. https://doi.org/10.1021/ja203780t.

(183) Nicolet, Y.; Amara, P.; Mouesca, J.-M.; Fontecilla-Camps, J. C. Unexpected Electron Transfer Mechanism upon AdoMet Cleavage in Radical SAM Proteins. *Proceedings of the National Academy of Sciences* **2009**, *106* (35), 14867–14871. https://doi.org/10.1073/pnas.0904385106.

(184) Lepore, B. W.; Ruzicka, F. J.; Frey, P. A.; Ringe, D. The X-Ray Crystal Structure of Lysine-2,3-Aminomutase from *Clostridium Subterminale*. *Proceedings of the National Academy of Sciences* **2005**, *102* (39), 13819–13824. https://doi.org/10.1073/pnas.0505726102.

(185) Lees, N. S.; Chen, D.; Walsby, C. J.; Behshad, E.; Frey, P. A.; Hoffman, B. M. How an Enzyme Tames Reactive Intermediates: Positioning of the Active-Site Components of Lysine 2,3-Aminomutase during Enzymatic Turnover As Determined by ENDOR

Spectroscopy. *J Am Chem Soc* **2006**, *128* (31), 10145–10154. https://doi.org/10.1021/ja061282r.

(186) Donnan, P. H.; Mansoorabadi, S. O. Broken-Symmetry Density Functional Theory Analysis of the Ω Intermediate in Radical *S* -Adenosyl- <scp>l</Scp> -Methionine Enzymes: Evidence for a Near-Attack Conformer over an Organometallic Species. *J Am Chem Soc* **2022**, *144* (8), 3381–3385. https://doi.org/10.1021/jacs.2c00678.

(187) Zhang, Q.; van der Donk, W. A.; Liu, W. Radical-Mediated Enzymatic Methylation: A Tale of Two SAMS. *Accounts of Chemical Research* **2012**, *45* (4). https://doi.org/10.1021/ar200202c.

(188) Bauerle, M. R.; Schwalm, E. L.; Booker, S. J. Mechanistic Diversity of Radical S-Adenosylmethionine (SAM)-Dependent Methylation. *Journal of Biological Chemistry* **2015**, *290* (7). https://doi.org/10.1074/jbc.R114.607044.

(189) Kowalak, J. A.; Bruenger, E.; McCloskey, J. A. Posttranscriptional Modification of the Central Loop of Domain V in Escherichia Coli 23 S Ribosomal RNA. *Journal of Biological Chemistry* **1995**, *270* (30), 17758–17764. https://doi.org/10.1074/jbc.270.30.17758.

(190) Benítez-Páez, A.; Villarroya, M.; Armengod, M.-E. The *Escherichia Coli* RlmN Methyltransferase Is a Dual-Specificity Enzyme That Modifies Both RRNA and TRNA and Controls Translational Accuracy. *RNA* **2012**, *18* (10), 1783–1795. https://doi.org/10.1261/rna.033266.112.

(191) Toh, S.-M.; Xiong, L.; Bae, T.; Mankin, A. S. The Methyltransferase YfgB/RlmN Is Responsible for Modification of Adenosine 2503 in 23S RRNA. *RNA* **2008**, *14* (1), 98–106. https://doi.org/10.1261/rna.814408.

(192) Boal, A. K.; Grove, T. L.; McLaughlin, M. I.; Yennawar, N. H.; Booker, S. J.; Rosenzweig, A. C. Structural Basis for Methyl Transfer by a Radical SAM Enzyme. *Science (1979)* **2011**, *332* (6033), 1089–1092. https://doi.org/10.1126/science.1205358.

(193) Grove, T. L.; Benner, J. S.; Radle, M. I.; Ahlum, J. H.; Landgraf, B. J.; Krebs, C.; Booker, S. J. A Radically Different Mechanism for *S* -Adenosylmethionine–Dependent Methyltransferases. *Science (1979)* **2011**, *332* (6029), 604–607. https://doi.org/10.1126/science.1200877.

(194) Silakov, A.; Grove, T. L.; Radle, M. I.; Bauerle, M. R.; Green, M. T.; Rosenzweig, A. C.; Boal, A. K.; Booker, S. J. Characterization of a Cross-Linked Protein–Nucleic Acid Substrate Radical in the Reaction Catalyzed by RlmN. *J Am Chem Soc* **2014**, *136* (23), 8221–8228. https://doi.org/10.1021/ja410560p.

(195) Yan, F.; LaMarre, J. M.; Röhrich, R.; Wiesner, J.; Jomaa, H.; Mankin, A. S.; Fujimori, D. G. RlmN and Cfr Are Radical SAM Enzymes Involved in Methylation of Ribosomal RNA. *J Am Chem Soc* **2010**, *132* (11), 3953–3964. https://doi.org/10.1021/ja910850y.

(196) Kaminska, K. H.; Purta, E.; Hansen, L. H.; Bujnicki, J. M.; Vester, B.; Long, K. S. Insights into the Structure, Function and Evolution of the Radical-SAM 23S RRNA Methyltransferase Cfr That Confers Antibiotic Resistance in Bacteria. *Nucleic Acids Research* **2010**, *38* (5), 1652–1663. https://doi.org/10.1093/nar/gkp1142.

(197) Grove, T. L.; Livada, J.; Schwalm, E. L.; Green, M. T.; Booker, S. J.; Silakov, A. A Substrate Radical Intermediate in Catalysis by the Antibiotic Resistance Protein Cfr. *Nature Chemical Biology* **2013**, *9* (7), 422–427. https://doi.org/10.1038/nchembio.1251.

(198) Wang, S. C. Cobalamin-Dependent Radical *S* -Adenosyl- <scp>l</Scp> -Methionine Enzymes in Natural Product Biosynthesis. *Natural Product Reports* **2018**, *35* (8), 707–720. https://doi.org/10.1039/C7NP00059F.

(199) Bridwell-Rabb, J.; Drennan, C. L. Vitamin B 12 in the Spotlight Again. *Current Opinion in Chemical Biology* **2017**, *37*, 63–70. https://doi.org/10.1016/j.cbpa.2017.01.013.

(200) Dowling, D. P.; Croft, A. K.; Drennan, C. L. Radical Use of Rossmann and TIM Barrel Architectures for Controlling Coenzyme B $_{12}$ Chemistry. *Annual Review of Biophysics* **2012**, *41* (1), 403–427. https://doi.org/10.1146/annurev-biophys-050511-102225.

(201) Bridwell-Rabb, J.; Grell, T. A. J.; Drennan, C. L. A Rich Man, Poor Man Story of *S* -Adenosylmethionine and Cobalamin Revisited. *Annual Review of Biochemistry* **2018**, *87* (1), 555–584. https://doi.org/10.1146/annurev-biochem-062917-012500.

(202) Knox, H. L.; Sinner, E. K.; Townsend, C. A.; Boal, A. K.; Booker, S. J. Structure of a B12-Dependent Radical SAM Enzyme in Carbapenem Biosynthesis. *Nature* **2022**, *602* (7896), 343–348. https://doi.org/10.1038/s41586-021-04392-4.

(203) Matthews, R. G. Cobalamin-Dependent Methyltransferases. *Accounts of Chemical Research* **2001**, *34* (8), 681–689. https://doi.org/10.1021/ar0000051.

(204) Kim, H. J.; Liu, Y.; McCarty, R. M.; Liu, H. Reaction Catalyzed by GenK, a Cobalamin-Dependent Radical *S* -Adenosyl- <scp>l</Scp> -Methionine Methyltransferase in the Biosynthetic Pathway of Gentamicin, Proceeds with Retention of Configuration. *J Am Chem Soc* **2017**, *139* (45), 16084–16087. https://doi.org/10.1021/jacs.7b09890.

(205) McLaughlin, M. I.; Pallitsch, K.; Wallner, G.; van der Donk, W. A.; Hammerschmidt, F. Overall Retention of Methyl Stereochemistry during B $_{12}$ -Dependent Radical SAM

Methyl Transfer in Fosfomycin Biosynthesis. *Biochemistry* **2021**, *60* (20), 1587–1596. https://doi.org/10.1021/acs.biochem.1c00113.

(206) Marous, D. R.; Lloyd, E. P.; Buller, A. R.; Moshos, K. A.; Grove, T. L.; Blaszczyk, A. J.; Booker, S. J.; Townsend, C. A. Consecutive Radical *S* -Adenosylmethionine Methylations Form the Ethyl Side Chain in Thienamycin Biosynthesis. *Proceedings of the National Academy of Sciences* **2015**, *112* (33), 10354–10358. https://doi.org/10.1073/pnas.1508615112.

(207) Wang, Y.; Schnell, B.; Baumann, S.; Müller, R.; Begley, T. P. Biosynthesis of Branched Alkoxy Groups: Iterative Methyl Group Alkylation by a Cobalamin-Dependent Radical SAM Enzyme. *J Am Chem Soc* **2017**, *139* (5), 1742–1745. https://doi.org/10.1021/jacs.6b10901.

(208) Kudo, F.; Zhang, J.; Sato, S.; Hirayama, A.; Eguchi, T. Functional Characterization of 3-Aminobenzoic Acid Adenylation Enzyme PctU and UDP- *N* -Acetyl- <scp>d</Scp> -Glucosamine: 3-Aminobenzoyl-ACP Glycosyltransferase PctL in Pactamycin Biosynthesis. *ChemBioChem* **2019**, *20* (19), 2458–2462. https://doi.org/10.1002/cbic.201900239.

(209) Watanabe, K.; Hotta, K.; Nakaya, M.; Praseuth, A. P.; Wang, C. C. C.; Inada, D.; Takahashi, K.; Fukushi, E.; Oguri, H.; Oikawa, H. *Escherichia Coli* Allows Efficient Modular Incorporation of Newly Isolated Quinomycin Biosynthetic Enzyme into Echinomycin Biosynthetic Pathway for Rational Design and Synthesis of Potent Antibiotic Unnatural Natural Product. *J Am Chem Soc* **2009**, *131* (26), 9347–9353. https://doi.org/10.1021/ja902261a.

(210) Chew, A. G. M.; Frigaard, N.-U.; Bryant, D. A. Bacteriochlorophyllide *c* C-8 ^{2} and C-12 ^{1} Methyltransferases Are Essential for Adaptation to Low Light in *Chlorobaculum Tepidum*. *Journal of Bacteriology* **2007**, *189* (17), 6176–6184. https://doi.org/10.1128/JB.00519-07.

(211) Parent, A.; Guillot, A.; Benjdia, A.; Chartier, G.; Leprince, J.; Berteau, O. The B $_{12}$ -Radical SAM Enzyme PoyC Catalyzes Valine C $_{\beta}$ -Methylation during Polytheonamide Biosynthesis. *J Am Chem Soc* **2016**, *138* (48), 15515–15518. https://doi.org/10.1021/jacs.6b06697.

(212) Allen, K. D.; Wang, S. C. Initial Characterization of Fom3 from Streptomyces Wedmorensis: The Methyltransferase in Fosfomycin Biosynthesis. *Archives of Biochemistry and Biophysics* **2014**, *543*, 67–73. https://doi.org/10.1016/j.abb.2013.12.004.

(213) Seto, H.; Kuzuyama, T.; Seto, H.; Kuzuyama, T. Bioactive Natural Products with Carbon–Phosphorus Bonds and Their Biosynthesis. *Natural Product Reports* **1999**, *16* (5), 589–596. https://doi.org/10.1039/a809398i.

(214) Welander, P. v.; Summons, R. E. Discovery, Taxonomic Distribution, and Phenotypic Characterization of a Gene Required for 3-Methylhopanoid Production. *Proceedings of the National Academy of Sciences* **2012**, *109* (32), 12905–12910. https://doi.org/10.1073/pnas.1208255109.

(215) Kim, H. J.; Liu, Y.; McCarty, R. M.; Liu, H. Reaction Catalyzed by GenK, a Cobalamin-Dependent Radical *S* -Adenosyl- <scp>l</Scp> -Methionine Methyltransferase in the Biosynthetic Pathway of Gentamicin, Proceeds with Retention of Configuration. *J Am Chem Soc* **2017**, *139* (45), 16084–16087. https://doi.org/10.1021/jacs.7b09890.

(216) Huang, C.; Huang, F.; Moison, E.; Guo, J.; Jian, X.; Duan, X.; Deng, Z.; Leadlay, P. F.; Sun, Y. Delineating the Biosynthesis of Gentamicin X2, the Common Precursor of the Gentamicin C Antibiotic Complex. *Chemistry & Biology* **2015**, *22* (2), 251–261. https://doi.org/10.1016/j.chembiol.2014.12.012.

(217) Kim, H. J.; McCarty, R. M.; Ogasawara, Y.; Liu, Y.; Mansoorabadi, S. O.; LeVieux, J.; Liu, H. GenK-Catalyzed C-6′ Methylation in the Biosynthesis of Gentamicin: Isolation and Characterization of a Cobalamin-Dependent Radical SAM Enzyme. *J Am Chem Soc* **2013**, *135* (22), 8093–8096. https://doi.org/10.1021/ja312641f.

(218) Chew, A. G. M.; Frigaard, N.-U.; Bryant, D. A. Bacteriochlorophyllide *c* C-8 ^{2} and C-12 ^{1} Methyltransferases Are Essential for Adaptation to Low Light in *Chlorobaculum Tepidum*. *Journal of Bacteriology* **2007**, *189* (17), 6176–6184. https://doi.org/10.1128/JB.00519-07.

(219) Bridwell-Rabb, J.; Zhong, A.; Sun, H. G.; Drennan, C. L.; Liu, H. A B12-Dependent Radical SAM Enzyme Involved in Oxetanocin A Biosynthesis. *Nature* **2017**, *544* (7650), 322–326. https://doi.org/10.1038/nature21689.

(220) Zhong, A.; Lee, Y.-H.; Liu, Y.; Liu, H. Biosynthesis of Oxetanocin-A Includes a B_{12}-Dependent Radical SAM Enzyme That Can Catalyze Both Oxidative Ring Contraction and the Demethylation of SAM. *Biochemistry* **2021**, *60* (7), 537–546. https://doi.org/10.1021/acs.biochem.0c00915.

(221) Bridwell-Rabb, J.; Kang, G.; Zhong, A.; Liu, H.; Drennan, C. L. An HD Domain Phosphohydrolase Active Site Tailored for Oxetanocin-A Biosynthesis. *Proceedings of the National Academy of Sciences* **2016**, *113* (48), 13750–13755. https://doi.org/10.1073/pnas.1613610113.

(222) Knox, H. L.; Chen, P. Y.-T.; Blaszczyk, A. J.; Mukherjee, A.; Grove, T. L.; Schwalm, E. L.; Wang, B.; Drennan, C. L.; Booker, S. J. Structural Basis for Non-Radical Catalysis by TsrM, a Radical SAM Methylase. *Nature Chemical Biology* **2021**, *17* (4), 485–491. https://doi.org/10.1038/s41589-020-00717-y.

(223) Blaszczyk, A. J.; Wang, B.; Silakov, A.; Ho, J. v.; Booker, S. J. Efficient Methylation of C2 in L-Tryptophan by the Cobalamin-Dependent Radical S-Adenosylmethionine Methylase TsrM Requires an Unmodified N1 Amine. *Journal of Biological Chemistry* **2017**, *292* (37), 15456–15467. https://doi.org/10.1074/jbc.M117.778548.

(224) Bridwell-Rabb, J.; Li, B.; Drennan, C. L. Cobalamin-Dependent Radical *S* -Adenosylmethionine Enzymes: Capitalizing on Old Motifs for New Functions. *ACS Bio & Med Chem Au* **2022**, acsbiomedchemau.1c00051. https://doi.org/10.1021/acsbiomedchemau.1c00051.

(225) Zhang, Q.; van der Donk, W. A.; Liu, W. Radical-Mediated Enzymatic Methylation: A Tale of Two SAMS. *Accounts of Chemical Research* **2012**, *45* (4), 555–564. https://doi.org/10.1021/ar200202c.

(226) Allen, K. D.; Xu, H.; White, R. H. Identification of a Unique Radical *S* -Adenosylmethionine Methylase Likely Involved in Methanopterin Biosynthesis in Methanocaldococcus Jannaschii. *Journal of Bacteriology* **2014**, *196* (18), 3315–3323. https://doi.org/10.1128/JB.01903-14.

(227) Deobald, D.; Adrian, L.; Schöne, C.; Rother, M.; Layer, G. Identification of a Unique Radical SAM Methyltransferase Required for the Sp3-C-Methylation of an Arginine Residue of Methyl-Coenzyme M Reductase. *Scientific Reports* **2018**, *8* (1), 7404. https://doi.org/10.1038/s41598-018-25716-x.

(228) Rivas, M.; Becerra, A.; Peretó, J.; Bada, J. L.; Lazcano, A. Metalloproteins and the Pyrite-Based Origin of Life: A Critical Assessment. *Origins of Life and Evolution of Biospheres* **2011**, *41* (4), 347–356. https://doi.org/10.1007/s11084-011-9238-1.

(229) Beinert, H. Iron-Sulfur Proteins: Ancient Structures, Still Full of Surprises. *JBIC Journal of Biological Inorganic Chemistry* **2000**, *5* (1), 2–15. https://doi.org/10.1007/s007750050002.

(230) Beinert, H.; Holm, R. H.; Münck, E. Iron-Sulfur Clusters: Nature's Modular, Multipurpose Structures. *Science (1979)* **1997**, *277* (5326), 653–659. https://doi.org/10.1126/science.277.5326.653.

(231) Johnson, D. C.; Dean, D. R.; Smith, A. D.; Johnson, M. K. STRUCTURE, FUNCTION, AND FORMATION OF BIOLOGICAL IRON-SULFUR CLUSTERS. *Annual Review of Biochemistry* **2005**, *74* (1), 247–281. https://doi.org/10.1146/annurev.biochem.74.082803.133518.

(232) Frazzon, J. Formation of Iron–Sulfur Clusters in Bacteria: An Emerging Field in Bioinorganic Chemistry. *Current Opinion in Chemical Biology* **2003**, *7* (2), 166–173. https://doi.org/10.1016/S1367-5931(03)00021-8.

(233) Hagen, K. S.; Reynolds, J. G.; Holm, R. H. Definition of Reaction Sequences Resulting in Self-Assembly of [Fe4S4(SR)4]2- Clusters from Simple Reactants. *J Am Chem Soc* **1981**, *103* (14), 4054–4063. https://doi.org/10.1021/ja00404a013.

(234) Hagen, K. S.; Watson, A. D.; Holm, R. H. Synthetic Routes to Iron Sulfide (Fe2S2, Fe3S4, Fe4S4, and Fe6S9), Clusters from the Common Precursor Tetrakis(Ethanethiolate)Ferrate(2-) Ion ([Fe(SC2H5)4]2-): Structures and Properties of [Fe3S4(SR)4]3- and Bis(Ethanethiolate)Nonathioxohexaferrate(4-) Ion

([Fe6S9(SC2H5)2]4-), Examples of the Newest Types of Fe-S-SR Clusters. *J Am Chem Soc* **1983**, *105* (12), 3905–3913. https://doi.org/10.1021/ja00350a028.

(235) Spiro, T. G. Iron-Sulfur Proteins. *Wiley-Interscience* **1982**, 1–66.

(236) Harrop, T. C.; Tonzetich, Z. J.; Reisner, E.; Lippard, S. J. Reactions of Synthetic [2Fe-2S] and [4Fe-4S] Clusters with Nitric Oxide and Nitrosothiols. *J Am Chem Soc* **2008**, *130* (46), 15602–15610. https://doi.org/10.1021/ja8054996.

(237) Hagen, K. S.; Reynolds, J. G.; Holm, R. H. Definition of Reaction Sequences Resulting in Self-Assembly of [Fe4S4(SR)4]2- Clusters from Simple Reactants. *J Am Chem Soc* **1981**, *103* (14), 4054–4063. https://doi.org/10.1021/ja00404a013.

(238) Grimshaw, J. Electrochemistry of the Sulphonium Group. In *The Sulfonium Group: Vol. 1 (1981)*; John Wiley & Sons, Ltd.: Chichester, UK; pp 141–155. https://doi.org/10.1002/9780470771648.ch7.

(239) Hinckley, G. T.; Frey, P. A. Cofactor Dependence of Reduction Potentials for [4Fe-4S] $^{2+/1+}$ in Lysine 2,3-Aminomutase. *Biochemistry* **2006**, *45* (10), 3219–3225. https://doi.org/10.1021/bi0519497.

(240) Wang, S. C.; Frey, P. A. Binding Energy in the One-Electron Reductive Cleavage of *S* -Adenosylmethionine in Lysine 2,3-Aminomutase, a Radical SAM Enzyme. *Biochemistry* **2007**, *46* (45), 12889–12895. https://doi.org/10.1021/bi701745h.

(241) Dey, A.; Peng, Y.; Broderick, W. E.; Hedman, B.; Hodgson, K. O.; Broderick, J. B.; Solomon, E. I. S K-Edge XAS and DFT Calculations on SAM Dependent Pyruvate Formate-Lyase Activating Enzyme: Nature of Interaction between the Fe_4S_4 Cluster and SAM and Its Role in Reactivity. *J Am Chem Soc* **2011**, *133* (46), 18656–18662. https://doi.org/10.1021/ja203780t.

(242) Sweeney, W. v.; Rabinowitz, J. C. Proteins Containing 4Fe-4S Clusters: An Overview. *Annual Review of Biochemistry* **1980**, *49* (1), 139–161. https://doi.org/10.1146/annurev.bi.49.070180.001035.

(243) Hearshen, D.; Hagen, W.; Sands, R.; Grande, H.; Crespi, H.; Gunsalus, I.; Dunham, W. An Analysis of g Strainin the EPR of Two [2Fe-2S] Ferredoxins. Evidence for a Protein Rigidity Model. *Journal of Magnetic Resonance* **1986**, *69*, 440–459.

(244) Fluck, E. Mößbauer-Spektroskopie: Mössbauer Spectroscopy and Transition Metal Chemistry (Inorganic Chemistry Concepts 3). Von Ph. Gütlich, R. Link Und A. Trautwein. Springer Verlag, Berlin, Heidelberg, New York 1978. X, 280 S., 160 Abb., 19 Tab., Geb. DM 76,-. *Nachrichten aus Chemie, Technik und Laboratorium* **1979**, *27* (8), 509–509. https://doi.org/10.1002/nadc.19790270821.

(245) Johnson, D. C.; Dean, D. R.; Smith, A. D.; Johnson, M. K. STRUCTURE, FUNCTION, AND FORMATION OF BIOLOGICAL IRON-SULFUR CLUSTERS. *Annual Review of Biochemistry* **2005**, *74* (1), 247–281. https://doi.org/10.1146/annurev.biochem.74.082803.133518.

(246) Wandersman, C.; Delepelaire, P. BACTERIAL IRON SOURCES: From Siderophores to Hemophores. *Annu. Rev. Microbiol* **2004**, *58*, 611–658. https://doi.org/10.1146/annurev.micro.58.030603.123811.

(247) Wilks, A.; Burkhard, K. A. First Published as an Advance Article on the Web 11th. **2006**. https://doi.org/10.1039/b604193k.

(248) Wandersman, C.; Stojiljkovic, I. Bacterial Heme Sources: The Role of Heme, Hemoprotein Receptors and Hemophores. *Current Opinion in Microbiology* **2000**, *3* (2), 215–220. https://doi.org/10.1016/S1369-5274(00)00078-3.

(249) Schryvers, A. B.; Stojiljkovic, I. Iron Acquisition Systems in the Pathogenic Neisseria. *Molecular Microbiology* **1999**, *32* (6), 1117–1123. https://doi.org/10.1046/j.1365-2958.1999.01411.x.

(250) Runyen-Janecky, L. J. Role and Regulation of Heme Iron Acquisition in Gram-Negative Pathogens. *Frontiers in Cellular and Infection Microbiology* **2013**, *3*. https://doi.org/10.3389/fcimb.2013.00055.

(251) Fetherston, J. D.; Bertolino, V. J.; Perry, R. D. YbtP and YbtQ: Two ABC Transporters Required for Iron Uptake in Yersinia Pestis. *Molecular Microbiology* **1999**, *32* (2), 289–299. https://doi.org/10.1046/j.1365-2958.1999.01348.x.

(252) Brimberry, M.; Toma, M. A.; Hines, K. M.; Lanzilotta, W. N. HutW from *Vibrio Cholerae* Is an Anaerobic Heme-Degrading Enzyme with Unique Functional Properties. *Biochemistry* **2021**, *60* (9). https://doi.org/10.1021/acs.biochem.0c00950.

(253) Frey, P. A.; Booker, S. J. Radical Mechanisms of S-Adenosylmethionine-Dependent Enzymes; 2001. https://doi.org/10.1016/S0065-3233(01)58001-8.

(254) Frey, P. A.; Hegeman, A. D.; Ruzicka, F. J. The Radical SAM Superfamily. *Critical Reviews in Biochemistry and Molecular Biology* **2008**, *43* (1). https://doi.org/10.1080/10409230701829169.

(255) Quitterer, F.; List, A.; Eisenreich, W.; Bacher, A.; Groll, M. Crystal Structure of Methylornithine Synthase (PylB): Insights into the Pyrrolysine Biosynthesis. *Angewandte Chemie International Edition* **2012**, *51* (6). https://doi.org/10.1002/anie.201106765.

(256) Nicolet, Y.; Pagnier, A.; Zeppieri, L.; Martin, L.; Amara, P.; Fontecilla-Camps, J. C. Crystal Structure of HydG from *Carboxydothermus Hydrogenoformans* : A Trifunctional

[FeFe]-Hydrogenase Maturase. *ChemBioChem* **2015**, *16* (3). https://doi.org/10.1002/cbic.201402661.

(257) Boal, A. K.; Grove, T. L.; McLaughlin, M. I.; Yennawar, N. H.; Booker, S. J.; Rosenzweig, A. C. Structural Basis for Methyl Transfer by a Radical SAM Enzyme. *Science (1979)* **2011**, *332* (6033). https://doi.org/10.1126/science.1205358.

(258) Grell, T. A. J.; Kincannon, W. M.; Bruender, N. A.; Blaesi, E. J.; Krebs, C.; Bandarian, V.; Drennan, C. L. Structural and Spectroscopic Analyses of the Sporulation Killing Factor Biosynthetic Enzyme SkfB, a Bacterial AdoMet Radical Sactisynthase. *Journal of Biological Chemistry* **2018**, *293* (45). https://doi.org/10.1074/jbc.RA118.005369.

(259) Grove, T. L.; Himes, P. M.; Hwang, S.; Yumerefendi, H.; Bonanno, J. B.; Kuhlman, B.; Almo, S. C.; Bowers, A. A. Structural Insights into Thioether Bond Formation in the Biosynthesis of Sactipeptides. *J Am Chem Soc* **2017**, *139* (34). https://doi.org/10.1021/jacs.7b01283.

(260) Yuan, Y.; Zallot, R.; Grove, T. L.; Payan, D. J.; Martin-Verstraete, I.; Šepić, S.; Balamkundu, S.; Neelakandan, R.; Gadi, V. K.; Liu, C.-F.; Swairjo, M. A.; Dedon, P. C.; Almo, S. C.; Gerlt, J. A.; de Crécy-Lagard, V. Discovery of Novel Bacterial Queuine Salvage Enzymes and Pathways in Human Pathogens. *Proceedings of the National Academy of Sciences* **2019**, *116* (38). https://doi.org/10.1073/pnas.1909604116.

(261) Berkovitch, F.; Nicolet, Y.; Wan, J. T.; Jarrett, J. T.; Drennan, C. L. Crystal Structure of Biotin Synthase, an *S* -Adenosylmethionine-Dependent Radical Enzyme. *Science (1979)* **2004**, *303* (5654). https://doi.org/10.1126/science.1088493.

(262) Vey, J. L.; Yang, J.; Li, M.; Broderick, W. E.; Broderick, J. B.; Drennan, C. L. Structural Basis for Glycyl Radical Formation by Pyruvate Formate-Lyase Activating Enzyme.

Proceedings of the National Academy of Sciences **2008**, *105* (42). https://doi.org/10.1073/pnas.0806640105.

(263) Goldman, P. J.; Grove, T. L.; Sites, L. A.; McLaughlin, M. I.; Booker, S. J.; Drennan, C. L. X-Ray Structure of an AdoMet Radical Activase Reveals an Anaerobic Solution for Formylglycine Posttranslational Modification. *Proceedings of the National Academy of Sciences* **2013**, *110* (21). https://doi.org/10.1073/pnas.1302417110.

(264) Goldman, P. J.; Grove, T. L.; Booker, S. J.; Drennan, C. L. X-Ray Analysis of Butirosin Biosynthetic Enzyme BtrN Redefines Structural Motifs for AdoMet Radical Chemistry. *Proceedings of the National Academy of Sciences* **2013**, *110* (40). https://doi.org/10.1073/pnas.1312228110.

(265) Dowling, D. P.; Bruender, N. A.; Young, A. P.; McCarty, R. M.; Bandarian, V.; Drennan, C. L. Radical SAM Enzyme QueE Defines a New Minimal Core Fold and Metal-Dependent Mechanism. *Nature Chemical Biology* **2014**, *10* (2). https://doi.org/10.1038/nchembio.1426.

(266) Bruender, N. A.; Grell, T. A. J.; Dowling, D. P.; McCarty, R. M.; Drennan, C. L.; Bandarian, V. 7-Carboxy-7-Deazaguanine Synthase: A Radical *S* -Adenosyl-<scp>l</Scp> -Methionine Enzyme with Polar Tendencies. *J Am Chem Soc* **2017**, *139* (5). https://doi.org/10.1021/jacs.6b11381.

(267) Bridwell-Rabb, J.; Zhong, A.; Sun, H. G.; Drennan, C. L.; Liu, H. A B12-Dependent Radical SAM Enzyme Involved in Oxetanocin A Biosynthesis. *Nature* **2017**, *544* (7650). https://doi.org/10.1038/nature21689.

(268) Fujimori, D. G. Radical SAM-Mediated Methylation Reactions. *Current Opinion in Chemical Biology* **2013**, *17* (4). https://doi.org/10.1016/j.cbpa.2013.05.032.

(269) LaMattina, J. W.; Nix, D. B.; Lanzilotta, W. N. Radical New Paradigm for Heme Degradation in *Escherichia Coli* O157:H7. *Proceedings of the National Academy of Sciences* **2016**, *113* (43). https://doi.org/10.1073/pnas.1603209113.

(270) Mathew, L. G.; Beattie, N. R.; Pritchett, C.; Lanzilotta, W. N. New Insight into the Mechanism of Anaerobic Heme Degradation. *Biochemistry* **2019**, *58* (46). https://doi.org/10.1021/acs.biochem.9b00841.

(271) Grell, T. A. J.; Bell, B. N.; Nguyen, C.; Dowling, D. P.; Bruender, N. A.; Bandarian, V.; Drennan, C. L. Crystal Structure of AdoMet Radical Enzyme 7-carboxy-7-deazaguanine Synthase from <scp> *Escherichia Coli* </Scp> Suggests How Modifications near [4Fe–4S] Cluster Engender Flavodoxin Specificity. *Protein Science* **2019**, *28* (1), 202–215. https://doi.org/10.1002/pro.3529.

(272) Young, A. P.; Bandarian, V. Eukaryotic TYW1 Is a Radical SAM Flavoenzyme. *Biochemistry* **2021**, *60* (27), 2179–2185. https://doi.org/10.1021/acs.biochem.1c00349.

(273) Bruender, N. A.; Young, A. P.; Bandarian, V. Chemical and Biological Reduction of the Radical SAM Enzyme CPH $_4$ Synthase. *Biochemistry* **2015**, *54* (18), 2903–2910. https://doi.org/10.1021/acs.biochem.5b00210.

(274) Grell, T. A. J.; Bell, B. N.; Nguyen, C.; Dowling, D. P.; Bruender, N. A.; Bandarian, V.; Drennan, C. L. Crystal Structure of AdoMet Radical Enzyme 7-carboxy-7-deazaguanine Synthase from <scp> *Escherichia Coli* </Scp> Suggests How Modifications near [4Fe–4S] Cluster Engender Flavodoxin Specificity. *Protein Science* **2019**, *28* (1). https://doi.org/10.1002/pro.3529.

(275) Arcinas, A. J.; Maiocco, S. J.; Elliott, S. J.; Silakov, A.; Booker, S. J. Ferredoxins as Interchangeable Redox Components in Support of MiaB, a Radical S-Adenosylmethionine Methylthiotransferase. *Protein Science* **2019**, *28* (1). https://doi.org/10.1002/pro.3548.

(276) Young, A. P.; Bandarian, V. Eukaryotic TYW1 Is a Radical SAM Flavoenzyme. *Biochemistry* **2021**, *60* (27). https://doi.org/10.1021/acs.biochem.1c00349.

(277) McLean, K. J.; Luciakova, D.; Belcher, J.; Tee, K. L.; Munro, A. W. Biological Diversity of Cytochrome P450 Redox Partner Systems; 2015. https://doi.org/10.1007/978-3-319-16009-2_11.

(278) DAIBER, A.; SHOUN, H.; ULLRICH, V. Nitric Oxide Reductase (P450) From. *Journal of Inorganic Biochemistry* **2005**, *99* (1). https://doi.org/10.1016/j.jinorgbio.2004.09.018.

(279) Otto, B. R.; Verweij-van Vught, A. M. J. J.; Maclaren, D. M. Transferrins and Heme-Compounds as Iron Sources for Pathogenic Bacteria. *Critical Reviews in Microbiology* **1992**, *18* (3). https://doi.org/10.3109/10408419209114559.

(280) Torres, A. G.; Redford, P.; Welch, R. A.; Payne, S. M. TonB-Dependent Systems of Uropathogenic *Escherichia Coli* : Aerobactin and Heme Transport and TonB Are Required for Virulence in the Mouse. *Infection and Immunity* **2001**, *69* (10). https://doi.org/10.1128/IAI.69.10.6179-6185.2001.

(281) Dickey, S. W.; Cheung, G. Y. C.; Otto, M. Different Drugs for Bad Bugs: Antivirulence Strategies in the Age of Antibiotic Resistance. *Nature Reviews Drug Discovery* **2017**, *16* (7), 457–471. https://doi.org/10.1038/nrd.2017.23.

(282) Lanz, N. D.; Grove, T. L.; Gogonea, C. B.; Lee, K.-H.; Krebs, C.; Booker, S. J. RlmN and AtsB as Models for the Overproduction and Characterization of Radical SAM Proteins. https://doi.org/10.1016/B978-0-12-394291-3.00030-7.

(283) Rossi Fanelli, A.; Antonini, E.; Caputo, A. 27 (I944) 355. 15 F. BINKLEY. *Arch. Biochem. Biophys* **1957**, *30* (11), 381–412.

(284) Ascoli, F.; Rossi Fanelli, M. R.; Antonini, E. Preparation and Properties of Apohemoglobin and Reconstituted Hemoglobins. *Methods in Enzymology* **1981**, *76* (C), 72–87. https://doi.org/10.1016/0076-6879(81)76115-9.

(285) Dolphin, David. The Porphyrins V7 : Biochemistry, Part B. **1979**, 573.

(286) Ran, Y.; Liu, M.; Zhu, H.; Nygaard, T. K.; Brown, D. E.; Fabian, M.; Dooley, D. M.; Lei, B. Spectroscopic Identification of Heme Axial Ligands in HtsA That Are Involved in Heme Acquisition by *Streptococcus Pyogenes*. *Biochemistry* **2010**, *49* (13). https://doi.org/10.1021/bi901987h.

(287) Kakar, S.; Hoffman, F. G.; Storz, J. F.; Fabian, M.; Hargrove, M. S. Structure and Reactivity of Hexacoordinate Hemoglobins. *Biophysical Chemistry* **2010**, *152* (1–3). https://doi.org/10.1016/j.bpc.2010.08.008.

(288) Hofbauer, S.; Hagmüller, A.; Schaffner, I.; Mlynek, G.; Krutzler, M.; Stadlmayr, G.; Pirker, K. F.; Obinger, C.; Daims, H.; Djinović-Carugo, K.; Furtmüller, P. G. Structure and Heme-Binding Properties of HemQ (Chlorite Dismutase-like Protein) from Listeria Monocytogenes. *Archives of Biochemistry and Biophysics* **2015**, *574*, 36–48. https://doi.org/10.1016/j.abb.2015.01.010.

(289) Smith, A. D.; Wilks, A. Differential Contributions of the Outer Membrane Receptors PhuR and HasR to Heme Acquisition in Pseudomonas Aeruginosa. *Journal of Biological Chemistry* **2015**, *290* (12), 7756–7766. https://doi.org/10.1074/jbc.M114.633495.

(290) Zhang, J.; Pierick, A. ten; van Rossum, H. M.; Maleki Seifar, R.; Ras, C.; Daran, J.-M.; Heijnen, J. J.; Aljoscha Wahl, S. Determination of the Cytosolic NADPH/NADP Ratio in

Saccharomyces Cerevisiae Using Shikimate Dehydrogenase as Sensor Reaction. *Scientific Reports* **2015**, *5* (1), 12846. https://doi.org/10.1038/srep12846.

(291) Goldbeck, O.; Eck, A. W.; Seibold, G. M. Real Time Monitoring of NADPH Concentrations in Corynebacterium Glutamicum and Escherichia Coli via the Genetically Encoded Sensor MBFP. *Frontiers in Microbiology* **2018**, *9*. https://doi.org/10.3389/fmicb.2018.02564.

(292) Rose, M. Y.; Olson, J. S. The Kinetic Mechanism of Heme Binding to Human Apohemoglobin. *Journal of Biological Chemistry* **1983**, *258* (7). https://doi.org/10.1016/S0021-9258(18)32622-X.

(293) Brown, W. D.; Snyder, H. E. Nonenzymatic Reduction and Oxidation of Myoglobin and Hemoglobin by Nicotinamide Adenine Dinucleotides and Flavins. *Journal of Biological Chemistry* **1969**, *244* (24). https://doi.org/10.1016/S0021-9258(18)63463-5.

(294) Zhang, L.; Kudo, T.; Takaya, N.; Shoun, H. The B′ Helix Determines Cytochrome P450nor Specificity for the Electron Donors NADH and NADPH. *Journal of Biological Chemistry* **2002**, *277* (37), 33842–33847. https://doi.org/10.1074/jbc.M203923200.

(295) Sekine, Y.; Tanzawa, T.; Tanaka, Y.; Ishimori, K.; Uchida, T. Cytoplasmic Heme-Binding Protein (HutX) from *Vibrio Cholerae* Is an Intracellular Heme Transport Protein for the Heme-Degrading Enzyme, HutZ. *Biochemistry* **2016**, *55* (6), 884–893. https://doi.org/10.1021/acs.biochem.5b01273.

(296) Wardman, P.; Candeias, L. P. Fenton Chemistry: An Introduction. *Radiat Res* **1996**, *145* (5), 523–531.

(297) Ray, P. D.; Huang, B.-W.; Tsuji, Y. Reactive Oxygen Species (ROS) Homeostasis and Redox Regulation in Cellular Signaling. *Cellular Signalling* **2012**, *24* (5), 981–990. https://doi.org/10.1016/j.cellsig.2012.01.008.

(298) Suits, M. D. L.; Lang, J.; Pal, G. P.; Couture, M.; Jia, Z. Structure and Heme Binding Properties of *Escherichia Coli* O157:H7 ChuX. *Protein Science* **2009**, NA-NA. https://doi.org/10.1002/pro.84.

(299) Su, T.; Chi, K.; Wang, K.; Guo, L.; Huang, Y. Expression, Purification and Preliminary Crystallographic Analysis of a Haem-Utilizing Protein, HutX, from *Vibrio Cholerae*. *Acta Crystallographica Section F Structural Biology Communications* **2015**, *71* (2), 141–144. https://doi.org/10.1107/S2053230X14027666.

(300) Rivera, M. Bacterioferritin: Structure Function and Protein–Protein Interactions; 2013; pp 135–178. https://doi.org/10.1142/9789814407755_0041.

(301) Andrews, S. C. The Ferritin-like Superfamily: Evolution of the Biological Iron Storeman from a Rubrerythrin-like Ancestor. *Biochimica et Biophysica Acta (BBA) - General Subjects* **2010**, *1800* (8), 691–705. https://doi.org/10.1016/j.bbagen.2010.05.010.

(302) Mouriño, S.; Giardina, B. J.; Reyes-Caballero, H.; Wilks, A. Metabolite-Driven Regulation of Heme Uptake by the Biliverdin IXβ/δ-Selective Heme Oxygenase (HemO) of Pseudomonas Aeruginosa. *Journal of Biological Chemistry* **2016**, *291* (39), 20503–20515. https://doi.org/10.1074/jbc.M116.728527.

(303) Dent, A. T.; Mouriño, S.; Huang, W.; Wilks, A. Post-Transcriptional Regulation of the Pseudomonas Aeruginosa Heme Assimilation System (Has) Fine-Tunes Extracellular

Heme Sensing. *Journal of Biological Chemistry* **2019**, *294* (8), 2771–5555. https://doi.org/10.1074/jbc.RA118.006185.

(304) Nelson, C. E.; Huang, W.; Brewer, L. K.; Nguyen, A. T.; Kane, M. A.; Wilks, A.; Oglesby-Sherrouse, A. G. Proteomic Analysis of the Pseudomonas Aeruginosa Iron Starvation Response Reveals PrrF Small Regulatory RNA-Dependent Iron Regulation of Twitching Motility, Amino Acid Metabolism, and Zinc Homeostasis Proteins. *Journal of Bacteriology* **2019**, *201* (12). https://doi.org/10.1128/JB.00754-18.

(305) Lamousé-Smith, E.; Kelly, D.; de Cremoux, I. Designing Bugs as Drugs: Exploiting the Gut Microbiome. *Am J Physiol Gastrointest Liver Physiol* **2021**, *320* (3), G295–G303. https://doi.org/10.1152/ajpgi.00381.2019.

(306) Chiu, L.; Bazin, T.; Truchetet, M.-E.; Schaeverbeke, T.; Delhaes, L.; Pradeu, T. Protective Microbiota: From Localized to Long-Reaching Co-Immunity. *Front Immunol* **2017**, *8*, 1678. https://doi.org/10.3389/fimmu.2017.01678.

(307) Shanahan, F. Gut Microbes: From Bugs to Drugs. *Am J Gastroenterol* **2010**, *105* (2), 275–279. https://doi.org/10.1038/ajg.2009.729.

(308) Hornef, M. Pathogens, Commensal Symbionts, and Pathobionts: Discovery and Functional Effects on the Host. *ILAR J* **2015**, *56* (2), 159–162. https://doi.org/10.1093/ilar/ilv007.

(309) Venema, K.; van den Abbeele, P. Experimental Models of the Gut Microbiome. *Best Practice & Research Clinical Gastroenterology* **2013**, *27* (1), 115–126. https://doi.org/10.1016/j.bpg.2013.03.002.

(310) Kumar, M.; Ji, B.; Zengler, K.; Nielsen, J. Modelling Approaches for Studying the Microbiome. *Nature Microbiology* **2019**, *4* (8), 1253–1267. https://doi.org/10.1038/s41564-019-0491-9.

Figure 1.1 Iron acquisition strategies at the host-pathogen interface.

Labile iron is sequestered from pathogens by iron trafficking and storage proteins including transferrin and lactoferrin. Invading bacteria have evolved both Fe^{3+} and Fe^{2+} iron uptake systems to acquire iron during infection. Heme bound iron is stored and utilized by haptoglobin and hemoglobin respectively. However, bacteria have evolved strategies to sense and procure heme and degrade it as a source of iron.

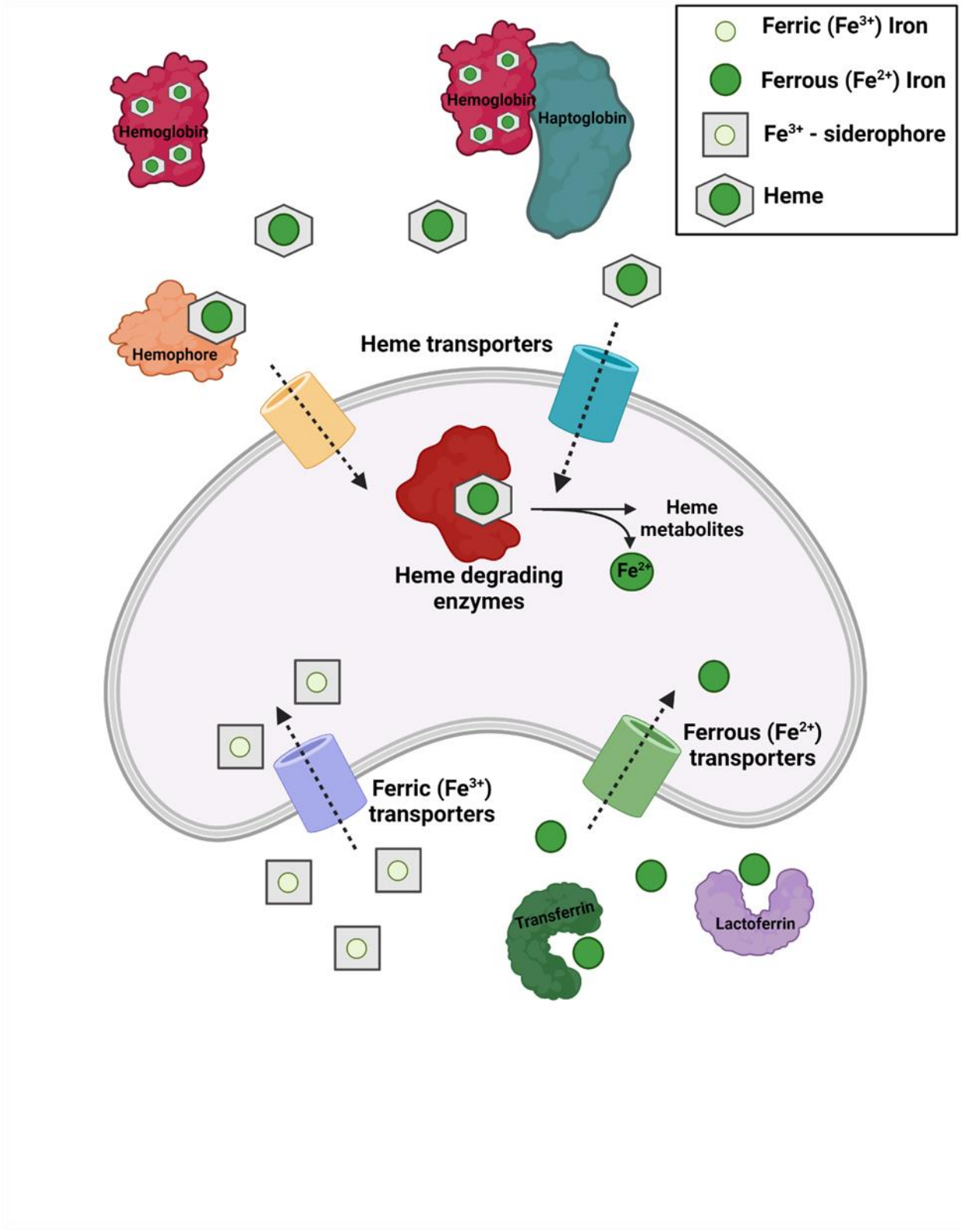
Ferric (Fe^{3+}) Iron
Ferrous (Fe^{2+}) Iron
Fe^{3+} - siderophore
Heme
Hemoglobin
Hemoglobin
Haptoglobin
Hemophore
Heme transporters
Heme metabolites
Fe^{2+}
Heme degrading enzymes
Ferrous (Fe^{2+}) transporters
Ferric (Fe^{3+}) transporters
Transferrin
Lactoferrin

Figure 1.2 Siderophore mediated uptake in Gram-negative bacteria.

Fe^{3+} siderophores are actively taken up across the outer membrane (OM) into the periplasm by the TonB/ExBD-dependent OM receptors. Siderophores are transported across the cytoplasmic membrane (CM) via ABC transporters where reductases release Fe^{2+} for utilization.

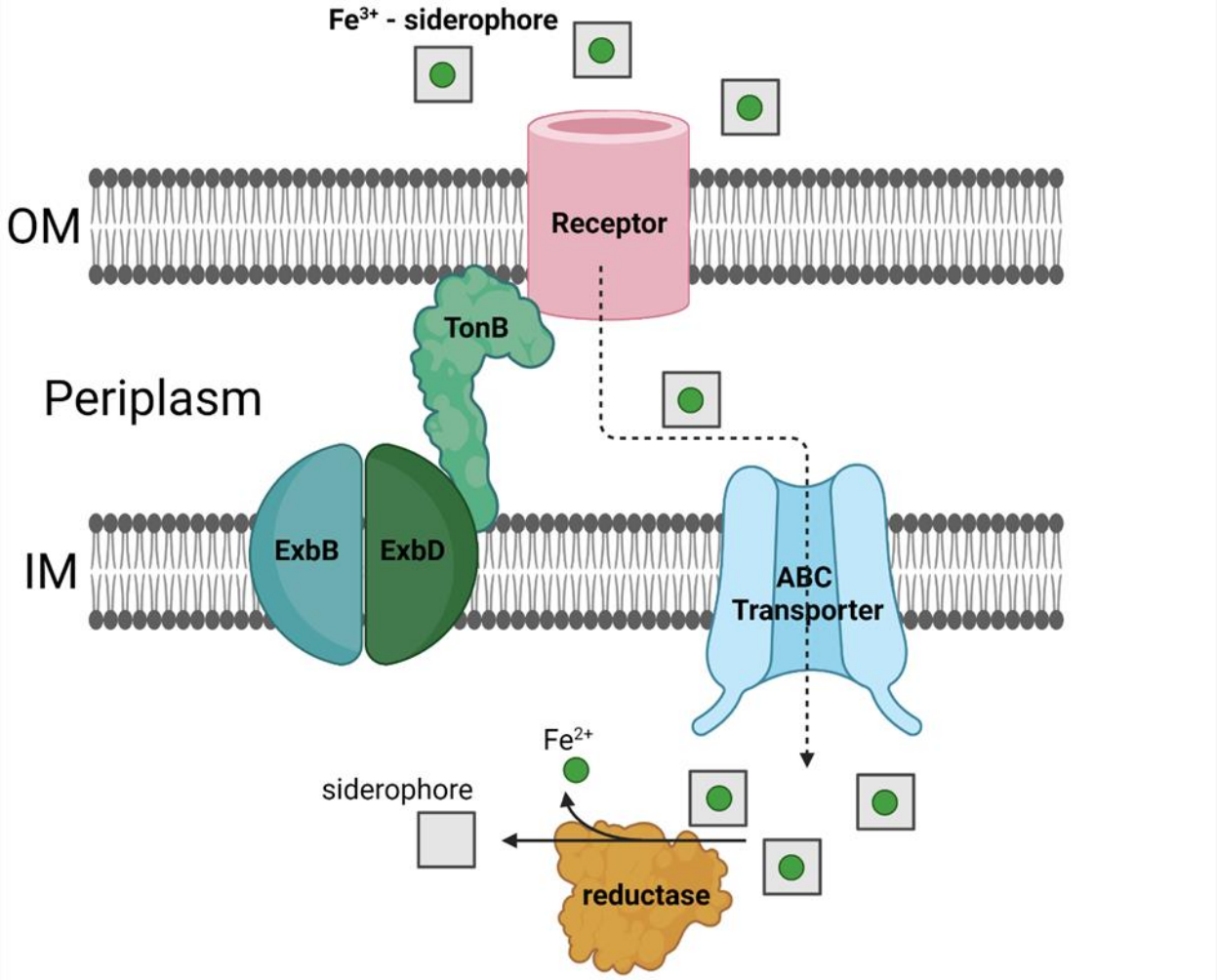
Fe3+ - siderophore
OM
Receptor
TonB
Periplasm
IM
ExbB
ExbD
ABC
Transporter
Fe2+
siderophore
reductase

Figure 1.3 Heme uptake in *Vibrio cholerae*

Heme is taken up by three non-redundant heme uptake systems, the HutA, HutR, and HasR. The HutA system takes up heme as well as heme from hemoglobin. HasR is a hemophore receptor system shown to take up free heme. There is no known hemophore in *V. cholerae,* but the receptor has homology with hemophore recetpros in *Pseudomonas aeruginosa* and *Serratia marcescens.* All three receptors are TonB depencent. Following internalization through one of these three receptors, heme is bound to the inner membrane permease, HutB, which delivers heme to the inner membrane permease, HutC/HutD. In the cytosol, it has been shown that HutX binds heme; however, its role in delivering heme to either aerobic heme degrading enzyme, HutZ or anaerobic heme degrading enzyme, HutW, is unclear. HutZ degrades heme under oxygenic conditions to β/δ biliverdin with concurrent release of CO and Fe^{2+}. Under anaerobic conditions, HutW, a radical *S*-adenosylmethionine (SAM) enzyme uses two molecules of the cofactor SAM through a radical-based mechanism to open the heme porphyrin ring with release of iron. Moreover, it has been shown that HutW is able to use NADPH to reduce the RS catalytic [4Fe-4S] cluster and product.

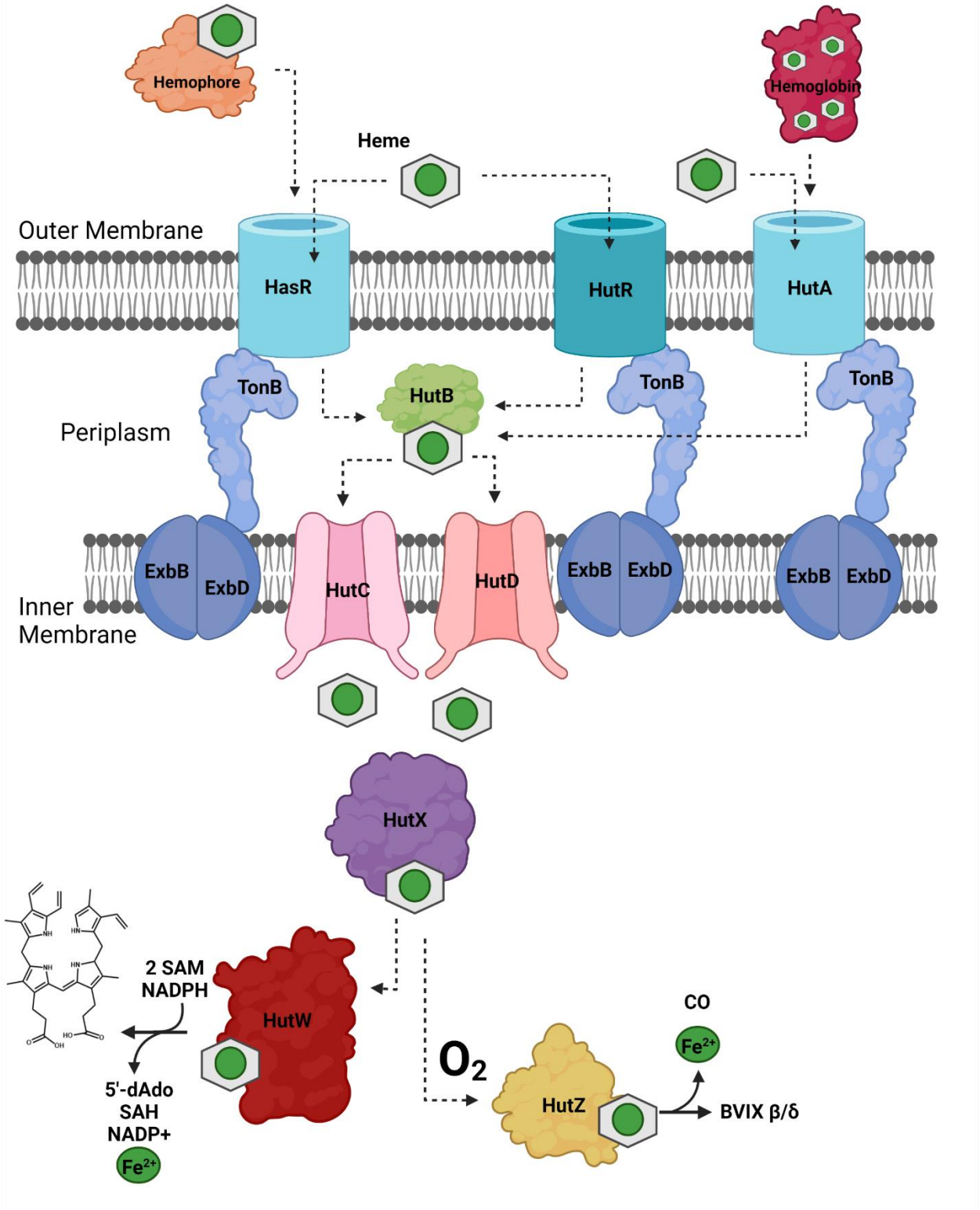
Hemophore
Hemoglobin
Heme
Outer Membrane
HasR
HutR
HutA
TonB
HutB
TonB
TonB
Periplasm
ExbB
ExbD
HutC
HutD
ExbB
ExbD
ExbB
ExbD
Inner Membrane
HutX
2 SAM
NADPH
HutW
5'-dAdo
SAH
NADP+
Fe2+
O2
CO
Fe2+
HutZ
BVIX β/δ

Figure 1.3 Heme metabolites for canonical and non-canonical heme degradation

Canonical heme degradation metabolites in green produce either BVIXα (HOs) or BVIXβ/δ (HemO). Non-canonical heme degradation products in blue (staphylobilins) or purple (mycobilins) catalyzed via ISdG/I or MhuD, respectively. The product of anaerobic heme degradation by ChuW (anaerobilin) and HutW is shown in brown.

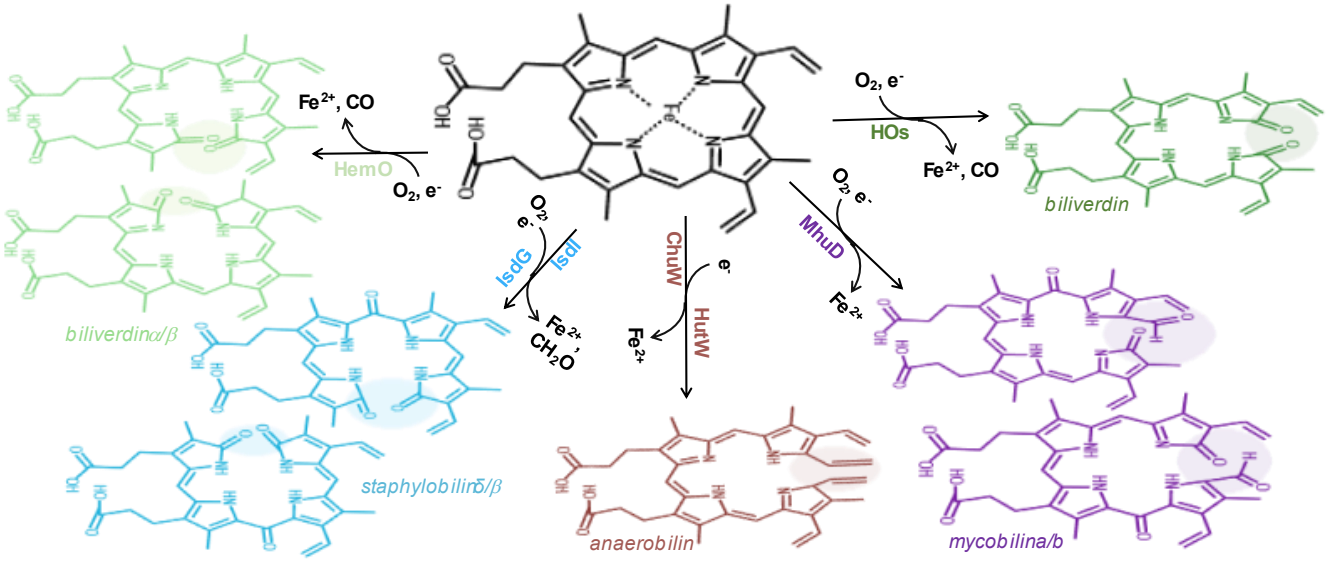
Fe2+, CO
HemO
O2, e-
O2, e-
HOs
Fe2+, CO
biliverdin
biliverdinα/β
IsdG
IsdI
O2, e-
Fe2+, CH2O
ChuW
HutW
e-
Fe2+
MhuD
O2, e-
Fe2+
staphylobilinδ/β
anaerobilin
mycobilina/b

Figure 1.4 Proposed mechanism for non-canonical heme degradation

Overview of proposed mechanism for IsdG/I and formation of staphylobilin and MhuD non-canonical heme degradation to mycobilin-a/mycobilin-b.

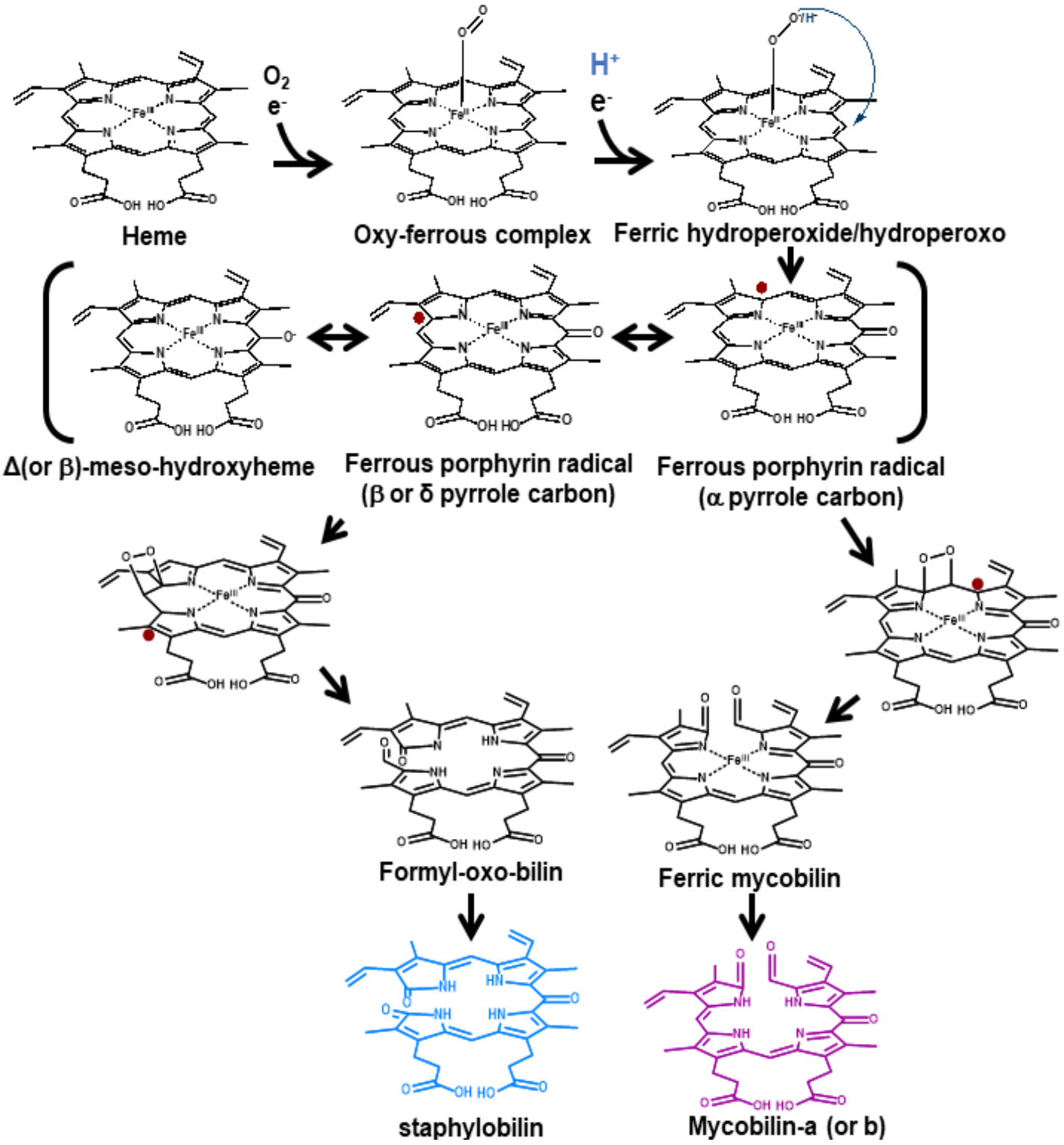
O2
e-
H+
e-
Heme
Oxy-ferrous complex
Ferric hydroperoxide/hydroperoxo
Δ(or β)-meso-hydroxyheme
Ferrous porphyrin radical
(β or δ pyrrole carbon)
Ferrous porphyrin radical
(α pyrrole carbon)
Formyl-oxo-bilin
Ferric mycobilin
staphylobilin
Mycobilin-a (or b)

Figure 1.5 Formation of the Ω species

Pathways for liberating 5’-dAdo• for H atom abstraction through formation of catalytically competent Ω upon SAM cleavage. Ω may be formed via reductive SAM cleavage then recombination of the 5′-dAdo· with the [4Fe-4S] cluster (pathway 1) or directly (pathway 2) via concerted reductive cleavage/Fe-C bond formation or nucleophilic attack of the unique iron on the 5’ carbon.

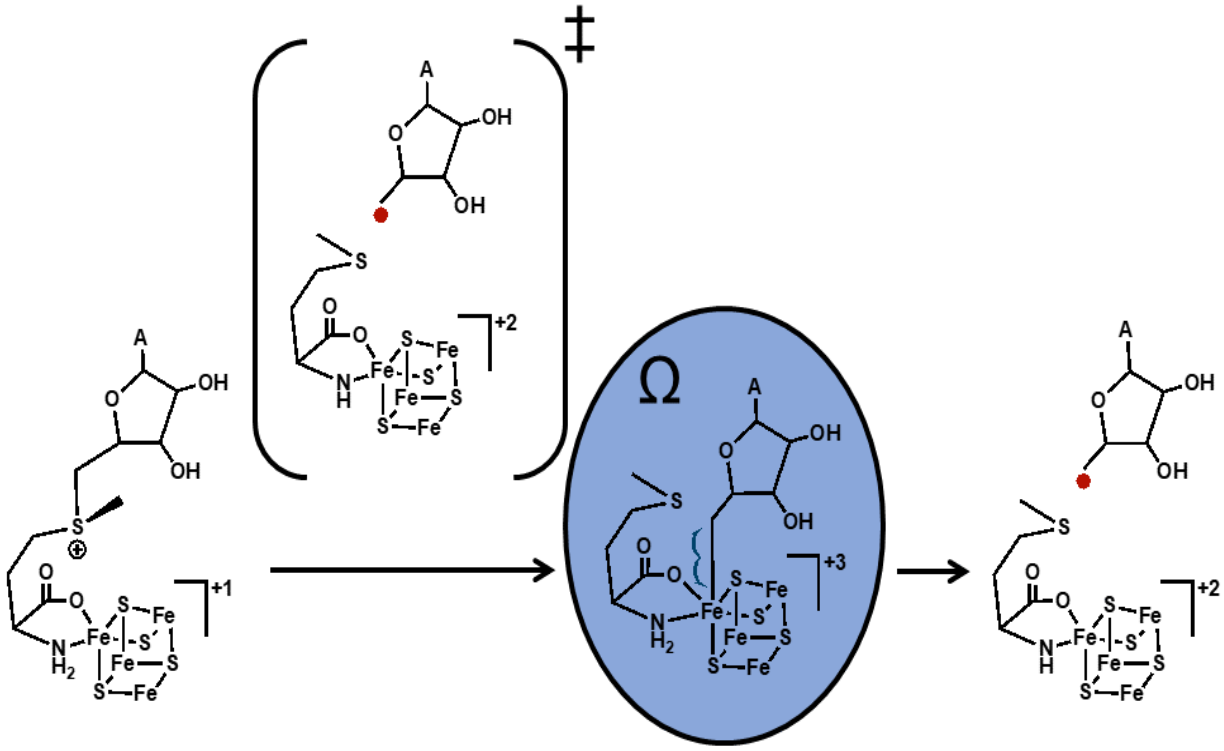
‡
Ω
A
OH
O
S
Fe
N
H
+1
+2
+3

Figure 1.6 Radical *S*-adenosylmethionine methyltransferase classes

Radical *S*-adenosylmethionine methylases are grouped into four classes based on protein architecture, cofactor requirement, and predicted mechanism of catalysis. Class A methylases use two cysteine residues to methylate sp^2 -hybridized carbon centers. Class B methylases require a cobalamin cofactor to methylate both sp^2 -hybridized and sp^3-hybridized carbon centers as well as phosphinate phosphorous atoms. Class C methylases bind two molecules of SAM to methylate sp^2-hybridized carbon centers. Class D methylases use methylenetetrahydrofolate as the source of the methyl group added to sp^2-hybridized carbon centers.

Class A	Class B	Class C	Class D
Radical SAM	Radical SAM + Cobalamin Binding Domain	Radical SAM + HemN Domain	Radical SAM + Folate Binding Domain
Cofactor	**Cofactor**	**Cofactor**	**Cofactor**
	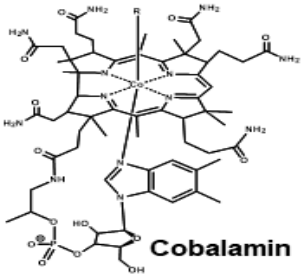 Cobalamin	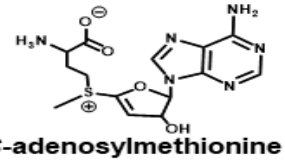 *S*-adenosylmethionine	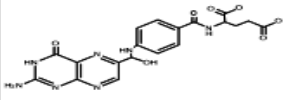 Folate
Example Enzyme(s)	**Example Enzyme(s)**	**Example Enzyme(s)**	**Example Enzyme(s)**
RlmN Cfr	PhpK Fom3 OxsB TsrM TokK	HemN ChuW/HutW NosN/NocN YktT	MJ0619
RNA Modification	***sp²* and *sp³* Centers**	***sp²* Carbon Center**	**Methanopterin Modification**
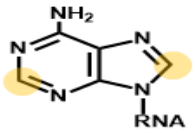	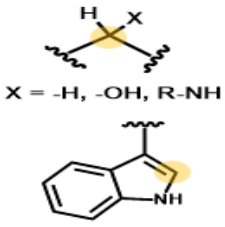 X = -H, -OH, R-NH	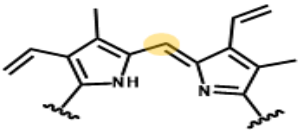	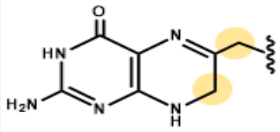
Unclassified	**Cofactor**	**Example Enzyme(s)**	**MCR Methylation**
	Unknown	MA4551	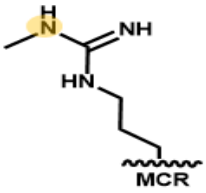 MCR

CHAPTER TWO

MAKING AND BREAKING CARBON-CARBON BONDS IN CLASS C RADICAL SAM METHYLTRANSFERSES[1]

[1]Brimberry, Marley A., Mathew, Liju, Lanzilotta, William. 2022. *J. Inorg. Biochem.*226:111636.

Accepted by The Journal of Inorganic Biochemistry. Reprinted here with permission from the publisher.

Abstract

Radical S-adenosylmethionine (SAM) enzymes utilize a $[4Fe\text{-}4S]^{1+}$ cluster and S-(5′-adenosyl)-L-methionine, (SAM), to generate a highly reactive radical and catalyze what is arguably the most diverse set of chemical reactions for any known enzyme family. At the heart of radical SAM catalysis is a highly reactive 5′ -deoxyadenosyl radical intermediate (5′ -dAdo●) generated through reductive cleavage of SAM or nucleophilic attack of the unique iron of the $[4Fe\text{-}4S]^{+}$ cluster on the 5′ C atom of SAM. Spectroscopic studies reveal the 5′ -dAdo● is transiently captured in an Fe–C bond (Ω species). In the presence of substrate, homolytic scission of this metal-carbon bond regenerates the 5′ -dAdo● for catalytic hydrogen atom abstraction. While reminiscent of the adenosylcobalamin mechanism, radical SAM enzymes appear to encompass greater catalytic diversity. In this review we discuss recent developments for radical SAM enzymes involved in unique chemical rearrangements, specifically regarding class C radical SAM methyltransferases. Illuminating this class of radical SAM enzymes is especially significant as many enzymes have been shown to play critical roles in pathogenesis and the synthesis of novel antimicrobial compounds

Introduction

Arguably the most catalytically diverse enzyme superfamily found in Nature, the radical *S*-(5′-adenosyl)-L-methionine (SAM) enzymes utilize an iron-sulfur cluster (formally $[4Fe\text{-}4S]^{1+}$) and SAM to initiate radical reactions throughout all domains of life [1,2]. Due to their substrate diversity, radical SAM enzymes have limited sequence homology and initially a minimal sequence motif, focused on the cluster binding site (CX_3CX_2C), was used to identify these enzymes [1]. Early biochemical characterization had shown that reduction of the $[4Fe\text{-}4S]^{2+}$ cluster to the catalytically-active $[4Fe\text{-}4S]^{+}$ state in vitro could be accomplished by using sodium dithionite or other strong reducing agents such as titanium (III)citrate [3]. However, later work revealed that artifacts arose when dithionite is used as a reductant in some systems [4] and therefore the preferred method is to use a physiological electron donor, such as a NADPH and/or a flavodoxin reducing system [5,6]. At the center of the radical SAM mechanism is a unique Fe site within the [4Fe-4S] cluster that is chelated by the α-amino and α-carboxylate groups of SAM [7]. Reductive cleavage of SAM by the $[4Fe\text{-}4S]^{1+}$ cluster generates a 5′-deoxyadenosyl radical intermediate (5′-dAdo●) [1]. The proposed mechanism for generation of this universal radical intermediate involves electron transfer from a $[4Fe\text{-}4S]^{1+}$ cluster to the SAM sulfonium ion, promoting S-[5′-C] bond cleavage and formation of the 5′-dAdo● [1] radical intermediate [8]. Recently, using advanced spectroscopic techniques, Horitani et al. demonstrated the 5′-dAdo● will add to the $[4Fe\text{-}4S]^{2+}$ and generate an organometallic intermediate, termed "Ω" (Fig. 1), where the unique iron of the [4Fe-4S] cluster is covalently bound to 5′- dAdo through an Fe–C bond [9]. While the precise role in a universal mechanism remains unknown, this organometallic intermediate has since been identified in several radical SAM enzymes and may be common to all [10,11]. Similar to adenosylcobalamin, Ω intermediate formation safely stores the radical until homolytic scission of the Fe–C bond

regenerates the 5′-dAdo●, once substrate is properly positioned. The 5′-dAdo● then initiates catalysis through hydrogen atom abstraction from the substrate. Mechanistically speaking, this is where the common structure/function properties of radical SAM enzymes end, and the radical rearrangements become extremely diverse. In fact, radical SAM enzymes are often divided according to the type of chemistry they initiate and/or additional structural motifs they possess. At present, Radical SAM enzyme classes have expanded to include glycyl radical enzyme activating enzymes [12,13], enzymes catalyzing sulfur insertion [14–18], mutases [19,20], enzymes involved in metallocofactor biosynthesis [21], enzymes involved in complex dehydrogenation reactions [22], and methyltransfer reactions that may or may not involve additional chemical rearrangements [23]. Radical SAM methyltransferases (RSMTs) are further subdivided into four classes based upon protein architecture, cofactor/cosubstrate requirement, and predicted catalytic mechanism [23–25]. Class A methyltransferases methylate sp2-hybridized carbon centers of RNA bases using two conserved cysteine residues within the active site. Class B enzymes utilize a cobalamin cofactor to facilitate the methylation of both sp2-hybridized and sp3-hybridized centers [26]. Class C enzymes have high sequence homology with the enzyme anaerobic coproporphyrinogen III oxidase (initially named HemN, now CpdH) [27] and methylate sp2-hybridized centers but are catalytically diverse in their substrates (Fig. 2). These reactions include biosynthesis of several natural products, as well as critical steps in anaerobic metabolism [28–31]. Lastly, Class D methyltransferases use methylenetetrahydrofolate to methylate sp2-hybridized centers [23]. In this review we focus on the class C RSMTs and identify some underlying mechanistic themes running through this important class of metalloenzymes.

1.1. Anaerobic heme biosynthesis and implications for the class C RSMT mechanism

Identified as an oxygen-independent coproporphyrinogen III oxidase, CpdH is essential to anaerobic heme biosynthesis, catalyzing the oxidative decarboxylation of two propionate groups of coproporphyrinogen III to protoporphyrinogen IX [32]. CpdH was one of the first radical SAM enzymes to be characterized biochemically when the requirement for SAM precursors, L-Methionine, and ATP was recognized in cell free assays [33–36]. CpdH was also one of the first radical SAM enzymes to be structurally characterized, revealing the (βα)6 TIM barrel, a structural fold fairly conserved in the core of radical SAM enzymes.{2014 #1}Although controversial at first, a mechanistically important observation was the presence of two SAM binding sites (Fig. 3) in the crystallographic model of CpdH [37]. The first molecule of SAM (SAM1) coordinates the unique iron atom of the catalytic [4Fe-4S] cluster, as expected. As can be seen in Fig. 3 the second molecule (SAM2) binds adjacent to the first SAM molecule and interacts with several residues that were later found to be highly conserved across the class C RSMT family [38]. Mutagenesis of the amino acid residues binding SAM2 supports an essential function in catalysis [38].

Based on the crystal structure and subsequent EPR studies of reduced $[4Fe\text{-}4S]^{1+}$ CpdH interacting with SAM and substrate coproporphyrinogen III, a catalytic mechanism was proposed [38,39]. The first step of the mechanism was based on a substrate-derived signal using coproporphyrinogen III that was regio-specifically labelled (15N or 2H) and revealed an allylic radical with the majority of spin density on the β-carbon of the propionate side chain (Fig. 4, Step II) [38,39]. Layer et al. demonstrated early on that conversion of coproporphyrinogen III to protoporphyrin IX required two molecules of SAM and the intermediate porphyrin (initially termed “harderoporphyrinogen”, now mono- vinyl, monopropionyl deuteroporphyrinogen) could exit and re-enter the active site [40]. CpdH has subsequently been re-named to CpdH to more

accurately depict the function and additional changes that have been observed in our understanding of heme biosynthetic pathways [27]. This intermediate is shown in Fig. 4, step III. In order to properly position the next propionate group for catalysis, the porphyrin must rotate 90◦, relative to the previous orientation. If the monovinyl, monopropionyl deuteroporphyrinogen intermediate (Fig. 4, Step III) is not rotated, then an adduct could form (Fig. 4, Step IV). However, initially there was no evidence for this adduct and it was suggested that the second SAM molecule (SAM2) was simply repositioned along with the intermediate to facilitate a second round of reductive cleavage by the catalytic [4Fe-4S] cluster. Regardless of the precise mechanism, one thing that could be agreed upon is that following the first decarboxylation/oxidation, the products of the reductive cleavage of SAM1 must exit the active site and a new molecule of SAM, (originally thought to be SAM2) must bind to the catalytic [4Fe-4S] cluster for the next round of catalysis. However, because a rational conclusion was to think that catalysis was limited to only the SAM molecule bound to the catalytic cluster (where reductive cleavage and formation of the 5′-dAdo● occurs), the role of the second SAM remained controversial.

The controversy was eventually addressed when evidence for a mechanistic connection between all class C RSMT enzymes was revealed through a detailed investigation of CpdH by Ji et al. in 2019 [41]. These investigators provided data that directly addressed two mechanistic points. First, the work provided evidence that during turnover, SAM2 functions in a “hydrogen atom relay” and is not cleaved, supporting a significantly different role for SAM2. In the modified mechanism, a third molecule of SAM (SAM3) enters the active site along with the monovinyl, monopropionyl deuteroporphyrinogen intermediate, specifically replacing the cleavage products of SAM1 (methionine and 5′-deoxyadenosine) at the catalytic [4Fe-4S] cluster. Second, they provided evidence for an unproductive shunt by isolating and identifying the SAM2- porphyrin

adduct shown in Fig. 4 (Step IV). Turnover experiments using isotopically-labelled SAM unequivocally demonstrated that the adduct was the result a SAM1-derived 5′-dAdo● abstracting a hydrogen atom from the methyl group of SAM2 and the subsequent methylene radical adding to an improperly positioned intermediate [41]. Specifically, if the monovinyl, monopropionyl deuteroporphyrinogen intermediate had not been repositioned, the SAM2 methylene radical attacks the double bond of the vinyl group, forming the adduct.

In addition to the mechanistic connection between CpdH and the class C RSMTs, Ji et al. also advanced the CpdH mechanism by proposing a new role for SAM2 in a hydrogen atom relay. This work correctly differentiated the roles of the two SAM binding sites in the oxidative decarboxylation reaction and identified the SAM2 binding site as the site for decarboxylation of both propionates. In light of their work, it stands to reason that the CpdH active site adopts two different conformations depending on whether coproporphyrinogen III or the monovinyl,monopropionyl deuteroporphyrinogen intermediate is bound. Since proper control of the radical requires a distinct electrostatic environment, problems will arise if another molecule of SAM (SAM3) binds to the catalytic [4Fe-4S] cluster prior to intermediate reorientation. In this case, reductive cleavage of SAM3 leads to hydrogen atom relay mal- function, and covalent adduct formation (Fig. 4, IV). In this sense, the CpdH covalent adduct is an evolutionary whisper of the mechanistic role of two SAM molecules in the class C RSMTs because, as will be discussed, methylene radical formation is a mechanistic feature that differentiates these enzymes from other RSMTs. Members in this subclass are found across diverse bacterial phyla and share sequence homology with CpdH 42]. To date, the majority of enzymes [30,31,43] appear to be involved in the biosynthesis of complex secondary metabolites [29,44–47]. The following sections will discuss representative reactions of class C RSMT and the enzymes that catalyze them.

1.2. Cyclopropanation: YtkT, and Jaw5

Two radical SAM enzymes have now been identified in the cyclopropanation of natural products. YtkT was identified from a cluster of genes involved in the biosynthesis of Yatakemycin (YTM) and the enzyme C10Q is involved in the synthesis of a similar compound termed CC-1065 [44,48]. Yatakemycin is a DNA alkylating agent with broad activity against bacteria, fungal pathogens and a tumor cell line [49] (Fig. 5). Deletion of the ytkT gene resulted in accumulation of a metabolic product similar to YTM which lacked the cyclopropane ring. This indicated that YtkT was responsible for providing the methyl group essential for spirocyclopropane ring formation [44]. YtkT Purification and reconstitution under experimental conditions typical for RS enzymes (anaerobic, strong reductant, SAM, etc.) resulted in conversion of the intermediate metabolite to YTM via methylation of a sp2-hybridized carbon atom [44]. The proposed mechanism of YtkT involved an enzymatic methyl-transfer from SAM to a double bond followed by transfer of a proton from the methyl group coupled to ring closing [44]; however, research on these enzymes remains sparse. In fact, only a single paper has appeared on the mechanism of the cyclopropanation catalyzed by C10P and C10Q in CC-1065 biosynthesis [48].

Jaw5 is another enzyme that catalyzes cyclopropanation during the synthesis of the antifungal agent, jawsamycin [50]. Based on sequence similarity to CpdH, and assignment of other open reading frames in this polyketide biosynthetic pathway, Jaw5 was proposed to be responsible for the installation of the cyclopropane modification Fig. 6. Two mechanisms for Jaw5 have been presented [23,51], both require two molecules of SAM and a methylene radical intermediate. In the first mechanism, the methylene radical adds to the ene-one of the substrate, yielding a substrate radical that attacks the bridging methylene carbon of SAM to generate the cyclopropane product. An unexplained facet of this mechanism it that the radical cation of SAH will require additional

reduction at a later step. In an alternative mechanism, the reduction step occurs sooner and the methylene radical is reduced to an ylide that attacks the ene-one followed by carbanion formation and subsequence production of cyclopropane and SAH. Both of these mechanisms were reviewed by Bauerle et al. [23] but an alternative mechanism, that has not been investigated further, is the possibility that Jaw5 functions with other proteins in the operon as part of a larger protein complex during the stepwise synthesis of jawsamycin

1.3. Thiopeptide biosynthesis: TbtI and NosN/NocN

Antibiotic biosynthesis represents another natural product pathway that often requires a class C RSMT, and with the rising incidence of antibiotic resistance [52] thiopeptide antibiotics may provide a viable solution. The ribosomally synthesized and posttraslationally modified peptide (RiPP) thiopeptide, thiomuracin, was shown to be dependent upon the gene tbtI, an annotated radical SAM enzyme [43,53]. Through in vitro reconstitution and enzymatic timing, Mahanta et al. demonstrated that TbtI methylates the thiazole natural product [31,43] (Fig. 7). A more detailed investigation from this same group was one of the first investigations to address how two molecules of SAM, initially seen in the CpdH crystal structure, could be involved in the class C RSMT mechanism. Using deuterated SAM (D3 at the methyl position only), Zhang et al later demonstrated that during TbtI catalysis, the 5′-dAdo product contained a single deuterium atom, providing evidence that SAM1 generates a 5′-dAdo● that abstracts a hydrogen atom from the methyl group of SAM2 during catalysis, producing a methylene radical as an intermediate [30]. A mass increase of +2 in the TbtA hexazole core confirmed that the two deuterium atoms were

incorporated into the substrate, with further assays suggesting that the third proton was contributed from solvent [30].

Synthesis of the antibiotic thiopeptide nosiheptide (NOS), and similarly nocathiacin, involve two class C RSMTs, NosN and NocN, respectively [28,54,55]. Initial cloning, sequencing, and characterization indicated that the indolic acid side chain ring is synthesized by genes nosL and nosN [54]. Overall, the NOS biosynthetic pathway involves a complex set of posttranslational modifications to a short (13 amino acid) peptide (NosM) [28]. A homologous set of genes are involved in the biosynthesis of nocathiacin (specifically nocI, nocN, and nocK, the latter is a gene fusion and contains both NosK and NosJ homologs) [56]. Nocathiacin's core macrocycle is initiated by thiazole formation, a cyclodehydration of the thiol side chains of six cysteine residues and is catalyzed by NosF, NosG, as well as NosH. Only one cysteine (Cys8) is left intact for acylation with 3-methyl-2-indolic acid (MIA) [57].

NosL catalyzes the conversion of tryptophan to MIA [58] and has been shown to tolerate fluorinated L-tryptophan substrates [59]. Initially, Yu et al proposed that NosN transferred a methyl group onto the indole side ring followed by hydroxylation and formation of the ester linkage [60]. Because of this activity, NosN was proposed to belong to the class C radical SAM methyltransferase family, although NosN waslater shown to be multi-functional [29]. A bottleneck in understanding the NosN mechanism was the availability of substrate. A significant advance was made when it was shown that MIA or 3,4-dimethyl-2-indolic acid (DMIA) could be transferred to a substrate analog, N-acetylcysteamine (SNAC) [45]. It was also suggested that the mechanism of NosN might be different, as 5′-methylthioadenosine (MTA) formation was detected during formation of 3,4-dimethylindolic acid (DMIA)-SNAC [45]. However, a subsequent investigation using MIA-SNAC as a substrate for NosN did not detect any MTA production [29]. LaMattina et

al. also identified the 4-methylene-3-methlindolic acid-SNAC (MMIA-SNAC) intermediate and used isotopically labelled SAM to demonstrate that SAM, and not MTA, is the source of the methyl group on MMIA-SNAC. Specifically, when [methyl-2H3]-SAM was used in their assay, the MMIA-SNAC generated showed a mass shift of +2, while the 5′-dAdo produced had a mass shift of +1 [29]. These findings support the common theme among class C RSMT catalyzed reactions that a SAM- derived 5′-dAdo● abstracts the hydrogen atom from the methyl group of another molecule of SAM to generate a methylene radical that adds to a double bond on the substrate. In the case of NosN, the methylation is followed by ester linkage formation [29,57,61]. Regardless, the reported chemistry supports the utilization of two molecules of SAM, a unifying feature of all class C RSMTs. Generally speaking, the operon responsible for thiomuracin synthesis phylogenetically clusters within a group of enzymes responsible for thiazole C-methylation and Trp C-methylation, suggesting that TbtI and NosN have a more distant relationship to other CpdH-like or class C RSMT members [43].

1.4. Anaerobic heme degradation

Biochemical characterization of CpdH (Initial named HemN), coupled with the minimal sequence motif used to identify radical SAM enzymes, lead to the mis-annotation of a number of CpdH-like genes as “anaerobic coproporphyrinogen III oxidase” [62]. Since that time, three functional classes have emerged from the collection of proteins initially annotated as CpdH [62]. This includes genuine CpdH enzymes [40], heme chaperone proteins (HemW) [63], and anaerobic heme degrading enzymes (ChuW) [64]. ChuW was identified in the hemolytic pathogen *E. coli* O157:H7 [65,66] as part of a heme uptake and degradation operon. This operon is expressed when iron levels are low under the control of the ferric uptake regulator (Fur). Low iron levels induce the “Coli heme utilization” (Chu) operon and ChuW is expressed, along with the proteins ChuX

and ChuY, from a single promoter. All three genes are part of a larger heme uptake operon that is common to several enteric pathogens, including Vibrio cholerae [64,67–69]. Deletion of the entire operon, in several organisms, has been shown to impair the ability of the organism to utilize heme as the sole iron source [70–72]. Subsequent work has demonstrated that these operons contain enzymes involved in degradation of heme under both aerobic and anaerobic conditions [65]. In *E. coli* O157:H7, ChuW was shown to catalyze the anaerobic degradation of heme [64]. Similar to what has been proposed for other class C RSMTs, the reaction was proposed to proceed through formation of a methylene radical, addition of that methylene radical to a double bond followed by beta-scission of the porphyrin ring. The net result is the release of iron and production of a reactive tetrapyrrole termed "anaerobilin" [64,69]. The structure of anaerobilin is shown in Fig. 8, intermediate VI. Evidence that anaerobilin is toxic comes from characterization of a ChuY deletion strain [73]. ChuY has been shown to be an NADPH-dependent anaerobilin reductase [68]. The ability of the ChuY knockout strain to successfully infect human cells was greatly impaired [73]. This observation is consistent with the role of ChuY in reducing the reactivity of anaerobilin, similar to the function of biliverdin reductase in the aerobic catabolism of heme.

In the current mechanism proposed for ChuW, it has been shown that the iron atom is not required for catalysis [69]. This is consistent with mechanisms proposed for other class C RSMT enzymes and underscores an exceptional level of control that the peptide environment imposes on the radical species being generated. A central tenant in the mechanism of class C RSMTs is the requirement for two molecules of SAM. One SAM molecule is responsible for generation of the 5′-dAdo● that abstracts a hydrogen atom from a second SAM molecule to generate a methylene radical. For ChuW, the methylene radical adds to a double bond at the meso carbon atom of the porphyrin ring [69]. A more general theme for all class C RSMTs is that the methylene radical is

adds to a sp2-hybridized carbon center. For ChuW, and presumably HutW, protonation of the porphyrin ring facilitates a β-scission reaction and accounts for the incorporation of a single, non-exchangeable proton in the anaerobilin product [64]. Similar to Jaw5, further reduction, hydride formation and protonation may all be required to quench the radical, depending on the precise mechanism and the exact product structure [64].

Although the ChuW and HutW proteins are phylogenetically distinct [74] when their protein sequences are compared, the two proteins likely perform similar chemistry when considered in the context of their heme uptake operons. Specifically, *E. coli* O157:H7 encodes chuW, chuX, and chuY behind a single promoter [66]. Similarly, *V. cholerae*, encodes hutW, hutX, and hutZ behind a single promoter [67]. A significant curiosity has arisen regarding the function of the third gene in each of these operons (ChuY in *E. coli* and HutZ in *V. cholerae*). ChuY utilizes NADPH to reduce the ChuW turnover product. In contrast, HutZ has a notably different structure and reported function when compared to ChuY. ChuY contains a Rossman fold and distinct NADPH binding site while HutZ has a split barrel fold and no recognizable site for nucleotide binding. It stands to reason that if the "W" genes are class C RSMTs responsible for the anaerobic opening of the porphyrin ring and iron liberation, then both organisms must deal with the resulting toxic tetrapyrrole product (Fig. 8, Intermediate VI). ChuY has been shown to perform this function in *E. coli* O157:H7 [68], but there is no homologous enzyme in *V. cholerae*. This enigma was recently addressed when it was discovered that recombinantly-produced HutW could catalyze opening of the porphyrin ring as well as reduction of the tetrapyrrole product [75]. An interesting aspect of the investigation was the observation that NADPH could be used as the electron source without any intermediary electron transfer proteins such as a flavodoxin/ferredoxin or the (flavodoxin/ferredoxin):NADP+ oxidoreductase [75]. How this electron transfer occurs is unclear

but direct electron transfer from NADPH to heme has been observed. Specifically for the “class X" cytochrome P450s. These P450 enzymes, such as P450nor, were the first P450s discovered to directly utilize NADPH [76–78]. Based on this literature, electron bifurcation mechanisms, and studies focused on the transient species observed during NAD(P)H oxidation it is tempting to speculate on a new mechanism for the class C RSMT HutW (Fig. 8). The mechanism shown in Fig. 8 also addresses at least one issue that was unresolved for the proposed ChuW mechanism. Specifically, in order to open the porphyrin ring, at least two electrons and two protons are required. One electron is required for reductive cleavage of SAM (radical generation) and the other for reduction of a radical intermediate on the tetrapyrrole. Given that the substrate heme most likely contains a ferrous iron atom in vivo, it was convenient to suggest that one electron could come from the ferrous heme. It has since been demonstrated that metal-free porphyrins can be used as substrates for ChuW and HutW, thus eliminating a possible role for the metal ion in the reaction [69,75].

Despite the differences in the electron transfer mechanisms described above, there are mechanistic similarities between ChuW and HutW, an acidic residue has been proposed to donate the first proton to the tetrapyrrole intermediate in both enzymes. A second proton and electron are required to quench the radical intermediate that is generated. In this regard, the mechanism proposed for HutW (Fig. 8) addresses this issue. Specifically, a radical ion is formed following reduction of the [4Fe-4S] cluster. The reduced (formally 1+) cluster reductively cleaves SAM1 to generate a 5′-dA radical (5′-dA•) that extracts a hydrogen atom from SAM2 to generate a methylene radical. The methylene radical adds to the double bond of the porphyrin ring and protonation by the enzyme sets a radical rearrangement into motion that results in breaking of the porphyrin ring. Consistent with what has been proposed in the literature for a multistep hydride

transfer [79], a powerful one-electron oxidant, such as the radical intermediate shown in Fig. 8, will complete the multistep electron transfer process and oxidation of the first molecule of NADPH (Fig. 8, conversion of molecule V to molecule VI). Two additional hydride transfers will further reduce the tetrapyrrole as shown in Fig. 8. The product (Fig. 8, molecule 8) has been identified by mass spectroscopy and fragmentation but it is important to note that it has not been isolated in quantities that are suitable for NMR or small molecule crystallography [75].

The proposed mechanism and observations reported by Brimberry et al. raise significant questions regarding the electron transfer reaction and the specific sequence of events. In particular, does the [4Fe-4S] cluster participate in the reduction of the tetrapyrrole or do conformational changes facilitate the direct transfer of a hydride to the bridging β-and δ-carbon atoms? Evidence presented for P450nor would suggest that the latter is true [78]. In this case, an exciting proposal is one whereby conformation-dependent electron transfer pathways exist in HutW. In this case, the first electron transfer pathway involves transfer of a single electron to the [4Fe-4S]2+ cluster while the second electron transfer pathway directs electrons and a proton to the bridging β- and δ-carbon atoms of the tetrapyrrole intermediate (Fig. 8, conversion of molecule V to molecule VI).

2. Conclusions

Given the mechanistic diversity that has been reported for the class C RSMTs and the critical role that these enzymes play in the biosynthesis of novel therapeutic compounds, a complete understanding the structure/function relationships will have tremendous potential for biotechnological innovation. In addition, the unique combination of control exerted on the organic radical(s) require for catalysis, combined with what seems to be an ever-increasing repertoire of inorganic cata-lytic diversity associated with the [4Fe-4S] cluster, will also have much broader implications

References

[1] .B. Broderick, B.R. Duffus, K.S. Duschene, E.M. Shepard, Radical S- adenosylmethionine enzymes, Chem. Rev. 114 (8) (2014) 4229–4317, https://doi. org/10.1021/cr4004709. 24476342, 4002137.

[2] Heidi J. Sofia, G. Chen, Beth G. Hetzler, Jorge F. Reyes-Spindola, Nancy E. Miller, Radical SAM, a novel protein superfamily linking unreslved steps in familiar biosynthetic pathways with radical mechanisms: functional characterization using new analysis and information visualization methods, Nucleic Acids Res. 29 (5) (2001).

[3] K.D. Allen, S.C. Wang, Spectroscopic characterization and mechanistic investigation of P-methyl transfer by a radical SAM enzyme from the marine bacterium Shewanella denitrificans OS217, Biochim. Biophys. Acta 1844 (12) (2014) 2135–2144. Epub 2014/09/17.

[4] N.A. Bruender, A.P. Young, V. Bandarian, Chemical and biological reduction of the radical SAM enzyme CPH4 synthase, Biochemistry 54 (18) (2015) 2903–2910, https://doi.org/10.1021/acs.biochem.5b00210. 25933252.

[5] T.L. Grove, K.H. Lee, J. St Clair, C. Krebs, S.J. Booker, In vitro characterization of AtsB, a radical SAM formylglycine-generating enzyme that contains three [4Fe-4S] .B. Broderick, B.R. Duffus, K.S. Duschene, E.M. Shepard, Radical S- adenosylmethionine enzymes, Chem. Rev. 114 (8) (2014) 4229–4317, https://doi. org/10.1021/cr4004709. 24476342, 4002137.

[2] Heidi J. Sofia, G. Chen, Beth G. Hetzler, Jorge F. Reyes-Spindola, Nancy E. Miller, Radical SAM, a novel protein superfamily linking unreslved steps in familiar biosynthetic pathways with radical mechanisms: functional characterization using new analysis and information visualization methods, Nucleic Acids Res. 29 (5) (2001).

[3] K.D. Allen, S.C. Wang, Spectroscopic characterization and mechanistic investigation of P-methyl transfer by a radical SAM enzyme from the marine bacterium Shewanella denitrificans OS217, Biochim. Biophys. Acta 1844 (12) (2014) 2135–2144. Epub 2014/09/17.

[4] N.A. Bruender, A.P. Young, V. Bandarian, Chemical and biological reduction of the radical SAM enzyme CPH4 synthase, Biochemistry 54 (18) (2015) 2903–2910, https://doi.org/10.1021/acs.biochem.5b00210. 25933252.

[5] T.L. Grove, K.H. Lee, J. St Clair, C. Krebs, S.J. Booker, In vitro characterization of AtsB, a radical SAM formylglycine-generating enzyme that contains three [4Fe-4S]

[54] L.D. Yi Yu, Qi Zhang, Rijing Liao, Ying Ding, Haixue Pan, Evelyn Wedt-Pienkowski, Gongli Tang, Ben Shen, Wen Liu, Nosiheptide biosynthesis feature a unique indole side ring formation on the characteristic thiopeptide framework, ACS Chem. Biol. 4 (10) (2010).

[55] D.M. Bhandari, D. Fedoseyenko, T.P. Begley, Mechanistic studies on tryptophan lyase (NosL): identification of cyanide as a reaction product, J. Am. Chem. Soc. 140 (2) (2018) 542–545. Epub 2017/12/13.

[56] Y. Ding, Y. Yu, H. Pan, H. Guo, Y. Li, W. Liu, Moving posttranslational modifications forward to biosynthesize the glycosylated thiopeptide nocathiacin I in nocardia sp. ATCC202099, Mol. BioSyst. 6 (7) (2010) 1180–1185. Epub 2010/05/18.

[57] Y. Qiu, Y. Du, F. Zhang, R. Liao, S. Zhou, C. Peng, Y. Guo, W. Liu, Thiolation protein-based transfer of indolyl to a ribosomally synthesized polythiazolyl peptide intermediate during the biosynthesis of the side-ring system of nosiheptide, J. Am. Chem. Soc. 139 (50) (2017) 18186–18189. Epub 2017/12/05.

[58] Q. Zhang, Y. Li, D. Chen, Y. Yu, L. Duan, B. Shen, W. Liu, Radical-mediated enzymatic carbon chain fragmentation-recombination, Nat. Chem. Biol. 7 (3) (2011) 154–160, https://doi.org/10.1038/nchembio.512.

[59] Q. Zhang, Y. Li, D. Chen, Y. Yu, L. Duan, B. Shen, W. Liu, Radical-mediated enzymatic carbon chain fragmentation-recombination, Nat. Chem. Biol. 7 (3) (2011) 154–160, https://doi.org/10.1038/nchembio.512. 21240261, 3079562.

[60] Y. Yu, L. Duan, Q. Zhang, R. Liao, Y. Ding, H. Pan, E. Wendt-Pienkowski, G. Tang, B. Shen, W. Liu, Nosiheptide biosynthesis featuring a unique indole side ring formation on the characteristic thiopeptide framework, ACS Chem. Biol. 4 (10) (2009) 855–864. Epub 2009/08/15.

[61] Y. Qiu, Y. Du, S. Wang, S. Zhou, Y. Guo, W. Liu, Radical S-adenosylmethionine protein NosN forms the side ring system of nosiheptide by functionalizing the polythiazolyl peptide S-conjugated indolic moiety, Org. Lett. 21 (5) (2019) 1502–1505. Epub 2019/02/21.

[62] H.A. Dailey, S. Gerdes, T.A. Dailey, J.S. Burch, J.D. Phillips, Noncanonical coproporphyrin-dependent bacterial heme biosynthesis pathway that does not use protoporphyrin, Proc. Natl. Acad. Sci. U. S. A. 112 (7) (2015), https://doi.org/ 10.1073/pnas.1416285112, 2210–5, 25646457, 4343137.

[63] V. Haskamp, S. Karrie, T. Mingers, S. Barthels, F. Alberge, A. Magalon, K. Muller, E. Bill, W. Lubitz, K. Kleeberg, P. Schweyen, M. Broring, M. Jahn, D. Jahn, The radical SAM protein HemW is a heme chaperone, J. Biol. Chem. 293 (7) (2018) 2558–2572. Epub 2017/12/29.

[64] J.W. LaMattina, D.B. Nix, W.N. Lanzilotta, Radical new paradigm for heme degradation in Escherichia coli O157:H7, Proc. Natl. Acad. Sci. U. S. A. 113 (43) (2016) 12138–12143. Epub 2016/10/30.

[65] S.M. Payne, A.R. Mey, Iron uptake in Shigella and Escherichia coli, in: P. Cornelis, S. C. Andrews (Eds.), Iron Uptake and Homeostasis in Microorganisms, 2010, pp. 87–100.

[66] A.G. Torres, S.M. Payne, Haem iron-transport system in enterohaemorrhagic Escherichia coli O157:H7, Mol. Microbiol. 23 (4) (1997) 825–833. Epub 1997/02/01, 9157252.

[67] E.E. Wyckoff, M. Schmitt, A. Wilks, S.M. Payne, HutZ is required for efficient heme utilization in Vibrio cholerae, J. Bacteriol. 186 (13) (2004) 4142–4151, https://doi.org/10.1128/JB.186.13.4142-4151.2004. 15205415, 421608.

[68] J.W. LaMattina, M. Delrossi, K.G. Uy, N.D. Keul, D.B. Nix, A.R. Neelam, W. N. Lanzilotta, Anaerobic heme degradation: ChuY is an anaerobilin reductase that exhibits kinetic cooperativity, Biochemistry 56 (6) (2017) 845–855. Epub 2017/01/04.

[69] L.G. Mathew, N.R. Beattie, C. Pritchett, W.N. Lanzilotta, New insight into the mechanism of anaerobic heme degradation, Biochemistry 58 (46) (2019) 4641–4654. Epub 2019/10/28.

[70] D.A. Occhino, E.E. Wyckoff, D.P. Henderson, T.J. Wrona, S.M. Payne, Vibrio cholerae iron transport: haem transport genes are linked to one of two sets of tonB, exbB, exbD genes, Mol. Microbiol. 29 (6) (1998) 1493–1507. Epub 1998/10/22.

[71] M. Mills, S.M. Payne, Genetics and regulation of heme iron transport in Shigella dysenteriae and detection of an analogous system in Escherichia coli O157:H7, J. Bacteriol. 177 (11) (1995), 3004–9, 7768795. PMC176986.

[72] A.N. Septer, Y. Wang, E.G. Ruby, E.V. Stabb, A.K. Dunn, The haem-uptake gene cluster in Vibrio fischeri is regulated by Fur and contributes to symbiotic colonization, Environ. Microbiol. 13 (11) (2011) 2855–2864, https://doi.org/10.1111/j.1462-2920.2011.02558.x. 21883801, 4000482.

[73] H. Kim, A.K. Chaurasia, T. Kim, J. Choi, S.C. Ha, D. Kim, K.K. Kim, Structural and functional study of ChuY from Escherichia coli strain CFT073, Biochem. Biophys. Res. Commun. 482 (4) (2017) 1176–1182. Epub 2016/12/07.

[74] D. Wilkens, R. Meusinger, S. Hein, J. Simon, Sequence analysis and specificity of distinct types of menaquinone methyltransferases indicate the widespread potential of methylmenaquinone production in bacteria and archaea, Environ. Microbiol. 23 (3) (2020) 1407–1421, https://doi.org/10.1111/1462-2920.15344,
33264482.

[75] M. Brimberry, M.A. Toma, K.M. Hines, W.N. Lanzilotta, HutW from Vibrio cholerae is an anaerobic heme-degrading enzyme with unique functional properties, Biochemistry 60 (9) (2021) 699–710. Epub 2021/02/19.

[76] L. Zhang, T. Kudo, N. Takaya, H. Shoun, The B' helix determines cytochrome P450nor specificity for the electron donors NADH and NADPH, J. Biol. Chem. 277 (37) (2002) 33842–33847. Epub 2002/07/10.

[77] T. Tosha, T. Nomura, T. Nishida, N. Saeki, K. Okubayashi, R. Yamagiwa, M. Sugahara, T. Nakane, K. Yamashita, K. Hirata, G. Ueno, T. Kimura, T. Hisano, K. Muramoto, H. Sawai, H. Takeda, E. Mizohata, A. Yamashita, Y. Kanematsu, Y. Takano, E. Nango, R. Tanaka, O. Nureki, O. Shoji, Y. Ikemoto, H. Murakami, S. Owada, K. Tono, M. Yabashi, M. Yamamoto, H. Ago, S. Iwata, H. Sugimoto, Y. Shiro, M. Kubo, Capturing an initial intermediate during the P450nor enzymatic reaction using time-resolved XFEL crystallography and caged-substrate, Nat. Commun. 8 (1) (2017) 1585. Epub 2017/11/18.

[78] R. Oshima, S. Fushinobu, F. Su, L. Zhang, N. Takaya, H. Shoun, Structural evidence for direct hydride transfer from NADH to cytochrome P450nor, J. Mol. Biol. 342 (1) (2004) 207–217. Epub 2004/08/18.

[79] J. Gebicki, A. Marcinek, J. Zielonka, Transient species in the stepwise interconversion of NADH and NAD+, Acc. Chem. Res. 37 (2003) 379–386.

[80] M. Horitani, K. Shisler, W.E. Broderick, R.U. Hutcheson, K.S. Duschene, A.R. Marts, B.M. Hoffman, J.B. Broderick, Radical SAM catalysis via an organometallic intermediate with an Fe [5'-C]-deoxyadenosyl bond, Science 352 (6287) (2016), https://doi.org/10.1126/science.aaf5327, 822–5, 27174986. PMC4929858.

[81] G. Layer, J. Moser, D.W. Heinz, D. Jahn, W.D. Schubert, Crystal structure of coproporphyrinogen III oxidase reveals cofactor geometry of radical SAM enzymes, EMBO J. 22 (23) (2003) 6214–6224, https://doi.org/10.1093/emboj/cdg598.14633981, 291839.

[82] M. Yoshida, M. Ezaki, M. Hashimoto, M. Yamashita, N. Shigematsu, M. Okuhara, M. Kohsaka, K. Horikoshi, A novel antifungal antibiotic, FR-900848 I. Production, isolation, physicochemical and biological properties, J. Antibiot. 43 (7) (1990) 748–754.

Figure 2.1

Fig. 1. Formation of the 5′ -deoxyadenosyl radical in the radical SAM protein superfamily and generation of the catalytically competent methylene radical. (A) Recent work has shown that the 5′ -dAdo• is formed through an "Ω" intermediate, involving a Fe C bond formed upon reductive cleavage of SAM [80]. Specifically, Ω may be formed directly by concerted reductive cleavage and nucleophilic attack of the unique iron on the 5′-carbon, or through an intermediate where SAM is reductively cleaved followed by recombination of the 5′-dAdo• with the [4Fe-4S]2+. (B) Generation of a methylene radical in the class C RSMTs. The 5′-dAdo• generated at the catalytic [4Fe-4S] cluster abstracts a hydrogen atom from the methyl group of a second molecule of SAM bound at distinct site. In CpdH SAM2 functions as part of a hydrogen atom relay [41], while class C RSMTs have evolved to exploit a methylene radical to catalyze difficult methylation reactions.

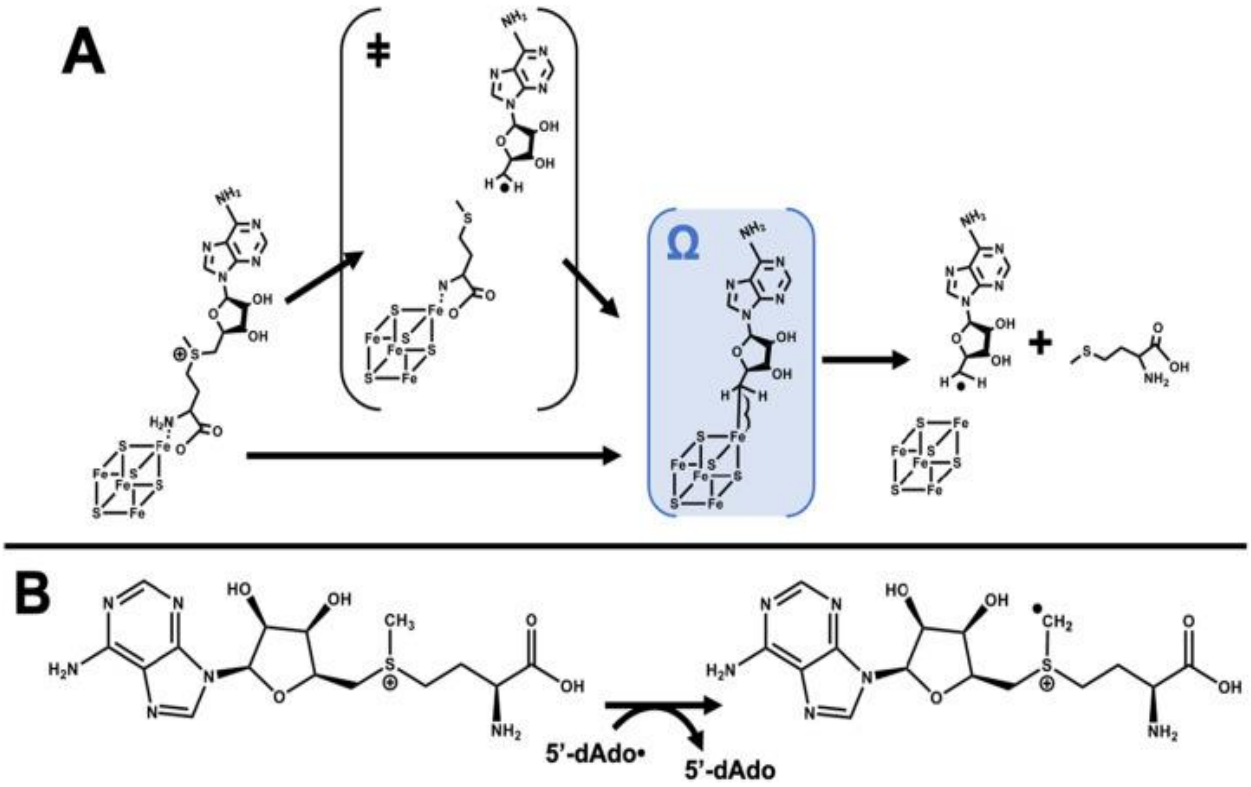
A
‡
Ω
B
5'-dAdo•
5'-dAdo

Figure 2.2

Representative class C radical SAM methyltransferases (RSMTs). Class C RSMT are differentiated, as shown in the bottom panel, by their radical SAM domain and CpdH domain. NosN/NocN, YtkT, Jaw5, and TbtI are involved in carbon-carbon bond forming reactions while ChuW/HutW and CpdH are implicated in carbon-carbon bond breaking

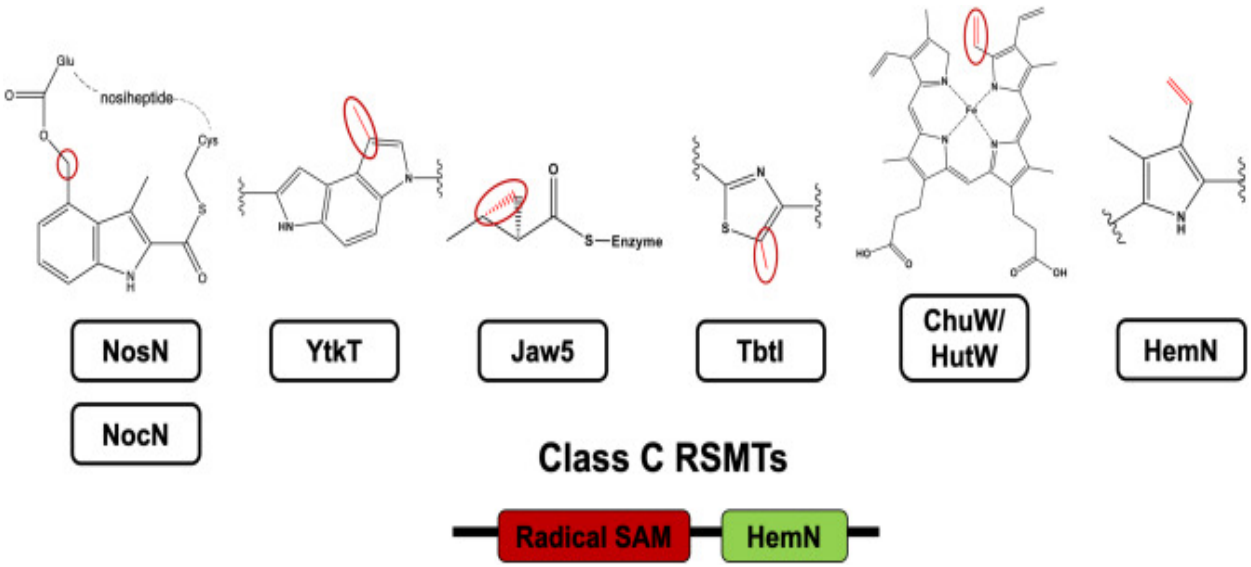
Glu
nosiheptide
Cys
S—Enzyme
NosN
NocN
YtkT
Jaw5
TbtI
ChuW/
HutW
HemN

Class C RSMTs
Radical SAM
HemN

Figure 2.3

Cartoon representation of the CpdH model (PDB ID) highlighting the relative spatial orientation of the [4Fe-4S] cluster, two SAM molecules, as well as the catalytic TIM-barrel (green) and C-terminal (magenta) domain [81]. The [4Fe-4S] cluster is shown as spheres with the cysteine ligand and both SAM molecules (SAM1 and SAM2) shown in stick format. Iron, sulfur, carbon, nitrogen, and oxygen are colored orange, cyan, tan, blue, and red, respectively. (For interpretation of the references to colour in this figure legend, the reader is referred to the web version of this article.)

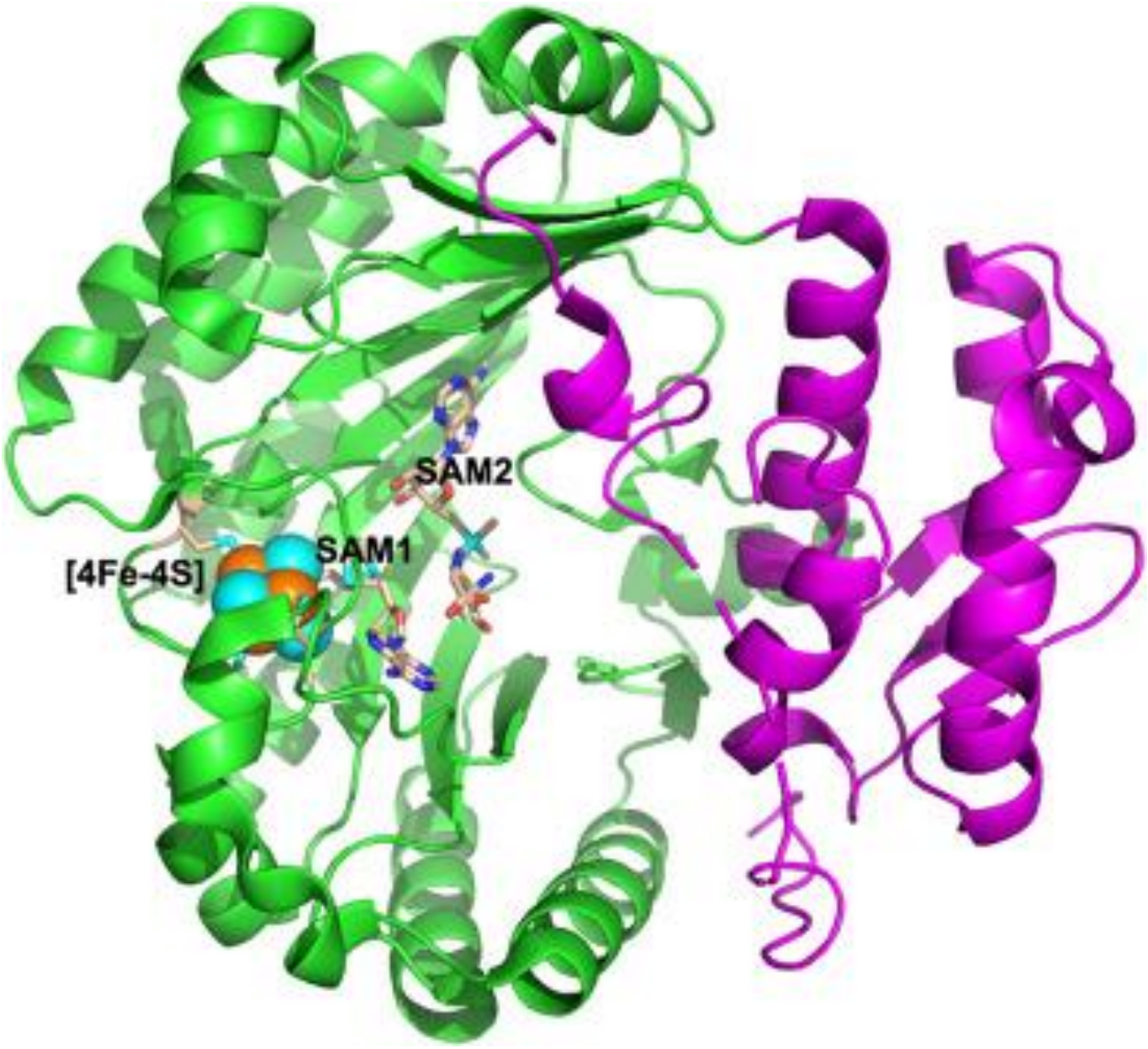
SAM2
SAM1
[4Fe-4S]

Figure 2.4

Proposed mechanism of Adduct formation in CpdH (formally termed HemN). Substrate (I) and two molecules of SAM (SAM1 and SAM2) are bound in the active site of CpdH. SAM1 coordinates the [4Fe-4S] cluster and is reductively cleaved to generate the 5′-dAdo radical (5′-dAdo•) and l-methionine. The 5′-dAdo• then abstracts a hydrogen atom from the methyl group of the SAM2 to generate a transient methylene radical. This radical is responsible for abstracting a hydrogen from the substrate to form a transient substrate radical (II) [41]. Previous investigations have shown that radical rearrangement leads to the monovinyl-tripropionic porphyrin intermediate (III) which must be re-oriented within the active site [40], a step that may involve exiting the active site altogether. If the intermediate is not reoriented then another round of radical generation will result in the covalent adduct (IV).

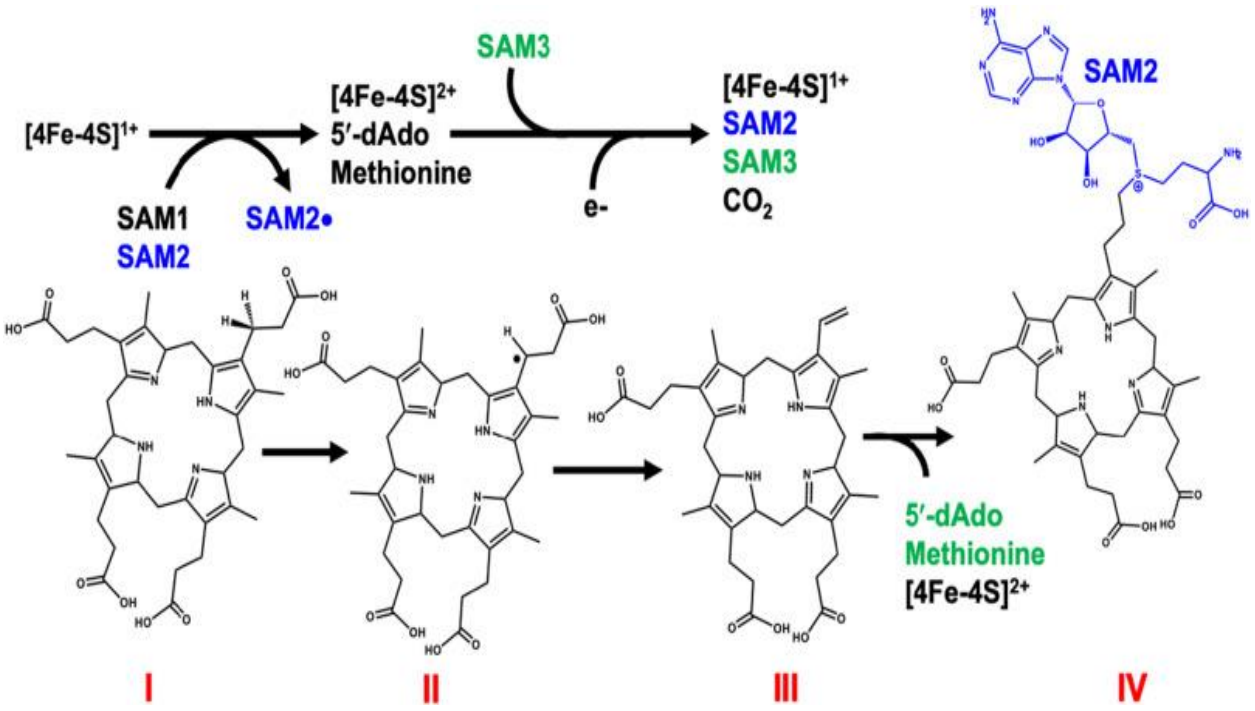
SAM3
[4Fe-4S]1+
[4Fe-4S]2+
5′-dAdo
Methionine
[4Fe-4S]1+
SAM2
SAM3
CO2
e-
SAM1
SAM2
SAM2•
SAM2
5′-dAdo
Methionine
[4Fe-4S]2+
I
II
III
IV

Figure 2.5

The general mechanism of the class C radical S-Adenosyl-L-methionine thiazole methyl transferase, YtkT. The reaction has been shown to require two molecules of SAM and the red circle highlights the methyl group that is added by YtkT. Figure adapted from [46]. Evidence for formation of a methylene radical and radical addition to a sp2 hybridized carbon center was confirmed, for the first time, through the detection of a SAM-substrate adduct [48]. .(For interpretation of the references to color in this figure legend, the reader is referred to the web version of this article.)

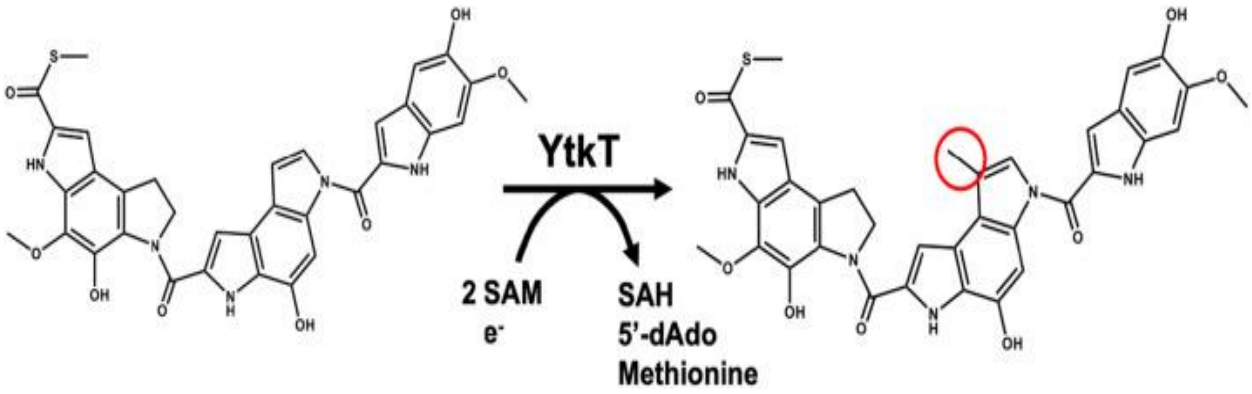
YtkT
2 SAM
e-
SAH
5'-dAdo
Methionine

Figure 2.6

General mechanism proposed for a novel class C RSMT, termed “cyclopropanase” [47], that catalyzes the addition of cyclopropyl groups in the biosynthesis of the antifungal agent jawsamycin [82]. Two mechanisms have been proposed, the first involving a methylene radical form on the second SAM molecule, which undergoes radical addition to the α,β-unsaturated polyketide chain. In a second mechanism the SAM methylene radical is transformed to its SAM ylide by acquiring an electron before adding to substrate with SAH being the leaving group during formation of the cyclopropyl moiety.

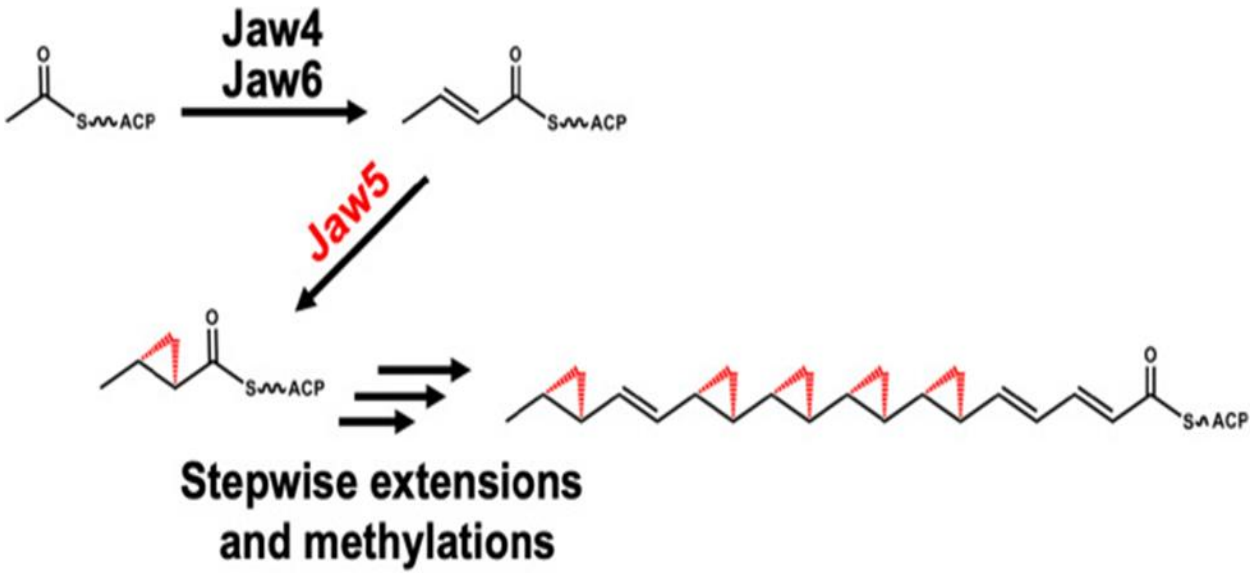
Jaw4
Jaw6
Jaw5
Stepwise extensions
and methylations

Figure 2.7

Methylation reaction catalyzed by the enzyme TbtI in the biosynthesis of thiomuracin, a ribosomally synthesized peptide antibiotic. The figure has been adapted from Zhang et al. [30] and highlights the hydrogen atom transfer events. Investigation of TbtI also produced a SAM adduct consistent with addition of a SAM-derived methylene radical to a carbon-carbon double bond.

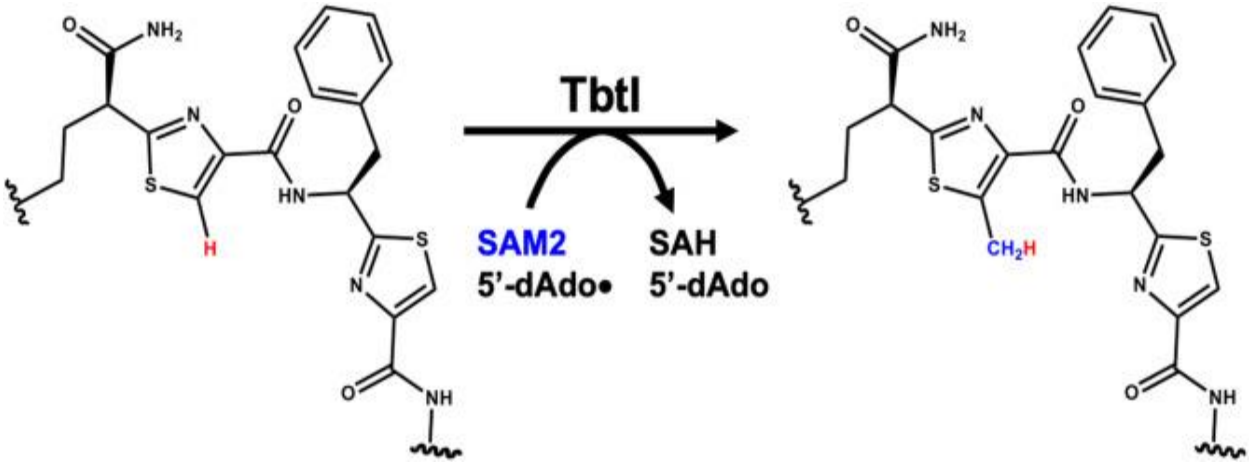
Tbtl
SAM2
5'-dAdo•
SAH
5'-dAdo

Figure 2.8

Anaerobic heme degradation mechanism proposed for the enzyme HutW in Vibrio cholera

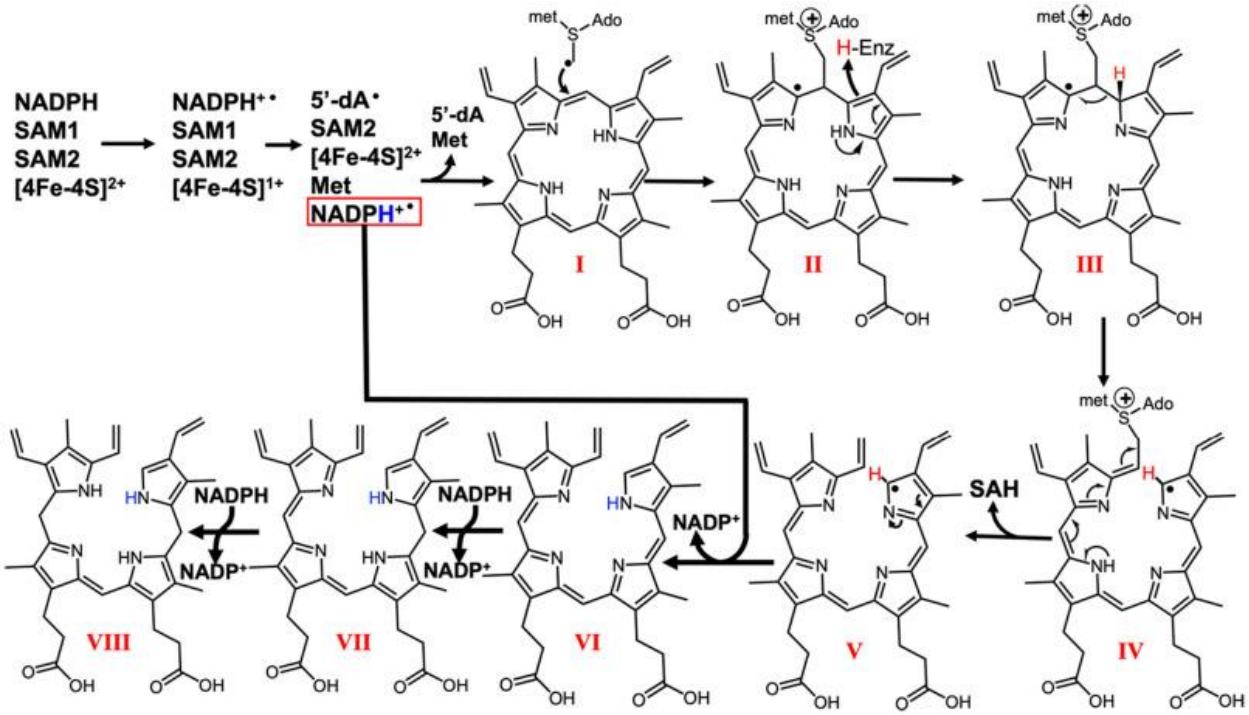
NADPH
SAM1
SAM2
[4Fe-4S]2+
NADPH+•
SAM1
SAM2
[4Fe-4S]1+
5'-dA•
SAM2
[4Fe-4S]2+
Met
NADPH+•
5'-dA
Met
met
Ado
H-Enz
I
II
III
IV
V
VI
VII
VIII
SAH
NADP+
NADPH

CHAPTER THREE

HUTW FROM VIBRIO CHOLERAE IS AN ANAEROBIC HEME-DEGRADING ENZYME WITH UNIQUE FUNCTIONAL PROPERTIES[2]

[2]Brimberry, Marley, Ana Marina Toma, Hines, Kelly M., Lanzilotta, William N. 2021.

Biochemistry. 60, 699-710.

Accepted by Biochemistry. Reprinted here with permission from the publisher.

Abstract

Increasing antibiotic resistance, and a growing recognition of the importance of the human microbiome, demand that new therapeutic targets be identified. Characterization of metabolic pathways that are unique to enteric pathogens represents a promising approach. Iron is often the rate-limiting factor for growth, and Vibrio cholerae, the causative agent of cholera, has been shown to contain numerous genes that function in the acquisition of iron from the environment. Included in this arsenal of genes are operons dedicated to obtaining iron from heme and heme-containing proteins. Given the persistence of cholera, an important outstanding question is whether V. cholerae is capable of anaerobic heme degradation as was recently reported for enterohemorrhagic Escherichia coli O157:H7. In this work, we demonstrate that HutW from V. cholerae is a radical S-adenosylmethionine methyl transferase involved in the anaerobic opening of the porphyrin ring of heme. However, in contrast to the enzyme ChuW, found in enterohemorrhagic E. coli O157:H7, there are notable differences in the mechanism and products of the HutW reaction. Of particular interest are data that demonstrate HutW will catalyze ring opening as well as tetrapyrrole reduction and can utilize reduced nicotinamide adenine dinucleotide phosphate as an electron source. The biochemical and biophysical properties of HutW are presented, and the evolutionary implications are discussed.

Introduction

Iron is a necessary micronutrient for all cellular organisms. The importance of iron for bacterial survival and pathogenesis is evident by the variety of highly conserved and broadly employed iron acquisition strategies among bacterial pathogens.[1,2] In addition to iron-siderophore scavenging mechanisms, many bacterial pathogens also contain systems for the utilization of heme as an iron source, either as free heme or from various heme-containing proteins.[3,4] Some pathogenic bacteria have been shown to encode a heme oxygenase-type enzyme that catalyzes the regiospecific conversion of heme into biliverdin IXα, CO, and free iron.[5−10] These HO-like enzymes were thought to be the only heme-degrading enzymes; however, characterization of noncanonical enzymes from Staphylococcus aureus (IsdG and IsdI) and Mycobacterium tuberculosis (MhuD) has begun to shed light on the diversity of aerobic bacterial heme-degrading systems.[11,12]

The enterohemorrhagic pathogens Escherichia coli O157:H7 and Vibrio cholerae inhabit anaerobic environments. Both have stimulated growth rates in the presence of heme or hemoglobin and can use heme as the sole iron source.[13,14] A radical S-adenosylmethionine (SAM) enzyme that liberates iron from heme under strictly anaerobic conditions in E. coli O157:H7 was recently identified and characterized.[15] The enzyme, ChuW, is expressed in a Fur-dependent manner under iron-limiting conditions along with two other proteins, ChuX and ChuY, that are downstream in the same operon. V. cholerae, the causative agent of the severe diarrheal disease cholera, also expresses proteins for the uptake and utilization of heme as an iron source.[16] Three genes that are linked to the V. cholerae operon for heme transport and in a region containing several potential binding sites for the iron regulator protein Fur, *hutWXZ*, were discovered to be required for growth on heme as the sole iron source.[13] Specifically, similar to the *chuWXY* genes of the E. coli O157:H7

serotype, the *hutWXZ* genes of V. cholerae constitute an operon divergently transcribed from the tonB1 operon initially identified in the uptake of extracellular heme.[16]

Upon comparison of the proteins of the E. coli O157:H7 (Chu) and V. cholerae (Hut) operons, several things are noteworthy. The level of sequence identity between ChuW and HutW is 39%, and they contain the catalytic [4Fe-4S] cluster binding motif common to all RS enzymes. Additional shared motifs include those for ligating two molecules of SAM, as is seen in class C radical SAM methyltransferases, and binding heme. Likewise, the sequence identity of ChuX from E. coli O157:H7 is 59% when compared to HutX. Alignment of the functional dimer from each of the crystal structures that are available for ChuX and HutX results in a root-mean-square deviation (RMSD) of 1.2 Å.[17,18] Both of these proteins have been shown to bind heme. In contrast to ChuW, HutW has not been isolated and has not been characterized biochemically. At the present time, no structure is available for ChuW or HutW.

A distinct difference is found in the third gene of these operons (*chuWXY* vs *hutWXZ*). Specifically, previous work has shown that ChuY (from enterohemorrhagic E. coli O157:H7) and HutZ (from V. cholerae) have different three dimensional structures and different functions.[19–21] However, ChuY and HutZ are found in the same relative location within their respective operons. Moreover, in both cases, gene expression is Fur-regulated and similar phenotypes are observed for the knockout strains.[13,22] Finally, it has been shown that HutZ is necessary for heme utilization as an iron source,[13] while deletion of ChuY weakens the ability of the pathogen to infect human cells.[22] The two available crystal structures for ChuY [Protein Data Bank (PDB) entries 5FFQ and 5GUY] reveal a nucleotide binding motif consistent with a NADPH-dependent reductase. In keeping with this observation, it has been shown that ChuY functions to reduce the tetrapyrrole product of ChuW.[19,22] Coupled with the recent observation that both ChuX and ChuY stimulate

the activity of ChuW,[23] a reasonable conclusion is that all three proteins function in a catabolic pathway responsible for the anaerobic degradation of heme. However, our understanding of heme degradation in V. cholerae is not clear as the function of HutW has not been addressed. In addition, we have not assessed whether similar functional synergy exists among HutW, HutX, and HutZ as has been reported for ChuW, ChuX, and ChuY.[23] Given that ChuY and HutZ have reportedly different functions and distinctly different protein structures, our hypothesis is that important functional differences exist. In the preliminary characterization of HutZ, Wyckoff *et al.* stopped short of describing HutZ as a heme oxygenase due to the lack of catalytic activity under physiologically relevant conditions.[13] In contrast, Uchida *et al*. later showed that ascorbic acid could be used to obtain spectroscopic intermediates that were similar to what had been reported for human heme oxygenase 1 (hHO-1).[21] Of significant interest was the proposal that peroxide may be a transient intermediate. Specifically, it has long been known that hydrogen peroxide (H_2O_2) can substitute for molecular oxygen (O_2) and two reducing equivalents in the HO-1 reaction[24] resulting in the formation of the ferric HO-1/verdoheme complex when a stoichiometric amount of peroxide and heme are reacted. HutZ appears to be capable of similar chemistry, based on the observed spectroscopic signatures. Furthermore, entirely on the basis of changes in the ultraviolet−visible spectrum, the addition of a chemical reductant, like ascorbic acid, to the HutZ/verdoheme complex leads to what appears to be a HutZ/biliverdin complex, although the tetrapyrrole product of this reaction has yet to be isolated and characterized.[21]

In light of these observations, and the similar environment colonized by both pathogens, the enigma appears to be how these proteins (ChuWXY vs HutWXZ) may have functionally diverged to accomplish a similar task in the same ecological niche. Our current hypothesis posits that HutW is a radical SAM enzyme capable of opening the porphyrin ring of heme to release iron

in an oxygen-independent reaction, although this hypothesis has not been tested. ChuX and HutX are structurally identical, and the RMSD for all backbone carbon atoms is <0.5 Å. Therefore, if HutW does catalyze a reaction similar to that of ChuW, then it stands to reason that HutX will function similarly to ChuX and bind free iron and/or the tetrapyrrole product of HutW. Given that ChuY and HutZ both contain nucleotide binding domains but have notably different overall folds, an exciting possibility is that the tetrapyrrole product of HutW is different from ChuW. In this case, HutZ may serve dual functions. Specifically, HutZ may be capable of catalyzing heme degradation in the presence of molecular oxygen (explaining the lack of a ChuS homologue in V. cholerae) but then also functioning as a reductase under anaerobic conditions to clear the product of HutW (explaining the lack of a ChuY homologue in V. cholerae), produced during anaerobic heme degradation. Alternatively, HutW may utilize a different mechanism, when compared to ChuW, to open the porphyrin ring of heme.

To address whether HutW is a radical SAM enzyme involved in anaerobic heme degradation, and generation of potentially new tetrapyrrole catabolites, and to address new functions for HutX and HutZ, we have isolated and characterized the recombinant proteins. Our results show that HutW is indeed a radical SAM enzyme capable of catalyzing anaerobic heme degradation, albeit with significantly different mechanistic features. Moreover, we show that while inclusion of HutX in the assay does increase the rate of HutW turnover, inclusion of HutZ does not. We also demonstrate that HutW can utilize NADPH as a substrate, a significant first for any RS enzyme. Both of these observations are in marked contrast to what was reported for ChuW from the O157:H7 serotype of E. coli. The physiological implications for utilization of heme as an iron source by V. cholerae are discussed.

Materials and Methods

Overproduction, Purification, and Reconstitution of HutW.

The gene encoding HutW was codon-optimized for expression in E. coli and synthesized de novo by DNA 2.0 (now ATUM, Newark, CA). This plasmid (kanamycin resistant) utilized a standard T7, isopropyl β-D-1-thiogalactopyranoside (IPTG)-inducible, promoter and was co-transformed along with the pDB1282 plasmid[25] (ampicillin resistant), containing the *isc* operon, into E. coli BL21(DE3). A 20 mL starter culture of LB medium was inoculated with a single colony and incubated overnight at 37 °C while being shaken at 250 rpm. Flasks (4 L) containing M9 medium (1 L) were inoculated with the overnight starter culture to initiate growth (180 rpm at 37 °C). Expression of the genes encoded on plasmid pDB1282 was induced at an OD600 of 0.3 with 0.2% arabinose. Expression of the *hutW* gene was subsequently induced with 0.2 mM IPTG at an OD600 of 0.6, and the mixture incubated overnight for 18 h at 17 °C while being shaken at 180 rpm. The cells were harvested, flash-frozen, and stored at −80 °C. For purification, 30 g of frozen cell paste was resuspended in 150 mL of anaerobic lysis buffer containing 50 mM Tris (pH 7.5), 250 mM KCl, 10% (v/v) glycerol, PMSF (1 mM), DNase1 (100 μg/mL), and lysozyme (1 mg/mL). Resuspended cells were degassed with argon while being stirred. Solubilized cells were then lysed anaerobically by equilibrating a closed-system French press with anaerobic buffer while maintaining a stream of argon in the drawing and collection flasks. The lysate was centrifuged at 60000g for 1.5 h. The supernatant was collected and purified anaerobically by a cobalt affinity column pre-equilibrated with buffer. After application of the supernatant, the column was washed with a buffer containing 0 and 10 mM imidazole before elution with 250 mM imidazole. Protein was diluted to 1 mg/mL, and the [4Fe-4S] cluster was reconstituted following previously established methods.[25] Briefly, the protein was diluted in 100 mM HEPES (pH 8.0), 300 mM KCl,

10% glycerol, and 10 mM DTT. Then, 100 mM ferric chloride was added to 4 times the protein concentration. After the solution had been allowed to incubate for 30 min, 15 μL of 100 mM sodium sulfide was added every 10 min until reaching 1 equiv of the iron concentration. After incubation in the glovebox for 12 h, excess iron−sulfur clusters were removed by centrifugation and the supernatant was run over a DEAE-Sepharose anion exchange column in the glovebox. The reconstituted enzyme was eluted using a stepwise (0.1 M steps) gradient (0-1 M KCl) in buffer. Protein fractions were concentrated anaerobically and applied on a G25 size exclusion column pre-equilibrated with a buffer containing 100 mM HEPES (pH 8.0), 300 mM KCl, and 10% glycerol. Protein fractions were concentrated anaerobically before being stored in liquid nitrogen.

HutX and HutZ Expression and Purification.

Unlike HutW, HutX and HutZ do not contain any cofactors that would require a unique expression protocol. The gene for HutZ was optimized for expression and cloned into the pD431-SR vector by ATUM. The gene for HutX was amplified from genomic V. cholerae DNA (a generous gift from S. Payne) and cloned into the commercially available pTrcHisA vector. Expression of both proteins was carried out in E. coli BL21(DE3) cells and the aforementioned IPTG-inducible expression plasmids (the HutZ expression vector is kanamycin resistant, while the HutX expression vector is carbenicillin resistant). Expression of HutZ and HutX was performed in LB medium (1 L) inoculated with a 10 mL starter culture and grown at 37 °C while being shaken at 200 rpm. Once an OD600 of 0.6 was achieved, IPTG was added to a final concentration of 1 mM. Cultures were grown for an additional 6 h before being harvested by centrifugation, frozen, and stored at −80 °C. Frozen cell pellets (50 g) were solubilized in 200 mL of a buffer containing 50 mM Tris (pH 7.5) and 250 mM KCl supplemented with PMSF (1 mM), lysozyme (1 mg/mL), and DNase (1 mg/mL). Cells were lysed aerobically with a French pressure cell, and the lysate was

centrifuged at 100000g for 1.15 h. The supernatant was applied to a TALON column that was pre-equilibrated with a buffer containing 50 mM Tris (pH 7.5), 250 mM KCl, and 10% glycerol. The column was washed with the same buffer also containing 0 and 10 mM imidazole buffer before elution with a buffer containing 250 mM imidazole. Protein fractions were analyzed by sodium dodecyl sulfate−polyacrylamide gel electrophoresis (SDS−PAGE) for homogeneity. Protein-containing fractions were pooled and concentrated prior to being frozen at −80 °C.

Ultraviolet−Visible (UV−vis) Activity Assays.

All UV− vis spectra were recorded on an HP 8453 diode array spectrophotometer running on OlisWorks using a Peltier temperature controller set to 25 °C and a stir speed of 1200 rpm. Unless indicated in the figure legend, assays were conducted anerobically with degassed buffer containing 5% DMSO (from a porphyrin stock), 10 μM HutW, 1 mM SAM, and 20 μM heme, protoporphyrin IX, deuteroheme, or deuteroporphyrin IX. Initially, sodium dithionite (2 mM) was used as the reducing agent until it was discovered that NADPH could drive the reaction. Turnover was initiated by the addition of SAM unless indicated otherwise. Spectra were recorded from 350 to 900 nm every minute. Assays were run for as long as 30 min, but for the majority of porphyrins investigated, all spectral changes were completed within 4−5 min. Extinction coefficients were also determined by the isosbestic point at 418 nm using the relationship $A = l\varepsilon(C_{substrate} + C_{product})$.

Quantification of Fe−S Cluster Content and Labile Iron after Turnover.

Quantification of the iron content in active preparations of HutW (presumably containing a [4Fe4S] cluster) was performed as previously described.[26] To quantify the labile iron present in assays pre- and postturnover, the assay was modified to include HutW (10 μM), heme (50 μM), SAM (1 mM), and either NADPH (10 mM) or sodium dithionite (2 mM) as the reductant. Aliquots for quantification were taken at the indicated time points. Iron standards were prepared in acid-

washed glassware at a concentration of 0.5 mM ferrous ammonium sulfate heptahydrate and diluted to various concentrations between 0.012 and 0.2 mM in 50 mM Tris (pH 8.0), 250 mM KCl, and 10% glycerol. After acid precipitation and heat incubation at 80 °C, 750 μL of dH2O was added, and samples were centrifuged. Supernatants were transferred to new microcentrifuge tubes followed by addition of 50 μL of 10% hydroxylamine and 250 μL of 0.1% bathophenanthroline. Samples were incubated at room temperature for 1 h, and the absorbance at 535 nm was taken. All iron standards were performed in triplicate as well as the samples for HutW. The same protocol was used to detect the total amount of iron available to the chelator in the HutW assay before and after turnover. Any protein-bound iron is released during acid hydrolysis, whereas heme-bound iron is not.

Electron Paramagnetic Resonance (EPR) Spectroscopy.

Samples were prepared, sealed, and flash-frozen in an anaerobic chamber. For all samples, the protein concentration was 400 μM in the presence of 3 mM sodium dithionite. When SAM was added to the sample, it was at a concentration of 1 mM. All EPR spectra were recorded at 12 K with a microwave power of 0.1 mW, a microwave frequency of 9.352 GHz, a modulation amplitude of 4.0 G, and a modulation frequency of 100 kHz.

High-Performance Liquid Chromatography (HPLC) Analysis.

Turnover assays of HutW were performed anaerobically in a 2 mL reaction volume with final concentrations of 1 mM SAM, 100 μM heme, 100 μM HutW, in 50 mM Tris (pH 8.0), 250 mM KCl, and 10% glycerol buffer. The reductant was either sodium dithionite (2 mM) or NADPH (10 mM). Due to the detection limits of our HPLC instrument, aliquots were taken at various time points during an assay. These are noted in the respective figure legends and include 0 min, 15 min, 30 min, 60 min, 90 min, and overnight (approximately 12 h). Sample aliquots (150 μL) were taken

and quenched with 1% TFA (v/v, final) and centrifuged to remove the precipitant, and the supernatant was applied to a C18 HPLC column (15 cm × 4.6 mm). SAM cleavage products were separated by a gradient of acetonitrile in 0.1% TFA at a flow rate of 1 mL/min and monitored at 260 nm. The column was washed following each injection for 5 min with 100% acetonitrile. A standard curve was constructed by spiking the assay solution with various concentrations of SAM, SAH, or 5′-dA and integrating the respective peak areas.

Mass Spectrometry.

Samples were diluted to approximately 10 μM in methanol containing 0.1% formic acid. The solutions were infused directly into the electrospray source of the ion mobility mass spectrometer (Waters Synapt XS) at a flow rate of 660 μL/h using an external syringe pump following mass calibration to 1 ppm over the range of m/z 50−1200. Data were acquired in positive ionization mode (capillary, +3 kV; source temperature, 120 °C; cone gas, 10 L/h; desolvation gas, 500 L/h at 350 °C) over a period of 5 min with a scan time of 1 s. The ion mobility separation was achieved using nitrogen drift gas and traveling wave settings of 550 m/s and 40 V. The tandem MS experiment was performed using a 25 eV collision energy that was applied to the transfer cell of the instrument. The exact calculated masses of the products were extracted from the ion mobility arrival time distribution within a window of 0.01 Da

Results

Isolation and Purification of HutW.

HutW is the first of three genes expressed in an iron-dependent (Fur promoter) manner as part of a larger heme utilization (Hut) operon (Figure 1A). In addition to the similar organization of the operon, HutW shares 39% sequence identity with ChuW, a radical SAM methyl transferase (RSMT) involved in anaerobic heme degradation.[15] Therefore, similar to the expression of other

radical SAM enzymes, expression of HutW was performed using an additional plasmid to increase the level of iron−sulfur cluster biosynthesis during expression.[23,25] Anaerobic isolation (Figure 1B) and reconstitution of HutW yielded a purified enzyme with 4.4 ± 0.7 iron atoms per protein. The UV−vis spectrum had a broad adsorption feature with a maximum near 400 nm, indicative of the coordination of a [4Fe-4S]+ cluster (Figure S1). To further investigate the cluster content, the EPR spectra of HutW in the presence of sodium dithionite were recorded and revealed a broad signal centered on a g of 1.93 (Figure 1C). These observations are similar to what has been observed for other radical SAM enzymes that contain only the catalytic [4Fe-4S] cluster in the reduced state (formally 1+).[27] In addition, when SAM is added to the mixture, a significant change in the line shape of the EPR signal ($g_{\parallel} = 1.99$, and $g_{\perp} = 1.93$) occurs that is consistent with SAM binding to the unique iron site (Figure 1D) of the [4Fe-4S]+ cluster.

Finally, when purified HutW was passed through a calibrated size exclusion column, the elution volume was consistent with a monomer (Figure S2).

Heme Binding.

To investigate heme binding by HutW, we monitored the absorption spectrum of a buffered solution of heme following the addition of purified HutW. A red shift in the major Soret band (from 385 to 422 nm) is observed and can be utilized to follow heme binding (Figure 2). Under reducing conditions, the observation of a major Soret band at ∼420 nm, and an α band at 556 nm, for heme-bound HutW, are spectral properties consistent with those of a reduced ferrous six-coordinate low-spin heme complex.[24,28,29] Addition of an increasing concentration of HutW to a

hemin solution (20 μM) produces a binding isotherm (Figure 2) that can be used to calculate binding affinities.

Specifically, HutW−heme titration was performed under strictly anaerobic conditions using either ferrous or ferric heme. The dissociation constant (K_d) for the HutW−hemin or −heme complexes was determined by fitting the data to a rectangular hyperbole giving Kd values of 1.4 ± 0.5 and 3.6 ± 0.9 μM for the binding of ferric and ferrous heme, respectively. These Kd values are in a range that is similar to what has been reported for other bacterial heme-degrading enzymes.[12,30,31] The binding also appears to saturate at 10 μM, which is a 1:1 HutW:heme ratio.

Turnover of HutW Using Metalated and Nonmetalated Porphyrins.

Despite the 39% sequence identity shared with ChuW, HutW is phylogenetically distinct[32] with significant sequence divergence occurring in an extended Nterminal domain. Therefore, although we hypothesized that HutW is a RSMT involved in anaerobic degradation, it is possible that significant differences in the catalytic mechanism exist. To assess our hypothesis and the porphyrin-degrading activity of HutW, we performed assays monitoring the UV−vis spectrum during incubation of the protein with one of several porphyrins or metalated porphyrins. This was performed in the presence of the chemical components typically required of a radical SAM enzyme, specifically, SAM as well as a source of low-potential electrons. No changes were seen if SAM was omitted from the assay, regardless of the source of electrons. We observed distinct changes in the absorption spectra for all of the porphyrins investigated (Figure 3). Progress curves for heme turnover are shown in Figure S3. The data in Figure 3 show the changes observed for heme (Figure 3A), deuteroheme (Figure 3C), protoporphrin IX (Figure 3B), or deuteroprotoporphyrin IX (Figure 3D). Rates were calculated from the progress curves, as described in Materials and Methods (Table 1), and reveal that the physiological substrate, heme,

has the fastest turnover rate (Figure 1A), resulting in a decrease in the intensity of the major Soret band at 407 nm and Q-bands concurrent with an increase in absorbance at 451 and 795 nm.

Deuteroheme (Figure 3C), a more soluble heme analogue, exhibited similar spectroscopic changes, including a decrease in the intensity of the major Soret band as well as increases in the absorption at longer wavelengths (448 and 775 nm). For ChuW, the mechanism of porphyrin degradation has also been shown to be independent of the metal ion,[23] and therefore, we wanted to address if the metal ion was required in the HutW. mechanism. Similar to heme and deuteroheme, the equivalent nonmetalated porphyrin molecules, protoporphyrin IX (Figure 3B) and deuteroporphyrin IX (Figure 3D), were also viable substrates. The absorption changes observed for all of the porphyrin substrates investigated are consistent with turnover regardless of the metalation state of the substrate. In addition, mesoheme and coproporphyrin III exhibited similar spectral changes (Figure S4). No spectroscopic changes were observed when N-methylprotoporphyrin was investigated, suggesting that "bent" porphyrins are not viable substrates.

Analysis of the Tetrapyrrole Product by Ion Mobility Mass Spectrometry.

The tetrapyrrole product of ChuW has been shown to be a hydrophobic, light/redox sensitive compound that is difficult to isolate and/or solubilize,[15] thus making analysis difficult. However, the field of lipidomics has experienced similar challenges that have resulted in new mass spectrometry methods to characterize hydrophobic compounds.[33,34] To this end, we analyzed HutW assay solutions before and after turnover using hydrophobic liquid chromatography (HILIC) paired with ion mobility mass spectrometry (IM-MS). When sodium dithionite was used as the electron source, a major peak was observed at m/z 583.3 (38.5% m + 1 for 13C), consistent with a more reduced form of anaerobilin (Figure 4). Initially, this is not that surprising, given that the

midpoint reduction potential of dithionite approaches −0.8 V at pH 8.0.35 Specifically, compared to the anaerobilin molecule produced by ChuW, at least two more electrons and protons appear to have been added giving rise to the tetrapyrrole shown in Figure 4A. To further assess the structure of the tetrapyrrole product, fragmentation of the peak at m/z 583.3 was performed (Figure 4). Interestingly, of the 107 likely fragments predicted by the MetFrag36 software (https://ipbhalle.github.io/MetFrag/), we observe 106 of the fragments with intensities of >200 counts (Figure S5). These results confirm that a more reduced form of anaerobilin is the product of HutW heme degradation (Figure 4A), again with the caveat that sodium dithionite is the reductant in these experiments. However, given that previous experiments using titanium(III) citrate as the reductant for ChuW did not result in production of a more reduced form of anaerobilin,[23] we favor a model whereby HutW is indeed functionally different from ChuW. Sodium dithionite and titanium(III) citrate are strong reductants, so reduction should be thermodynamically favorable. However, unknown kinetic factors related to the pathway for electron transfer cannot be ruled out at this time.

Iron Release and Other Turnover Products.

HutW is part of an operon that is required for *V. cholerae* to use heme as an iron source; therefore, we determined the concentration labile iron before and after turnover (Figure 5A). Similar to what has been reported for ChuW, we observe an increase in the labile iron that is proportional to the amount of heme degraded during the assay. As mentioned previously, sequence homology also indicates that HutW is a class C radical SAM methyltransferase (RSMT). Class C RSMTs require two molecules of SAM per turnover. They have been shown to use a mechanism whereby one SAM molecule is converted to 5′-dA for radical generation while the second molecule of SAM is converted to S-adenosyl-L-homocysteine (SAH).[37] Therefore, we employed HPLC to

analyze the products of the dithionite driven HutW reaction. It is important to note that, due to the detection limits of our HPLC system and the low solubility of the tetrapyrrole products, these assays are run for an extended period and do not represent a steady state. However, this does provide insight into the relative ratio of products. On the basis of the data shown in Figure 5B (trace ii), and integration of the respective peaks, 340 μmol of SAH and 745 μmol of 5′-dA have been produced when dithionite is used as the reductant. This is indicative of the "abortive cleavage" of SAM, an observation that has been reported for other RS enzymes.[38] Due to the extended length of the assay required for HPLC analysis, a small amount of breakdown products is observed in the control experiment in the absence of externally added dithionite (Figure 5B, trace iii), but this is in marked contrast to the fact that no SAH is produced in the absence of heme and abortive cleavage observed only when dithionite is added (Figure 5, trace v). These observations are not unexpected and, as we will demonstrate, are most likely an artifact of the electron source, as others have also reported.[38]

HutX Increases the HutW Turnover Rate.

The enzymes HutW, HutX, and HutZ are expressed from the same operon, suggesting that they may work synergistically during heme acquisition and degradation. To address this, we investigated the effect of HutX and HutZ on the turnover rate observed for HutW. The rationale for this experiment is based on the observation that product release has been shown to be the ratelimiting step for the heme oxygenase reaction. This can be altered by the inclusion of biliverdin reductase in the assay, resulting in a significantly faster turnover rate.[39,40] Similarly, when HutX was included in the HutW assay, the turnover rate appeared to increase (Table 1).

However, inclusion of purified HutZ, the third enzyme from the same operon in the V. cholerae, failed to increase the rate of turnover. This is distinctly different from the increase in

specific activity reported for enterohemorrhagic E. coli O157:H7 when the third gene (*chuY*), shown to be an "anaerobilin reductase", is included.19 In fact, we hypothesize that one reason HutZ does not accelerate the HutW reaction is due to the higher affinity for heme (K_d = 0.052 ± 0.004 μM at pH 8.0) that has been reported.[20] These observations are consistent with previous work supporting a role for HutZ in heme degradation under aerobic growth or oxidizing conditions.[21] These observations may also explain the lack of a ChuS homologue in V. cholerae, where ChuS, from E. coli O157:H7, has been shown to catalyze heme degradation under aerobic conditions in vitro.[31]

NADPH Is an Acceptable Electron Donor for the HutW Reaction.

Every radical SAM enzyme requires a source of low-potential electrons. Ultimately, in vivo these electrons come from NADH or NADPH by way of ferredoxin or flavodoxin and the respective oxidoreductases. However, in the course of expression and isolation of these enzymes, it may or may not be possible to obtain the physiologically relevant. electron transfer proteins. Therefore, chemical reductants such as sodium dithionite or titanium(III) citrate are often used in the laboratory. As others have observed, and we clearly see in Figure 5B, strong chemical reductants can lead to unproductive cleavage of SAM. Interestingly, HutW is phylogenetically distinct from ChuW and contains a glycine rich NAD(P) binding motif (328GCGAGGNMGG337).[32,41] Given this observation and the lack of a ChuY homologue in V. cholerae, we decided to test whether NADPH would support HutW turnover. Surprisingly, utilization of NADPH as the electron donor in the HutW assay resulted in changes in the absorption

spectra that were similar to what was observed when sodium dithionite was used as the electron donor (Figure 6A).

In addition, a similar increase in the concentration of labile iron was also observed (Figure 6B). The specific activity using NADPH was calculated from the linear portion of the progress curves (Figure S3), as described in Materials and Methods, and resulted in a rate of 148.3 ± 14.0 nmol min−1 mg−1 . To identify the tetrapyrrole product(s), we subjected the NADPH-dependent turnover samples to IM-MS (Figure 7).

Similar to the turnover sample using sodium dithionite as the reductant, the major product was associated with a peak at m/z 583.3 (Figure 7). However, in contrast to the assay using sodium dithionite, an additional peak that was not observed in the pre-turnover sample but was present post-turnover, albeit at much weaker level, was a peak at m/z 581.3 (Figure 7). This peak is consistent with an intermediate state of reduction as anaerobilin is reduced in two-electron/proton increments. Finally, we subjected the NADPH-dependent turnover samples to HPLC analysis and found production of SAH and 5′-A (Figure 8). Again, the detection limits of our HPLC system require that we run the assay for an extended period. The integrated areas indicate the production of 634 μmol of SAH and 742 μmol of 5′-A. While not quite stoichiometric, this is a significant improvement over what was observed when sodium dithionite was used as the electron source. Regardless, comparison of the data in Figure 8, with the data from the dithionite-driven turnover presented in Figure 5, indicates a significant decrease in the rate of abortive cleavage. More importantly, the observation that the physiological reductant, NADPH, can be used to drive the ring-opening reaction catalyzed by HutW, as well as reduction of the initial tetrapyrrole product, is significant in light of the lack of a ChuY homologue in *V. cholerae*

Discussion

The human gut represents a set of complex and unique microbial habitats where organisms, including the host cells, must compete for the available micronutrients.[42] A new theory has emerged that suggests commensal organisms live synergistically with one another and the host. In contrast to this collaborative relationship, enteric pathogens appear to have evolved mechanisms to rapidly acquire or steal nutrients from the commensal flora and host cells, an advantage that is amplified during systemic infection and the induction of certain host defense mechanisms. However, it is reasonable to assert that our current understanding of the human microbiome is still in its infancy. In part, understanding the human microbiome is challenging because a significant portion of the gut ecology is represented by strictly anaerobic commensal organisms that are difficult to culture. Moreover, many commensal organisms form consortiums, dependent on one another for specific, sometimes unknown, metabolites. Given the rise in antibiotic resistance, understanding how pathogenic bacteria compete in this environment is a major global interest. The utilization of heme as an iron source represents a nutrient acquisition mechanism that is found in pathogenic organisms, but not commensal bacteria, and is often essential to pathogenesis.[13] Therefore, a complete understanding of the novel mechanisms for pathogenic heme degradation, and the secondary messaging that triggers pathogenesis, represents a largely unexplored avenue of antibiotic development. In particular, while extensive work has been performed on the aerobic pathways for heme catabolism,[43] our understanding of unique anaerobic pathways remains deficient.

Anaerobic Heme Degradation by HutW in V. cholerae.

It is clear that survival in the complex ecology of the human microbiome requires an organism to rapidly adapt to nutrient availability. In this work, we demonstrate that HutW is a radical SAM

enzyme involved in anaerobic heme degradion in V. cholerae. The protein sequence, iron analysis, and EPR spectra of HutW presented in this work are all consistent with the presence of a single $[4Fe\text{-}4S]^{+}$ cluster in the active enzyme (Figure 1). Moreover, the EPR signal for the $[4Fe\text{-}4S]^{+}$ cluster undergoes SAM-dependent changes that are consistent with what has been reported for other radical SAM enzymes containing only the catalytic [4Fe-4S] cluster.[44] Finally, the presence of this cluster is required for heme degradation.

On the basis of changes in the major Soret band of heme, we found that HutW binds ferrous heme with a K_d of 3.6 ± 0.9 μM (Figure 2), consistent with other proteins involved in heme degradation.[17,30,45] Moreover, upon anaerobic incubation with SAM and sodium dithionite, the UV absorption spectra reveal changes consistent with opening of the porphyrin ring (Figure 3). Care must be taken when powerful chemical reductants such as sodium dithionite or titanium-(III)citrate are utilized as this can lead to product artifacts. Regardless, similar to what was reported for ChuW in E. coli O157:H7, the iron atom does not appear to be involved in the mechanism of ring opening.[23] Analysis of the pre- and postturnover assay by IM-MS confirmed the formation of a linear tetrapyrrole (Figure 4). We also observe a concurrent increase in the level of labile iron in the assay when metalated porphyrins were used as the substrate, consistent with the liberation of iron from the porphyrin macrocycle (Figure 5). Taken together, these data support a role for HutW in the anaerobic degradation of heme and iron release. Similar to what was reported for ChuW, from enterohemorrhagic E. coli, the mechanism of ring opening involves two molecules of SAM, one being required for radical generation and the other involved in formation of a transient methylene radical. Consistent with what has been recently reported for other class C RSMT enzymes, both 5′-dA and SAH are produced (Figure 5). However, the ability to utilize NADPH directly is an unexpected and significant difference in the mechanism of HutW. This observation

must be considered in the larger context of heme acquisition/utilization by enteric pathogens and the enzymes involved. Specifically, while titanium(III) citrate was not capable of reducing the tetrapyrrole product of ChuW,[23] this organism has an additional enzyme, ChuY, that utilizes NADPH to catalyze a four-electron reduction.[19] To the best of our knowledge, there is no ChuY homologue in V. cholerae. In that context, the observation that HutW can catalyze the ring opening and four-electron reduction of anerobilin, regardless of electron source, certainly makes sense. However, when considering electron transfer reactions, it is important to recognize that there is a thermodynamic component and a kinetic component. The former is dependent on the midpoint reduction potential of the donor and acceptor, while the latter is often hidden within the subtle elements of protein structure and the specific electron transfer pathway. This is being investigated further, but the ability to utilize NADPH directly, instead of via a flavodoxin and ferredoxin/ flavodoxin NADP oxidoreductase, would seem advantageous.

HutW Is a Class C RSMT.

The results reported herein are consistent with HutW functioning as a class C radical SAM methyltransferase (RSMT) that shares some sequence and mechanistic homology with ChuW but is phylogenetically distinct.[32] Currently, the proposed mechanism for ChuW and other class C RSMT involves two molecules of SAM, as first observed in the HemN crystal structure.[49] The first molecule of SAM is required for generation of the 5′-deoxyadenosyl radical (5′-dA•). This radical, proposed to be common to all radical SAM enzymes, abstracts a hydrogen atom from the second molecule of SAM (SAM2) yielding a methylene radical. A unique aspect of the class C RSMT mechanism is that the methylene radical on SAM2 is added to a double bond, methylating an otherwise unreactive sp^2 -hybridized carbon center.[46] This is in contrast to an enzyme that uses the methylene radical to abstract a hydrogen atom from the substrate molecule. The latter has now

been shown to be the case for HemN, as a SAM2−prophyrin adduct was recently captured,[47] confirming an evolutionary/mechanistic connection between HemN and the class C RSMTs. Specifically, in the HemN mechanism SAM2 functions as part of a "hydrogen atom relay" network, while the methylene radical in class C RSMTs serves to methylate what would be otherwise unreactive sp^2 -hybridized carbon centers.[27,37,48,49] Therefore, an equal ratio of 5′-deoxyadenosine (5′-dA) to the Sadenosylhomocysteine (SAH) product is expected for any class C RSMT. We looked for both 5′-dA and SAH production during HutW turnover by HPLC and observed a much larger peak for 5′-dA when using the chemical reductant sodium dithionite (Figure 5), compared to when NADPH is used (Figure 8). This is consistent with the "abortive cleavage" of SAM that others have reported for radical SAM enzymes when chemical reductants are used.[38]

Mechanism and Function of HutW versus ChuW.

A significant, and potentially problematic, step in the catabolism of heme is the production of reactive tetrapyrrole intermediates. Specifically, production of the biliverdin or anaerobilin intermediate occurs via the aerobic or anaerobic pathway, respectively. Accumulation of these intermediates is often toxic, and therefore, organisms contain specific reductases to prevent accumulation.[19,50,51] The source of the toxicity appears to be ring conjugation and the general aromaticity of the compounds, making the tetrapyrrole highly reactive and insoluble. Therefore, it is not surprising that these reductases eliminate some of the toxicity by reducing the double bonds between the pyrrole ring and a bridging carbon atom.[19,52] While we have shown that HutW is an anaerobic heme-degrading enzyme, like ChuW, functional differences between the enzymes must

be considered in the larger context of what is known about utilization of heme as an iron source as well as the organization of these genes in the two organisms.

Pathogenic strains of *E. coli*, such as serotype O157:H7, and *V. cholerae* contain similar operons for the utilization of heme as an iron source.[1,53] Likewise, expression of genes within both operons has been shown to be regulated in a Fur-dependent manner and they have been shown to encode a number of proteins with homologous functions. For example, homologous proteins are involved in heme uptake, transport/storage within the periplasm, and the ATP-dependent transport from the periplasm into the cytoplasm. However, following transport into the cytoplasm, the fate of heme seems to differ in the two organisms. For pathogenic *E. coli* O157:H7, evidence has been presented that identifies ChuS as both a heme oxygenase[54] and a heme storage/transfer protein.[23] The latter role is consistent with the structural homology and significant sequence identity (66%) to the heme storage protein PhuS in Pseudomonas aeruginosa. [55,56] Moreover, little is known about how the externally obtained heme is incorporated into the pathogen's own heme proteins or how the degradation products of heme are sequestered. Specifically, how do the pathogens detoxify the tetrapyrrole products or transport or store the iron that is released following catalysis? These are important questions because the only single-gene deletions that have been shown to result in a fitness phenotype during growth on heme as the sole iron source in pathogenic *E. coli* O157:H7 or *V. cholerae* are deletions of ChuY or HutZ, respectively.[13,22] Similar to the role of biliverdin reductase, ChuY has been shown to utilize NADPH to reduce anaerobilin.[19] Even though the *hutZ* gene is found in an orientation similar to that of the *chuY* gene, HutZ has been shown to be a peroxide-dependent heme oxygenase, potentially explaining the phenotype of the deletion strain. However, there is no ChuY homologue in *V. cholerae*. Therefore, the discovery that HutW can utilize NADPH to catalyze not only the opening of the porphyrin ring but also the reduction of

anaerobilin suggests that HutW performs the function of both ChuW and ChuY. However, deletion of HutZ would still be problematic as it is required for aerobic heme degradation, consistent with the observed phenotype for the deletion strain.[13] This conclusion is also consistent with sequence motifs unique to HutW and the observation that HutW is phylogenetically distinct, as discussed above.

HutX Stimulates HutW Catalysis.

HutX is transcribed from the gene immediately following HutW in the same operon. Therefore, it is plausible that HutX is also involved in the anaerobic breakdown of heme, by binding the freed iron atom, the linear tetrapyrrole, delivering heme to HutW, or through some other mechanism, such as allosteric modulation of HutW activity. From the current literature, HutX is annotated as a heme binding protein. Therefore, we hypothesize that HutX could function to deliver heme to HutW under anaerobic conditions, or HutZ aerobically for degradation, fulfilling its role as a general heme binding protein. Additionally, recently a new role for ChuX (the homologous protein from *E. coli* O157:H7) was proposed where the ChuX protein works synergistically with the ChuW protein as a chaperone to transiently sequester the iron atom and/or the tetrapyrrole product.[23] The evidence presented here demonstrates that HutX stimulates the heme degradation activity of HutW (Table 1). Whether this is through binding and facilitation of removal of iron or the tetrapyrrole product is currently under investigation. Regardless, HutX binding one of the products of HutW catalysis is in agreement with both the organization of the genes within the heme utilization operon and our evidence that HutX stimulates HutW activity.

Conclusions.

We have provided experimental evidence that HutW is a class C RSMT involved in the liberation of iron from heme. HutW is expressed along with several other proteins involved in heme

acquisition under iron-depleted conditions.[13] The observation that NADPH will catalyze the ring opening and subsequent reduction of the tetrapyrrole product is a significant new observation that is consistent with the lack of a ChuY homologue in *V. cholerae*. In evolutionary terms, the conservation of an enzyme that releases iron from heme under anaerobic conditions across enteric pathogens makes sense, as any nutritional advantage would be significant in the crowded and competitive environment of the human gut. Future work will interrogate the precise mechanism of NADPH-dependent turnover. Specifically, to provide insight into the reaction mechanism and how interactions with HutX modulate the mechanism, these studies will be coupled to biophysical investigations, to shed light on potentially unexplored avenues for antimicrobial development. Finally, this work, and future investigations, will expand our understanding of the poorly understood class C RS enzymes involved in the synthesis of natural compounds with therapeutic properties.

FUNDING

Funding from the National Institute of General Medical Sciences (Grant R01GM124203) to W.N.L. and startup funds from The University of Georgia to K.M.H. is gratefully acknowledged. The authors also acknowledge that funding for the EMXplus EPR and cryogen-free Stinger cooling system was provided by a grant from the NSF Major Research Instrumentation (MRI) program in the Division of Chemistry (CHE-1827968).

ACKNOWLEDGMENTS

The authors would like to thanks Dr. Amy Medlock for critical reviews during the preparation of this manuscript.

SUPPORTING INFORMATION

The UV-visible spectra of as-isolated HutW, analysis of HutW on a calibrated size exclusion column, the progress curves for HutW turnover (with heme substrate) using Dt and NADPH, and the complete breakdown of the MS fragmentation are included as supplemental information.

ACCESSION CODES

Information on the enzymes being studied in this work can be found under the UniProt IDs A0A3G4VEL8 and Q9KL40 for HutW and HutX, respectively.

References

1. Payne, S. M., and Mey, A. R. (2010) Iron uptake in Shigella and Escherichia coli. In Iron Uptake and Homeostasis in Microorganisms (Cornelis, P., and Andrews, S. C., Eds.) pp 87−100, Caister Academic Press.
2. Payne, S. M., Wyckoff, E. E., Murphy, E. R., Oglesby, A. G., Boulette, M. L., and Davies, N. M. (2006) Iron and pathogenesis of Shigella: iron acquisition in the intracellular environment. BioMetals 19, 173−180.
3. Wandersman, C., and Delepelaire, P. (2004) Bacterial iron sources: from siderophores to hemophores. Annu. Rev. Microbiol. 58, 611−647.
4. Wilks, A., and Burkhard, K. A. (2007) Heme and virulence: how bacterial pathogens regulate, transport and utilize heme. Nat. Prod. Rep. 24, 511−522.
5. Poss, K. D., and Tonegawa, S. (1997) Reduced stress defense in heme oxygenase 1-deficient cell. Proc. Natl. Acad. Sci. U. S. A. 94, 10925−10930.
6. Schmitt, M. P. (1997) Utilization of Host Iron Sources by Corynebacterium diphtheriae: Identification of a Gene Whose Product Is Homologous to Eukaryotic Heme Oxygenases and Is Required for Acquisition of Iron from Heme and Hemoglobin. J. Bacteriol. 179, 838−845.
7. Genco, C. A., and Dixon, D. W. (2001) Emerging strategies in microbial haem capture. Mol. Microbiol. 39, 1−11.
8. Wilks, A., and Schmitt, M. P. (1998) Expression and characterization of a heme oxygenase (Hmu O) from Corynebacterium diphtheriae. Iron acquisition requires oxidative cleavage of the heme macrocycle. J. Biol. Chem. 273, 837−841.

9. Zhu, W., Wilks, A., and Stojiljkovic, I. (2000) Degradation of Heme in Gram-Negative Bacteria: the Product of the hemO Gene of Neisseriae Is a Heme Oxygenase. J. Bacteriol. 182, 6783−6790.
10. Ratliff, M., Zhu, W., Deshmukh, R., Wilks, A., and Stojiljkovic, I. (2001) Homologues of neisserial heme oxygenase in gram-negative bacteria: degradation of heme by the product of the pigA gene of Pseudomonas aeruginosa. J. Bacteriol. 183, 6394−6403.
11. Nambu, S., Matsui, T., Goulding, C. W., Takahashi, S., and Ikeda-Saito, M. (2013) A new way to degrade heme: the Mycobacterium tuberculosis enzyme MhuD catalyzes heme degradation without generating CO. J. Biol. Chem. 288, 10101−10109.
12. Skaar, E. P., Gaspar, A. H., and Schneewind, O. (2004) IsdG and IsdI, heme-degrading enzymes in the cytoplasm of Staphylococcus aureus. J. Biol. Chem. 279, 436−443.
13. Wyckoff, E. E., Schmitt, M., Wilks, A., and Payne, S. M. (2004) HutZ is required for efficient heme utilization in Vibrio cholerae. J. Bacteriol. 186, 4142−4151.
14. Law, D., and Kelly, J. (1995) Use of heme and hemoglobin by Escherichia coli O157 and other Shiga-like-toxin-producing E. coli serogroups. Infect. Immun. 63, 700−702.
15. LaMattina, J. W., Nix, D. B., and Lanzilotta, W. N. (2016) Radical new paradigm for heme degradation in Escherichia coli O157:H7. Proc. Natl. Acad. Sci. U. S. A. 113, 12138−12143.
16. Mey, A. R., and Payne, S. M. (2001) Haem utilization in Vibrio cholerae involves multiple TonB-dependent haem receptors. Mol. Microbiol. 42, 835−849.
17. Sekine, Y., Tanzawa, T., Tanaka, Y., Ishimori, K., and Uchida, T. (2016) Cytoplasmic Heme-Binding Protein (HutX) from Vibrio cholerae Is an Intracellular Heme Transport Protein for the HemeDegrading Enzyme, HutZ. Biochemistry 55, 884−893.

18. Suits, M. D., Lang, J., Pal, G. P., Couture, M., and Jia, Z. (2009) Structure and heme binding properties of Escherichia coli O157:H7 ChuX. Protein Sci. 18, 825−838.
19. LaMattina, J. W., Delrossi, M., Uy, K. G., Keul, N. D., Nix, D. B., Neelam, A. R., and Lanzilotta, W. N. (2017) Anaerobic Heme Degradation: ChuY Is an Anaerobilin Reductase That Exhibits Kinetic Cooperativity. Biochemistry 56, 845−855.
20. Uchida, T., Dojun, N., Sekine, Y., and Ishimori, K. (2017) Heme Proximal Hydrogen Bonding between His170 and Asp132 Plays an Essential Role in the Heme Degradation Reaction of HutZ from Vibrio cholerae. Biochemistry 56, 2723−2734.
21. Uchida, T., Sekine, Y., Matsui, T., Ikeda-Saito, M., and Ishimori, K. (2012) A heme degradation enzyme, HutZ, from Vibrio cholerae. Chem. Commun. (Cambridge, U. K.) 48, 6741−6743.
22. Kim, H., Chaurasia, A. K., Kim, T., Choi, J., Ha, S. C., Kim, D., and Kim, K. K. (2017) Structural and functional study of ChuY from Escherichia coli strain CFT073. Biochem. Biophys. Res. Commun. 482, 1176−1182.
23. Mathew, L. G., Beattie, N. R., Pritchett, C., and Lanzilotta, W. N. (2019) New Insight into the Mechanism of Anaerobic Heme Degradation. Biochemistry 58, 4641−4654.
24. Wilks, A., and Ortiz de Montellano, P. R. (1993) Rat liver heme oxygenase. High level expression of a truncated soluble form and nature of the meso-hydroxylating species. J. Biol. Chem. 268, 22357− 22362.
25. Lanz, N. D., Grove, T. L., Gogonea, C. B., Lee, K. H., Krebs, C., and Booker, S. J. (2012) RlmN and AtsB as models for the overproduction and characterization of radical SAM proteins. Methods Enzymol. 516, 125−152.

26. Lovenberg, W., Buchanan, B. B., and Rabinowitz, J. C. (1963) Studies on the Chemical Nature of Clostridial Ferredoxin. J. Biol. Chem. 238, 3899−3913.

27. Layer, G., Grage, K., Teschner, T., Schunemann, V., Breckau, D., Masoumi, A., Jahn, M., Heathcote, P., Trautwein, A. X., and Jahn, D. (2005) Radical S-adenosylmethionine enzyme coproporphyrinogen III oxidase HemN: functional features of the [4Fe-4S] cluster and the two bound S-adenosyl-L-methionines. J. Biol. Chem. 280, 29038− 29046.

28. Wilks, A., and Moenne-Loccoz, P. (2000) Identification of the proximal ligand His-20 in heme oxygenase (Hmu O) from Corynebacterium diphtheriae. Oxidative cleavage of the heme macrocycle does not require the proximal histidine. J. Biol. Chem. 275, 11686−11692.

29. Rublevskaya, I., and Maines, M. D. (1994) Interaction of Feprotoporphyrin IX and heme analogues with purified recombinant heme oxygenase-2, the constitutive isozyme of the brain and testes. J. Biol. Chem. 269, 26390−26395.

30. Matthews, S. J., Pacholarz, K. J., France, A. P., Jowitt, T. A., Hay, S., Barran, P. E., and Munro, A. W. (2019) MhuD from Mycobacterium tuberculosis: Probing a Dual Role in Heme Storage and Degradation. ACS Infect. Dis. 5, 1855−1866.

31. Suits, M. D., Pal, G. P., Nakatsu, K., Matte, A., Cygler, M., and Jia, Z. (2005) Identification of an Escherichia coli O157:H7 heme oxygenase with tandem functional repeats. Proc. Natl. Acad. Sci. U. S. A. 102, 16955−16960.

32. Wilkens, D., Meusinger, R., Hein, S., and Simon, J. (2020) Sequence analysis and specificity of distinct types of menaquinone methyltransferases indicate the widespread potential of methylmenaquinone production in bacteria and archaea. Environ. Microbiol., DOI: 10.1111/1462-2920.15344.

33. Appala, K., Bimpeh, K., Freeman, C., and Hines, K. M. (2020) Recent applications of mass spectrometry in bacterial lipidomics. Anal. Bioanal. Chem. 412, 5935−5943.
34. Hines, K. M., and Xu, L. (2019) Lipidomic consequences of phospholipid synthesis defects in Escherichia coli revealed by HILICion mobility-mass spectrometry. Chem. Phys. Lipids 219, 15−22.
35. Mayhew, S. G. (1978) The redox potential of dithionite and SO-2 from equilibrium reactions with flavodoxins, methyl viologen and hydrogen plus hydrogenase. Eur. J. Biochem. 85, 535−547.
36. Wolf, S., Schmidt, S., Muller-Hannemann, M., and Neumann, S. (2010) In silico fragmentation for computer assisted identification of metabolite mass spectra. BMC Bioinf. 11, 148−160.
37. Zhang, Z., Mahanta, N., Hudson, G. A., Mitchell, D. A., and van der Donk, W. A. (2017) Mechanism of a Class C Radical S-Adenosyll-methionine Thiazole Methyl Transferase. J. Am. Chem. Soc. 139, 18623−18631.
38. Bruender, N. A., Young, A. P., and Bandarian, V. (2015) Chemical and Biological Reduction of the Radical SAM Enzyme CPH4 Synthase. Biochemistry 54, 2903−2910.
39. Wilks, A., and Ortiz de Montellano, P. R. (1993) Rat liver heme oxygenase. High level expression of a truncated soluble form and nature of the meso-hydroxylating species. J. Biol. Chem. 268, 22357− 22362.
40. Wilks, A. (2002) Heme oxygenase: evolution, structure, and mechanism. Antioxid. Redox Signaling 4, 603−614.

41. Hua, Y. H., Wu, C. Y., Sargsyan, K., and Lim, C. (2015) Sequence-motif detection of NAD(P)-binding proteins: discovery of a unique antibacterial drug target. Sci. Rep. 4, 6471−6478.

42. Celis, A. I., and Relman, D. A. (2020) Competitors versus Collaborators: Micronutrient Processing by Pathogenic and Commensal Human-Associated Gut Bacteria. Mol. Cell 78, 570−576.

43. Wilks, A., and Ikeda-Saito, M. (2014) Heme utilization by pathogenic bacteria: not all pathways lead to biliverdin. Acc. Chem. Res. 47, 2291−2298.

44. Galambas, A., Miller, J., Jones, M., McDaniel, E., Lukes, M., Watts, H., Copie, V., Broderick, J. B., Szilagyi, R. K., and Shepard, E. M. (2019) Radical S-adenosylmethionine maquette chemistry: Cx3Cx2C peptide coordinated redox active [4Fe-4S] clusters. JBIC, J. Biol. Inorg. Chem. 24, 793−807.

45. Bhakta, M. N., and Wilks, A. (2006) The mechanism of heme transfer from the cytoplasmic heme binding protein PhuS to the deltaregioselective heme oxygenase of Pseudomonas aeruginosa. Biochemistry 45, 11642−11649.

46. Jin, W. B., Wu, S., Xu, Y. F., Yuan, H., and Tang, G. L. (2020) Recent advances in HemN-like radical S-adenosyl-l-methionine enzyme-catalyzed reactions. Nat. Prod. Rep. 37, 17−28.

47. Ji, X., Mo, T., Liu, W. Q., Ding, W., Deng, Z., and Zhang, Q. (2019) Revisiting the Mechanism of the Anaerobic Coproporphyrinogen III Oxidase HemN. Angew. Chem., Int. Ed. 58, 6235−6238.

48. Layer, G., Pierik, A. J., Trost, M., Rigby, S. E., Leech, H. K., Grage, K., Breckau, D., Astner, I., Jansch, L., Heathcote, P., Warren, M. J., Heinz, D. W., and Jahn, D. (2006)

The substrate radical of Escherichia coli oxygen-independent coproporphyrinogen III oxidase HemN. J. Biol. Chem. 281, 15727−15734.

49. Layer, G., Verfurth, K., Mahlitz, E., and Jahn, D. (2002) Oxygen-independent coproporphyrinogen-III oxidase HemN from Escherichia coli. J. Biol. Chem. 277, 34136−34142.
50. Kutty, R. K., and Maines, M. D. (1981) Purification and characterization of biliverdin reductase from rat liver. J. Biol. Chem. 256, 3956−3962.
51. Rigney, E., Mantle, T. J., and Dickinson, F. M. (1989) The kinetics of ox kidney biliverdin reductase in the pre-steady state. Evidence that the dissociation of bilirubin is the rate-determining step. Biochem. J. 259, 709−713.
52. Kikuchi, A., Park, S. Y., Miyatake, H., Sun, D., Sato, M., Yoshida, T., and Shiro, Y. (2001) Crystal structure of rat biliverdin reductase. Nat. Struct. Biol. 8, 221−225.
53. O'Malley, S. M., Mouton, S. L., Occhino, D. A., Deanda, M. T., Rashidi, J. R., Fuson, K. L., Rashidi, C. E., Mora, M. Y., Payne, S. M., and Henderson, D. P. (1999) Comparison of the heme iron utilization systems of pathogenic Vibrios. J. Bacteriol. 181, 3594− 3598.
54. Suits, M. D., Pal, G. P., Nakatsu, K., Matte, A., Cygler, M., and Jia, Z. (2005) Identification of an Escherichia coli O157:H7 heme oxygenase with tandem functional repeats. Proc. Natl. Acad. Sci. U. S. A. 102, 16955−16960.
55. Tripathi, S., O'Neill, M. J., Wilks, A., and Poulos, T. L. (2013) Crystal structure of the Pseudomonas aeruginosa cytoplasmic heme binding protein, Apo-PhuS. J. Inorg. Biochem. 128, 131−136.

56. O'Neill, M. J., and Wilks, A. (2013) The P. aeruginosa heme binding protein PhuS is a heme oxygenase titratable regulator of heme uptake. ACS Chem. Biol. 8, 1794−1802.

Figure 3.1

Genetic organization of the heme utilization operon in *V. cholerae*, SDS−PAGE of purified HutW, and EPR spectra. **(A)** HutW is genetically adjacent to the heme uptake machinery that is expressed during iron starvation. **(B)** SDS−PAGE showing molecular weight standards and the isolated HutW used in this study. EPR spectra of **(C)** purified HutW with 3 mM sodium dithionite before and **(D)** after the addition of 1 mM SAM. All EPR spectra were recorded at 12 K with a microwave power of 0.1 mW, a microwave frequency of 9.352 GHz, a modulation amplitude of 4.0 G, and a modulation frequency of 100 kHz

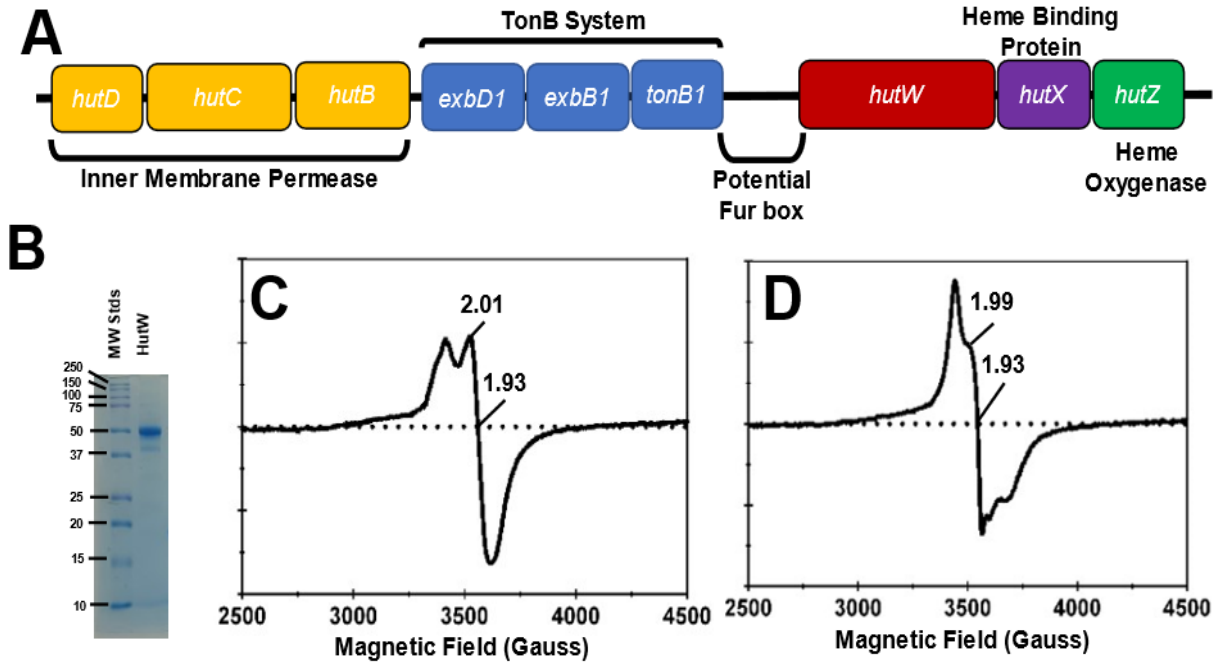
A
TonB System
Heme Binding Protein
hutD
hutC
hutB
exbD1
exbB1
tonB1
hutW
hutX
hutZ
Inner Membrane Permease
Potential Fur box
Heme Oxygenase
B
MW Stds
HutW
250
150
100
75
50
37
25
20
15
10
C
2.01
1.93
2500
3000
3500
4000
4500
Magnetic Field (Gauss)
D
1.99
1.93
2500
3000
3500
4000
4500
Magnetic Field (Gauss)

Figure 3.2

Ferric (red circles) and ferrous (black circles) heme binding to ferric HutW. Titration of increasing amounts of HutW (1−20 μM) into a solution of hemin (10 μM). The shift in the heme Soret peak was monitored and plotted as a function of protein concentration. Saturation was reached at a 1:1 protein:heme ratio (10 μM). The data were fit to a standard binding isotherm represented by a rectangular hyperbola using PRISM as described in the text. Dissociation constants were 1.27 and 3.64 μM for the ferrous and ferric heme, respectively.

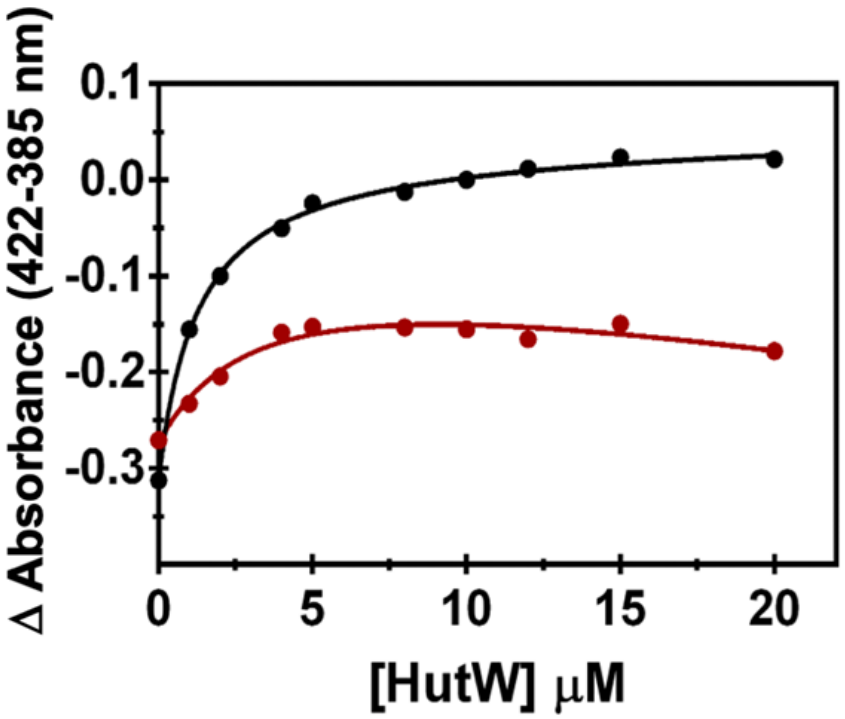
Δ Absorbance (422-385 nm)
0.1
0.0
-0.1
-0.2
-0.3
0
5
10
15
20
[HutW] μM

Table 3.1 Specific Activities for HutW-Catalyzed Porphyrin Degradation Reactions

Protein components in assay	*Substrate*	*Specific Activity [nmol•min^{-1}• (mg HutW)$^{-1}$]*
HutW	Heme	226.5 $\pm$ 15.6[1]
HutW (NADPH)[2]	Heme	346.2 $\pm$ 22.5
HutW	Deuteroheme	132.3 $\pm$ 46.7
HutW	Protoporphyrin IX	191.1 $\pm$ 4.3
HutW	Deuteroporphyrin IX	174.8 $\pm$ 14.5
HutW and one equivalent of HutX	Heme	552.8 $\pm$ 17.6

[1]Error represents average deviation from the mean for three measurements.
[2]NAPDH was the reductant in these assays. Unless stated otherwise, sodium dithionite (2 mM) is the electron source.

Figure 3.3

UV−vis absorbance spectra monitoring the anaerobic degradation of **(A)** heme, **(B)** protoporphyrin IX, **(C)** deuteroheme, and **(D)** deuteroporphyrin IX catalyzed by HutW. HutW assays were performed as described in Materials and Methods, and spectral changes were recorded every 2 min for 6 min. The structure of each substrate is shown as an inset in the respective panels, and the arrows indicate the direction of spectral changes during the assay.

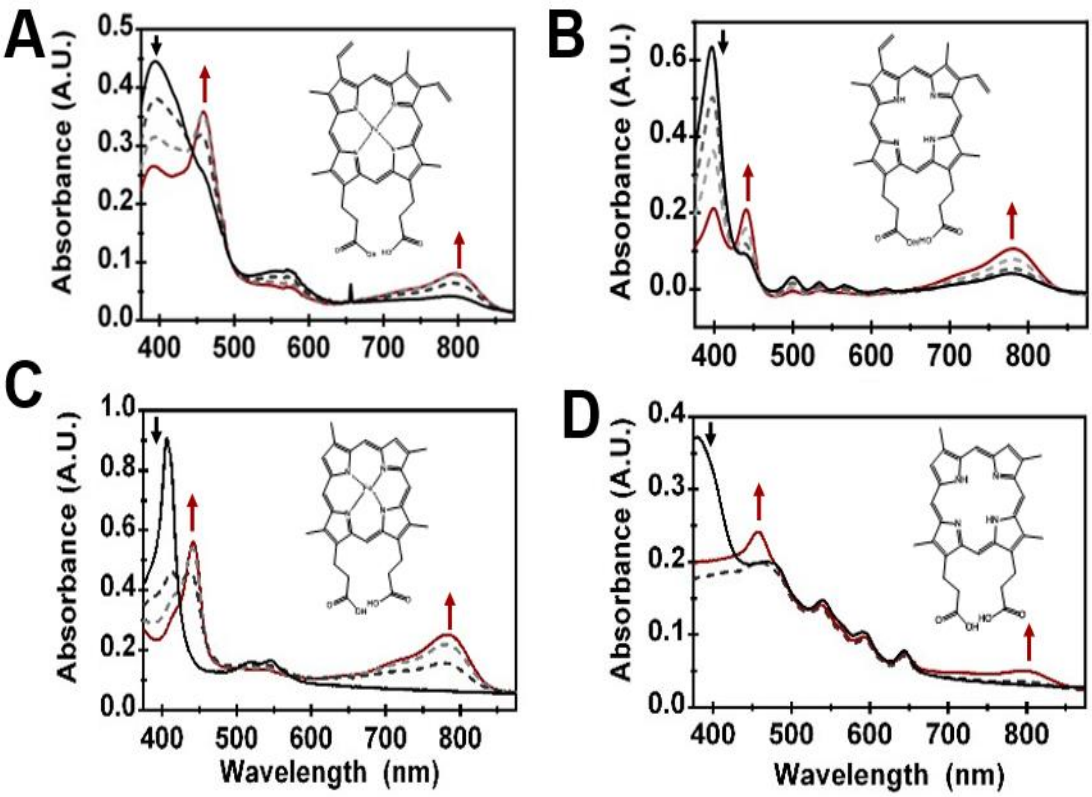
A
B
C
D
Absorbance (A.U.)
Wavelength (nm)
400
500
600
700
800

Figure 3.4

(A) Ion mobility mass spectrometry (IM-MS) of the tetrapyrrole product produced in the HutW reaction and **(B)** MS/MS fragment peaks and some representative fragment structures. Pre- and post-turnover samples were prepared and analyzed by IM-MS as described in Materials and Methods. Comparison of pre- and post-turnover data showed the appearance of a peak at m/z 583.3 (A) that was subjected to fragmentation (B). The five most abundant fragment peaks and structures are labeled (B). One hundred six of the 107 fragments predicted by MetFrag were observed with intensities of >200 counts

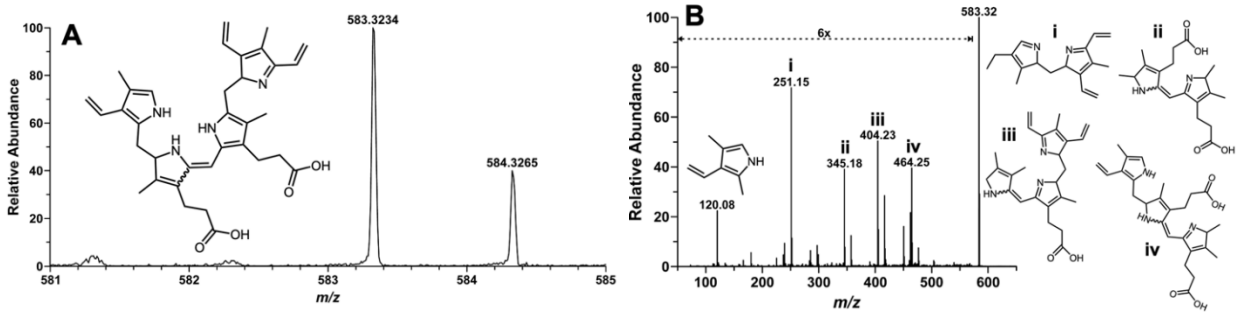
A
583.3234
584.3265
Relative Abundance
m/z
B
6x
583.32
i
251.15
ii
345.18
iii
404.23
iv
464.25
120.08
Relative Abundance
m/z

Figure 3.5

(A) Detection of labile iron and **(B)** SAM turnover products for the dithionite-driven HutW reaction. The total labile iron was measured, and HPLC analysis was performed as described in *Materials and Methods.* **(A)** The labile iron was measured prior to the initiation of the reaction (t = 0) and after 30 min (t = 30). **(B)** HPLC traces showing the chromatogram for some standards (i) and the results of a 90 min assay containing the complete reaction mix (ii) or in the absence of dithionite (iii), the absence of enzyme (iv), the absence of heme (v), and the absence of externally added SAM (vi).

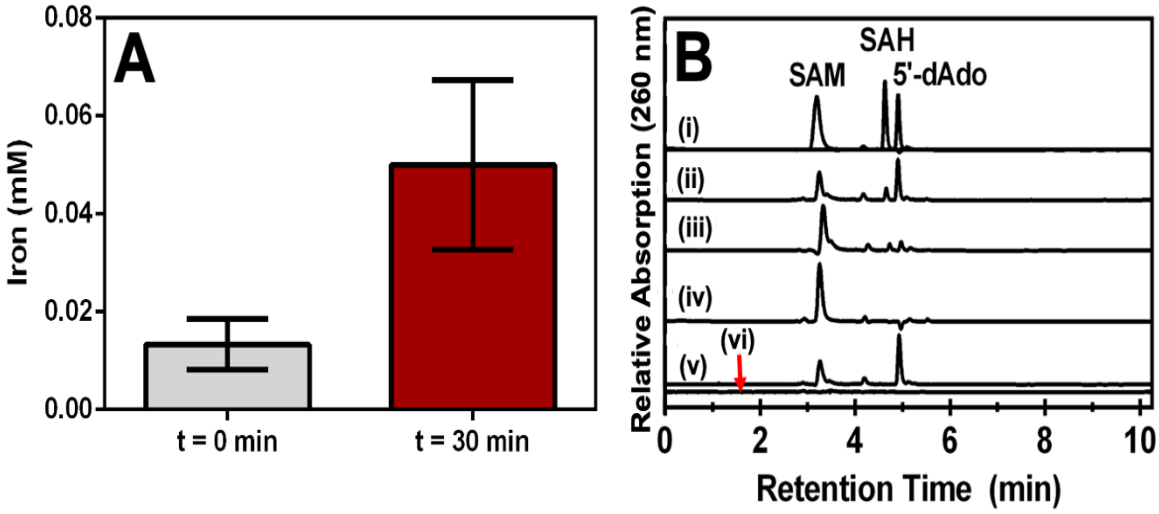
A
Iron (mM)
0.08
0.06
0.04
0.02
0.00
t = 0 min
t = 30 min
B
SAH
SAM
5'-dAdo
(i)
(ii)
(iii)
(iv)
(v)
(vi)
Relative Absorption (260 nm)
0
2
4
6
8
10
Retention Time (min)

Figure 3.6

NADPH-dependent turnover of HutW monitored by following **(A)** the UV−vis spectra and **(B)** changes in the concentration of the labile iron in the assay. Assay conditions were identical to those shown in Figure 3, except that NADPH (10 mM) was used as the reductant instead of sodium dithionite. In addition, the assay was conducted for 30 min, with a scan recorded every 6 min. The assay was performed as described in Materials and Methods to include HutW (10 μM) and heme (20 μM) and initiated by the addition of SAM (1 mM).

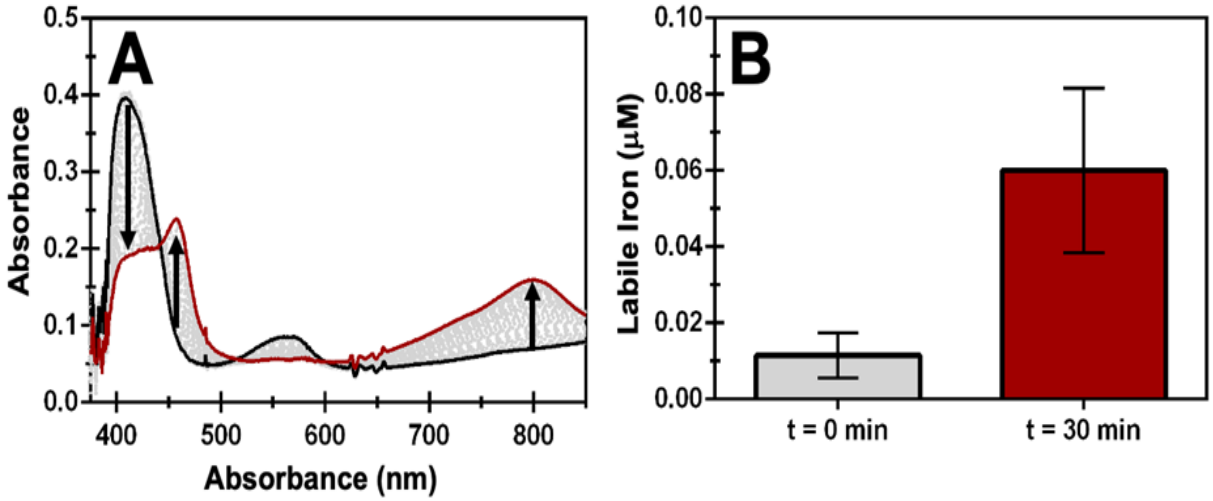
A
Absorbance
0.5
0.4
0.3
0.2
0.1
0.0
400
500
600
700
800
Absorbance (nm)
B
Labile Iron (μM)
0.10
0.08
0.06
0.04
0.02
0.00
t = 0 min
t = 30 min

Figure 3.7

Ion mobility mass spectrometry (IM-MS) of tetrapyrrole product produced in the NADPH-dependent HutW reaction. The NADPH dependent assay was performed and subjected to IM-MS as described in Materials and Methods. Similar to the dithionite-driven assay (Figure 4), a strong peak at m/z 583.3 appeared in the post-turnover sample.

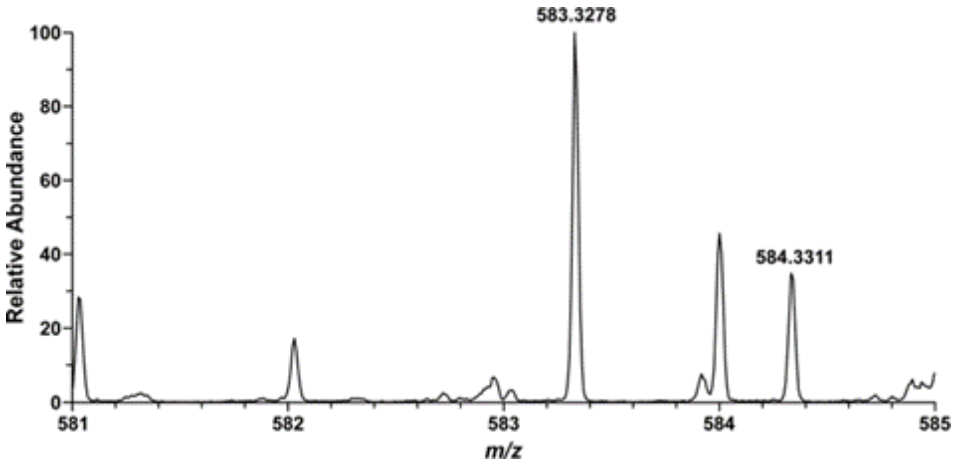
583.3278
584.3311
100
80
60
40
20
0
Relative Abundance
581
582
583
584
585
m/z

Figure 3.8

HPLC analysis of the NADPH-driven turnover reaction of HutW. HPLC analysis was performed as described in Materials and Methods. Traces show the chromatogram for standards (i), and the results of an overnight assay containing the complete reaction mix (ii) or in the absence of NADPH (iii), the absence of enzyme (iv), the absence of heme (v), and the absence of externally added SAM (vi).

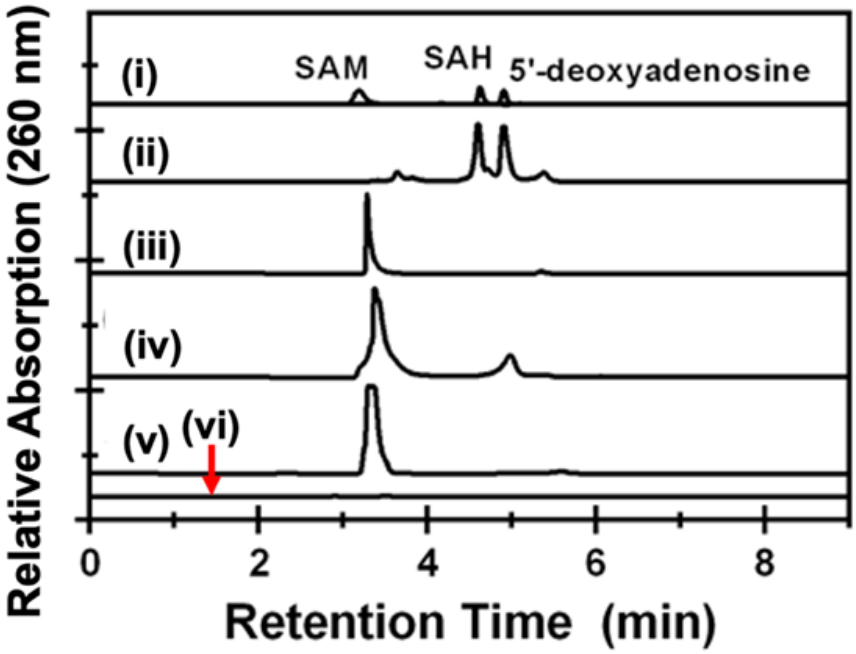
Relative Absorption (260 nm)
(i)
SAM
SAH
5'-deoxyadenosine
(ii)
(iii)
(iv)
(v)
(vi)
0
2
4
6
8
Retention Time (min)

Supplementary Figure 3.1

UV-visible spectrum of “as-isolated” HutW (10 μM).

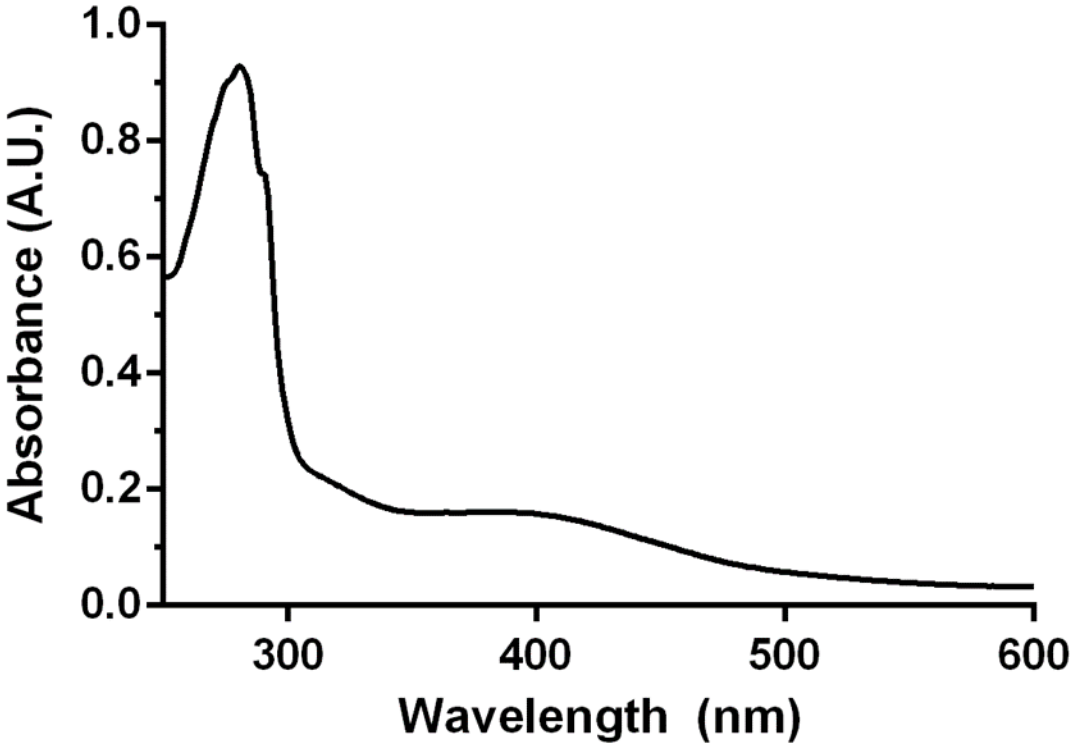
1.0
0.8
0.6
0.4
0.2
0.0
Absorbance (A.U.)
300
400
500
600
Wavelength (nm)

Supplementary Figure 3.2

Plot showing the relative elution volume of purified HutW (Blue Circle) relative to various protein standards (Black Circles) on a calibrated size exclusion column.

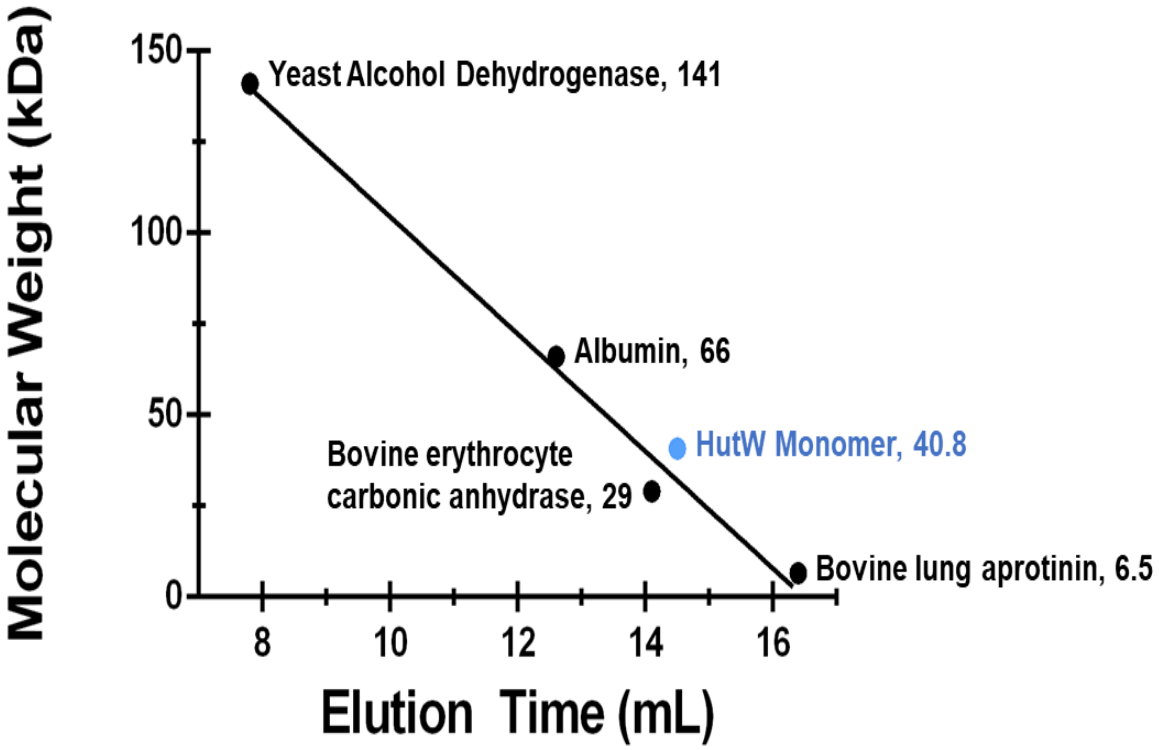
Molecular Weight (kDa)
150
100
50
0
Yeast Alcohol Dehydrogenase, 141
Albumin, 66
HutW Monomer, 40.8
Bovine erythrocyte
carbonic anhydrase, 29
Bovine lung aprotinin, 6.5
8
10
12
14
16
Elution Time (mL)

Supplementary Figure 3.3

Progress curves for the turnover of heme by HutW when either sodium dithionite **(Panels A & B)** or NADPH **(Panel C & D)** is utilized as the reductant. Panels A & C show the decrease in absorbance at 402nm, indicative of heme degradation while Panels B & D follow the increase in absorbance at 795nm, indicative of product formation.

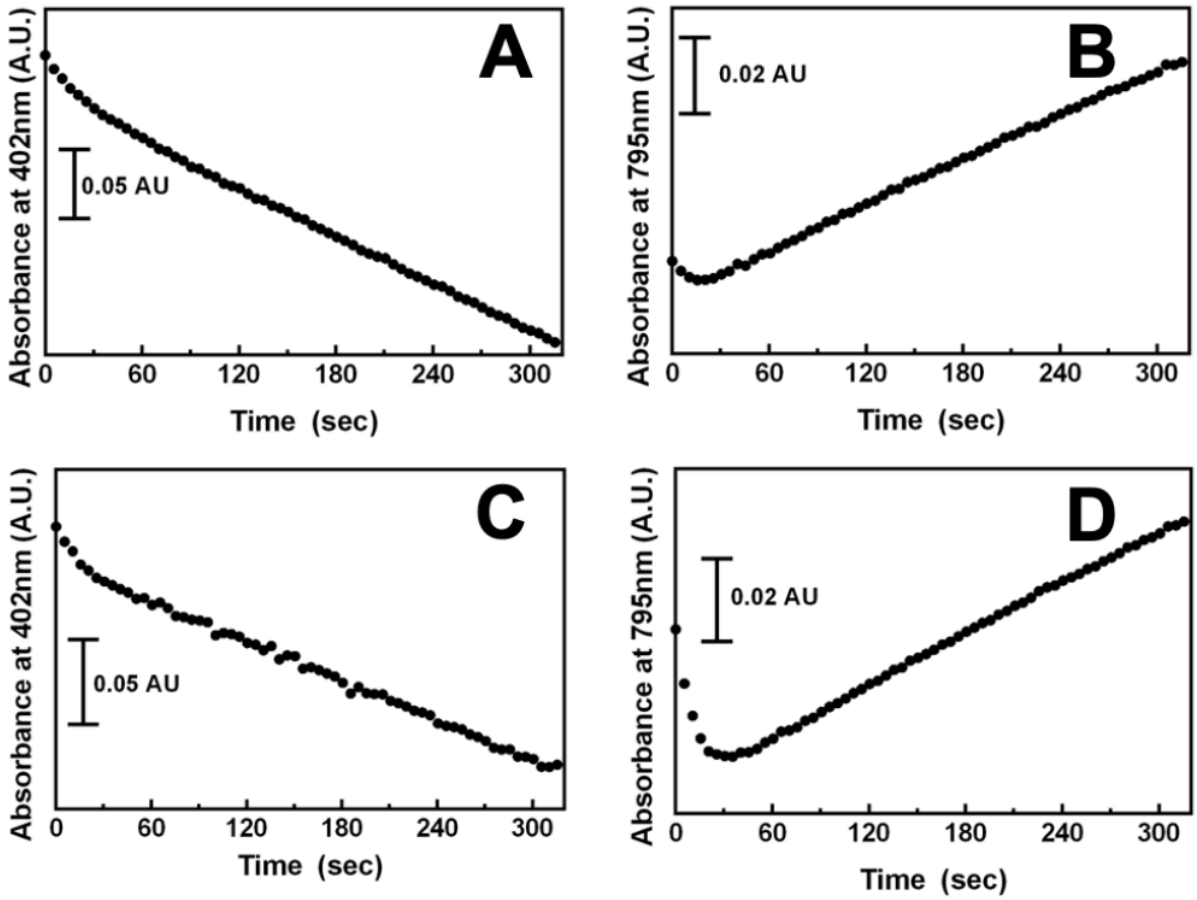
A
Absorbance at 402nm (A.U.)
0.05 AU
0
60
120
180
240
300
Time (sec)
B
Absorbance at 795nm (A.U.)
0.02 AU
0
60
120
180
240
300
Time (sec)
C
Absorbance at 402nm (A.U.)
0.05 AU
0
60
120
180
240
300
Time (sec)
D
Absorbance at 795nm (A.U.)
0.02 AU
0
60
120
180
240
300
Time (sec)

Supplementary Figure 3.4

UV-visible absorbance spectra monitoring the anaerobic degradation of mesoheme using either sodium dithionite **(Panel A)** or NADPH **(Panel B)** as the reductant. Coproporphyrin III degradation using sodium dithionite **(Panel C)** or NADPH **(Panel D)** as the reductant is also shown. Assays were performed as described in the Materials and Methods and spectral changes were recorded every 2 minutes for 8 minutes. Arrows indicate the direction of spectral changes during the assay, with the initial scan being the solid black line, and the final scan (at 8 minutes) the red line.

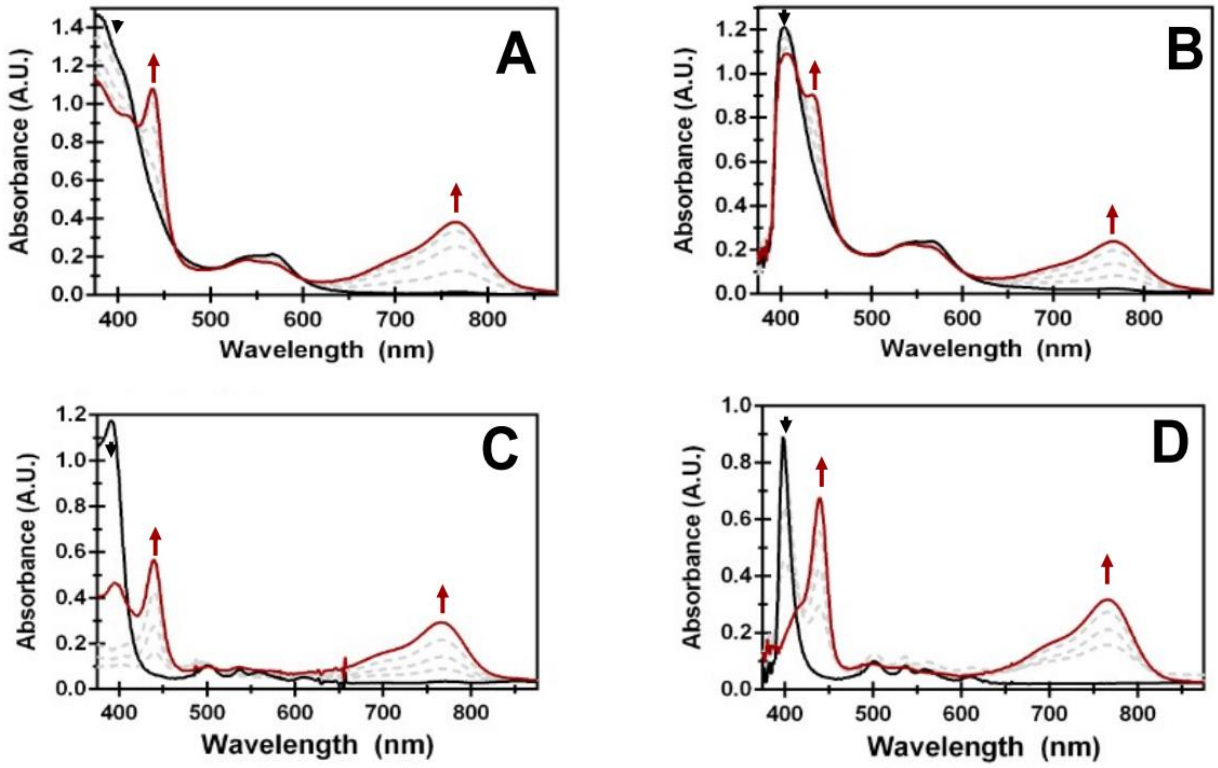
A
B
C
D
Absorbance (A.U.)
Wavelength (nm)
400
500
600
700
800

Supplementary Figure 3.5

Raw MS and MS/MS data **(Panel A)** as well as information on the 106 (of 107) fragments that were observed **(Panels B-J)** with greater than 200 counts. Fragments were predicted by the MetFrag software (https://msbi.ipb-halle.de/MetfragBeta).

A

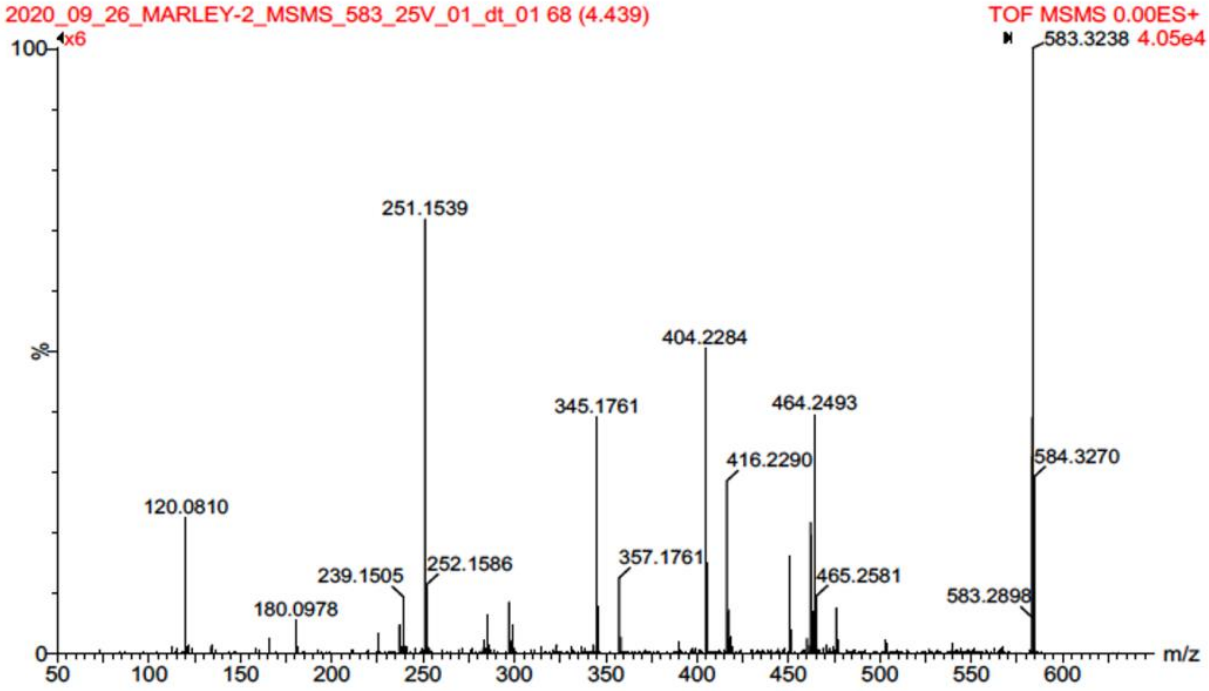
2020_09_26_MARLEY-2_MSMS_583_25V_01_dt_01 68 (4.439)
TOF MSMS 0.00ES+
x6
583.3238 4.05e4
100
%
0
251.1539
404.2284
345.1761
464.2493
416.2290
584.3270
120.0810
239.1505
252.1586
357.1761
465.2581
583.2898
180.0978
50
100
150
200
250
300
350
400
450
500
550
600
m/z

B

Precursor

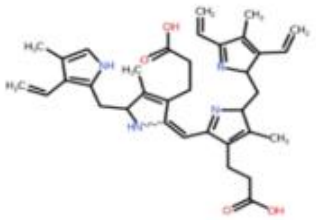

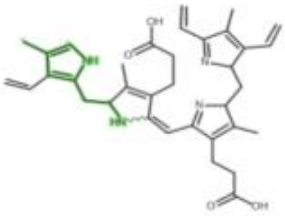

Fragment 1

Formula [C7H9N2-H]+
Mass 120.06823
Peak m/z 120.0733

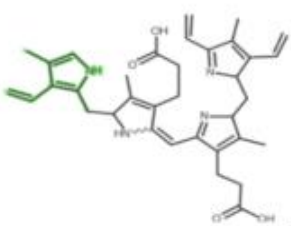

Fragment 2

Formula [C8H10N]+
Mass 120.08082
Peak m/z 120.0771

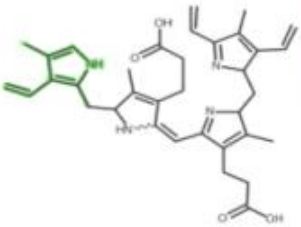

Fragment 3

Formula [C8H10N]+
Mass 120.08082
Peak m/z 120.081

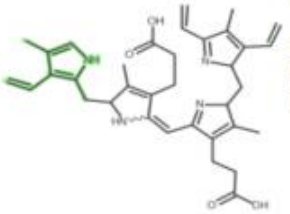

Fragment 4

Formula [C8H10N]+
Mass 120.08082
Peak m/z 120.0848

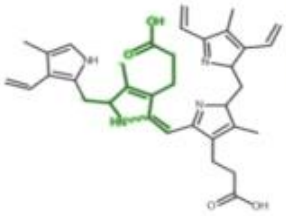

Fragment 5

Formula [C10H13NO2]+H+
Mass 180.10196
Peak m/z 180.0978

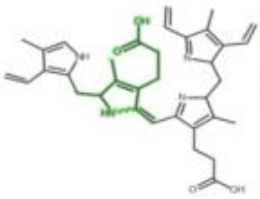

Fragment 6

Formula [C10H13NO2]+H+
Mass 180.10196
Peak m/z 180.1026

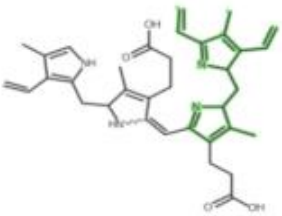

Fragment 7

Formula [C15H16N2]+H+
Mass 225.1387
Peak m/z 225.1334

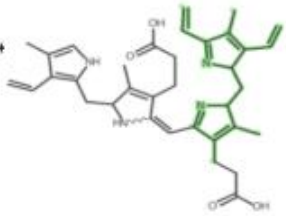

Fragment 8

Formula [C16H18N2-H]+
Mass 237.1387
Peak m/z 237.1306

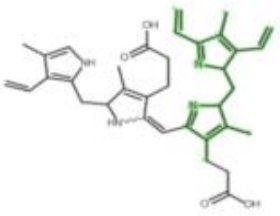

Fragment 9

Formula [C16H18N2-H]+
Mass 237.1387
Peak m/z 237.1361

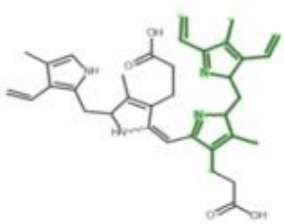

Fragment 10

Formula [C16H18N2-H]+
Mass 237.1387
Peak m/z 237.1415

C

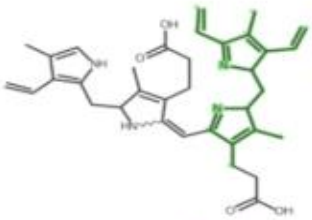

Fragment 11

Formula [C16H18N2]+H+
Mass 239.15436
Peak m/z 239.1451

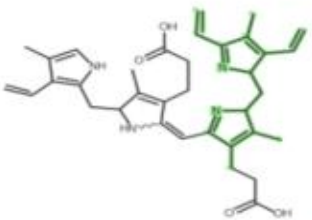

Fragment 12

Formula [C16H18N2]+H+
Mass 239.15436
Peak m/z 239.1505

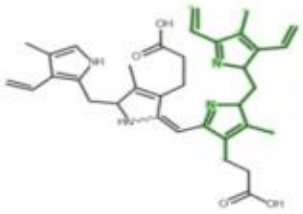

Fragment 13

Formula [C16H18N2]+H+
Mass 239.15436
Peak m/z 239.1559

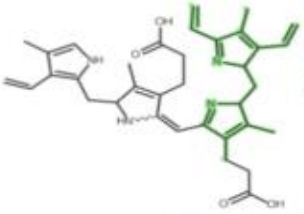

Fragment 14

Formula [C16H18N2]+H+
Mass 239.15436
Peak m/z 239.1614

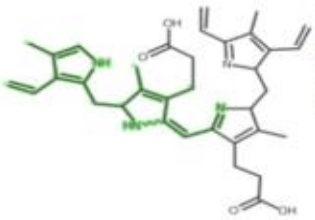

Fragment 15

Formula [C16H18N3-H]+
Mass 251.14177
Peak m/z 251.1371

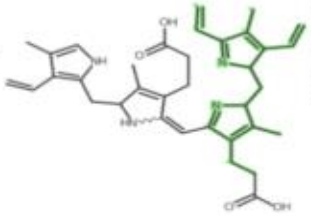

Fragment 16

Formula [C17H20N2-H]+
Mass 251.15436
Peak m/z 251.1427

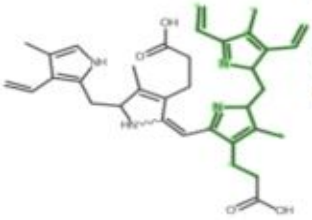

Fragment 17

Formula [C17H20N2-H]+
Mass 251.15436
Peak m/z 251.1483

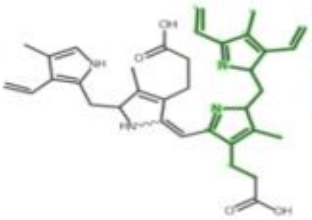

Fragment 18

Formula [C17H20N2-H]+
Mass 251.15436
Peak m/z 251.1539

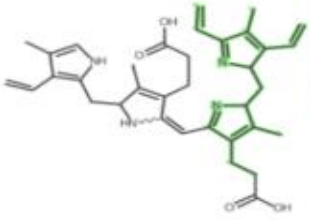

Fragment 19

Formula [C17H20N2-H]+
Mass 251.15436
Peak m/z 251.1595

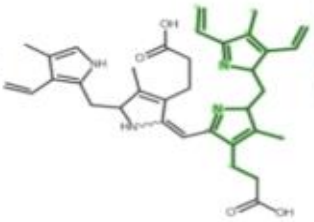

Fragment 20

Formula [C17H20N2-H]+
Mass 251.15436
Peak m/z 251.165

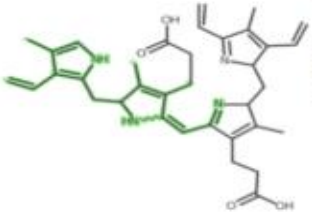

Fragment 21

Formula [C16H18N3]+
Mass 252.1496
Peak m/z 252.1474

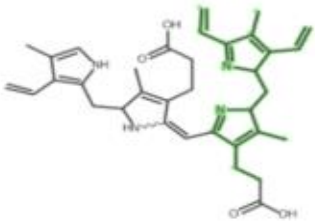

Fragment 22

Formula [C17H20N2]+
Mass 252.16219
Peak m/z 252.153

D

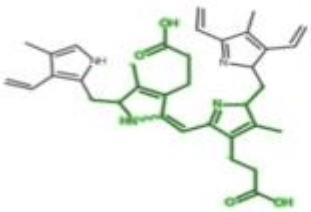

Fragment 35

Formula [C19H24N2O4]+H+
Mass 345.18098
Peak m/z 345.1696

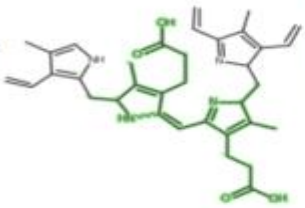

Fragment 36

Formula [C19H24N2O4]+H+
Mass 345.18098
Peak m/z 345.1761

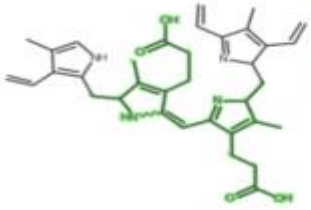

Fragment 37

Formula [C19H24N2O4]+H+
Mass 345.18098
Peak m/z 345.1826

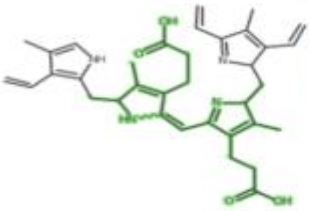

Fragment 38

Formula [C19H24N2O4]+H+
Mass 345.18098
Peak m/z 345.1892

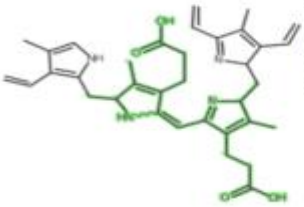

Fragment 39

Formula [C19H24N2O4]+H+
Mass 345.18098
Peak m/z 345.1957

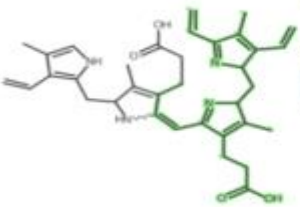

Fragment 40

Formula [C22H24N2O2-2H]+
Mass 346.16767
Peak m/z 346.1705

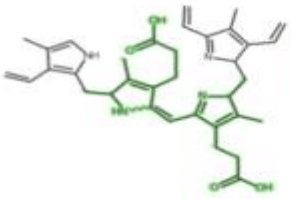

Fragment 41

Formula [C19H24N2O4+H]+H+
Mass 346.18881
Peak m/z 346.177

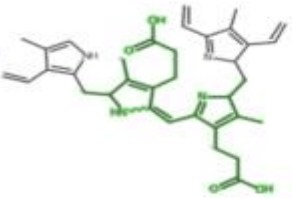

Fragment 42

Formula [C19H24N2O4+H]+H+
Mass 346.18881
Peak m/z 346.1836

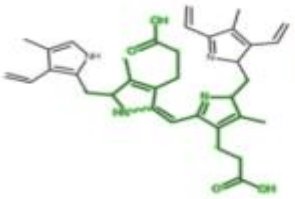

Fragment 43

Formula [C19H24N2O4+H]+H+
Mass 346.18881
Peak m/z 346.1901

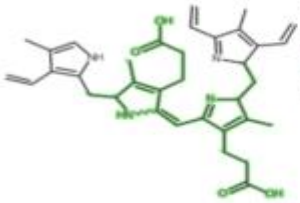

Fragment 44

Formula [C20H25N2O4]+
Mass 357.18098
Peak m/z 357.1628

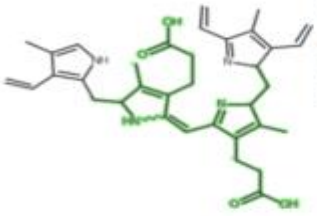

Fragment 45

Formula [C20H25N2O4]+
Mass 357.18098
Peak m/z 357.1694

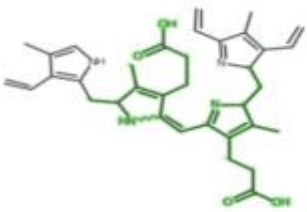

Fragment 46

Formula [C20H25N2O4]+
Mass 357.18098
Peak m/z 357.1761

F

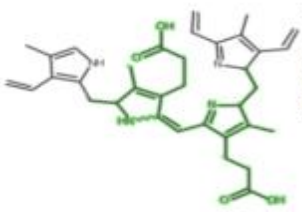

Fragment 47

Formula [C20H25N2O4]+
Mass 357.18098
Peak m/z 357.1827

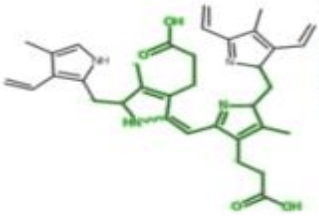

Fragment 48

Formula [C20H25N2O4]+
Mass 357.18098
Peak m/z 357.1894

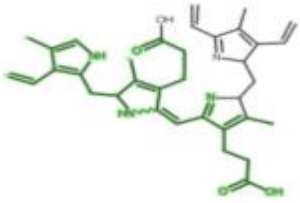

Fragment 49

Formula [C24H28N3O3-2H]+
Mass 404.19697
Peak m/z 404.2071

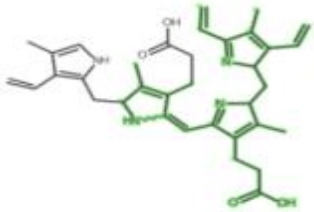

Fragment 50

Formula [C25H29N3O2]+H+
Mass 404.23338
Peak m/z 404.2142

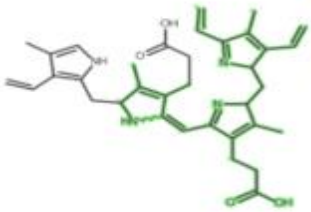

Fragment 51

Formula [C25H29N3O2]+H+
Mass 404.23338
Peak m/z 404.2213

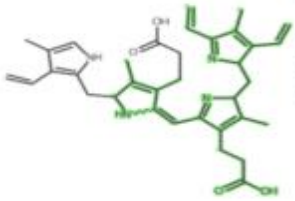

Fragment 52

Formula [C25H29N3O2]+H+
Mass 404.23338
Peak m/z 404.2284

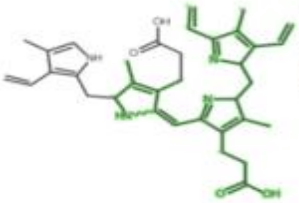

Fragment 53

Formula [C25H29N3O2]+H+
Mass 404.23338
Peak m/z 404.2354

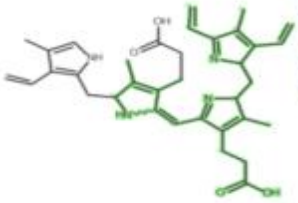

Fragment 54

Formula [C25H29N3O2]+H+
Mass 404.23338
Peak m/z 404.2425

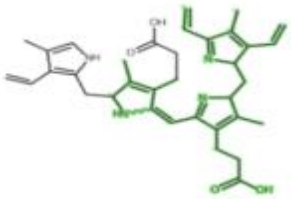

Fragment 55

Formula [C25H29N3O2]+H+
Mass 404.23338
Peak m/z 404.2496

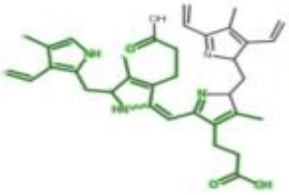

Fragment 56

Formula [C24H28N3O3-H]+
Mass 405.2048
Peak m/z 405.2193

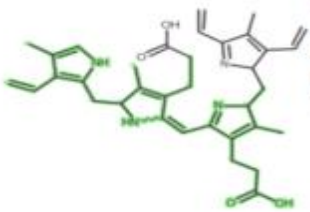

Fragment 57

Formula [C25H31N3O2]+
Mass 405.24121
Peak m/z 405.2264

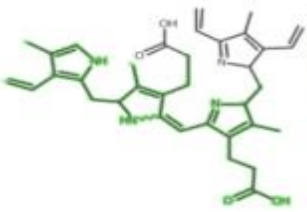

Fragment 58

Formula [C25H31N3O2]+
Mass 405.24121
Peak m/z 405.2335

G

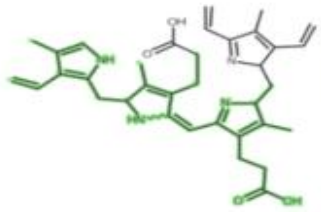

Fragment 59

Formula [C25H31N3O2]+
Mass 405.24121
Peak m/z 405.2406

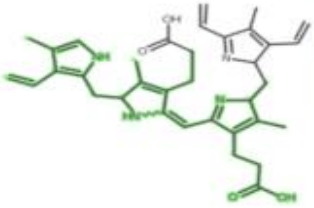

Fragment 60

Formula [C25H31N3O2]+
Mass 405.24121
Peak m/z 405.2477

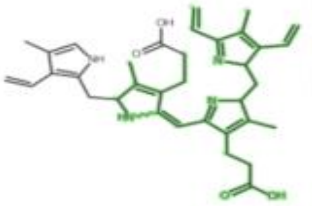

Fragment 61

Formula [C26H31N3O2-H]+
Mass 416.23338
Peak m/z 416.2147

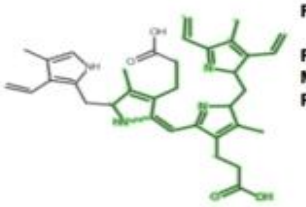

Fragment 62

Formula [C26H31N3O2-H]+
Mass 416.23338
Peak m/z 416.2218

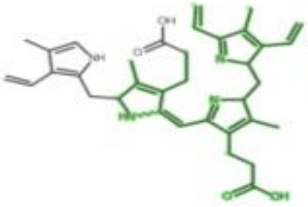

Fragment 63

Formula [C26H31N3O2-H]+
Mass 416.23338
Peak m/z 416.229

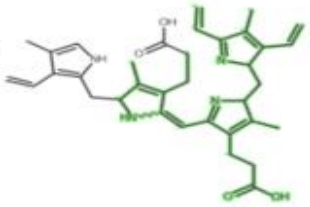

Fragment 64

Formula [C26H31N3O2-H]+
Mass 416.23338
Peak m/z 416.2362

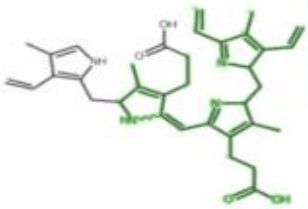

Fragment 65

Formula [C26H31N3O2-H]+
Mass 416.23338
Peak m/z 416.2433

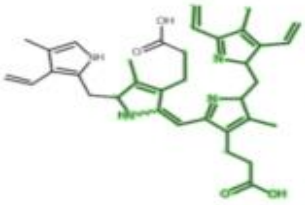

Fragment 66

Formula [C26H31N3O2-H]+
Mass 416.23338
Peak m/z 416.2505

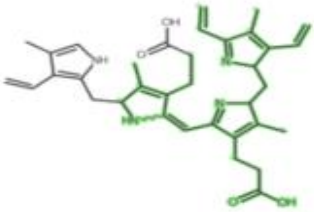

Fragment 67

Formula [C26H31N3O2]+
Mass 417.24121
Peak m/z 417.2202

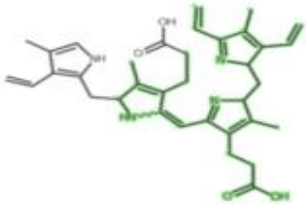

Fragment 68

Formula [C26H31N3O2]+
Mass 417.24121
Peak m/z 417.2274

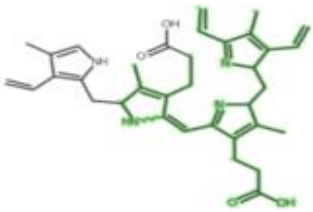

Fragment 69

Formula [C26H31N3O2]+
Mass 417.24121
Peak m/z 417.2346

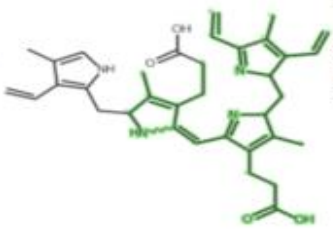

Fragment 70

Formula [C26H31N3O2]+
Mass 417.24121
Peak m/z 417.2418

H

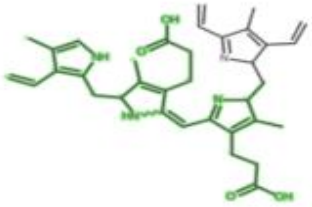

Fragment 71

Formula [C26H32N3O4]+
Mass 450.23886
Peak m/z 450.218

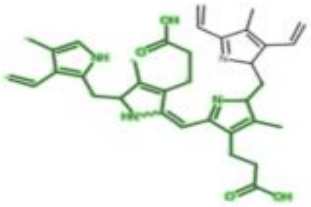

Fragment 72

Formula [C26H32N3O4]+
Mass 450.23886
Peak m/z 450.2255

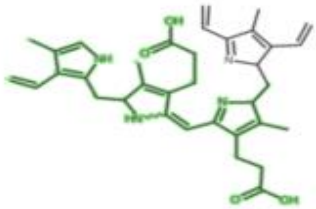

Fragment 73

Formula [C26H32N3O4]+
Mass 450.23886
Peak m/z 450.233

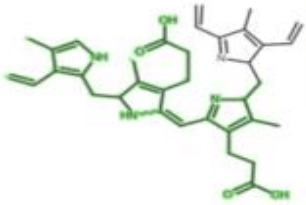

Fragment 75

Formula [C26H32N3O4]+
Mass 450.23886
Peak m/z 450.2479

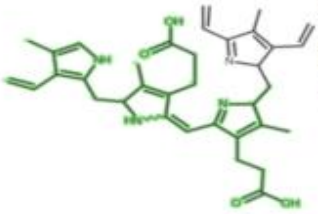

Fragment 74

Formula [C26H32N3O4]+
Mass 450.23886
Peak m/z 450.2404

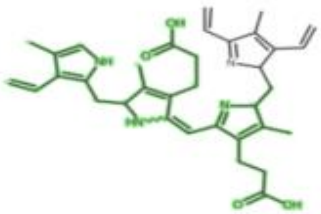

Fragment 76

Formula [C26H32N3O4]+
Mass 450.23886
Peak m/z 450.2554

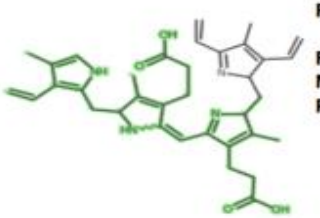

Fragment 77

Formula [C26H32N3O4]+H+
Mass 451.24669
Peak m/z 451.234

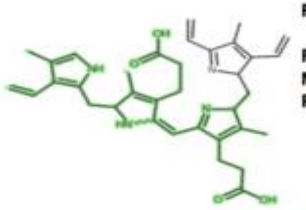

Fragment 78

Formula [C26H32N3O4]+H+
Mass 451.24669
Peak m/z 451.2415

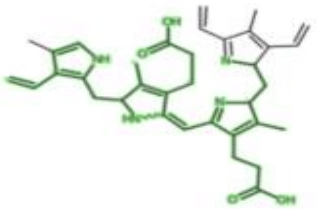

Fragment 79

Formula [C26H30N4O4]+
Mass 462.22627
Peak m/z 462.2122

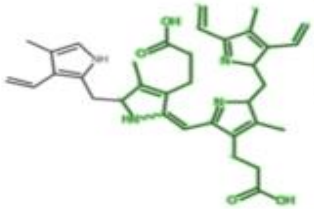

Fragment 80

Formula [C27H32N3O4]+
Mass 462.23886
Peak m/z 462.2198

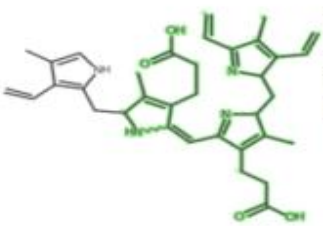

Fragment 81

Formula [C27H32N3O4]+
Mass 462.23886
Peak m/z 462.2274

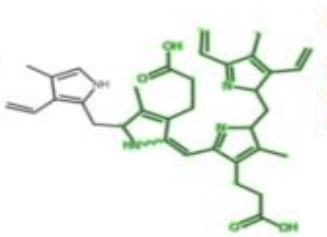

Fragment 82

Formula [C27H32N3O4]+
Mass 462.23886
Peak m/z 462.2349

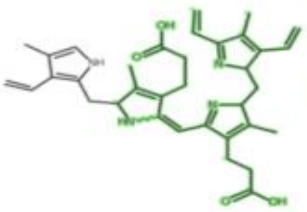

Fragment 83

Formula [C27H32N3O4]+
Mass 462.23886
Peak m/z 462.2425

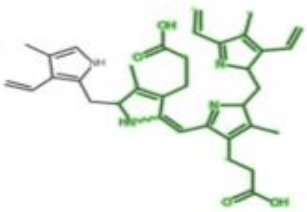

Fragment 84

Formula [C27H32N3O4]+
Mass 462.23886
Peak m/z 462.25

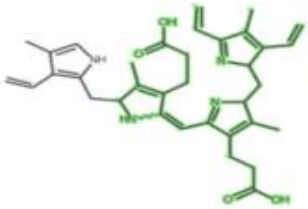

Fragment 85

Formula [C27H32N3O4]+
Mass 462.23886
Peak m/z 462.2576

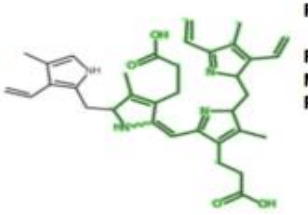

Fragment 86

Formula [C27H32N3O4]+H+
Mass 463.24669
Peak m/z 463.2264

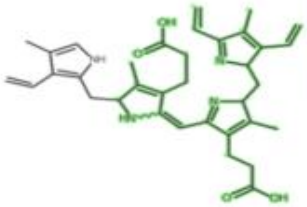

Fragment 87

Formula [C27H32N3O4]+H·
Mass 463.24669
Peak m/z 463.234

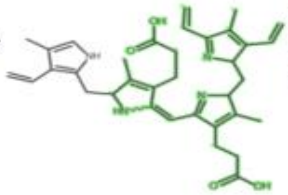

Fragment 88

Formula [C27H32N3O4]+H+
Mass 463.24669
Peak m/z 463.2415

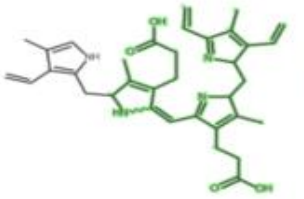

Fragment 89

Formula [C27H32N3O4]+H+
Mass 463.24669
Peak m/z 463.2491

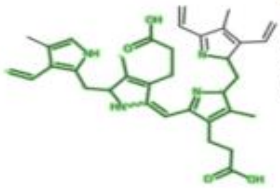

Fragment 90

Formula [C26H30N4O4+H]+H+
Mass 464.24193
Peak m/z 464.2266

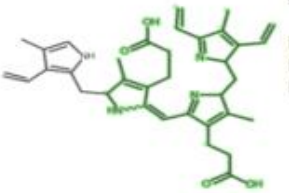

Fragment 91

Formula [C27H32N3O4+H]+H+
Mass 464.25452
Peak m/z 464.2342

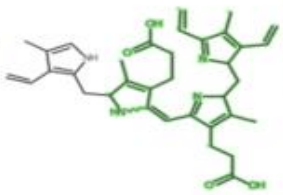

Fragment 92

Formula [C27H32N3O4+H]+H+
Mass 464.25452
Peak m/z 464.2417

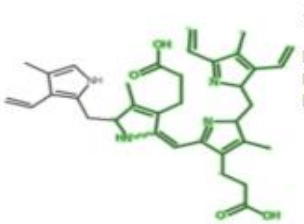

Fragment 93

Formula [C27H32N3O4+H]+H+
Mass 464.25452
Peak m/z 464.2493

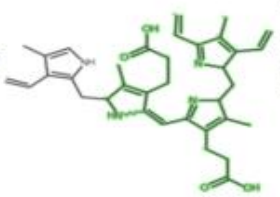

Fragment 94

Formula [C27H32N3O4+H]+H+
Mass 464.25452
Peak m/z 464.2569

J

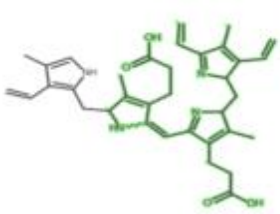

Fragment 95

Formula [C27H32N3O4+H]+H+
Mass 464.25452
Peak m/z 464.2645

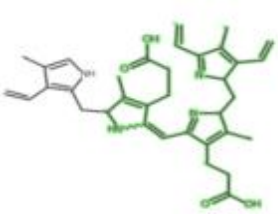

Fragment 96

Formula [C27H32N3O4+H]+H+
Mass 464.25452
Peak m/z 464.272

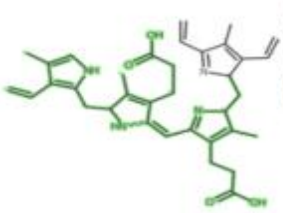

Fragment 97

Formula [C27H33N3O4+H]+H+
Mass 465.26235
Peak m/z 465.243

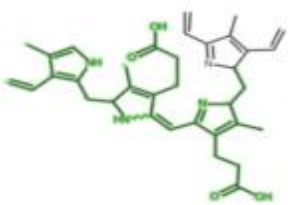

Fragment 98

Formula [C27H33N3O4+H]+H+
Mass 465.26235
Peak m/z 465.2505

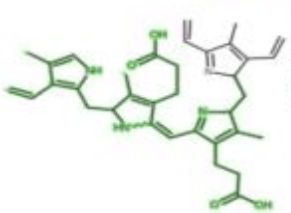

Fragment 99

Formula [C27H33N3O4+H]+H+
Mass 465.26235
Peak m/z 465.2581

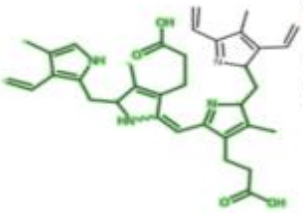

Fragment 100

Formula [C27H33N3O4+H]+H+
Mass 465.26235
Peak m/z 465.2657

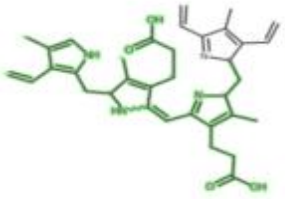

Fragment 101

Formula [C27H33N3O4+H]+H+
Mass 465.26235
Peak m/z 465.2733

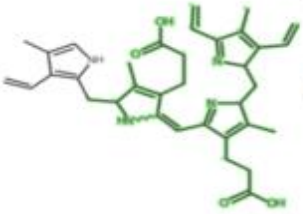

Fragment 102

Formula [C28H34N3O4]+
Mass 476.25452
Peak m/z 476.2357

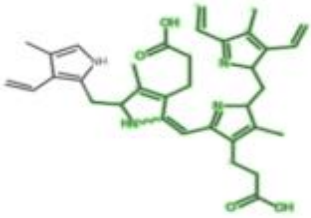

Fragment 103

Formula [C28H34N3O4]+
Mass 476.25452
Peak m/z 476.2434

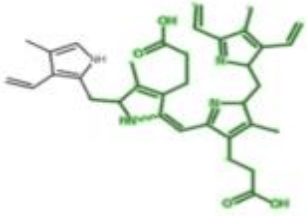

Fragment 104

Formula [C28H34N3O4]+
Mass 476.25452
Peak m/z 476.2511

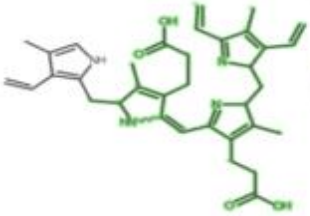

Fragment 105

Formula [C28H34N3O4]+
Mass 476.25452
Peak m/z 476.2588

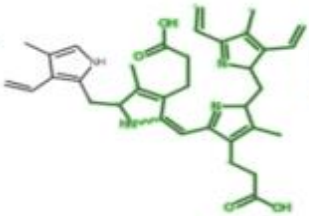

Fragment 106

Formula [C28H34N3O4]+
Mass 476.25452
Peak m/z 476.2664

CHAPTER FOUR

PORPHYRIN-RING-MEDIATED ELECTRON TRANSFER IN A RADICAL SAM ENZYME HUTW[3]

[3]Brimberry, Marley, Corrigan, Patrick, Silakov, Alexey, and Lanzilotta, William.

To be submitted to Biochemistry

ABSTRACT

Bacteria that infect the anaerobic human gut must compete for essential nutrients, including iron. Several enteric pathogens, including *Vibrio cholerae* and *Escherichia coli* O157:H7, have evolved the ability to obtain iron from heme in this environment. Our laboratory has demonstrated that a radical *S*-adenosylmethionine (SAM) methyltransferase (RSMT) is responsible for opening of the porphyrin ring and releasing iron from heme. Interestingly, the enzyme in *V. cholerae*, HutW, has recently been shown to utilize NADPH directly when SAM is utilized to initiate the reaction. However, how NADPH, a hydride donor, catalyzes the single electron reduction of a [4Fe-4S] cluster was not addressed. In this work we provide evidence that the porphyrin ring, and/or the subsequent tetrapyrrole intermediate, is facilitating electron transfer from NADPH to the [4Fe-4S] cluster. This study adds to the growing body of work in radical SAM enzymology, and further expands the repertoire of electron transfer pathways being identified in these enzymes.

INTRODUCTION

Several pathogenic bacteria utilize various iron-acquisition strategies including utilization of heme as an iron source, either as free heme or from various heme-containing proteins.[1,2] Additionally, the regulation of many virulence factors is dependent on iron acquisition from the host.[3–6] It has been established that, once internalized into the bacterium, the iron is liberated from the porphyrin macrocycle through heme oxygenase-type enzymes that catalyze the regiospecific conversion of heme into biliverdin IXα, CO, and free iron. However, the diversity of aerobic heme degrading enzymes has significantly expanded with the discovery of the noncanonical enzymes IsdG and IsdI from *Staphylococcus aureus* as well as MhuD from *Mycobacterium tuberculosis*.[7,8] In addition to these aerobic heme degrading enzymes, research has shown that pathogens such as the enterohemorrhagic *Escherichia coli* O157:H7 and *Vibrio cholera* encode radical *S*-adenosylmethionine (SAM) enzymes that liberate iron from heme under anaerobic conditions.[9–11] The radical SAM (RS) enzyme in *E. coli* O157:H7, ChuW, is responsible for opening the porphyrin ring through a radical mechanism. A second enzyme, ChuY, is a NADPH-dependent reductase that reduces the tetrapyrrole product of ChuW.[12] However, unlike the organism *E. coli* O157:H7, *V. cholera* does not an enzyme homologous to ChuY. In contrast, we have shown that the RS enzyme HutW can catalyze anaerobic ring-opening as well as tetrapyrrole reductions.[13] The observation of direction reduction by NADPH is significant for several reasons, discussed below.

Members of the RS enzyme superfamily are characterized by their [4Fe-4S] cluster coordinated by a cysteine rich motif, typically CxxCxxC.[14–16] Three of the iron ions in the cluster are ligated by the conserved cysteine resides in the motif while the remaining iron ligates the α-

amino and α-carboxy moieties of SAM in the catalytic complex[17–31]. Reductive cleavage of SAM by the [4Fe-4S] cluster (formally in the +1 oxidation state) results in the formation of methionine and a 5′-deoxyadenosyl radical (dAdo•). Mechanistically, this has been proposed to proceed through an organometallic intermediate.[15,16,32–34] RS enzymes are further classified by their domain structure and chemical transformation. As such, both HutW and ChuW are further identified as class C RS methyltransferases (RSMTs), that utilize SAM as a methyl donor in addition to using SAM for radical generation.[35–37] In general, class C RSMTs have been shown to methylate an inert sp^2-hybridized carbon or phosphorus center. Other RSMTs target different substrates and each class employs a distinct cofactor/cosubstrate ensemble.[37–39] The anaerobic heme degrading enzymes HutW and ChuW have been shown to utilize two molecules of SAM, in a mechanism that has presumable evolved from HemN.[36] The first SAM molecule is reductively cleaved by the iron-sulfur cluster to yield the 5′-deoxyadenosyl radical (5′-dAdo•), which rapidly abstracts a hydrogen atom from the second molecule of SAM to produce a methylene radical, a common intermediate for the class C RSMTs.[10,11] For both enzymes, the methylene radical has been proposed to add to a double bond specifically, the bridging carbon atom at the *meso* position of the porphyrin ring, resulting in β-scission of the carbon-carbon bond and liberation of the iron atom.[13,40,41] While these two enzymes do share a mutual mechanistic framework, there are several noteworthy differences including the electron source and tetrapyrrole product. In *E. coli*, the flavodoxin/flavodoxin reductase system with NADPH was able to be employed as the electron source.[40,41] Neither *E. coli* flavodoxin nor *V. cholerae* flavodoxin was able to reconstitute activity in HutW. Instead, we demonstrated that HutW could employ NADPH as a sole electron source, when the reaction is initiated by addition of SAM, resulting in opening of the porphyrin ring.

Furthermore, when NADPH is the reductant, the product of HutW has been shown to be a more reduced tetrapyrrole by comparison to the product of the ChuW reaction.[9,10,13,35,36]

The source of electrons has been shown to influence the catalytic mechanism of some RS enzymes, underscoring the importance of the redox partner in RS enzyme mechanism.[42–44] Interestingly, the enzyme MiaB comes from the organism *Thermatoga maritima*, an organism containing no flavodoxin homologs but five ferredoxins with a ferredoxin-NADP+ oxidoreductase that support the RS enzymatic activity.[45,46] Additionally, recent work by Young and Bandarian has shown that *Saccharomyces cerevisiae* TYW1 contains a flavodoxin-like domain that co-purifies with FMN bound, indicating that a redox domain is built into this enzyme.[47] These researchers further showed that *Sc*TYW1 was active with either nicotinamide cofactor.[47] These observations, when considered in light of NADPH-dependent reduction of HutW, are reminiscent of the family of cytochrome P450s. In particular, genomic sequencing of P450s has shown that in addition to the two major classes of P450 redox partners, there are specific electron delivery domains as well as P450s that react directly with hydrogen peroxide or NAD(P)H to facilitate oxidative or reductive catalysis.[48] P450s that have evolved to function without the use of redox partners are the CYP55A P450 subfamily of enzymes, including the prototype enzyme CYP55A1 (P450nor) from the fungus *Fusarium oxysporum* .[49,50] We propose that, similar to cytochrome P450s, RS enzymes have evolved diverse mechanisms for electron transfer that include enzymes linked to their partner machinery as well as domains that may bypass the requirement for a particular redox partner.

In this work, we further investigate the mechanism of electron transfer in the anaerobic heme degrading enzyme HutW. Evidence is presented that indicates the porphyrin ring is essential to electron transfer from NADPH to the [4Fe-4S] cluster. Given that several enteric pathogens encode “W”-type enzymes, with or without the requisite reductase proteins, these data may provide

insight into an emerging class of RS enzyme.[14,51,52] Moreover, further characterization of the heme degradation strategy in *V. cholera* will illuminate unexplored avenues for antimicrobial development in multiple enteric pathogens. This is underscored by the observation that these catabolic pathways are critical for infection and virulence, but not necessarily for survival outside a host, where it is less likely that poor antibiotic stewardship will exacerbate resistance. Finally, methods that reduce bacterial colonization will slow resistance development by exerting less selective evolutionary pressure on the bacteria.[53]

RESULTS AND DISCUSSION

Reduction of the [4Fe-4S] cluster in HutW. A common mechanistic theme for all RS enzymes is that reductive cleavage of SAM requires the [4Fe-4S] cluster to be in the reduced (formally 1+) state. Moreover, an intriguing observation is that the source of electrons can influence the chemistry of RS enzymes and therefore electron transfer to the catalytic cluster, as well as subsequent electron/proton transfer steps, are of considerable interest towards understanding the mechanism of RS enzymes.[44]

The UV-visible spectrum for reconstituted HutW (100 μM) is shown in Figure 1, Panel A and reveals a broad shoulder from 400 to 420 nm, consistent with the presence of an oxidized (formally 2+) [4Fe-4S] cluster. The addition of a 10X molar excess of either sodium dithionite (dashed line) or 5X molar excess of NADPH (dotted line) shows a bleaching of this feature, consistent with reduction of the [4Fe-4S] cluster in the presence of either reductant. Notably, sodium dithionite appears to result in a greater decrease in the adsorption in the 400-420 nm range compared to the change seen with NADPH (Figure 1, Panel A). These data indicate that both sodium dithionite and NADPH can reduce the [4Fe-4S] cluster. Moreover, consistent with a greater reduction in absorption, sodium dithionite appears to reduce considerably more of the

cluster population. This hypothesis was investigated further by employing electron paramagnetic resonance (EPR) to monitor the redox state of the [4Fe-4S] cluster in the "as purified" enzyme as well as following the addition of sodium dithionite or NADPH (Figure 1, Panel B). Similar to the changes in the UV-visible spectra, the EPR spectra confirmed that reduction of the [4Fe-4S] cluster in the as-isolated HutW is occurring when either sodium dithionite or NADPH are present. However, upon closer examination of the UV-visible spectra with and without sodium dithionite, we noticed additional spectroscopic changes that are consistent with the reduction of a minor population of heme (Figure 2). Specifically, at the higher protein concentrations (100 μM), we observe a shift from a broad absorbance at 420 nm to a distinct peak at 422 nm, indicative of a major γ Soret (Figure 2, Panel A). Similarly, longer wavelength features also appeared when excess dithionite was added, as evidence by the appearance of a β peak at approximately 532 nm and a α peak at 560 nm (Figure 2 Panel B). Since the HutW in these experiments is that of that of freshly isolated and reconstituted enzyme, these data indicate that a small fraction of heme has remained tightly bound to the protein during purification. Likewise, the observed changes in the Soret peak and Q-bands, upon addition of dithionite, are consistent with reduction of heme and are characteristic of iron in a hexacoordinate complex, likely with two strong axial ligands.[54,55] These observations indicate that some heme is indeed co-purifying with HutW, a phenomena that has been observed for other heme or tetrapyrrole binding proteins.[56,57] Finally, this observation is important because there is precedent for electron transfer from NADPH facilitated through the porphyrin ring.[50,58,59]

NADPH substrate saturation. A high affinity for heme has been reported for HutW, but the binding constant for NADPH has not been investigated.[11,35] To investigate the affinity of NADPH for HutW, we determined the substrate saturation kinetics (K_M^{app}) and found HutW to

bind NADPH with a K_M^{app} of 7.3 ± 1.1 mM (Supplemental Figure 1). While we acknowledge that this is not a high affinity, it is consistent with what was observed for P450nor and NADPH, that had a K_M^{app} of approximately 4 mM.[60] Additionally, it indicates that HutW displays saturable kinetics with NADPH. In addition, given that cytoplasmic NADPH concentrations have been estimated to be anywhere from 0.31 to 22 mM, depending upon cellular conditions,[61,62] it is reasonable to propose that HutW may utilize NADPH as an electron source when inhabiting an anaerobic environment in the gut.

Preparation of heme-stripped HutW. To address the possibility that heme co-purifying with HutW and facilitating electron transfer from NADPH to the [4Fe-4S] cluster, we subjected the enzyme to additional purification steps that would remove any tightly bound heme. One such additional purification step includes treatment with apo-hemoglobin and apo-myoglobin that had been prepared as described previously.[63] Previous work has shown that bound heme can be removed by incubating the protein of interest with apo-hemoglobin, and/or apo-myoglobin, because of their high affinity for heme.[64] Purified HutW, containing an intact [4Fe-4S] cluster, was treated in this manner and is referred to as heme-stripped HutW.

Reduction of the [4Fe-4S] cluster in heme-stripped HutW. To establish if heme may be facilitating reduction of the cluster, increasing amounts of NADPH were injected into a protein sample of either HutW or heme-stripped HutW and the absorption changes were recorded (Figure 3). The as-purified enzyme shows a reduction in the absorbance of the iron-sulfur cluster within the 400-420 nm range (Figure 3, Panel A) when increasing amounts of NADPH are titrated. However, for heme-stripped HutW, the decrease in absorption upon the addition of NADPH, was substantially less (Figure 3, Compare Panel A and Panel B). These data indicate that less reduction has occurred and is consistent with the proposal that the porphyrin ring of heme is facilitating

electron transfer from NADPH to the [4Fe-4S] cluster. To validate our UV-visible absorbance results with the heme-stripped HutW, and further address the oxidation state of the [4Fe-4S] cluster when NADPH, or sodium dithionite are present, we turned to EPR. As a reminder Figure 1, Panel B, shows the EPR spectra for the $[4Fe\text{-}4S]^{+}$ cluster of HutW, following the addition of sodium dithionite and has a broad signal centered at a *g* of 2.01, as previously reported.[11] To address whether the adventitiously bound heme was mediating electron transfer from NADPH to the [4Fe-4S] cluster, we analyzed heme-stripped HutW sample. The EPR spectra indicate that sodium dithionite is still capable of reducing the [4Fe-4S] cluster in heme-stripped HutW (Figure 4, Panel A, trace 2). In contrast, the addition of NADPH to the same sample of heme-stripped HutW did not result in any reduction of the [4Fe-4S] cluster (Figure 4, Panel B, trace 3). In fact, reduction of the cluster by NADPH was only rescued if heme was added back to the sample (Figure 4, Panel C). This further supports our hypothesis that the porphyrin ring, and potentially a tetrapyrrole intermediate, is mediating NADPH-dependent reduction of the Fe-S cluster in HutW.

NAD(P)H reduction of heme has been shown for hemoglobin and myoglobin, and we propose a similar mechanism in HutW, where the reduction of the [4Fe-4S] cluster reduction is mediated through electron transfer from NADPH through the heme porphyrin ring, and ultimately to the [4Fe-4S] cluster.[65] Overall, similar to what has been reported for P450nor, these results support a role for the porphyrin ring in mediating electron transfer and alleviating the requirement for a system-specific redox protein. This adaptation potentially facilitates a quicker response to the metabolic needs of the cell.

CONCLUSIONS

A common mechanistic feature of all RS enzymes is the requirement for reduction of a [4Fe-4S] catalytic cluster from its resting state of +2 to the active state of +1.[16,66] The requisite

reduction of the [4Fe-4S] cluster prior to catalysis has been shown to be mediated through a variety of redox-active partner proteins.[42,43,46] Therefore, the discovery that NADPH would function as a direct electron source and catalyze ring opening as well as subsequent reduction of the tetrapyrrole product was surprising, but not unprecedented in the context of what is known about heme-dependent enzymes. Specifically, in addition to examples in the literature of NADPH reduction of heme in hemoglobin and/or myoglobin, direct electron transfer from NADPH to heme has also been observed for the CYP55A1 cytochrome P450s.[58,59,67,68]

NADPH reduction of HutW and subsequent reduction of the porphyrin intermediate/product, however, does present some additional challenges. In particular, at least two distinct electron transfer pathways must exist. Since NADPH is a hydride donor, one low potential electron must go to the [4Fe-4S] cluster while the second electron and a proton are transferred to the intermediate, as shown in Scheme 1. It is important to point out that the reduction or oxidation of a radical intermediate is another common step in all RS mechanisms. In this case, the substrate, and intermediate are the electron transfer conduit. The properties of the porphyrin macrocycle change as the heme is converted to iron and the methylated tetrapyrrole intermediate, yet both states (porphyrin and tetrapyrrole) could facilitate electron/proton transfer as shown in Scheme 1.

In the case of HutW, the current paradigm holds that SAM and heme binding occur prior to NADPH binding, avoiding the potential for radical generation in the absence of substrate. In the presence of heme, a single electron from NADPH leads to reduction of the [4Fe-4S] cluster with the subsequent reductive cleavage of the first SAM molecule and generation of the transient 5'-deoxyadenosyl radical (5'-dAdo•). Abstraction of a hydrogen atom from the second SAM molecule leads to transient formation of a methylene radical (Scheme 2), an intermediate postulated to be common to all Class C RSMTs. Addition of the methylene radical set-in motion

a radical rearrangement and β-scission of a carbon-carbon bond at the *meso* position of the porphyrin macrocycle. As is the case for all radical intermediates in RS enzyme mechanism, an oxidation or reduction, accompanied by proton transfer, must occur to resolve the radical. The direct utilization of NADPH (Scheme 1) is intriguing as the bifurcation of one electron to the cluster, conveniently, leaves a second electron and proton available to resolve the radical on the tetrapyrrole intermediate. In addition, HutW is expressed on an operon that is upregulated when the bacterium is in Fe-limiting conditions along with several other proteins that have been proposed to function in heme acquisition (HutX) or aerobic heme degradation (HutZ).[69–72] Although HutX was shown to function synergistically with HutW, neither HutX nor HutZ reduce the tetrapyrrole product of HutW. Therefore, the ability of HutW to utilize NADPH to catalyze the ring opening as well as the reduction of the tetrapyrrole provides a distinct advantage. Specifically, encoding one protein that performs the ring-opening as well as the reduction of the tetrapyrrole product is energetically advantageous to the organism.

FUNDING

Funding from the National Institute of General Medical Sciences (Grant R01GM124203) to W.N.L. is gratefully acknowledged.

ACKNOWLEDGMENTS

SUPPORTING INFORMATION

The longer wavelength (400-600 nm) UV-visible spectra of purified and reconstituted HutW at high protein concentrations, the UV-visible turnover assays of heme stripped HutW, and the binding curve for HutW and NADPH are included as supplemental information.

ACCESSION CODES

Information on the enzymes being studied in this work can be found under the UniProt IDs A0A3G4VEL8 for HutW.

REFERENCES

(1) Wandersman, C.; Delepelaire, P. BACTERIAL IRON SOURCES: From Siderophores to Hemophores. *Annu. Rev. Microbiol* **2004**, *58*, 611–658. https://doi.org/10.1146/annurev.micro.58.030603.123811.

(2) Wilks, A.; Burkhard, K. A. First Published as an Advance Article on the Web 11th. **2006**. https://doi.org/10.1039/b604193k.

(3) Wandersman, C.; Stojiljkovic, I. Bacterial Heme Sources: The Role of Heme, Hemoprotein Receptors and Hemophores. *Current Opinion in Microbiology* **2000**, *3* (2), 215–220. https://doi.org/10.1016/S1369-5274(00)00078-3.

(4) Schryvers, A. B.; Stojiljkovic, I. Iron Acquisition Systems in the Pathogenic Neisseria. *Molecular Microbiology* **1999**, *32* (6), 1117–1123. https://doi.org/10.1046/j.1365-2958.1999.01411.x.

(5) Runyen-Janecky, L. J. Role and Regulation of Heme Iron Acquisition in Gram-Negative Pathogens. *Frontiers in Cellular and Infection Microbiology* **2013**, *3*. https://doi.org/10.3389/fcimb.2013.00055.

(6) Fetherston, J. D.; Bertolino, V. J.; Perry, R. D. YbtP and YbtQ: Two ABC Transporters Required for Iron Uptake in Yersinia Pestis. *Molecular Microbiology* **1999**, *32* (2), 289–299. https://doi.org/10.1046/j.1365-2958.1999.01348.x.

(7) Nambu, S.; Matsui, T.; Goulding, C. W.; Takahashi, S.; Ikeda-Saito, M. A New Way to Degrade Heme. *Journal of Biological Chemistry* **2013**, *288* (14). https://doi.org/10.1074/jbc.M112.448399.

(8) Skaar, E. P.; Gaspar, A. H.; Schneewind, O. IsdG and IsdI, Heme-Degrading Enzymes in the Cytoplasm of Staphylococcus Aureus. *Journal of Biological Chemistry* **2004**, *279* (1). https://doi.org/10.1074/jbc.M307952200.

(9) Mathew, L. G.; Beattie, N. R.; Pritchett, C.; Lanzilotta, W. N. New Insight into the Mechanism of Anaerobic Heme Degradation. *Biochemistry* **2019**, *58* (46). https://doi.org/10.1021/acs.biochem.9b00841.

(10) LaMattina, J. W.; Nix, D. B.; Lanzilotta, W. N. Radical New Paradigm for Heme Degradation in *Escherichia Coli* O157:H7. *Proceedings of the National Academy of Sciences* **2016**, *113* (43). https://doi.org/10.1073/pnas.1603209113.

(11) Brimberry, M.; Toma, M. A.; Hines, K. M.; Lanzilotta, W. N. HutW from Vibrio Cholerae Is an Anaerobic Heme-Degrading Enzyme with Unique Functional Properties. *Biochemistry* **2021**, *60* (9). https://doi.org/10.1021/acs.biochem.0c00950.

(12) LaMattina, J. W.; Delrossi, M.; Uy, K. G.; Keul, N. D.; Nix, D. B.; Neelam, A. R.; Lanzilotta, W. N. Anaerobic Heme Degradation: ChuY Is an Anaerobilin Reductase That Exhibits Kinetic Cooperativity. *Biochemistry* **2017**, *56* (6). https://doi.org/10.1021/acs.biochem.6b01099.

(13) Brimberry, M.; Toma, M. A.; Hines, K. M.; Lanzilotta, W. N. HutW from *Vibrio Cholerae* Is an Anaerobic Heme-Degrading Enzyme with Unique Functional Properties. *Biochemistry* **2021**, *60* (9). https://doi.org/10.1021/acs.biochem.0c00950.

(14) Frey, P. A.; Booker, S. J. Radical Mechanisms of S-Adenosylmethionine-Dependent Enzymes; 2001. https://doi.org/10.1016/S0065-3233(01)58001-8.

(15) Frey, P. A.; Hegeman, A. D.; Ruzicka, F. J. The RS Superfamily. *Critical Reviews in Biochemistry and Molecular Biology* **2008**, *43* (1). https://doi.org/10.1080/10409230701829169.

(16) Broderick, J. B.; Duffus, B. R.; Duschene, K. S.; Shepard, E. M. Radical *S* -Adenosylmethionine Enzymes. *Chemical Reviews* **2014**, *114* (8). https://doi.org/10.1021/cr4004709.

(17) Quitterer, F.; List, A.; Eisenreich, W.; Bacher, A.; Groll, M. Crystal Structure of Methylornithine Synthase (PylB): Insights into the Pyrrolysine Biosynthesis. *Angewandte Chemie International Edition* **2012**, *51* (6). https://doi.org/10.1002/anie.201106765.

(18) Nicolet, Y.; Pagnier, A.; Zeppieri, L.; Martin, L.; Amara, P.; Fontecilla-Camps, J. C. Crystal Structure of HydG from *Carboxydothermus Hydrogenoformans* : A Trifunctional [FeFe]-Hydrogenase Maturase. *ChemBioChem* **2015**, *16* (3). https://doi.org/10.1002/cbic.201402661.

(19) Boal, A. K.; Grove, T. L.; McLaughlin, M. I.; Yennawar, N. H.; Booker, S. J.; Rosenzweig, A. C. Structural Basis for Methyl Transfer by a RS Enzyme. *Science (1979)* **2011**, *332* (6033). https://doi.org/10.1126/science.1205358.

(20) Grell, T. A. J.; Kincannon, W. M.; Bruender, N. A.; Blaesi, E. J.; Krebs, C.; Bandarian, V.; Drennan, C. L. Structural and Spectroscopic Analyses of the Sporulation Killing Factor Biosynthetic Enzyme SkfB, a Bacterial AdoMet Radical Sactisynthase. *Journal of Biological Chemistry* **2018**, *293* (45). https://doi.org/10.1074/jbc.RA118.005369.

(21) Grove, T. L.; Himes, P. M.; Hwang, S.; Yumerefendi, H.; Bonanno, J. B.; Kuhlman, B.; Almo, S. C.; Bowers, A. A. Structural Insights into Thioether Bond Formation in the Biosynthesis of Sactipeptides. *J Am Chem Soc* **2017**, *139* (34). https://doi.org/10.1021/jacs.7b01283.

(22) Yuan, Y.; Zallot, R.; Grove, T. L.; Payan, D. J.; Martin-Verstraete, I.; Šepić, S.; Balamkundu, S.; Neelakandan, R.; Gadi, V. K.; Liu, C.-F.; Swairjo, M. A.; Dedon, P. C.; Almo, S. C.; Gerlt, J. A.; de Crécy-Lagard, V. Discovery of Novel Bacterial Queuine Salvage Enzymes and Pathways in Human Pathogens. *Proceedings of the National Academy of Sciences* **2019**, *116* (38). https://doi.org/10.1073/pnas.1909604116.

(23) Berkovitch, F.; Nicolet, Y.; Wan, J. T.; Jarrett, J. T.; Drennan, C. L. Crystal Structure of Biotin Synthase, an *S* -Adenosylmethionine-Dependent Radical Enzyme. *Science (1979)* **2004**, *303* (5654). https://doi.org/10.1126/science.1088493.

(24) Vey, J. L.; Yang, J.; Li, M.; Broderick, W. E.; Broderick, J. B.; Drennan, C. L. Structural Basis for Glycyl Radical Formation by Pyruvate Formate-Lyase Activating Enzyme. *Proceedings of the National Academy of Sciences* **2008**, *105* (42). https://doi.org/10.1073/pnas.0806640105.

(25) Goldman, P. J.; Grove, T. L.; Sites, L. A.; McLaughlin, M. I.; Booker, S. J.; Drennan, C. L. X-Ray Structure of an AdoMet Radical Activase Reveals an Anaerobic Solution for Formylglycine Posttranslational Modification. *Proceedings of the National Academy of Sciences* **2013**, *110* (21). https://doi.org/10.1073/pnas.1302417110.

(26) Goldman, P. J.; Grove, T. L.; Booker, S. J.; Drennan, C. L. X-Ray Analysis of Butirosin Biosynthetic Enzyme BtrN Redefines Structural Motifs for AdoMet Radical Chemistry. *Proceedings of the National Academy of Sciences* **2013**, *110* (40). https://doi.org/10.1073/pnas.1312228110.

(27) Dowling, D. P.; Bruender, N. A.; Young, A. P.; McCarty, R. M.; Bandarian, V.; Drennan, C. L. RS Enzyme QueE Defines a New Minimal Core Fold and Metal-Dependent Mechanism. *Nature Chemical Biology* **2014**, *10* (2). https://doi.org/10.1038/nchembio.1426.

(28) Bruender, N. A.; Grell, T. A. J.; Dowling, D. P.; McCarty, R. M.; Drennan, C. L.; Bandarian, V. 7-Carboxy-7-Deazaguanine Synthase: A Radical *S* -Adenosyl- <scp>l</Scp> -Methionine Enzyme with Polar Tendencies. *J Am Chem Soc* **2017**, *139* (5). https://doi.org/10.1021/jacs.6b11381.

(29) Bridwell-Rabb, J.; Zhong, A.; Sun, H. G.; Drennan, C. L.; Liu, H. A B12-Dependent RS Enzyme Involved in Oxetanocin A Biosynthesis. *Nature* **2017**, *544* (7650). https://doi.org/10.1038/nature21689.

(30) Chen, D.; Walsby, C.; Hoffman, B. M.; Frey, P. A. Coordination and Mechanism of Reversible Cleavage of *S* -Adenosylmethionine by the [4Fe-4S] Center in Lysine 2,3-Aminomutase. *J Am Chem Soc* **2003**, *125* (39). https://doi.org/10.1021/ja036120z.

(31) Walsby, C. J.; Hong, W.; Broderick, W. E.; Cheek, J.; Ortillo, D.; Broderick, J. B.; Hoffman, B. M. Electron-Nuclear Double Resonance Spectroscopic Evidence That *S* -Adenosylmethionine Binds in Contact with the Catalytically Active [4Fe−4S] $^{+}$ Cluster of Pyruvate Formate-Lyase Activating Enzyme. *J Am Chem Soc* **2002**, *124* (12). https://doi.org/10.1021/ja012034s.

(32) Horitani, M.; Shisler, K.; Broderick, W. E.; Hutcheson, R. U.; Duschene, K. S.; Marts, A. R.; Hoffman, B. M.; Broderick, J. B. RS Catalysis via an Organometallic Intermediate with an Fe–[5′-C]-Deoxyadenosyl Bond. *Science (1979)* **2016**, *352* (6287). https://doi.org/10.1126/science.aaf5327.

(33) Byer, A. S.; Yang, H.; McDaniel, E. C.; Kathiresan, V.; Impano, S.; Pagnier, A.; Watts, H.; Denler, C.; Vagstad, A. L.; Piel, J.; Duschene, K. S.; Shepard, E. M.; Shields, T. P.; Scott, L. G.; Lilla, E. A.; Yokoyama, K.; Broderick, W. E.; Hoffman, B. M.; Broderick, J. B. Paradigm Shift

for Radical *S* -Adenosyl- <scp>l</Scp> -Methionine Reactions: The Organometallic Intermediate Ω Is Central to Catalysis. *J Am Chem Soc* **2018**, *140* (28). https://doi.org/10.1021/jacs.8b04061.

(34) Broderick, W. E.; Hoffman, B. M.; Broderick, J. B. Mechanism of Radical Initiation in the Radical *S* -Adenosyl- <scp>l</Scp> -Methionine Superfamily. *Accounts of Chemical Research* **2018**, *51* (11). https://doi.org/10.1021/acs.accounts.8b00356.

(35) Mathew, L. G.; Brimberry, M.; Lanzilotta, W. N. Class C RS Methyltransferases Involved in Anaerobic Heme Degradation. *ACS Bio & Med Chem Au* **2021**, acsbiomedchemau.1c00047. https://doi.org/10.1021/acsbiomedchemau.1c00047.

(36) Brimberry, M. A.; Mathew, L.; Lanzilotta, W. Making and Breaking Carbon-Carbon Bonds in Class C RS Methyltransferases. *Journal of Inorganic Biochemistry* **2022**, *226*, 111636. https://doi.org/10.1016/j.jinorgbio.2021.111636.

(37) Bauerle, M. R.; Schwalm, E. L.; Booker, S. J. Mechanistic Diversity of Radical S-Adenosylmethionine (SAM)-Dependent Methylation. *Journal of Biological Chemistry* **2015**, *290* (7). https://doi.org/10.1074/jbc.R114.607044.

(38) Zhang, Q.; van der Donk, W. A.; Liu, W. Radical-Mediated Enzymatic Methylation: A Tale of Two SAMS. *Accounts of Chemical Research* **2012**, *45* (4). https://doi.org/10.1021/ar200202c.

(39) Fujimori, D. G. RS-Mediated Methylation Reactions. *Current Opinion in Chemical Biology* **2013**, *17* (4). https://doi.org/10.1016/j.cbpa.2013.05.032.

(40) LaMattina, J. W.; Nix, D. B.; Lanzilotta, W. N. Radical New Paradigm for Heme Degradation in *Escherichia Coli* O157:H7. *Proceedings of the National Academy of Sciences* **2016**, *113* (43). https://doi.org/10.1073/pnas.1603209113.

(41) Mathew, L. G.; Beattie, N. R.; Pritchett, C.; Lanzilotta, W. N. New Insight into the Mechanism of Anaerobic Heme Degradation. *Biochemistry* **2019**, *58* (46). https://doi.org/10.1021/acs.biochem.9b00841.

(42) Grell, T. A. J.; Bell, B. N.; Nguyen, C.; Dowling, D. P.; Bruender, N. A.; Bandarian, V.; Drennan, C. L. Crystal Structure of AdoMet Radical Enzyme 7-carboxy-7-deazaguanine Synthase from <scp> *Escherichia Coli* </Scp> Suggests How Modifications near [4Fe–4S] Cluster Engender Flavodoxin Specificity. *Protein Science* **2019**, *28* (1), 202–215. https://doi.org/10.1002/pro.3529.

(43) Young, A. P.; Bandarian, V. Eukaryotic TYW1 Is a RS Flavoenzyme. *Biochemistry* **2021**, *60* (27), 2179–2185. https://doi.org/10.1021/acs.biochem.1c00349.

(44) Bruender, N. A.; Young, A. P.; Bandarian, V. Chemical and Biological Reduction of the RS Enzyme CPH $_4$ Synthase. *Biochemistry* **2015**, *54* (18), 2903–2910. https://doi.org/10.1021/acs.biochem.5b00210.

(45) Grell, T. A. J.; Bell, B. N.; Nguyen, C.; Dowling, D. P.; Bruender, N. A.; Bandarian, V.; Drennan, C. L. Crystal Structure of AdoMet Radical Enzyme 7-carboxy-7-deazaguanine Synthase from <scp> *Escherichia Coli* </Scp> Suggests How Modifications near [4Fe–4S] Cluster Engender Flavodoxin Specificity. *Protein Science* **2019**, *28* (1). https://doi.org/10.1002/pro.3529.

(46) Arcinas, A. J.; Maiocco, S. J.; Elliott, S. J.; Silakov, A.; Booker, S. J. Ferredoxins as Interchangeable Redox Components in Support of MiaB, a Radical S-Adenosylmethionine Methylthiotransferase. *Protein Science* **2019**, *28* (1). https://doi.org/10.1002/pro.3548.

(47) Young, A. P.; Bandarian, V. Eukaryotic TYW1 Is a RS Flavoenzyme. *Biochemistry* **2021**, *60* (27). https://doi.org/10.1021/acs.biochem.1c00349.

(48) McLean, K. J.; Luciakova, D.; Belcher, J.; Tee, K. L.; Munro, A. W. Biological Diversity of Cytochrome P450 Redox Partner Systems; 2015. https://doi.org/10.1007/978-3-319-16009-2_11.

(49) DAIBER, A.; SHOUN, H.; ULLRICH, V. Nitric Oxide Reductase (P450) From. *Journal of Inorganic Biochemistry* **2005**, *99* (1). https://doi.org/10.1016/j.jinorgbio.2004.09.018.

(50) Shoun, H.; Fushinobu, S.; Jiang, L.; Kim, S.-W.; Wakagi, T. Fungal Denitrification and Nitric Oxide Reductase Cytochrome P450nor. *Philosophical Transactions of the Royal Society B: Biological Sciences* **2012**, *367* (1593). https://doi.org/10.1098/rstb.2011.0335.

(51) Otto, B. R.; Verweij-van Vught, A. M. J. J.; Maclaren, D. M. Transferrins and Heme-Compounds as Iron Sources for Pathogenic Bacteria. *Critical Reviews in Microbiology* **1992**, *18* (3). https://doi.org/10.3109/10408419209114559.

(52) Torres, A. G.; Redford, P.; Welch, R. A.; Payne, S. M. TonB-Dependent Systems of Uropathogenic *Escherichia Coli* : Aerobactin and Heme Transport and TonB Are Required for Virulence in the Mouse. *Infection and Immunity* **2001**, *69* (10). https://doi.org/10.1128/IAI.69.10.6179-6185.2001.

(53) Dickey, S. W.; Cheung, G. Y. C.; Otto, M. Different Drugs for Bad Bugs: Antivirulence Strategies in the Age of Antibiotic Resistance. *Nature Reviews Drug Discovery* **2017**, *16* (7), 457–471. https://doi.org/10.1038/nrd.2017.23.

(54) Ran, Y.; Liu, M.; Zhu, H.; Nygaard, T. K.; Brown, D. E.; Fabian, M.; Dooley, D. M.; Lei, B. Spectroscopic Identification of Heme Axial Ligands in HtsA That Are Involved in Heme Acquisition by *Streptococcus Pyogenes*. *Biochemistry* **2010**, *49* (13). https://doi.org/10.1021/bi901987h.

(55) Kakar, S.; Hoffman, F. G.; Storz, J. F.; Fabian, M.; Hargrove, M. S. Structure and Reactivity of Hexacoordinate Hemoglobins. *Biophysical Chemistry* **2010**, *152* (1–3). https://doi.org/10.1016/j.bpc.2010.08.008.

(56) Hofbauer, S.; Hagmüller, A.; Schaffner, I.; Mlynek, G.; Krutzler, M.; Stadlmayr, G.; Pirker, K. F.; Obinger, C.; Daims, H.; Djinović-Carugo, K.; Furtmüller, P. G. Structure and Heme-Binding Properties of HemQ (Chlorite Dismutase-like Protein) from Listeria Monocytogenes. *Archives of Biochemistry and Biophysics* **2015**, *574*, 36–48. https://doi.org/10.1016/j.abb.2015.01.010.

(57) Smith, A. D.; Wilks, A. Differential Contributions of the Outer Membrane Receptors PhuR and HasR to Heme Acquisition in Pseudomonas Aeruginosa. *Journal of Biological Chemistry* **2015**, *290* (12), 7756–7766. https://doi.org/10.1074/jbc.M114.633495.

(58) Oshima, R.; Fushinobu, S.; Su, F.; Zhang, L.; Takaya, N.; Shoun, H. Structural Evidence for Direct Hydride Transfer from NADH to Cytochrome P450nor. *Journal of Molecular Biology* **2004**, *342* (1), 207–217. https://doi.org/10.1016/j.jmb.2004.07.009.

(59) Tosha, T.; Nomura, T.; Nishida, T.; Saeki, N.; Okubayashi, K.; Yamagiwa, R.; Sugahara, M.; Nakane, T.; Yamashita, K.; Hirata, K.; Ueno, G.; Kimura, T.; Hisano, T.; Muramoto, K.; Sawai, H.; Takeda, H.; Mizohata, E.; Yamashita, A.; Kanematsu, Y.; Takano, Y.; Nango, E.; Tanaka, R.; Nureki, O.; Shoji, O.; Ikemoto, Y.; Murakami, H.; Owada, S.; Tono, K.; Yabashi, M.; Yamamoto, M.; Ago, H.; Iwata, S.; Sugimoto, H.; Shiro, Y.; Kubo, M. Capturing an Initial Intermediate during the P450nor Enzymatic Reaction Using Time-Resolved XFEL Crystallography and Caged-Substrate. *Nature Communications* **2017**, *8* (1), 1585. https://doi.org/10.1038/s41467-017-01702-1.

(60) Zhang, L.; Kudo, T.; Takaya, N.; Shoun, H. The B′ Helix Determines Cytochrome P450nor Specificity for the Electron Donors NADH and NADPH. *Journal of Biological Chemistry* **2002**, *277* (37), 33842–33847. https://doi.org/10.1074/jbc.M203923200.

(61) Zhang, J.; Pierick, A. ten; van Rossum, H. M.; Maleki Seifar, R.; Ras, C.; Daran, J.-M.; Heijnen, J. J.; Aljoscha Wahl, S. Determination of the Cytosolic NADPH/NADP Ratio in Saccharomyces Cerevisiae Using Shikimate Dehydrogenase as Sensor Reaction. *Scientific Reports* **2015**, *5* (1), 12846. https://doi.org/10.1038/srep12846.

(62) Goldbeck, O.; Eck, A. W.; Seibold, G. M. Real Time Monitoring of NADPH Concentrations in Corynebacterium Glutamicum and Escherichia Coli via the Genetically Encoded Sensor MBFP. *Frontiers in Microbiology* **2018**, *9*. https://doi.org/10.3389/fmicb.2018.02564.

(63) Ascoli, F.; Rossi Fanelli, M. R.; Antonini, E. Preparation and Properties of Apohemoglobin and Reconstituted Hemoglobins. *Methods in Enzymology* **1981**, *76* (C), 72–87. https://doi.org/10.1016/0076-6879(81)76115-9.

(64) Rose, M. Y.; Olson, J. S. The Kinetic Mechanism of Heme Binding to Human Apohemoglobin. *Journal of Biological Chemistry* **1983**, *258* (7). https://doi.org/10.1016/S0021-9258(18)32622-X.

(65) Brown, W. D.; Snyder, H. E. Nonenzymatic Reduction and Oxidation of Myoglobin and Hemoglobin by Nicotinamide Adenine Dinucleotides and Flavins. *Journal of Biological Chemistry* **1969**, *244* (24). https://doi.org/10.1016/S0021-9258(18)63463-5.

(66) Holliday, G. L.; Akiva, E.; Meng, E. C.; Brown, S. D.; Calhoun, S.; Pieper, U.; Sali, A.; Booker, S. J.; Babbitt, P. C. Atlas of the RS Superfamily: Divergent Evolution of Function Using a "Plug and Play" Domain; 2018. https://doi.org/10.1016/bs.mie.2018.06.004.

(67) Zhang, L.; Kudo, T.; Takaya, N.; Shoun, H. The B′ Helix Determines Cytochrome P450nor Specificity for the Electron Donors NADH and NADPH. *Journal of Biological Chemistry* **2002**, *277* (37), 33842–33847. https://doi.org/10.1074/jbc.M203923200.

(68) Uchida, T.; Dojun, N.; Sekine, Y.; Ishimori, K. Heme Proximal Hydrogen Bonding between His170 and Asp132 Plays an Essential Role in the Heme Degradation Reaction of HutZ from *Vibrio Cholerae*. *Biochemistry* **2017**, *56* (21), 2723–2734. https://doi.org/10.1021/acs.biochem.7b00152.

(69) Sekine, Y.; Tanzawa, T.; Tanaka, Y.; Ishimori, K.; Uchida, T. Cytoplasmic Heme-Binding Protein (HutX) from *Vibrio Cholerae* Is an Intracellular Heme Transport Protein for the Heme-Degrading Enzyme, HutZ. *Biochemistry* **2016**, *55* (6), 884–893. https://doi.org/10.1021/acs.biochem.5b01273.

(70) Uchida, T.; Sekine, Y.; Dojun, N.; Lewis-Ballester, A.; Ishigami, I.; Matsui, T.; Yeh, S.-R.; Ishimori, K. Reaction Intermediates in the Heme Degradation Reaction by HutZ from Vibrio Cholerae. *Dalton Transactions* **2017**, *46* (25), 8104–8109. https://doi.org/10.1039/C7DT01562C.

(71) Wyckoff, E. E.; Schmitt, M.; Wilks, A.; Payne, S. M. HutZ Is Required for Efficient Heme Utilization in *Vibrio Cholerae*. *Journal of Bacteriology* **2004**, *186* (13), 4142–4151. https://doi.org/10.1128/JB.186.13.4142-4151.2004.

Figure 4.1

UV-visible (Panel A) and EPR spectroscopy (Panel B) following the reduction of the [4Fe-4S] cluster of the as-purified HutW (1) with sodium dithionite (NaDT) (2) or NADPH (3). EPR spectra were recorded at 10K with a microwave power of 0.1 mW, a modulation amplitude of 1 mT and 180 second scan time as further detailed in the Materials and Methods.

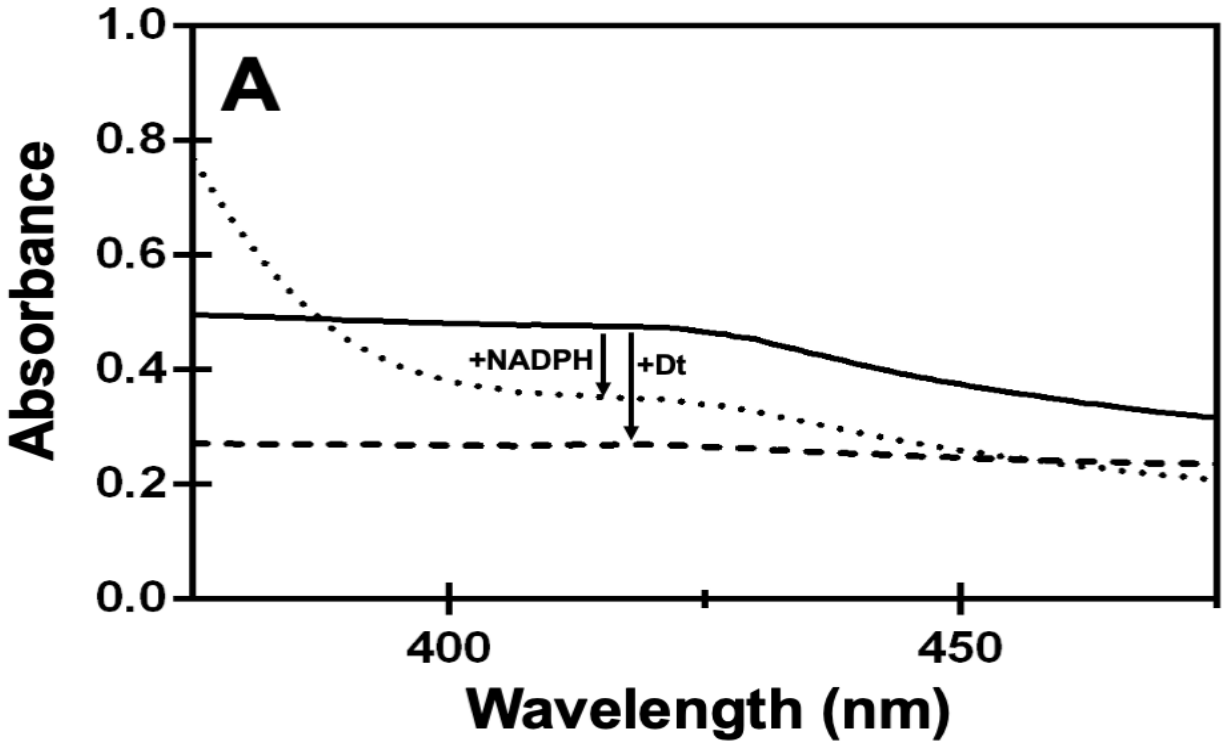
A
1.0
0.8
0.6
0.4
0.2
0.0
Absorbance
+NADPH
+Dt
400
450
Wavelength (nm)

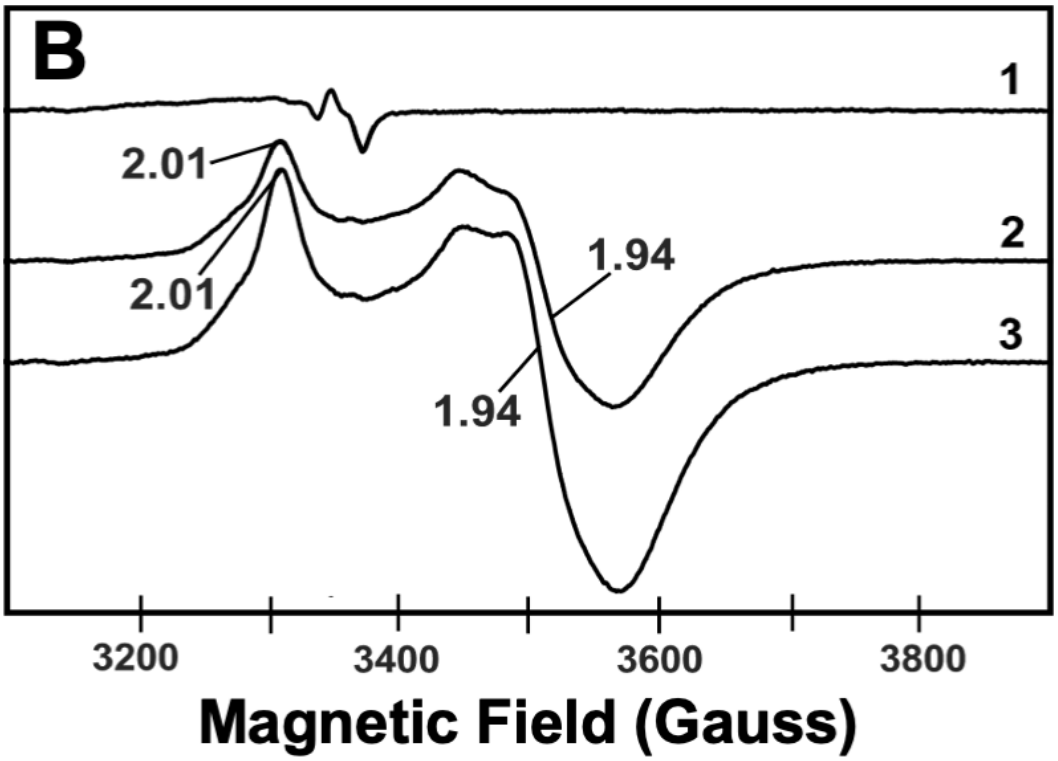
B
1
2
3
2.01
2.01
1.94
1.94
3200
3400
3600
3800
Magnetic Field (Gauss)

Figure 4.2

UV-visible spectra highlighting the appearance of a Soret band (Panel A) and β-bands (Panel B) following the addition of sodium dithionite to reconstituted HutW. HutW was isolated with the [4Fe-4S] cluster reconstituted as described in the Materials and Methods and UV-visible spectra was recorded (black line).

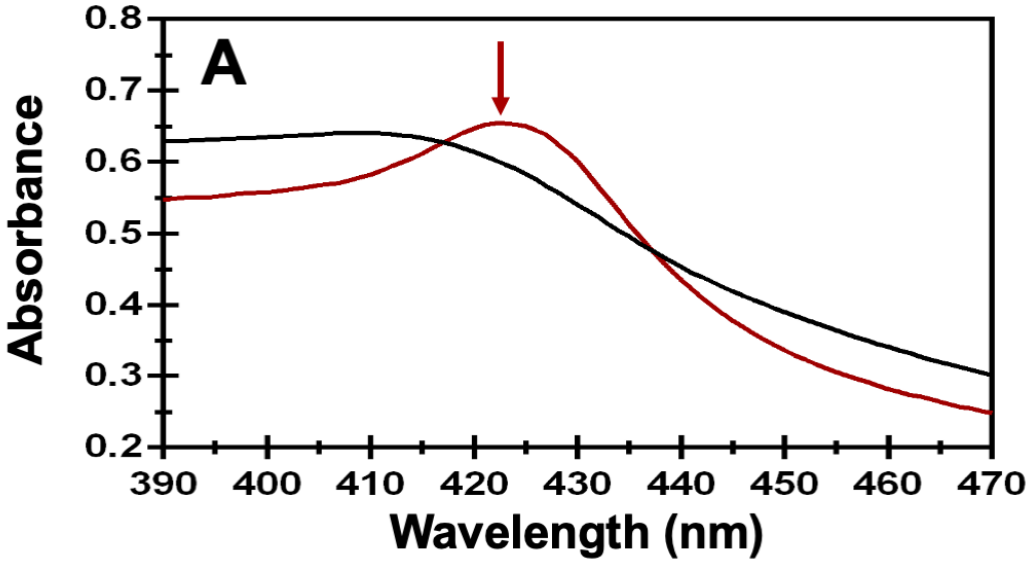
A
Absorbance
0.8
0.7
0.6
0.5
0.4
0.3
0.2
390
400
410
420
430
440
450
460
470
Wavelength (nm)

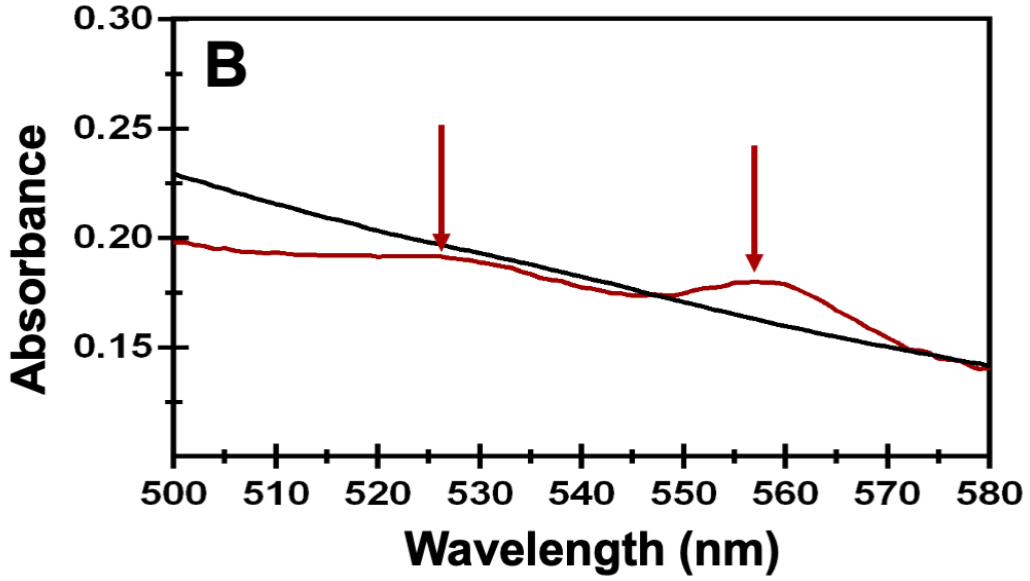
B
Absorbance
0.30
0.25
0.20
0.15
500
510
520
530
540
550
560
570
580
Wavelength (nm)

Figure 4.3

UV-visible spectroscopy of as-purified HutW (Panel A) and heme-stripped HutW (Panel B) titrated with NADPH. As-purified HutW prior to and following treatment with apo-Hemoglobin, as detailed in the Materials & Methods, was subjected to the addition NADPH as indicated in the figure panels.

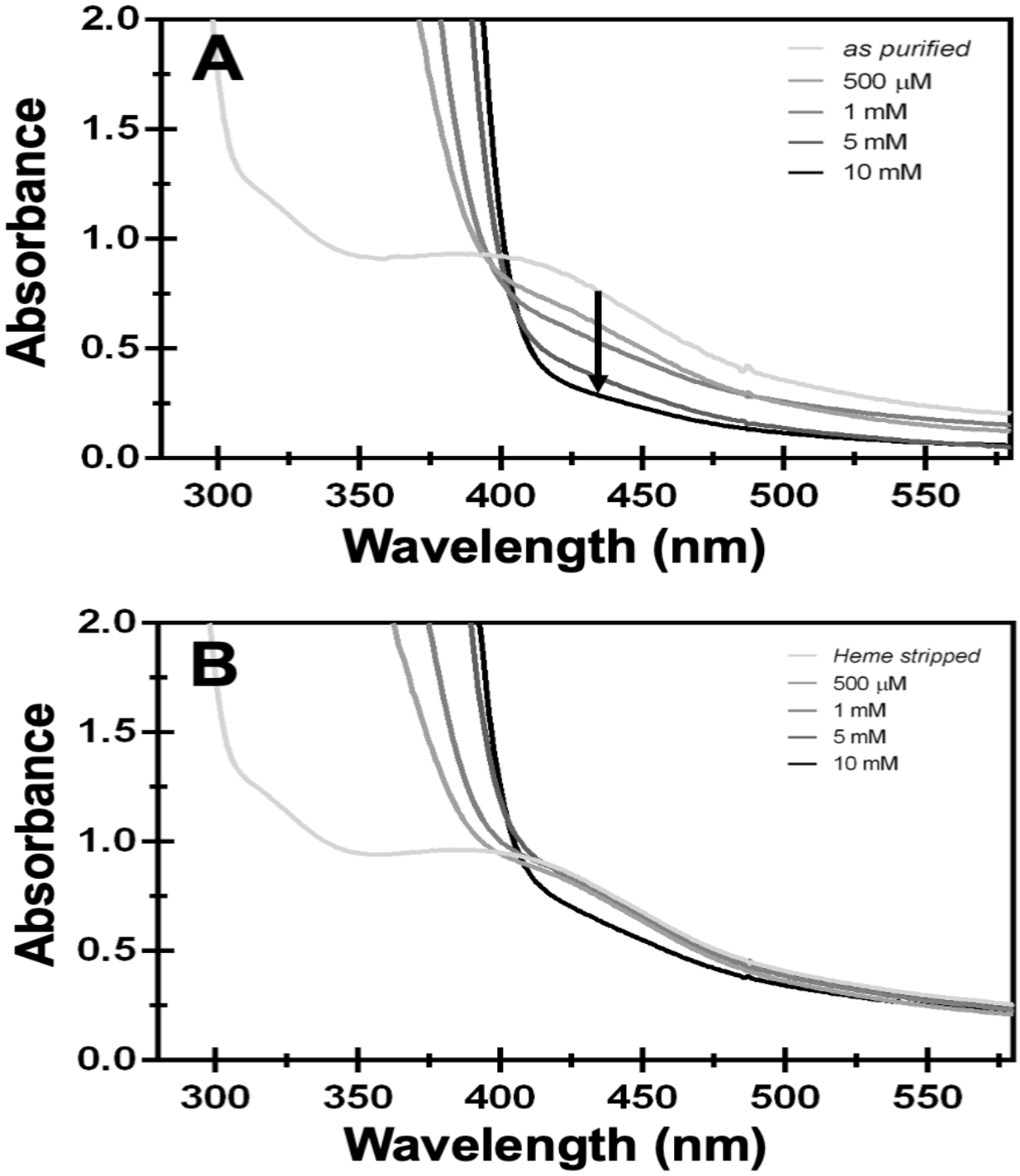
A
as purified
500 μM
1 mM
5 mM
10 mM
Absorbance
2.0
1.5
1.0
0.5
0.0
300
350
400
450
500
550
Wavelength (nm)
B
Heme stripped
500 μM
1 mM
5 mM
10 mM
Absorbance
2.0
1.5
1.0
0.5
0.0
300
350
400
450
500
550
Wavelength (nm)

Figure 4.4

EPR spectroscopy of heme-stripped HutW Panel A. UV-visible spectroscopy of heme-stripped HutW (solid red trace) following addition of sodium dithionite (dashed red) and NADPH (dotted red). Reconstituted HutW is shown for comparison (solid black). Panel B EPR spectra of heme-stripped HutW without added reductant (1), following addition of sodium dithionite (2), NADPH (3). Panel C EPR spectra of HutW (4) and heme-stripped HutW (5) with 50 μM heme added to sample prior to EPR. EPR spectra were recorded at 10K with a microwave power of 0.1 mW, a modulation amplitude of 1 mT and 180 second scan time as further detailed in the Materials and Methods.

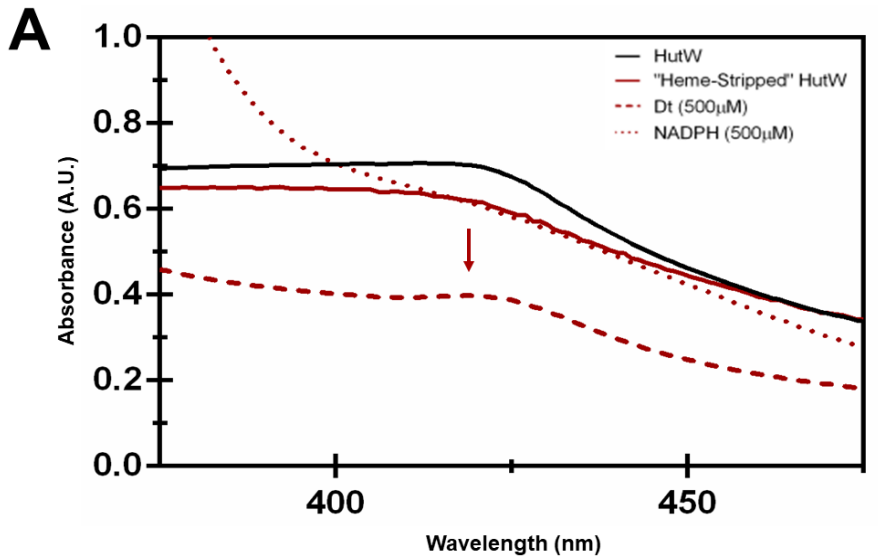
A
1.0
0.8
0.6
0.4
0.2
0.0
Absorbance (A.U.)
HutW
"Heme-Stripped" HutW
Dt (500μM)
NADPH (500μM)
400
450
Wavelength (nm)

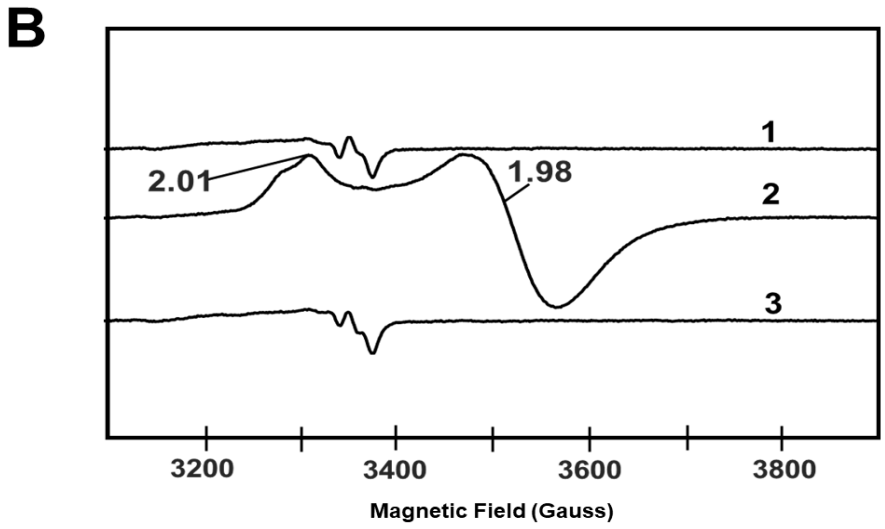
B
1
2.01
1.98
2
3
3200
3400
3600
3800
Magnetic Field (Gauss)

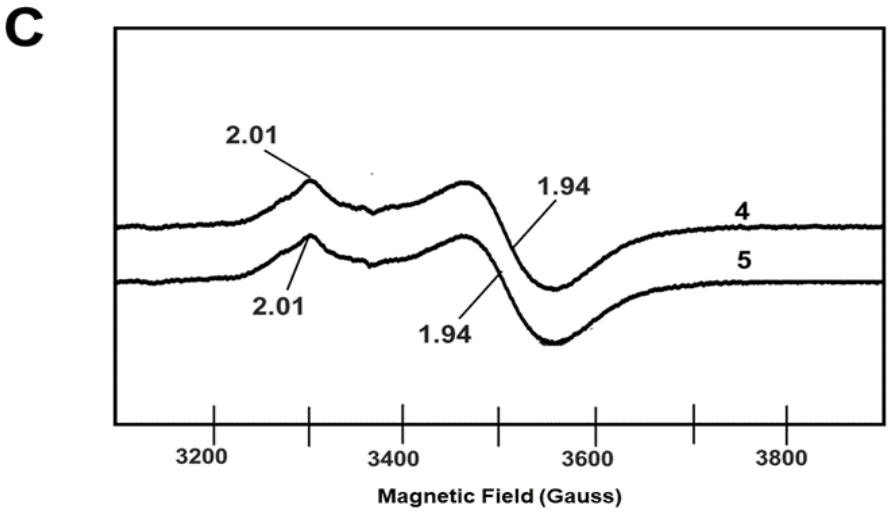
C
2.01
1.94
4
5
2.01
1.94
3200
3400
3600
3800
Magnetic Field (Gauss)

Scheme 4.1: Proposed bifurcation of reducing equivalents from NADPH to support HutW turnover.

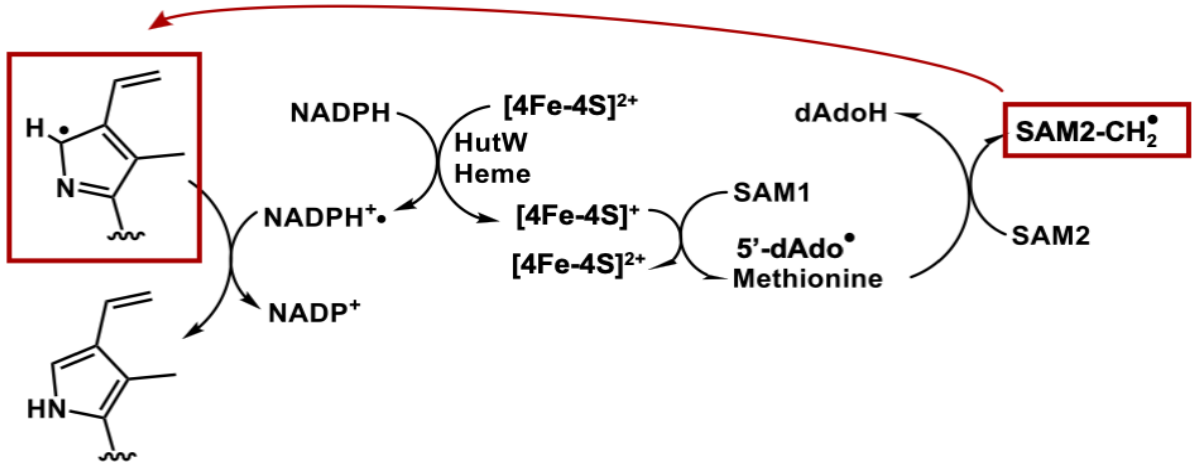

Figure S4.1

UV-visible absorbance assays of heme stripped HutW | (left) UV-visible assays of heme stripped HutW, with no SAM added. (Right) with addition of SAM. HutW assays were performed as described in Materials and Methods, and spectral changes were recorded every minute for 5 minutes.

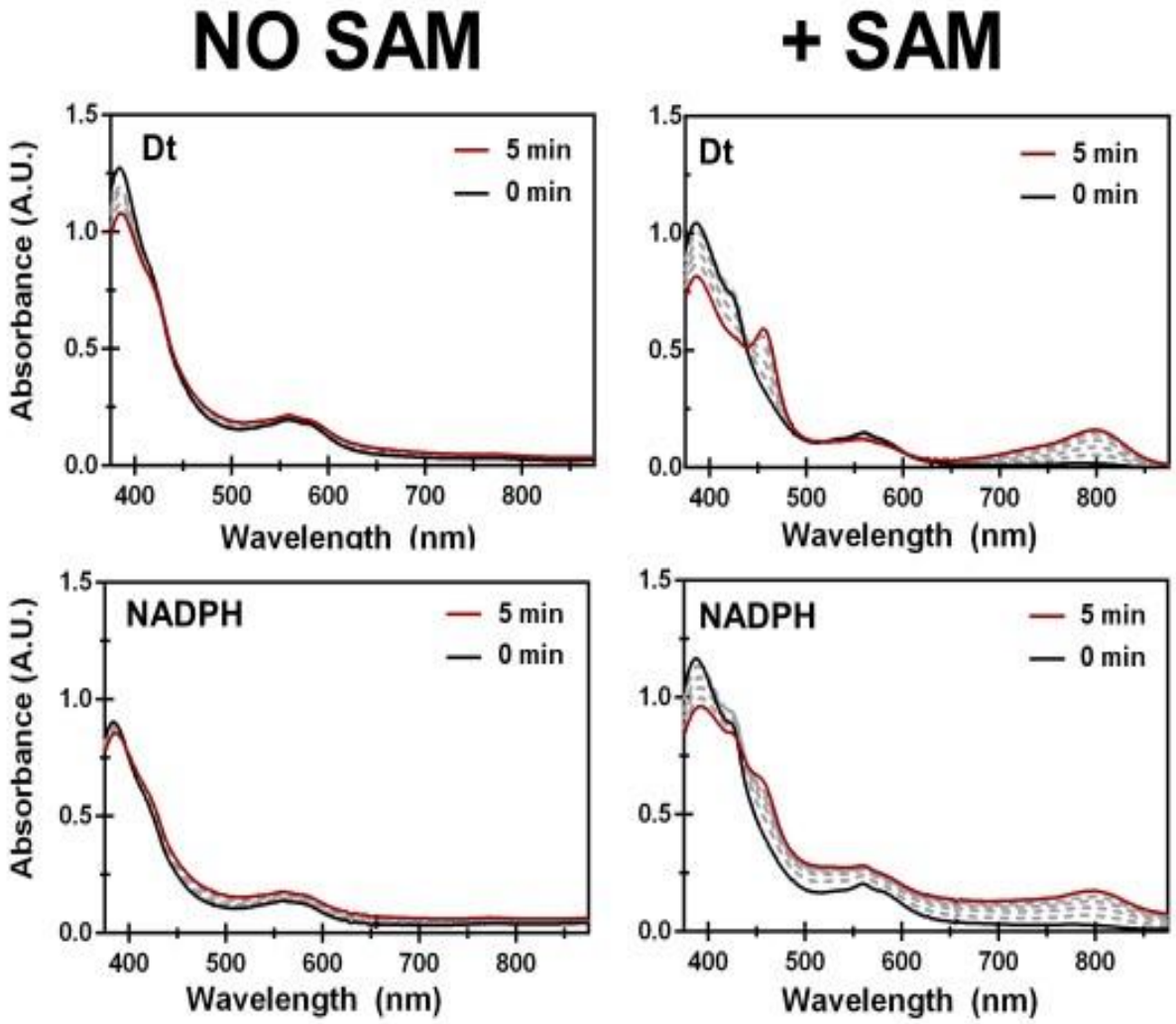
NO SAM
+ SAM
Dt
5 min
0 min
Absorbance (A.U.)
Wavelength (nm)
NADPH

Figure S4.2

Substrate saturation of HutW and NADPH | HutW specific activity calculated from the disappearance of the heme Soret peak at increasing concentrations of NADPH. Error bars represent the standard deviation of triplicate determinations, with the central point representing the average. K_M was determined using GraphpadPRISM one-state binding kinetics.

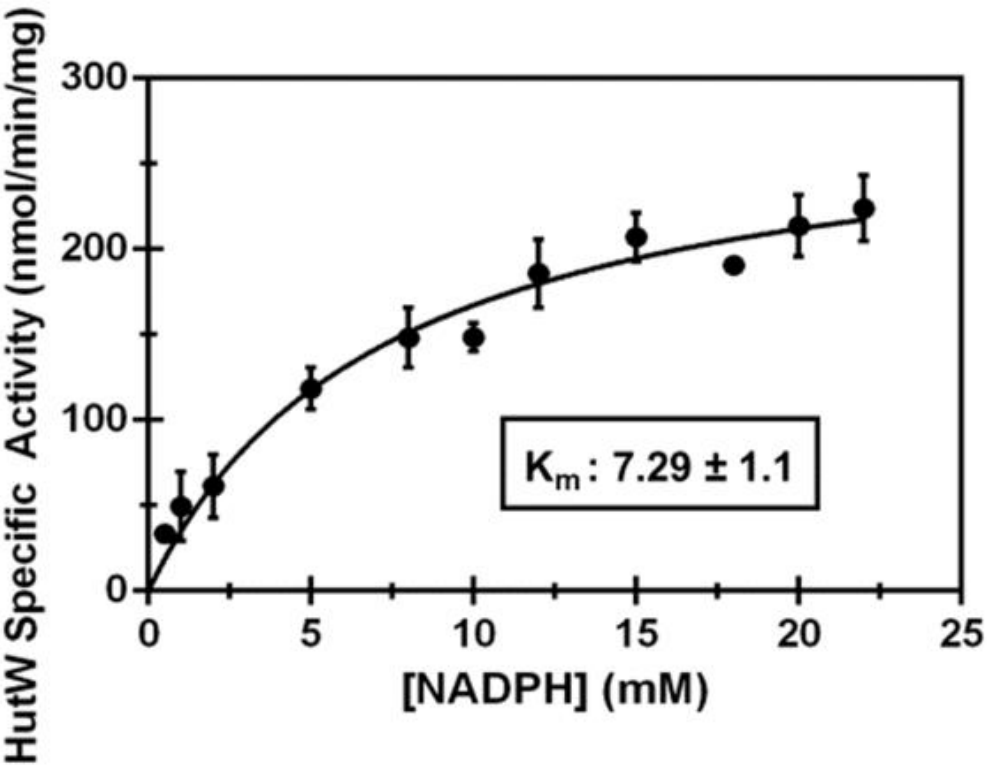
HutW Specific Activity (nmol/min/mg)
300
200
100
0
0
5
10
15
20
25
[NADPH] (mM)
K_m: 7.29 ± 1.1

Figure S4.3

UV-visible turnover assay of deuteroporphyrin IX using NADPH | UV-visible absorbance spectra monitoring the anaerobic degradation of deuteroporphyrin IX catalyzed by HutW with NADPH as the electron source. Assay was performed as described in Materials and Methods and the spectral changes were recorded every minute for 6 minutes. The structure of deuteroporphyrin IX is shown as an inset and the arrows indicate the direction of spectral changes during the assay.

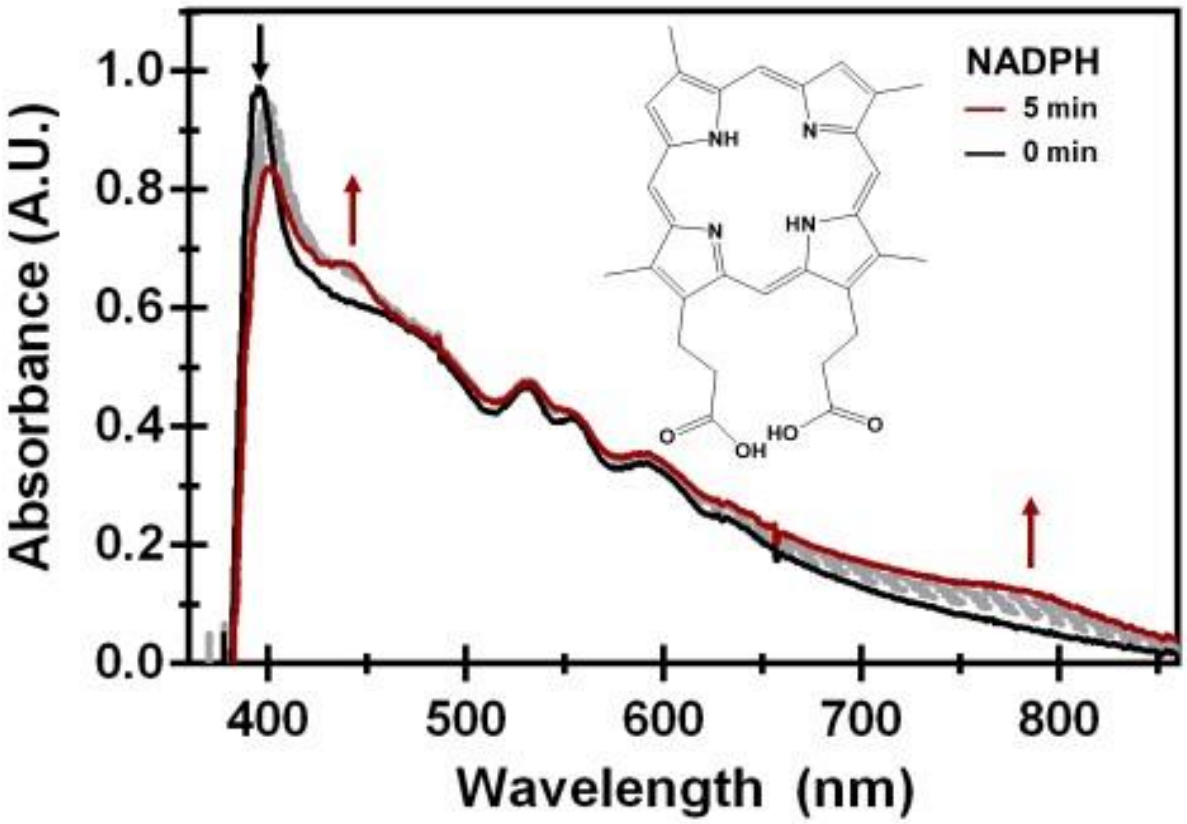
NADPH
5 min
0 min
Absorbance (A.U.)
1.0
0.8
0.6
0.4
0.2
0.0
400
500
600
700
800
Wavelength (nm)
NH
N
N
HN
O
OH
HO
O

Figure S4.5

UV-visible spectroscopy of heme stripped HutW [Fe-S] cluster | UV-visible spectra of heme stripped HutW (solid trace) treated with NADPH (dashed trace) followed by addition of heme (dotted trace).

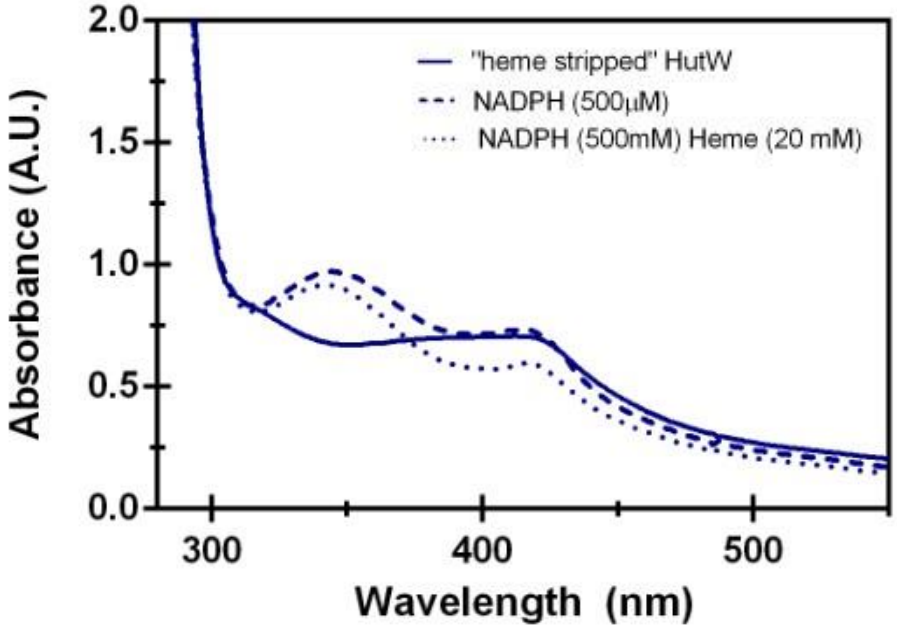
2.0
1.5
1.0
0.5
0.0
Absorbance (A.U.)
300
400
500
Wavelength (nm)
"heme stripped" HutW
NADPH (500μM)
NADPH (500mM) Heme (20 mM)

CHAPTER 5

FUTURE DIRECTIONS AND FINAL THOUGHTS

Pathogens that infect anaerobic environments within the host, where nutrients are severely limiting, must not only survive and colonize but outcompete the commensal bacteria inhabiting that environment. It is therefore not surprising that certain enteric pathogens encode genes for a means of anaerobically degrading heme as an iron source. In addition, many non-canonical heme oxygenases produce verdins that have evolved to suit the physiological needs of the invading bacteria. Moreover, evidence is emerging revealing that specific isoforms of biliverdin produced by *P. aeruginosa* HO, result in increased infectivity and pathogenicity. Taken together, it becomes clear that understanding not only the mechanism for anaerobic heme degradation but identifying the structures of the various tetrapyrrole products remains an intriguing and crucial avenue of future research.

Exploration of the "oxygen-independent coproporphyrinogen III oxidase like" Sequence Space

The identification of ChuW as an anaerobic heme degrading enzyme was interesting for several reasons. Not only did it represent a previously unrecognized means of degrading heme employed selectively by gut pathogens, but it demonstrated that the annotation of "Oxygen-

independent coproporphyrinogen III oxidase-like" nodes or genes, that was based on certain sequence motifs, did not reflect the true functionalities of these genes. That is, the true function of the" CgdH-like" (formerly "HemN-like") genes. Therefore, it would be interesting to characterize additional enzymes encoded by the genes originally annotated CgdH enzymes. Interestingly, the ChuW/HutW protein family diverges into distinct groups when using a UniProt ID CR of 0.881 (Figure 5.1).[1] Interestingly, at least part of this can be explained by differences in the operon structure. Specifically, the *E. coli* O157:H7 operon contains *chuWXY* and the *Vibrio spp* operon encodes *hutWXZ*, where the "W" and "X" genes appear to have very high sequence and structural identity, but the "Y" and "Z" gene do not. In addition to probing the precise role of these proteins in anaerobic heme degradation, addressing the functional role(s) these genes may have in pathogenesis is a priority. Additional future investigations should also include characterization of the proteins encoded by the UniProt IDs in other nodes of the sequence network. Specifically, are there other CgdH-like enzymes that include RS enzymes with the ability to use either NADPH or NADH to reduce the RS cluster.

Identification of Products

Work presented in this dissertation provides a rational basis for some of the differences in the heme utilization operons reported for *E. coli* and *V. cholerae.* In particular, the observation that HutW can utilize NADPH as a reductant and produces a more reduced tetrapyrrole product, by comparison to anaerobilin, may negate the need for a reductase. However, this remains to be definitively examined in vivo. In addition, small molecule, crystal structures, or NMR structure for both tetrapyrroles (anaerobilin and the HutW products) remain unavailable due to the photosensitivity and general reactivity of these hydrophobic molecules. Furthermore, the metabolic fate of the tetrapyrrole product as well as the iron atom remains to be determined.

Presumably, the tetrapyrrole is excreted while the iron is utilized by the pathogen. However, it is not known if the iron is in the ferric or ferrous form following release from ferric or ferrous heme, respectively. Iron is highly reactive and can promote the production of radical oxygen species (ROS) which react with proteins, lipids and DNA damaging and killing cells under aerobic conditions.[2,3] Both ChuX and HutX have been reported to bind heme with low micromolar affinities, but no structural data has been obtained for either protein with heme bound.[4,5] Based on computational modeling and structural analysis of several "X" proteins including *E. coli* ChuX (PDB ID 2OVI), *V. cholerae* HutX (PDB ID 5EXV), and *Anabaena variabilis* ChuX (PDB ID 3FM2) an alternative function was proposed where the "X" protein acts as a chaperone to transiently and safely sequester/transport the iron atom as well as the tetrapyrrole product.[6] Or, in analogy to bacterial HOs, such as *E. coli*, the free iron could bind an iron storage protein, either a bacterial ferritin or a bacterioferritin.[7,8] This would be intriguing because the ferritins function by utilizing O_2 or H_2O_2 to oxidize Fe^{2+} and compartmentalizing the resultant Fe^{3+}. Therefore, following ChuW/HutW iron release, first identifying the oxidation state of the iron atom then understanding how it is sequestered could identify a novel type of anaerobic iron-binding protein. Additionally, as mentioned previously, it is unknown how the potentially toxic tetrapyrrole product is dealt with *in vivio.* Furthermore, the verdin products of other HOs, have been shown to be involved in signaling pathways that feedback into infectivity and pathogenicity islands in *P. aeruginosa*, *M. tuberculosis*, and *S. aureus.*[9–13] An intriguing proposal would therefore be whether or not the tetrapyrrole products of anaerobic heme degradation have an additional role in signaling or pathogenesis.

Elucidation of the electron transfer pathway from NADPH to the HutW [4Fe-4S]

Direct electron transfer from NAD(P)H to a redox protein that contains only a one-electron redox center is usually impossible because NAD(P)H releases two electrons simultaneously, usually as a hydride ion (H^-), and the one-electron redox center cannot accept a hydride ion directly.[14,15] Therefore, in enzymatic reactions, electron carriers such as flavins, quinones, and cytochromes are used.[16–18] However, the mechanism for electron transfer from the hydride donor NADPH to reduce the [4Fe-4S] cluster must be rationalized. For a hydride transfer in HutW, NADPH donates a hydride ion (H-) to the heme porphyrin ring, for which there is evidence for in the cytochrome P450 superfamily including P450nor and P450BM-3.[19–23] Assuming that NAD(P)H reacts by hydride transfer, the hydride is donated to the heme porphyrin ring, forming a porphyrin radical.[24] An active site base could react with the proton from NAD(P)H. Other researchers have evaluated the ability of heme to be protonated or accept a hydride using density function theory calculations coupled with FTCIR mass spectrometry and found that the most stable isomer is a transfer to the β carbon atom of the vinyl.[25,26] Alternatively, the proton could react with an active site base and in a two-electron redox reaction, the ferric (Fe^{3+}) iron intercalated within the heme macrocycle reduced to ferrous heme (Fe^{2+}) and formation of the corresponding porphyrin π-cation radical. Either by two one-electron reductions or directly by a two-electron reduction step.[27] As with other redox active heme proteins, the nature of electron donor (organic or inorganic, cationic, neutral or anionic, low or high molar mass) and the actual substrate binding and oxidation site has great variability.

Where exactly the hydrogen is transferred could be evaluated using synthetic NADPH, including 4,4-^{2}H,^{2}H-NADPH and the kinetic isotope effect measured. One electron reduces the [4Fe-4S] cluster, based on the reduction potential of the cluster, and the [4Fe-4S] cluster

reductively cleaves the first molecule of SAM (SAM1) to 5′-deoxyadenosine radical, which abstracts a hydrogen atom from the second molecule of SAM (SAM2), forming a methylene radical. This methylene radical then adds to the bridging *meso* carbon of the porphyrin radical. Obviously, the oxidation state of the intermediate will need to be evaluated in future research, as discussed later in this section. The porphyrin ring is opened through β-scission. The porphyrin ring then undergoes radical rearrangement with quenching of the radical. A proton donated originally from NAD(P)H to an active site base then protonates the porphyrin, as detailed in Figure 5.3.

For the mechanism, reactive species such as radical cations and neutral radicals, both of the hydride donor, in this case, NAD(P)H and of the acceptor molecule (heme) are formed in the process. Such species are very reactive because they possess unpaired electrons. Localization of these electrons in different parts of a molecule may lead to the shortening or elongation of specific bonds. Determination of the spin density distribution provides information on the nature of the electronic ground state as well as on dynamic features of a species which can be spectroscopically characterized. Therefore, the hydride transfer mechanism, can be investigated in HutW by comparing the reactivities of different types of NAD(P)H analogues which have different donor abilities in the initial and second electron transfer sequence.[28,29] In this way, by using NAD(P)H donors with different reactivities, the rates of each electron transfer event can be modeled, and determined. As the energetics of initial electron transfer determines the energetics of the overall hydride transfer, I would predict that the rate would depend upon the reduction potential of the HutW [4Fe-4S] cluster. Therefore, determining the reduction potential of the cluster is of high importance to ascertain the mechanism of NADPH reduction.

Moreover, if HutW is indeed using a stepwise electron-proton-electron transfer, the hypothesis is that the first electron would reduce the [4Fe-4S], followed by protonation and radical

quenching of the tetrapyrrole product. Multi-heme containing proteins have the ability to store multiple reducing equivalents, and this is enabled by the presence of two pathways for electrons to flow to/from the active site.[30–34] This allows these enzymes to hold charge generated during catalysis, and could be linked to motions within the protein. This is similar to the system seen for bifurcating quinones in cytochrome bc_1, where the first electron transferred is delivered to an iron-sulfur cluster (Rieske center in the case of cytochrome bc_1), and the second bifurcated electron that reduces a low-potential heme.[35–37] With the caveat being that the electrochemical parameters of the cofactors in HutW have not been investigated, including the redox midpoint potentials (Em). Obviously, a baseline determination of the Em as well as the electronic state of the heme (high spin versus low spin) would first need to be conclusively determined. This could be done as, for example, low-spin and high spin heme cofactors are observed by UV-visible spectroscopy, EPR, resonance Raman, and potentially even NMR.[38] Furthermore, the state of the heme can be deconvoluted through electrochemical redox titrations monitored by either optical spectroscopy.[39] In a UV-visible spectrum, high-spin heme is distinguished by the Q-bands at 537 and 570 nm as well as at 618 nm, for approximate values.[40] . Furthermore, the dependence of the UV-visible absorbance signal size at different wavelengths and the applied ambient potential can be plotted to give the pH.[41] EPR can be used to determine both ferric and ferrous as well as low-spin high-spin heme, with low-spin heme being dominated by a rhombic signal centered around $g = 2$ and a high-spin heme population at $g = 6$ (approximate values).[42] Characterization using resonance Raman can also be utilized for HutW, with the porphyrin skeletal mode ν_4 correlating with the oxidation state of the iron (if the metal is involved in the electron transfer), and the ν_3, ν_2, and ν_{10} modes reporting on iron coordination and spin states.[43,44] Although we have shown that HutW is able to turnover non-metallated porphyrins when supplied NADPH as a reductant, suggesting that the iron

is non involved in the electron transfer. This finding reflects recent findings in *in silico* and in long-range electron transfer pathways which find the porphyrin ring itself to be the electron transfer mediator.[45–49] An interesting avenue of research would be to see if the electron transfer from NADPH to the [4Fe-4S] cluster of HutW is dependent upon the iron atom within the heme porphyrin ring, or if it is dependent upon the conjugated pi system of the porphyrin macrocycle. To probe this, the electron transfer of apo-HutW using non-metalated porphyrins (PPIX), alternatively metalated porphyrins such as cobalt protoporphyrin IX (Co-PPIX), and redox neutral metals such as magnesium (Mg) could be utilized.

Mechanistic characterization of HutW has much broader implications in the electron transfer mechanisms that facilitate electron transfer from NADPH to the [4Fe-4S] cluster. We have postulated a detailed mechanism using chemical logic and evidence attained from our research as well as being informed by other class C RSMTs including ChuW and the cytochrome P450s which have been shown to use NAD(P)H as a direct hydride donor. The reaction scheme proposed for HutW was based on a random association mechanism for substrate binding; however, a stopped-flow spectroscopic investigation combined with site-directed mutagenesis may provide more details into the sequence of mechanistic events and residues involved in binding either SAM cofactor or heme. Additionally, probing the electronic and spatial environment of the iron-sulfur cluster using isotopically labeled SAM, analogs of SAM, heme or ^{57}Fe in conjunction with EPR and hyperfine sublevel correlation spectroscopy (HYSCORE) may provide insights into the unique ability of HutW to use heme as a conduit to transfer electrons from NADPH to the [4Fe-4S] cluster.

Anaerobic Heme Degradation as an Antibiotic Target

Understanding the resistance mechanisms and developing alternative strategies to target bacterial pathogens is a priority in the development of new therapeutics. Targeting iron and heme

as global virulence regulators within Gram-positive and Gram-negative pathogens is a viable strategy. Moreover, heme is readily available within the human host environment and is an essential source of iron during chronic infection therefore discovering new drugs targeting heme acquisition systems is a feasible approach. Knockouts of *hutW* and the operon *hutWXZ* showed a reduced, but not eliminated ability to use heme as an iron source in liquid media; however, these results cannot be used to determine the competitiveness of the organism in the enteric environment.[50] It is well established that host microbiota generally play a beneficial role in preventing or fighting infection.[51–54] Therefore, if HutW confers an advantage during colonization and/or pathogenesis, the gene may be an effective antimicrobial target. Both mathematical models and experimental have been demonstrated to be useful for understanding the complex ecosystem of the human microbiome, and these models could be used to test the competitive ability of a Δ*hutW* strain of *V. cholera* within this environment.[55,56]

Final Thoughts

The significance of iron acquisition, especially during an infection, is highlighted by the numerous and redundant mechanisms observed in pathogens. In addition, heme is a significant and essential source of iron during infection in mammals, and the oxygen-independent heme degradation pathway observed in bacteria that infect and inhabit in the anaerobic environment of the distal intestine is a recent discovery. In this work, we have shown that *V. cholera* encodes a RS enzyme, HutW, which is not only able to catalyze radical methylation of the heme porphyrin ring to ultimately open the macrocycle to release intercalated iron but is also able to use NADPH to reduce the catalytically necessary [4Fe-4S] cluster. Encoding a means to be obtain iron from heme in the anaerobic distal intestine likely provides *V. cholerae* a competitive advantage during colonization that could be of interest in the development of antibiotics.

References

(1) Holliday, G. L.; Akiva, E.; Meng, E. C.; Brown, S. D.; Calhoun, S.; Pieper, U.; Sali, A.; Booker, S. J.; Babbitt, P. C. Atlas of the Radical SAM Superfamily: Divergent Evolution of Function Using a "Plug and Play" Domain; 2018. https://doi.org/10.1016/bs.mie.2018.06.004.

(2) Wardman, P.; Candeias, L. P. Fenton Chemistry: An Introduction. *Radiat Res* **1996**, *145* (5), 523–531.

(3) Ray, P. D.; Huang, B.-W.; Tsuji, Y. Reactive Oxygen Species (ROS) Homeostasis and Redox Regulation in Cellular Signaling. *Cellular Signalling* **2012**, *24* (5), 981–990. https://doi.org/10.1016/j.cellsig.2012.01.008.

(4) Suits, M. D. L.; Lang, J.; Pal, G. P.; Couture, M.; Jia, Z. Structure and Heme Binding Properties of *Escherichia Coli* O157:H7 ChuX. *Protein Science* **2009**, NA-NA. https://doi.org/10.1002/pro.84.

(5) Su, T.; Chi, K.; Wang, K.; Guo, L.; Huang, Y. Expression, Purification and Preliminary Crystallographic Analysis of a Haem-Utilizing Protein, HutX, from *Vibrio Cholerae*. *Acta Crystallographica Section F Structural Biology Communications* **2015**, *71* (2), 141–144. https://doi.org/10.1107/S2053230X14027666.

(6) Mathew, L. G.; Beattie, N. R.; Pritchett, C.; Lanzilotta, W. N. New Insight into the Mechanism of Anaerobic Heme Degradation. *Biochemistry* **2019**, *58* (46). https://doi.org/10.1021/acs.biochem.9b00841.

(7) Rivera, M. Bacterioferritin: Structure Function and Protein–Protein Interactions; 2013; pp 135–178. https://doi.org/10.1142/9789814407755_0041.

(8) Andrews, S. C. The Ferritin-like Superfamily: Evolution of the Biological Iron Storeman from a Rubrerythrin-like Ancestor. *Biochimica et Biophysica Acta (BBA) - General Subjects* **2010**, *1800* (8), 691–705. https://doi.org/10.1016/j.bbagen.2010.05.010.

(9) Kumar, A.; Deshane, J. S.; Crossman, D. K.; Bolisetty, S.; Yan, B.-S.; Kramnik, I.; Agarwal, A.; Steyn, A. J. C. Heme Oxygenase-1-Derived Carbon Monoxide Induces the Mycobacterium Tuberculosis Dormancy Regulon. *Journal of Biological Chemistry* **2008**, *283* (26), 18032–18039. https://doi.org/10.1074/jbc.M802274200.

(10) Streit, B. R.; Kant, R.; Tokmina-Lukaszewska, M.; Celis, A. I.; Machovina, M. M.; Skaar, E. P.; Bothner, B.; DuBois, J. L. Time-Resolved Studies of IsdG Protein Identify Molecular Signposts along the Non-Canonical Heme Oxygenase Pathway. *Journal of Biological Chemistry* **2016**, *291* (2), 862–871. https://doi.org/10.1074/jbc.M115.666560.

(11) Mouriño, S.; Giardina, B. J.; Reyes-Caballero, H.; Wilks, A. Metabolite-Driven Regulation of Heme Uptake by the Biliverdin IXβ/δ-Selective Heme Oxygenase (HemO) of Pseudomonas Aeruginosa. *Journal of Biological Chemistry* **2016**, *291* (39), 20503–20515. https://doi.org/10.1074/jbc.M116.728527.

(12) Dent, A. T.; Mouriño, S.; Huang, W.; Wilks, A. Post-Transcriptional Regulation of the Pseudomonas Aeruginosa Heme Assimilation System (Has) Fine-Tunes Extracellular Heme Sensing. *Journal of Biological Chemistry* **2019**, *294* (8), 2771–5555. https://doi.org/10.1074/jbc.RA118.006185.

(13) Nelson, C. E.; Huang, W.; Brewer, L. K.; Nguyen, A. T.; Kane, M. A.; Wilks, A.; Oglesby-Sherrouse, A. G. Proteomic Analysis of the Pseudomonas Aeruginosa Iron Starvation Response Reveals PrrF Small Regulatory RNA-Dependent Iron Regulation of Twitching Motility, Amino

Acid Metabolism, and Zinc Homeostasis Proteins. *Journal of Bacteriology* **2019**, *201* (12). https://doi.org/10.1128/JB.00754-18.

(14) Agarwal, P. K.; Webb, S. P.; Hammes-Schiffer, S. Computational Studies of the Mechanism for Proton and Hydride Transfer in Liver Alcohol Dehydrogenase. *J Am Chem Soc* **2000**, *122* (19), 4803–4812. https://doi.org/10.1021/ja994456w.

(15) Sawaya, M. R.; Kraut, J. Loop and Subdomain Movements in the Mechanism of *Escherichia Coli* Dihydrofolate Reductase: Crystallographic Evidence ‡. *Biochemistry* **1997**, *36* (3), 586–603. https://doi.org/10.1021/bi962337c.

(16) Garcia Costas, A. M.; Poudel, S.; Miller, A.-F.; Schut, G. J.; Ledbetter, R. N.; Fixen, K. R.; Seefeldt, L. C.; Adams, M. W. W.; Harwood, C. S.; Boyd, E. S.; Peters, J. W. Defining Electron Bifurcation in the Electron-Transferring Flavoprotein Family. *Journal of Bacteriology* **2017**, *199* (21). https://doi.org/10.1128/JB.00440-17.

(17) Wise, C. E.; Ledinina, A. E.; Yuly, J. L.; Artz, J. H.; Lubner, C. E. The Role of Thermodynamic Features on the Functional Activity of Electron Bifurcating Enzymes. *Biochimica et Biophysica Acta (BBA) - Bioenergetics* **2021**, *1862* (4), 148377. https://doi.org/10.1016/j.bbabio.2021.148377.

(18) Mitchell, P. Possible Molecular Mechanisms of the Protonmotive Function of Cytochrome Systems. *Journal of Theoretical Biology* **1976**, *62* (2), 327–367. https://doi.org/10.1016/0022-5193(76)90124-7.

(19) Shimizu, H.; Park, S.-Y.; Lee, D.-S.; Shoun, H.; Shiro, Y. Crystal Structures of Cytochrome P450nor and Its Mutants (Ser286→Val, Thr) in the Ferric Resting State at Cryogenic

Temperature: A Comparative Analysis with Monooxygenase Cytochrome P450s. *Journal of Inorganic Biochemistry* **2000**, *81* (3), 191–205. https://doi.org/10.1016/S0162-0134(00)00103-3.

(20) Kaspera, R.; Sahele, T.; Lakatos, K.; Totah, R. A. Cytochrome P450BM-3 Reduces Aldehydes to Alcohols through a Direct Hydride Transfer. *Biochemical and Biophysical Research Communications* **2012**, *418* (3), 464–468. https://doi.org/10.1016/j.bbrc.2012.01.040.

(21) Oshima, R.; Fushinobu, S.; Su, F.; Zhang, L.; Takaya, N.; Shoun, H. Structural Evidence for Direct Hydride Transfer from NADH to Cytochrome P450nor. *Journal of Molecular Biology* **2004**, *342* (1), 207–217. https://doi.org/10.1016/j.jmb.2004.07.009.

(22) WATSUJI, T.; TAKAYA, N.; NAKAMURA, A.; SHOUN, H. Denitrification of Nitrate by the Fungus *Cylindrocarpon Tonkinense*. *Bioscience, Biotechnology, and Biochemistry* **2003**, *67* (5), 1115–1120. https://doi.org/10.1271/bbb.67.1115.

(23) Daiber, A.; Nauser, T.; Takaya, N.; Kudo, T.; Weber, P.; Hultschig, C.; Shoun, H.; Ullrich, V. Isotope Effects and Intermediates in the Reduction of NO by P450NOR. *Journal of Inorganic Biochemistry* **2002**, *88* (3–4), 343–352. https://doi.org/10.1016/S0162-0134(01)00386-5.

(24) Shimizu, D.; Osuka, A. Porphyrinoids as a Platform of Stable Radicals. *Chemical Science* **2018**, *9* (6), 1408–1423. https://doi.org/10.1039/C7SC05210C.

(25) Mukherjee, S.; Mukherjee, M.; Bandyopadhyay, S.; Dey, A. Three Phases in PH Dependent Heme Abstraction from Myoglobin. *Journal of Inorganic Biochemistry* **2017**, *172*, 80–87. https://doi.org/10.1016/j.jinorgbio.2017.04.011.

(26) Chiavarino, B.; Crestoni, M. E.; Fornarini, S.; Rovira, C. Protonated Heme. *Chemistry - A European Journal* **2007**, *13* (3), 776–785. https://doi.org/10.1002/chem.200600748.

(27) Fukuzumi, S.; Ohkubo, K.; Tokuda, Y.; Suenobu, T. Hydride Transfer from 9-Substituted 10-Methyl-9,10-Dihydroacridines to Hydride Acceptors via Charge-Transfer Complexes and Sequential Electron−Proton−Electron Transfer. A Negative Temperature Dependence of the Rates. *J Am Chem Soc* **2000**, *122* (18), 4286–4294. https://doi.org/10.1021/ja9941375.

(28) Fukuzumi, S.; Mochizuki, S.; Tanaka, T. Acid-Catalyzed Electron-Transfer Processes in Reduction of Alpha-Haloketones by an NADH Model Compound and Ferrocene Derivatives. *J Am Chem Soc* **1989**, *111* (4), 1497–1499.

(29) Arciero, D. M.; Hooper, A. B. Hydroxylamine Oxidoreductase from Nitrosomonas Europaea Is a Multimer of an Octa-Heme Subunit. *Journal of Biological Chemistry* **1993**, *268* (20), 14645–14654. https://doi.org/10.1016/S0021-9258(18)82382-1.

(30) Igarashi, N.; Moriyama, H.; Fujiwara, T.; Fukumori, Y.; Tanaka, N. The 2.8 Å Structure of Hydroxylamine Oxidoreductase from a Nitrifying Chemoautotrophic Bacterium, Nitrosomonas Europaea. *Nature Structural Biology* **1997**, *4* (4), 276–284. https://doi.org/10.1038/nsb0497-276.

(31) Esteve-Núñez, A.; Sosnik, J.; Visconti, P.; Lovley, D. R. Fluorescent Properties of C-Type Cytochromes Reveal Their Potential Role as an Extracytoplasmic Electron Sink in Geobacter Sulfurreducens. *Environmental Microbiology* **2008**, *10* (2), 497–505. https://doi.org/10.1111/j.1462-2920.2007.01470.x.

(32) Rodrigues, M. L.; Oliveira, T. F.; Pereira, I. A. C.; Archer, M. X-Ray Structure of the Membrane-Bound Cytochrome c Quinol Dehydrogenase NrfH Reveals Novel Haem Coordination. *The EMBO Journal* **2006**, *25* (24), 5951–5960. https://doi.org/10.1038/sj.emboj.7601439.

(33) Schuetz, B.; Schicklberger, M.; Kuermann, J.; Spormann, A. M.; Gescher, J. Periplasmic Electron Transfer via the *c* -Type Cytochromes MtrA and FccA of *Shewanella Oneidensis* MR-1. *Applied and Environmental Microbiology* **2009**, *75* (24), 7789–7796. https://doi.org/10.1128/AEM.01834-09.

(34) Borek, A.; Ekiert, R.; Osyczka, A. Chapter 8. Advances in Understanding Mechanism and Physiology of Cytochromes *Bc*; pp 192–214. https://doi.org/10.1039/9781788010405-00192.

(35) Fisher, N.; Bowman, M. K.; Kramer, D. M. Electron Transfer Reactions at the Qo Site of the Cytochrome Bc 1 Complex: The Good, the Bad, and the Ugly; 2016; pp 419–434. https://doi.org/10.1007/978-94-017-7481-9_21.

(36) Crofts, A. R.; Hong, S.; Wilson, C.; Burton, R.; Victoria, D.; Harrison, C.; Schulten, K. The Mechanism of Ubihydroquinone Oxidation at the Qo-Site of the Cytochrome Bc1 Complex. *Biochimica et Biophysica Acta (BBA) - Bioenergetics* **2013**, *1827* (11–12), 1362–1377. https://doi.org/10.1016/j.bbabio.2013.01.009.

(37) Smith, K. M. *Porphyrins and Metallopophyrins*; Elsevier Science, 1975.

(38) Gębicki, J.; Marcinek, A.; Zielonka, J. Transient Species in the Stepwise Interconversion of NADH and NAD $^{+}$. *Accounts of Chemical Research* **2004**, *37* (6), 379–386. https://doi.org/10.1021/ar030171j.

(39) Jepkorir, G.; Rodríguez, J. C.; Rui, H.; Im, W.; Lovell, S.; Battaile, K. P.; Alontaga, A. Y.; Yukl, E. T.; Moënne-Loccoz, P.; Rivera, M. Structural, NMR Spectroscopic, and Computational Investigation of Hemin Loading in the Hemophore HasAp from *Pseudomonas Aeruginosa*. *J Am Chem Soc* **2010**, *132* (28), 9857–9872. https://doi.org/10.1021/ja103498z.

(40) Kraus, D. W.; Wittenberg, J. B. Hemoglobins of the Lucina Pectinata/Bacteria Symbiosis. I. Molecular Properties, Kinetics and Equilibria of Reactions with Ligands. *J Biol Chem* **1990**, *265* (27), 16043–16053.

(41) Brautigan, D. L.; Feinberg, B. A.; Hoffman, B. M.; Margoliash, E.; Preisach, J.; Blumberg, W. E. Multiple Low Spin Forms of the Cytochrome c Ferrihemochrome. EPR Spectra of Various Eukaryotic and Prokaryotic Cytochromes c. *J Biol Chem* **1977**, *252* (2), 574–582.

(42) Spiro, T.; Li, X. *Biological Applications of Raman Spectroscopy*; John Wiley & Sons, 1988; Vol. 3.

(43) Yukl, E. T.; Jepkorir, G.; Alontaga, A. Y.; Pautsch, L.; Rodriguez, J. C.; Rivera, M.; Moënne-Loccoz, P. Kinetic and Spectroscopic Studies of Hemin Acquisition in the Hemophore HasAp from *Pseudomonas Aeruginosa*. *Biochemistry* **2010**, *49* (31), 6646–6654. https://doi.org/10.1021/bi100692f.

(44) Gorby, Y. A.; Yanina, S.; McLean, J. S.; Rosso, K. M.; Moyles, D.; Dohnalkova, A.; Beveridge, T. J.; Chang, I. S.; Kim, B. H.; Kim, K. S.; Culley, D. E.; Reed, S. B.; Romine, M. F.; Saffarini, D. A.; Hill, E. A.; Shi, L.; Elias, D. A.; Kennedy, D. W.; Pinchuk, G.; Watanabe, K.; Ishii, S.; Logan, B.; Nealson, K. H.; Fredrickson, J. K. Electrically Conductive Bacterial Nanowires Produced by *Shewanella Oneidensis* Strain MR-1 and Other Microorganisms. *Proceedings of the National Academy of Sciences* **2006**, *103* (30), 11358–11363. https://doi.org/10.1073/pnas.0604517103.

(45) Reguera, G.; McCarthy, K. D.; Mehta, T.; Nicoll, J. S.; Tuominen, M. T.; Lovley, D. R. Extracellular Electron Transfer via Microbial Nanowires. *Nature* **2005**, *435* (7045), 1098–1101. https://doi.org/10.1038/nature03661.

(46) El-Naggar, M. Y.; Wanger, G.; Leung, K. M.; Yuzvinsky, T. D.; Southam, G.; Yang, J.; Lau, W. M.; Nealson, K. H.; Gorby, Y. A. Electrical Transport along Bacterial Nanowires from *Shewanella Oneidensis* MR-1. *Proceedings of the National Academy of Sciences* **2010**, *107* (42), 18127–18131. https://doi.org/10.1073/pnas.1004880107.

(47) Zhang, Y.; Xie, Z.; Lu, C.; Guo, J.; Chen, Z.; Li, H.; Song, Y.; Han, Y.; Hou, Y. Study on the Electron Transfer Capability of Porphyrin Ring and the Mechanisms in the Catalytic Denitrification. *Biochemical Engineering Journal* **2021**, *175*, 108010. https://doi.org/10.1016/j.bej.2021.108010.

(48) Agam, Y.; Nandi, R.; Kaushansky, A.; Peskin, U.; Amdursky, N. The Porphyrin Ring Rather than the Metal Ion Dictates Long-Range Electron Transport across Proteins Suggesting Coherence-Assisted Mechanism. *Proceedings of the National Academy of Sciences* **2020**, *117* (51), 32260–32266. https://doi.org/10.1073/pnas.2008741117.

(49) Wyckoff, E. E.; Schmitt, M.; Wilks, A.; Payne, S. M. HutZ Is Required for Efficient Heme Utilization in *Vibrio Cholerae*. *Journal of Bacteriology* **2004**, *186* (13), 4142–4151. https://doi.org/10.1128/JB.186.13.4142-4151.2004.

(50) Lamousé-Smith, E.; Kelly, D.; de Cremoux, I. Designing Bugs as Drugs: Exploiting the Gut Microbiome. *Am J Physiol Gastrointest Liver Physiol* **2021**, *320* (3), G295–G303. https://doi.org/10.1152/ajpgi.00381.2019.

(51) Chiu, L.; Bazin, T.; Truchetet, M.-E.; Schaeverbeke, T.; Delhaes, L.; Pradeu, T. Protective Microbiota: From Localized to Long-Reaching Co-Immunity. *Front Immunol* **2017**, *8*, 1678. https://doi.org/10.3389/fimmu.2017.01678.

(52) Shanahan, F. Gut Microbes: From Bugs to Drugs. *Am J Gastroenterol* **2010**, *105* (2), 275–279. https://doi.org/10.1038/ajg.2009.729.

(53) Hornef, M. Pathogens, Commensal Symbionts, and Pathobionts: Discovery and Functional Effects on the Host. *ILAR J* **2015**, *56* (2), 159–162. https://doi.org/10.1093/ilar/ilv007.

(54) Venema, K.; van den Abbeele, P. Experimental Models of the Gut Microbiome. *Best Practice & Research Clinical Gastroenterology* **2013**, *27* (1), 115–126. https://doi.org/10.1016/j.bpg.2013.03.002.

(55) Kumar, M.; Ji, B.; Zengler, K.; Nielsen, J. Modelling Approaches for Studying the Microbiome. *Nature Microbiology* **2019**, *4* (8), 1253–1267. https://doi.org/10.1038/s41564-019-0491-9.

Figure 5.1 SSN of “W” Class C RSMTs

HutW clusters to the RS SSN Megacluster-2-2 which is oxygen-independent copropoprphyrinogen III oxidase-like. Megacluster-2-2 is large and functionally diverse. A single alignment score threshold cannot be used to segregate the SSN into isofunctional clusters. And therefore a series of 20 SSNs were generated with increasing alignment scores. As the alignment score increases, the clusters decrease in complexity and size as they become isofunctional. The isofunctional cluster of HutW is with several Vibrio spp. where one is annotated as a coproporphyrinogenase III oxidase and the other is annotated as a “HutW- like RS enzyme” see annotations on figure.

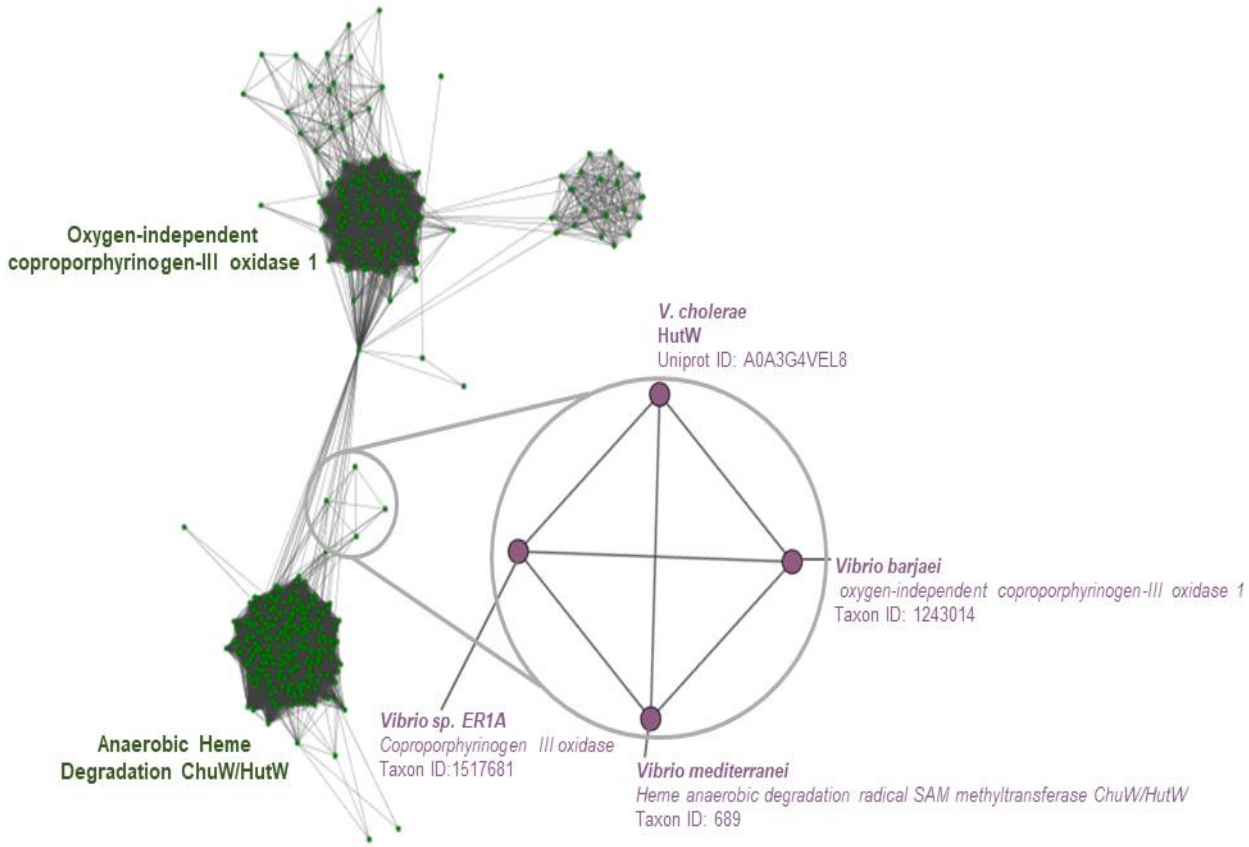
Oxygen-independent
coproporphyrinogen-III oxidase 1
V. cholerae
HutW
Uniprot ID: A0A3G4VEL8
Vibrio barjaei
oxygen-independent coproporphyrinogen-III oxidase 1
Taxon ID: 1243014
Vibrio sp. ER1A
Coproporphyrinogen III oxidase
Taxon ID:1517681
Vibrio mediterranei
Heme anaerobic degradation radical SAM methyltransferase ChuW/HutW
Taxon ID: 689
Anaerobic Heme
Degradation ChuW/HutW

Figure 5.2 Proposed HutW Mechanism

Proposed mechanism for the class C RSMT HutW incorporating the observation that NADPH can be used as a source of electrons. NADPH transfers a hydride, which is held intermittently by the heme porphyrin ring. One electron is transferred to the [4Fe-4S] cluster to produce [4Fe-4S]+ . The reduced iron-sulfur cluster cleaves one molecule of *S*-adenosylmethionine (SAM) to form a 5′-deoxyadenosine radical (5′-dAdo). The 5′-dAdo radical abstracts a hydrogen atom from a second molecule of SAM, which forms both 5′-deoxyadenosine and a methylene radical. The menthylene radical abstracts a hydrogen atom from the bound heme. The intermediate then undergoes radical rearrangement, which remains to be characterized. A radical, originally generated from NADPH, and a proton, likely held by an active site base as shown in the figure, are incorporated into the intermediate. The product shown is further reduced by NADPH to generate a tetrapyrrole where the bridging *meso* carbons are sp^3.

HutW proposed electron transfer pathway

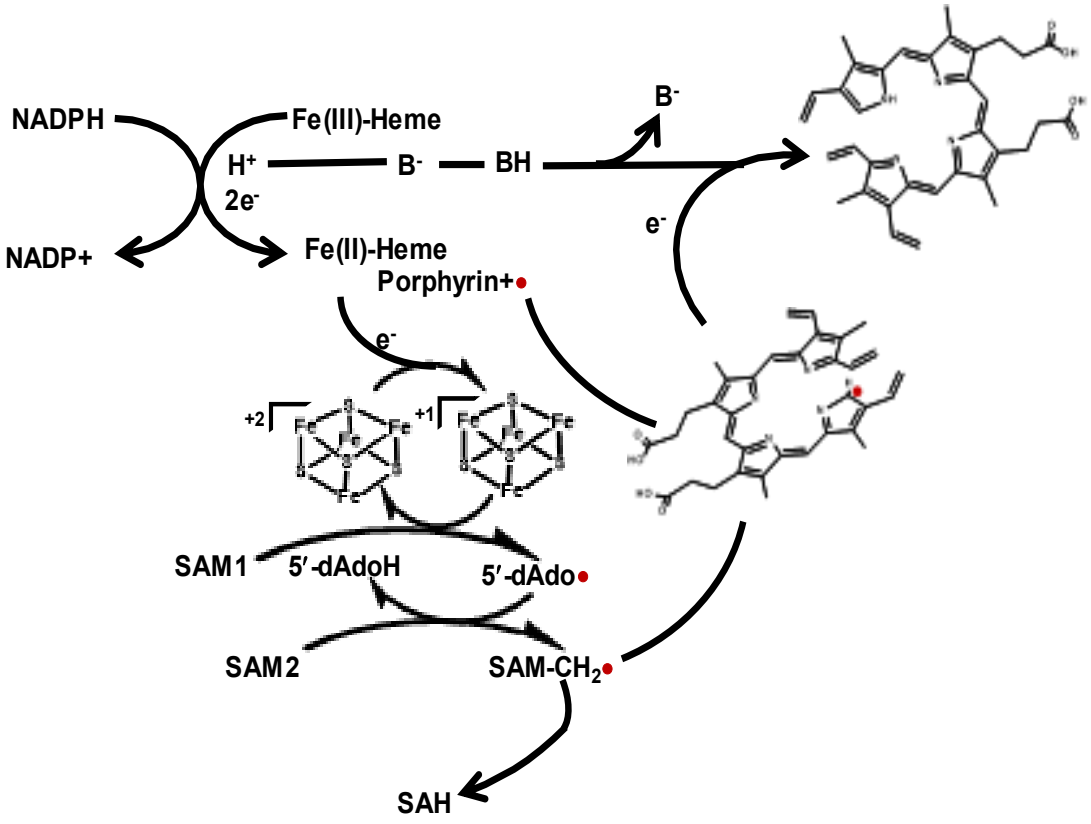

APPENDIX A

AXIAL HEME COORDINATION BY THE TYR-HIS MOTIF IN THE EXTRACELLULAR HEMOPHORE HASAP IS CRITICAL FOR THE RELEASE OF HEME TO THE HASR RECEPTOR OF *PSEUDOMONAS AERUGINOSA*[3]

[3]Alecia T. Dent, **Marley Brimberry**, Therese Albert, William N. Lanzilotta, Pierre Moënne-Loccoz, and Angela Wilks. (2021). Axial Heme Coordination by the Tyr-His Motif in the Extracellular Hemophore HasAp Is Critical for the Release of Heme to the HasR Receptor of *Pseudomonas aeruginosa*. *Biochemistry.* 60 (33), 2549-2559.

Abstract

Pseudomonas aeruginosa senses extracellular heme via an extra cytoplasmic function σ factor that is activated upon interaction of the hemophore holo-HasAp with the HasR receptor. Herein, we show Y75H holo-HasAp interacts with HasR but is unable to release heme for signaling and uptake. To understand this inhibition, we undertook a spectroscopic characterization of Y75H holo-HasAp by resonance Raman (RR), electron paramagnetic resonance (EPR), and X-ray crystallography. The RR spectra are consistent with a mixed six-coordinate high-spin (6cHS), six-coordinate low-spin (6cLS) heme configuration and an H_2 ^{18}O exchangeable FeIII−O stretching frequency with $^{16}O/^{18}O$ and H/D isotope shifts that support a two body Fe−OH_2 oscillator with (iron-hydroxy)-like character as both hydrogen atoms are engaged in short hydrogen bond interactions with protein side chains. Further support comes from the EPR spectrum of Y75H holo-HasAp that shows a LS rhombic signal with ligand-field splitting values intermediate between those of His-hydroxy and bis-His ferric hemes. The crystal structure of Y75H holo-HasAp confirmed the coordinated solvent molecule hydrogen bonded through H75 and H83. The long-range conformational rearrangement of HasAp upon heme binding can still take place in Y75H holo-HasAp, because the intercalation of a hydroxy ligand between the heme iron and H75 allows the variant to reproduce the heme binding pocket observed in wild-type holo-HasAp. However, in the absence of a covalent linkage to the Y75 loop combined with the malleability provided by the bracketing H75 and H83 hydrogen bonds, either the hydroxy sixth ligand remains bound after complexation of Y75H holo-HasAp with HasR or rearrangement and coordination of H85 prevent heme transfer.

Introduction

Iron is essential for the survival and virulence of nearly all bacterial pathogens. However, in the human body, iron is tightly bound by high-affinity binding proteins such as transferrin and ferritin.[1] The innate immune response further limits bioavailable iron by upregulating iron binding proteins such as lipocalin-2 and ferritin.[2] To combat iron deficiency within the host, bacterial pathogens have evolved systems that can scavenge iron and heme.[3–6] Pseudomonas aeruginosa is a major cause of infection in immune-compromised patients[7,8] and encodes several iron uptake systems, including the siderophore-based pyoverdine and pyochelin systems,[9,10] the ferrous uptake system (Feo),[11] and the heme assimilation (Has) and Pseudomonas heme uptake (Phu) systems.[12,13] Within the host, *P. aeruginosa* senses and alters gene expression in response to the extracellular iron source through cell surface signaling (CSS) systems that encode alternative σ factors. Extra cytoplasmic function (ECF) σ factors are proteins that form a complex with the core RNA polymerase, direct binding to the promoter region of target genes, and activate transcription.[14–17] P. aeruginosa encodes several ECF σ factors associated with the iron uptake systems, including iron starvation σ factors PvdS and FpvI. PvdS and FpvI respond to extracellular iron pyoverdine by upregulating expression of the pyoverdine biosynthesis genes and the cognate pyoverdine outer membrane (OM) receptor FpvA, respectively.[18–23] Several heme-dependent σ factors associated with heme uptake systems have also been identified in Gram-negative pathogens such as *Bordetella pertussis*,[24] *Serratia marcescens*,[25,26] and *P. aeruginosa*.[12]

The *P. aeruginosa* "Has" system senses heme through the interaction of a secreted extracellular hemophore, HasAp, that captures and releases heme to OM receptor HasR. Capture of the heme by the N-terminal plug domain of HasR results in inactivation of anti-σ factor HasS and release of σ factor HasI. HasI then binds to the hasR promoter, recruits the core RNA polymerase, and

upregulates transcription of the has operon. Simultaneously, heme released to HasR is transported through the receptor by the TonB-dependent coupling of the proton motive force of the cytoplasmic membrane. The Has system does not encode a periplasmic transport system, so heme is sequestered and translocated to the cytoplasm by the PhuT-PhuUV periplasmic ABC transport system. Within the cytoplasm, heme is transported to the iron-regulated heme oxygenase (HemO) by cytoplasmic heme binding protein PhuS.[27] HemO catalyzes the oxidative cleavage of heme releasing CO, iron, and heme metabolites biliverdin IXβ (BVIXβ) and IXδ (BVIXδ).[28] Furthermore, the *P. aeruginosa* Has and Phu systems have nonredundant roles in heme sensing and uptake, where the Has system is primarily required for sensing, and the Phu system is the major transporter.[13] In addition to heme-dependent transcriptional activation of the Has system by σ factor HasI, the *hasAp* transcript is also subject to post-transcriptional regulation by heme metabolite BVIXβ and/or BVIXδ.29,30 Multiple layers of transcriptional and post-transcriptional regulation over the Has system allow the bacteria to rapidly respond to changes in the host environment. The significance of heme sensing and uptake to *P. aeruginosa* pathogenesis is evident in the fact that clinical isolates from patients with chronic lung infection adapt over time to utilize heme while decreasing pyoverdine biosynthesis.[31] Furthermore, in a murine acute lung infection, the has system is the most upregulated set of genes and deletion of the HasR signaling receptor leads to a significant reduction in bacterial load and virulence.[32]

Given the significance of the Has system to bacterial survival and virulence, we sought to further investigate the molecular mechanism of heme-dependent signaling by the HasAp-HasR complex. Heme in HasAp is coordinated between two loops, one that includes conserved residue Tyr-75 and the other His-32.[33] Additionally, Tyr-75 engages in a hydrogen bond with His-83, stabilizing the loop in apo-HasAp and prepositioning Tyr-75 for coordination of the heme iron.

Previous spectroscopic and kinetic studies of the HasAp wild-type (WT) protein and the corresponding H32A heme coordination variant concluded heme rapidly binds to the Tyr-75 loop with a slower conformational closure of the His-32 loop.[33,34] Similar structural and kinetic studies of the HasAp Y75A and H83A variants concluded that hydrophobic π–π stacking and van der Waals interactions drive heme binding with the axial heme coordination, slowing the release of heme.[35] Such a mechanism allows HasAp to capture heme efficiently and with high affinity for delivery to its cognate receptor. In recent studies, we have begun to investigate the role of HasAp axial coordination in the release of heme to HasR by direct analysis of the transcriptional upregulation of the has operon following activation of the ECF σ factor system.[29,36] Taken together, our data utilizing WT holo-HasAp and the previously characterized Y75A, H32A, and H83A axial variants are consistent with a model in which holo-HasAp upon interaction with HasR causes a conformational rearrangement disrupting the hydrogen bond between Tyr-75 and His-83 that drives the concerted release of heme to HasR. In these same studies, we observed that a Y75H holo-HasAp variant did not activate the ECF σ factor system and interpreted this to be due to inhibition of the release of heme to HasR. Herein, we further show by surface plasmon resonance (SPR) that the Y75H holo-HasAp protein retains the ability to interact with the HasR receptor but is unable to support heme uptake on supplementation of the *P. aeruginosa ΔhasAp* strain. Spectroscopic and structural characterization of the Y75H holo-HasAp variant confirmed a similar overall structural fold and heme binding mode to that of WT holo-HasAp. However, rather than the anticipated bis-His ligation, the RR, EPR, and crystal structure are consistent with heme coordination through a water molecule that is strongly hydrogen bonded to H75 and H83. Furthermore, mutation of the Tyr-His motif causes a conformational rearrangement of the H32 loop that is also seen in the Y75A and H83A holo-HasAp crystal structures.[35] We propose this

strongly hydrogen bonded Fe-OH ligand inhibits the conformational rearrangement required to facilitate heme release.

Experimental Procedures

Bacterial Strains, Plasmids, and Proteins.

Bacterial strains and plasmids used in this study were as previously reported.[29] Escherichia coli strains were routinely grown in Luria-Bertani (LB) broth (American Bioanalytical) or on LB agar plates, and P. aeruginosa strains were freshly streaked and maintained on Pseudomonas isolation agar (PIA) (BD Biosciences). All strains were stored frozen at −80 °C in LB broth with 20% glycerol. All purified proteins were stored at −80 °C until further use.

Purification of HasAp WT and Y75H Proteins.

Protein expression was performed by a slight modification of the previously published method.[29] Briefly, WT and Y75H HasAp were expressed by culturing a single colony from freshly transformed E. coli BL21(DE) cells for 16 h in LB medium (100 mL) containing 100 μg/mL ampicillin at 37 °C while being shaken. The cells were harvested by centrifugation and washed twice in M9, and the cell pellet was resuspended and used to inoculate 4 × 1 L of M9 medium containing 100 μg/mL ampicillin to a final OD600 of 0.05. The cells were grown to an OD600 of ~1.0, induced with a final concentration of isopropyl β-D-thiogalactopyranoside (IPTG) of 1 mM, and grown for a further 16 h at 30 °C. Cells were harvested by centrifugation and stored at −80 °C until further use. Pellets were thawed and resuspended in 40 mL of lysis buffer [20 mM Tris-HCl (pH 7.5), 20 mM NaCl, and 1 mM EDTA] containing a protease inhibitor tablet (Roche), 1 mg/mL DNase, and 25 mg/mL lysozyme, stirred at 4 °C for 1 h, and passed through a model LM-20

microfluidizer at 20000 psi. The lysis suspension was centrifuged at 25000 rpm for 1 h, and the supernatant applied to a Q-Sepharose column (3 cm × 10 cm) pre-equilibrated with equilibration buffer [20 mM Tris-HCl (pH 7.5) and 20 mM NaCl]. The column was washed (3–5 column volumes) with equilibration buffer, and the protein eluted over a gradient from 20 to 600 mM NaCl in 20 mM Tris-HCl (pH 7.5). The purity of the eluted fractions was determined by SDS–PAGE, and the peak fractions were pooled and dialyzed in 4 L of 50 mM Tris-HCl (pH 7.5) containing 50 mM NaCl. The protein was concentrated and further purified on an AKTA FPLC instrument over a 26/60 Superdex 200 size exclusion column. Fractions containing purified protein were pooled, concentrated to 10 mg/mL, and stored at −80 °C. Apo-HasAp was reconstituted with heme prepared immediately prior to use by being dissolved in 0.1 mM NaOH and buffered with 10 mM Tris-HCl (pH 8). The final concentration of the heme stock was determined by the pyridine hemochrome method.37 WT and Y75H HasAp were reconstituted in a 1:1 ratio with hemin, incubated on ice for 30 min, and concentrated via an Amicon ultracentrifuge filter (30 MWCO). The integrity of protein secondary structure was determined by circular dichroism (CD) spectroscopy recorded on a Jasco J-810 spectropolarimeter as previously described.[29]

Purification and Reconstitution of HasR in SMALPS.

HasR was prepared as previously described.[38] Briefly, a single colony of freshly transformed *E. coli* BL21 (DE3) transformed with pHasR22b was used to inoculate 50 mL of non-inducing MDAG-135 medium containing 100 μg/mL Amp and grown overnight at 37 °C and 225 rpm. This culture was used to inoculate four 1 L flasks of autoinducing MDA-5052 medium containing 100 μg/mL Amp and grown for 10 h at 25 °C. Cells were harvested by centrifugation, resuspended in 40 mL of lysis buffer, and passed through a model LM-20 microfluidizer at 20000 psi. Cell debris was removed by centrifugation at 12000 rpm for 15 min, and the supernatant was centrifuged for

1 h at 25000 rpm to pellet the cellular membranes. Pelleted membranes were resuspended in 30 mL of lysis buffer with an added EDTA-free protease inhibitor tablet (Roche) overnight. The cytoplasmic membrane proteins were solubilized by addition of 2% (v/v) Triton X-100 (Sigma) and 0.5% (v/v) N-lauroylsarcosine sodium salt (Sigma). The membrane fractions were stirred at room temperature for 1 h and pelleted at 25000 rpm for 1 h at 4 °C. The supernatant was discarded, and the pelleted OM fraction was resuspended in 30 mL of lysis buffer containing an EDTA-free protease inhibitor cocktail tablet and stirred at 4 °C overnight.

The RC DC protein assay (Bio-Rad) was used to determine the total protein concentration, and the OM fragments were diluted to a final concentration of ~10 mg/mL. The styrene-maleic acid copolymer (Xiran SL30010 P20) was then added to the OM suspension to a final concentration of 2.5% (v/v) and inverted continuously at room temperature for 1 h. The suspension was frozen in liquid nitrogen and thawed at 42 °C a total of five times followed by passage through a microfluidizer at 20000 psi. This cycle was repeated once more; the final suspension was centrifuged at 25000 rpm for 1 h at 4 °C, and the supernatant containing the HasR in lipid nanodisc (HasR-SMALP) was collected. The supernatant was concentrated, and the HasR concentration was determined using an extinction coefficient of 126 mM^{-1} cm^{-1} after subtracting the blank containing the filtrate (to account for absorption of residual lipids and polymer).

Surface Plasmon Resonance of Holo-HasAp WT and Y75H Binding to HasR.

Holo-HasAp WT or Y75H protein was covalently bound to the surface of flow cells 2–4 of a CM5 chip to a final level of 50 RU using the NHS-EDC kit (GE Life Sciences, Piscataway, NJ). Flow cell 1 was used as a blank. HasR-his (0–1000 nM) in 120 μL of HBS-EP buffer (GE Life Sciences) was injected into flow cells 1–4 at 25 °C until the signal reached saturation. The surface was then washed with buffer for 3 min, and the dissociation of analyte–ligand complexes was followed over

time. The flow cells were regenerated by injecting 15 μL aliquots of 10 mM glycine (pH 1.5) followed by 15 μL aliquots of 10 mM NaOH, and the process was repeated. Values from the reference flow cell were subtracted to obtain the values for specific binding. The maximum response units during the steady-state phase were plotted as a function of HasR concentration, and data were fitted to a 1:1 binding model using BIAeval version 4.1 (Biacore).

[13C]Heme Uptake and Extraction of [13C]BVIX Isomers from Holo-HasAp WT- and Y75H-Supplemented Cultures.

[^{13}C]Heme uptake studies were performed as previously described.[36] Briefly, a single isolated colony of the *ΔhasAp* strain[29] was picked, inoculated into 10 mL of LB broth, and grown overnight at 37 °C. The cultures were then harvested and washed in 10 mL of M9 minimal medium (Nalgene). The iron levels in M9 medium were determined by ICP-MS to be <1 nM. Following centrifugation, the bacterial pellet was resuspended in 10 mL of M9 medium and used to inoculate 50 mL of fresh M9 low-iron medium to a starting OD600 of 0.04. Cultures were grown at 37 °C while being shaken for 3 h before the addition of 1 μM WT or Y75H [^{13}C]holo-HasAp. Cells were harvested by centrifugation, and the BVIX isomers were extracted as previously described.[30] Briefly, the cell medium was collected and filtered through a Nalgene vacuum filtration unit with a 0.22 μm PVDF membrane. The resulting flow-through was acidified to pH ~2.5 with 10% trifluoroacetic acid (TFA), supplemented with a final concentration of BVIXα dimethyl ester of 10 nM as an internal standard and loaded over a C_{18} Sep-Pak column (Waters). The column was previously flushed with 2 mL of acetonitrile (ACN), H2O, 0.1% TFA in H2O, and methanol in 0.1% TFA (10:90). Following sample application, the columns were washed with 4 mL of 0.1% TFA, 4 mL of an ACN/0.1% TFA mixture (20:80), and 2 mL of a methanol/0.1% TFA mixture

(50:50). Purified BVIX isomers were eluted in methanol, dried, and stored for up to 1 week at −80 °C prior to LC-MS/MS analysis.

LC-MS/MS Analysis of BVIX Isomers.

Samples were resuspended in 10 μL of DMSO, diluted to 100 μL with mobile phase ACN [50:50 (v/v)], centrifuged at 14000 rpm for 5 min at room temperature to remove particulates, and filtered through a 0.45 μm syringe filter prior to loading. BVIX isomers (2 μL) were separated and analyzed by LC-tandem mass spectrometry (MS/MS) (Waters TQ-XS triple-quadrupole mass spectrometer with an AQUITY H-Class UPLC instrument) as previously described with slight modification.[30] BVIX isomers were separated on an Ascentis RP-amide 2.7 μm C18 column (10 cm × 2.1 mm) at a flow rate of 0.4 mL/min. The mobile phase consisted of phase A (H2O/0.1% formic acid) and phase B (ACN/0.1% formic acid). The initial gradient is 64% A and 36% B. After 5 min, 55% A and 45% B, after 8 min 40% A and 60% B, after 8.5 min 5% A and 95% B, and after 10 min 64% A and 36% B. Fragmentation patterns of the precursor ions were detected at 583.21 ([^{12}C]BVIX) and 591.21 ([^{13}C]BVIX) using multiple-reaction monitoring (MRM). The source temperature was set to 150 °C, the capillary voltage to 3.60 kV, and the cone voltage to 43 V. The column was kept at 30 °C during separation. The precursor ions used in MRM for the α, β, and δ isomers of [^{12}C]BVIX are at 297.1, 343.1, and 402.2, respectively, with collision energies of 38, 36, and 30 V, respectively. The product ions used in MRM for the α, β, and δ isomers of [^{13}C]BVIX are at 301.1, 347.1, and 408.2, respectively, with a collision energy of 34 V for each.

Resonance Raman and EPR Spectroscopy.

All EPR and RR measurements were conducted on solutions containing 150–200 μM heme in 100 mM HEPES buffer (pH 7.5). Water exchange with $H_2{}^{18}O$ and D_2O was performed through

concentration and redilution of the protein solution with the HEPES buffer prepared in labeled water to reach labeling levels of >80%. The RR spectra were recorded on a custom McPherson 2061/207 spectrograph equipped with a liquid N_2-cooled CCD detector (LN1100PB, Princeton Instruments). The excitation wavelength at 407 nm was provided by a krypton laser (Innova 302C, Coherent) with attenuation of the Rayleigh scattering with a long-pass filter (RazorEdge, Semrock). Room-temperature RR spectra were recorded in a 90° scattering geometry, while RR spectra of frozen solutions maintained at 110 K with a liquid nitrogen coldfinger were recorded using a back-scattering geometry. Comparison of spectra obtained with short acquisition on rapidly spinning samples with longer acquisition on static samples confirmed the lack of photosensitivity of all samples with laser intensities maintained below 15 mW. Frequency calibrations using indene and aspirin standards are accurate with ±1 cm^{-1}.

EPR spectra were recorded on a Bruker E-500 X-band EPR spectrometer equipped with a superX microwave bridge and a dual-mode cavity with a helium flow cryostat (ESR900, Oxford Instruments). The microwave frequency was 9.67 GHz, the microwave power 1 mW, the modulation frequency 100 kHz, and the modulation amplitude 4 G.

Crystallography.

Diffraction quality crystals of the Y75H HasA variant were obtained when the purified enzyme (0.5 μL at 10 mg/mL) was mixed in a 1:1 ratio with a precipitating solution containing 0.1 M sodium chloride, 0.1 M HEPES (pH 7.5), and 1.6 M ammonium sulfate (100 μL reservoir) using a Mosquito (tpplabtech, Boston, MA) protein crystallization robot. Crystals appeared 4 weeks after incubation at 18 °C. Crystals of the H32A HasA variant were obtained when the purified enzyme (1 μL at 10 mg/mL) was mixed in a 1:1 ratio with a precipitating solution of 1 M sodium citrate, 0.1 M Tris (pH 7.0), and 0.2 M sodium chloride. Crystals of HasA H32A were obtained via sitting

drop diffusion. Crystals appeared after incubation for 1 week at 18 °C. Monochromatic data collection with 0.97 Å X-rays was performed at SER-CAT on beamline 22-ID at the Advanced Photon Source (Argonne, IL). Data were processed using SGXPRO, and 5% of the reflections were set aside for cross-validation.[39] Phases were obtained by molecular replacement using the WT HasAp [Protein Data Bank (PDB) entry 3ELL] model, and initial phasing was performed using PHENIX. Successive rounds of model building and refinement were performed using COOT and PHENIX.40,41 Data collection and refinement statistics are listed in Table 1.

Results

Surface Plasmon Resonance (SPR) Analysis of Interaction of Holo-HasAp WT and Y75H with HasR.

We previously characterized the heme binding properties of Y75H HasAp along with that of the Y75A, H32A, and H83A variants.29 The heme binding affinity (K_D) as determined by isothermal titration calorimetry for Y75H HasAp (1.1 ± 0.7 μM) is identical to that of WT HasAp (1.2 ± 0.8 μM). Whereas binding of heme to WT and Y75H HasAp was enthalpically driven, the Y75A variant showed an increase in entropy at the expense of enthalpic contributions that were attributed to stronger hydrophobic interaction of the heme with the Y75 loop and disorder in the loop upon loss of the coordinating ligand. Moreover, transcriptional reporter assays further showed the heme coordination mutants Y75A, H83A, and H32A holo-HasAp variants retained their ability to activate the ECF σ factor system. However, the holo-HasAp Y75H variant showed no transcriptional activation at the *hasR* promoter. We initially attributed this to the inability of holo-HasAp Y75H protein to release heme to HasR due to potentially stronger bis-His coordination.

We previously determined the relative K_D for binding of apo- and holo-HasAp WT to purified HasR WT in SMALPs as the analyte.[38] The calculated K_D for the binding of holo-HasAp to HasR as determined by steady-state association measurements with various analyte concentrations was 479 ± 20 nM. Herein, we determined the K_D for holo-HasAp Y75H to be 394 ± 5 nM (Figure 1). The similar binding affinity of holo-HasAp WT and Y75H protein for HasR ruled out disruption of the protein–protein interaction as the reason for Y75H holo-HasAp's inability to activate the ECF σ factor system. As transcriptional activation and heme transport require protein–protein interaction, conformational rearrangement, and energy-dependent uptake, any in vitro measurement of binding affinity (K_D) merely represents a determination of relative associations of the holo-HasAp and HasR proteins. To further determine if the inability to signal is due to heme retention in Y75H holo-HasAp, we also evaluated heme uptake in vivo utilizing our previously developed [^{13}C]heme uptake assay.

[^{13}C]Heme Isotopic Labeling and LC-MS/MS Analysis of the BVIX Isomers.

Heme release and transport were assessed by analysis of the BVIX metabolites following supplementation of cultures with either WT or Y75H [^{13}C]heme-HasAp. Supernatants were collected 4 h following supplementation, and the BVIX metabolites extracted and analyzed by LC-MS/MS. We confirmed that PAO1 WT cultures supplemented with [^{13}C]heme-HasAp were able to utilize the heme via the Has system (Figure 2A). The *ΔhasAp* cultures supplemented with Y75H [^{13}C]heme-HasAp variant were unable to utilize heme as an iron source as judged by the lack of [^{13}C]BVIXβ and BVIXδ metabolites (Figure 2B). This observation is consistent with recent studies of the heme uptake defective *hasRH624A* and *hasRH221R* allelic strains where free heme in solution, but not heme bound to HasAp, is accessible to the PhuR transporter.[36] The inability of

Y75H holo-HasAp to support heme uptake is also consistent with inhibition of heme release to HasR.

Spectroscopic Characterization of the Holo-hasAp Y75H Variant.

The room-temperature absorption spectra of WT and Y75H holo-HasAp show differences in their high-spin:low-spin ratios as judged by the increased intensity of the Q-bands at 537 and 570 nm and decreased high-spin marker at 618 nm in the holo-HasAp Y75H variant compared to WT (Figure 3A). To further confirm the coordination and the heme iron status of the Y75H holo-HasAp variant, we performed RR spectroscopy. The room-temperature RR spectrum of WT holo-HasAp obtained with Soret excitation shows a porphyrin skeletal frequency ν4 at 1370 cm−1 typical of ferric (Fe3+) hemes and ν3, ν2, and ν10 frequencies representative of both six-coordinate high-spin (6cHS) (1477, 1561, and 1605 cm−1, respectively) and six-coordinate low-spin (6cLS) (1503, 1579, and 1634 cm−1, respectively) conformers (Figure 3B,C). Y75H holo-HasAp shows similar RR frequencies from both 6cHS and 6cLS species compared to WT holo-HasAp, but the high-spin versus low-spin intensities are significantly lower in Y75H than in the WT. The vinyl stretching frequency at 1624 cm−1 and C–C–C deformation modes at 378 and 410–420 cm−1 from the porphyrin peripheral groups are not significantly affected by the Tyr-75 to His substitution, suggesting the heme seating is similar in both proteins. RR spectra of WT and Y75H holo-HasAp at 110 K show greatly decreased intensities for the 6cHS contribution and increased intensities for the 6cLS contribution (Figure 4A). Most importantly, low-frequency RR spectra of Y75H holo-HasAp recorded at 110 K show a ν(FeIII–OH) stretching frequency at 514 cm−1 identified through its downshift after incubation in $H_2{}^{18}O$ and D_2O (Figure 4B). This low-spin ν(FeIII–OH) frequency is ~40 cm−1 lower than in hydroxy complexes of vertebrate globins in alkaline buffers and is more in tune with frequencies observed in bacterially truncated hemoglobins, where the presence of

multiple hydrogen bond interactions with the coordinating hydroxy group weakens the FeIII–OH bond.[42]

While the 25 cm−1 downshift observed with 18O exchange matches reasonably well with the calculated shifts for a two-body Fe–OH harmonic oscillator (Δ18Ocalc = −21 cm−1), the large isotope shift observed with H/D exchange is more puzzling. One possible interpretation for these isotope shifts is that the 514 cm−1 band corresponds to a two-body Fe–OH2 oscillator with both H atoms engaged in short hydrogen bond interactions, leading to an iron(III)-hydroxo-like sixth ligand (Scheme 1). This analysis of the RR data is supported by the crystallography data (see the following section).

The EPR spectra of holo-HasAp WT and Y75H are dominated by a rhombic signal centered around g = 2, consistent with the 6cLS ferric heme species (Figure 5A). As previously observed for holo-HasAp WT,[34] a minor resonance at g = 6.1 corresponding to an axial high-spin heme population is also present in the holo-HasAp Y75H variant. The holo-HasAp WT 6cLS resonances at g = 2.83, 2.20, and 1.71 are identical to those previously reported.[34] In contrast, holo-HasAp Y75H shows broadened resonances at g = 2.89, 2.24, and 1.65. Using McGarvey's analysis of the tetragonal low-spin d5 ferric heme EPR signature[48] and Joshua Tesler's DLD5 program to calculate ligand-field splitting parameters, we compare holo-HasAp Y75H with other low-spin heme proteins as initially carried out by Blumberg and Peisach.[49] The resulting ligand-field splitting values are intermediate between those previously reported for bis-His and His-hydroxy ligated systems (Figure 5B).

Crystal Structure of the Holo-HasAp Y75H Variant.

The holo-HasAp Y75H structure, determined to 1.3 Å resolution, shows an overall αβ fold similar to that of holo-HasAp WT (Figure 6A). As for the holo-HasAp WT, the holo-HasAp Y75H structure consists of an extended "β-sheet wall" comprised of eight antiparallel β-strands connected by hairpin loops. Opposite of this "β-sheet wall" four α-helices pack to form a "α-helix wall". Additionally, the plane of the porphyrin ring for the heme in holo-HasAp Y75H is oriented in a similar manner when compared to that of the WT protein (Figure 6B). The Fe–NHis32 bond lengths in the WT and Y75H mutants are similar at 2.0 and 2.2 Å, respectively. The sixth coordination site of the heme iron is occupied by a solvent molecule in HasAp Y75H with an Fe–O bond length of 2.1 Å that mimics well the 2.0 Å Fe–OTyr75 distance observed in the WT structure (Figure 6B).[50] The distance from the His-Nε of H75 or H83 to the iron-bound solvent molecule is 2.5 Å. Interestingly, the Nδ atom of H83 that is located in the loop linking strands β3 and β4 forms a hydrogen bond with the phenol oxygen of Y75 in the apo- and holo-HasAp WT structures.[33] On the basis of stopped flow absorption and rapid freeze quench RR of heme binding to the WT, Y75A, and H83A variants, the authors proposed the Tyr75 Oη–His83 Nδ hydrogen bond facilitates heme loading by orienting Y75 to coordinate the heme iron. In the absence of the hydrogen bond in the Y75A variant, the conformational disorder in the loop may allow for transient coordination of H83 prior to loop closure and coordination of H32 that leads to displacement of H83 and coordination of a water molecule. A similar sequence of events may occur if heme binds to Y75H where coordination of H83 or H75 may occur prior to H32 loop closure and scission of the His coordination and replacement by a water molecule. The fact that the structures of the Y75 and H32 loops are very similar in the Y75H, Y75A, and H32A holo-HasAp structures with only a slight reorientation of R33, D39, and V38 rotating the H32 loop away from the heme is consistent with previous studies indicating heme binding is dominated by π–π stacking and hydrophobic

interactions with side chains in the Y75 loop (Figure 6). The crystal structure at 1.32 Å resolution is a good predictor of the hydrogen bonding network, consistent with the Fe–OH2 oscillator predicted by RR where the coordinated water molecule replacing Y75 is strongly hydrogen bonded through H75 and H83.

Discussion

On the basis of previous studies supplementing the *P. aeruginosa ΔhasAp* strain with WT or holo-HasAp Y75A or H83A variants, we proposed a model for heme-dependent activation of the CSS cascade. In this model, the release of heme from HasAp to HasR involves a concerted release of H32 and Y75 facilitated by weakening of the tyrosinate ligand on transient protonation by H83. This was in part based on the observation of a significant increase in the level of *hasR* mRNA (a result of activation of the CSS cascade for the Y75A or H83A HasAp variant) compared to that of WT holo-HasAp. This increase in the level of transcription given the fact the total heme available to the strains is identical was attributed to a nonphysiological kinetically trapped "signaling" intermediate that transports heme at a slower rate.[29] Interestingly, the crystal structure of the Y75A and H83A holo-HasAp proteins shows the overall fold and positioning of the heme to be almost identical to those of WT holo-HasAp.[35] The primary factor of importance is the ligation state of the iron atom.

In the H83A holo-HasAp structure, Y75 remains coordinated to the heme, whereas in Y75A holo-HasAp, an exogenous ligand replaces Y75 with H83A, occupying a similar position in the absence of the Y75 ligand. In the H83A holo-HasAp structures, a water molecule or an ethylene glycol from the cryoprotectant forms a hydrogen bond with Y75, essentially replacing

the Y75 Oη–H83 Nδ hydrogen bond in WT holo-HasAp.35 RR and EPR analyses of H83A holo-HasAp are consistent with a 6cHS/6cLS mixture as seen here with the Y75H variant. Previous spectroscopic studies of the *S. marcescens* H83A holo-HasA suggested that disruption of the hydrogen bond resulted in loss of the Tyr ligand,[51] but subsequent analysis of H83A holo-HasAp showed that the Tyr ligation is a weaker sixth ligand at room temperature but is retained and enforces the same rhombic low-spin ferric EPR signature at cryogenic temperatures as in WT holo-HasAp.[35] While the conformation of the Y75 loop in the Y75A and H83A mutants is similar to that of WT holo-HasAp, the conformation of the H32 loop in both mutants is more affected than in WT holo-HasAp. The reorientation of the H32 loop and several side chains, including R33, D39, and V38, rotate the loop away from the heme, potentially weakening the steric clash upon interaction with HasR. While not true for all crystal forms, it is important to note that R33 forms an important crystal contact in the WT holo-HasAp crystal lattice, and therefore, structural differences in the H32 loop need to be carefully interpreted. The most feasible hypothesis at this time is that modulation of the tyrosinate character of Y75, during interaction with HasR, is required for the concerted release of heme. The loss or disruption of this controlled release leads to the formation of the "kinetically" trapped intermediate. Furthermore, the region of the H32 loop most affected by the previous Y75 loop mutations is the region not visible in the crystal structure of the S. marcescens HasA–HasR complex.[52] Moreover, as the H32A mutation also gave a similar signaling profile, the data suggest that preferential loss of either ligand yields the "kinetically" trapped signaling intermediate.

In previous studies, we attributed the inability of the Y75H holo-HasAp to activate the CSS cascade to the potential of a stronger bis-His ligation.[29] In an effort to further understand the significance of the His-Tyr motif in controlling the release of heme to HasR, we performed

spectroscopic and structural analysis of the Y75H holo-HasAp variant. SPR analysis of the interaction of Y75H holo-HasAp with HasR confirmed the inability to trigger the CSS cascade was not due to disruption of the protein–protein interaction (Figure 1). Moreover, despite the retention of the protein–protein interaction, supplementation of the ΔhasAp strain with [13C]heme-loaded Y75H HasAp showed a growth defect consistent with the lack of [13C]heme-derived biliverdin metabolites compared to WT holo-HasAp supplementation (Figure 2). Taken together, the data are consistent with a stronger heme ligation inhibiting heme sensing and uptake by preventing the release of heme to the receptor.

The absorption, RR, and EPR spectroscopic analyses of Y75H holo-HasAp are consistent with predominantly 6CLS ferric heme species (Figures 3 and 4). Interestingly, rather than a bis-His signature, the detection of a ν(FeIII–OH) stretching frequency at 514 cm−1 in the Y75H holo-HasAp low-frequency RR spectrum is indicative of a hydroxy ligand that is strongly hydrogen bonded. Similarly, ligand-field analysis of the low-spin d5 ferric heme EPR signature reveals ligand-field splitting parameters that fall between a bis-His and His-hydroxy ligation to the heme. The crystal structure of Y75H holo-HasAp is further confirmation of a unique ligation within the heme pocket. As is the case for the Y75A and H83A holo-HasAp structures,[35] the heme seating in Y75H holo-HasAp is unchanged from that of WT holo-HasAp (Figure 6). Similarly, the Fe–N and Fe–O ligand bond lengths are similar within 0.2 and 0.1 Å, respectively. The most notable change in the Y75H holo-HasAp structure is in the H32 loop, where similar to the Y75A and H83A holo-HasAp variants (Figure 6C,D), the alternate conformation is rotated away from the heme (Figure 6B). However, as previously mentioned, extreme care must be taken to interpret these conformational changes as R33 is involved in a crystal contact in WT holo-HasAp, but not in the Y75H holo-HasAp crystal lattice. An alternative origin for heme retention in Y75H may be the

lack of a covalent linkage between the heme iron and the Y75 loop, providing sufficient flexibility to this His–hydroxy ligation motif to remain after complexation with HasR and to inhibit the transfer of the heme to HasR. Indeed, the hydrogen bonds from H83 and H75 optimize the coordination of a hydroxy group in place of the Tyr75 hydroxy group. More importantly, this new interaction provides sufficient malleability to this His-hydroxy-His binding motif, allowing significant rearrangement of the Y75 loop upon interaction with HasR without displacement and loss of the hydroxy ligating group. The current data suggest that a steric clash between the H32 loop of HasAp with L8 of HasR is not sufficient to drive the conformational rearrangement required to sever the Fe–N ligand but also modulation of the Fe–O bond on the opposite face of the heme to trigger the release of heme upon interaction with HasR.

The critical role of the Tyr-His motif in driving conformational rearrangement and heme release is further supported by the fact the H32 coordination is not conserved among HasA proteins. *Yersinia pestis* HasA encodes a Gln at position 32 with the heme solely ligated through the conserved Tyr-His motif.[53] Interestingly, the Y. pestis apo-HasA (HasAyp) structure is in a closed loop conformation almost identical to the holo-HasA structure, with the only significant difference being rearrangement of the R40 side chain on the distal face of the heme in the holo structure.[53] More evidence for the closed loop structure of apo-HasAyp is the extremely fast on rate of heme binding this hemophore displays compared to that of HasAp.[53] Interestingly, the R33A HasAp variant disrupts the “zipper-like” interaction of the H32 loop with the protein core required for stabilizing the apo-HasAp open conformation, allowing the H32 loop to adopt a closed conformation similar to that of HasAyp.[54] However, the R33A apo-HasAp closed conformation is less efficient in capturing heme than the apo-HasAyp conformation, suggesting there are subtle differences between R33A apo-HasAp and HasAyp in terms of the conformational dynamics and

kinetics of heme binding. The authors concluded that the apo-HasAyp closed conformation has evolved to optimize binding to the hydrophobic Y75 platform whereas in R33A apo-HasAp the closed H32 loop obstructs the heme binding pocket. Moreover, the fact that the ability of the H32A holo-HasAp variant to support heme transport is compromised suggests there may be subtle differences between the conformational dynamics and rearrangement between holo-HasAp WT and the H32 loop mutants on interaction with HasR. In this context, it would be interesting to see if the closed conformation of *Y. pestis* holo-HasAyp upon supplementation of the *P. aeruginosa ΔhasAp* allelic strain has a signaling and uptake profile similar to that of WT holo-HasAp or the H32A HasAp variant. Taken together with current studies of Y75H holo-HasAp, the accumulated data suggest the Tyr-His motif is critical for coupling modulation of the Fe–O ligand with conformational rearrangements in the H32 and Y75 loops of HasAp required to release heme to HasR. We hypothesize that the Tyr-His motif and its ability to actuate long-range conformational changes within the H(Q)32 loop constitute a conserved mechanism irrespective of a coordinating ligand to the heme. We are further investigating the mechanism of heme release and transport structurally analyzing the HasAp mutants in complex with HasR together with in vivo heme signaling and transport assays. In conclusion, our studies highlight the unique nature of the Tyr-His motif that couples conformational rearrangement on protein–protein interaction to controlled heme release. As such, the unique properties of the conserved Tyr-His motif have been exploited in a variety of bacterial heme transport systems in both Gram-negative and Gram-positive pathogens.[55–57]

References

(1) Otto BR, Verweij-Van Vught AM, and MacLaren DM (1992) Transferrins and heme-compounds as iron sources for pathogenic bacteria. Crit. Rev. Microbiol 18, 217–233. [PubMed: 1532495]

(2). Ganz T (2009) Iron in innate immunity: starve the invaders. Curr. Opin. Immunol 21, 63–67. [PubMed: 19231148]

(3). Payne SM, Mey AR, and Wyckoff EE (2016) Vibrio Iron Transport: Evolutionary Adaptation to Life in Multiple Environments. Microbiol. Mol. Biol. Rev 80, 69–90. [PubMed: 26658001]

(4). Sheldon JR, and Heinrichs DE (2015) Recent developments in understanding the iron acquisition strategies of gram positive pathogens. FEMS Microbiol Rev. 39, 592–630. [PubMed: 25862688]

(5). Contreras H, Chim N, Credali A, and Goulding CW (2014) Heme uptake in bacterial pathogens. Curr. Opin. Chem. Biol 19, 34–41. [PubMed: 24780277]

(6). Huang W, and Wilks A (2017) Extracellular Heme Uptake and the Challenge of Bacterial Cell Membranes. Annu. Rev. Biochem 86, 799–823. [PubMed: 28426241]

(7). Costerton JW (2001) Cystic fibrosis pathogenesis and the role of biofilms in persistent infection. Trends Microbiol. 9, 50–52. [PubMed: 11173226]

(8). Sadikot RT, Blackwell TS, Christman JW, and Prince AS (2005) Pathogen-host interactions in Pseudomonas aeruginosa pneumonia. Am. J. Respir. Crit. Care Med 171, 1209–1223. [PubMed: 15695491]

(9). Royt PW (1990) Pyoverdine-mediated iron transport. Fate of iron and ligand in Pseudomonas aeruginosa. Biol. Met 3, 28–33. [PubMed: 2119198] Dent et al.Page 13Biochemistry. Author manuscript; available in PMC 2021 December 15.Author ManuscriptAuthor ManuscriptAuthor ManuscriptAuthor Manuscript

(10). Heinrichs DE, Young L, and Poole K (1991) Pyochelin-mediated iron transport in Pseudomonas aeruginosa: involvement of a high-molecular-mass outer membrane protein. Infect. Immun 59, 3680–3684. [PubMed: 1910015]

(11). Hunter RC, Asfour F, Dingemans J, Osuna BL, Samad T, Malfroot A, Cornelis P, and Newman DK (2013) Ferrous iron is a significant component of bioavailable iron in cystic fibrosis airways. mBio 4, No. e00557–13.

(12). Ochsner UA, Johnson Z, and Vasil ML (2000) Genetics and regulation of two distinct haem-uptake systems, phu and has, in Pseudomonas aeruginosa. Microbiology 146 (Part 1), 185–198. [PubMed: 10658665]

(13). Smith AD, and Wilks A (2015) Differential Contributions of the Outer Membrane Receptors PhuR and HasR to Heme Acquisition in Pseudomonas aeruginosa. J. Biol. Chem 290, 7756–7766. [PubMed: 25616666]

(14). Llamas MA, Imperi F, Visca P, and Lamont IL (2014) Cell-surface signaling in Pseudomonas: stress responses, iron transport, and pathogenicity. FEMS Microbiol Rev. 38, 569–597. [PubMed: 24923658]

(15). Mascher T (2013) Signaling diversity and evolution of extracytoplasmic function (ECF) sigma factors. Curr. Opin. Microbiol 16, 148–155. [PubMed: 23466210]

(16). Helmann JD (2002) The extracytoplasmic function (ECF) sigma factors. Adv. Microb. Physiol 46, 47–110. [PubMed: 12073657]

(17). Sineva E, Savkina M, and Ades SE (2017) Themes and variations in gene regulation by extracytoplasmic function (ECF) sigma factors. Curr. Opin. Microbiol 36, 128–137. [PubMed: 28575802]

(18). Cunliffe HE, Merriman TR, and Lamont IL (1995) Cloning and characterization of pvdS, a gene required for pyoverdine synthesis in Pseudomonas aeruginosa: PvdS is probably an alternative sigma factor. J. Bacteriol 177, 2744–2750. [PubMed: 7751284]

(19). Leoni L, Ciervo A, Orsi N, and Visca P (1996) Iron-regulated transcription of the pvdA gene in Pseudomonas aeruginosa: effect of Fur and PvdS on promoter activity. J. Bacteriol 178, 2299–2313. [PubMed: 8636031]

(20). Leoni L, Orsi N, de Lorenzo V, and Visca P (2000) Functional analysis of PvdS, an iron starvation sigma factor of Pseudomonas aeruginosa. J. Bacteriol 182, 1481–1491. [PubMed: 10692351]

(21). Beare PA, For RJ, Martin LW, and Lamont IL (2003) Siderophore-mediated cell signalling in Pseudomonas aeruginosa: divergent pathways regulate virulence factor production and side-rophore receptor synthesis. Mol. Microbiol 47, 195–207. [PubMed: 12492864]

(22). Redly GA, and Poole K (2003) Pyoverdine-mediated regulation of FpvA synthesis in Pseudomonas aeruginosa: involvement of a probable extracytoplasmic-function sigma factor, FpvI. J. Bacteriol 185, 1261–1265. [PubMed: 12562796]

(23). Redly GA, and Poole K (2005) FpvIR control of fpvA ferric pyoverdine receptor gene expression in Pseudomonas aeruginosa: demonstration of an interaction between FpvI and FpvR and identification of mutations in each compromising this interaction. J. Bacteriol 187, 5648–5657. [PubMed: 16077110]

(24). Vanderpool CK, and Armstrong SK (2003) Heme-responsive transcriptional activation of Bordetella bhu genes. J. Bacteriol 185, 909–917. [PubMed: 12533466]

(25). Rossi MS, Paquelin A, Ghigo JM, and Wandersman C (2003) Haemophore-mediated signal transduction across the bacterial cell envelope in Serratia marcescens: the inducer and the transported substrate are different molecules. Mol. Microbiol 48, 1467–1480. [PubMed: 12791131]

(26). Biville F, Cwerman H, Letoffe S, Rossi MS, Drouet V, Ghigo JM, and Wandersman C (2004) Haemophore-mediated signalling in Serratia marcescens: a new mode of regulation for an extra cytoplasmic function (ECF) sigma factor involved in haem acquisition. Mol. Microbiol 53, 1267–1277. [PubMed: 15306027]

(27). Lansky IB, Lukat-Rodgers GS, Block D, Rodgers KR, Ratliff M, and Wilks A (2006) The cytoplasmic heme-binding protein (PhuS) from the heme uptake system of Pseudomonas Dent et al.Page 14Biochemistry. Author manuscript; available in PMC 2021 December 15.Author ManuscriptAuthor ManuscriptAuthor ManuscriptAuthor Manuscript

aeruginosa is an intracellular heme-trafficking protein to the delta-regioselective heme oxygenase. J. Biol. Chem 281, 13652–13662. [PubMed: 16533806]

(28). Ratliff M, Zhu W, Deshmukh R, Wilks A, and Stojiljkovic I (2001) Homologues of neisserial heme oxygenase in gram-negative bacteria: degradation of heme by the product of the pigA gene of Pseudomonas aeruginosa. J. Bacteriol 183, 6394–6403. [PubMed: 11591684]

(29). Dent AT, Mourino S, Huang W, and Wilks A (2019) Post-transcriptional regulation of the Pseudomonas aeruginosa heme assimilation system (Has) fine-tunes extracellular heme sensing. J. Biol. Chem 294, 2771–2785. [PubMed: 30593511]

(30). Mourino S, Giardina BJ, Reyes-Caballero H, and Wilks A (2016) Metabolite-driven Regulation of Heme Uptake by the Biliverdin IXbeta/delta-Selective Heme Oxygenase (HemO) of Pseudomonas aeruginosa. J. Biol. Chem 291, 20503–20515. [PubMed: 27493207] (31). Nguyen AT, O'Neill MJ, Watts AM, Robson CL, Lamont IL, Wilks A, and Oglesby-Sherrouse AG (2014) Adaptation of iron homeostasis pathways by a Pseudomonas aeruginosa pyoverdine mutant in the cystic fibrosis lung. J. Bacteriol 196, 2265–2276. [PubMed: 24727222]

(32). Damron FH, Oglesby-Sherrouse AG, Wilks A, and Barbier M (2016) Dual-seq transcriptomics reveals the battle for iron during Pseudomonas aeruginosa acute murine pneumonia. Sci. Rep 6, 39172. [PubMed: 27982111]

(33). Jepkorir G, Rodriguez JC, Rui H, Im W, Lovell S, Battaile KP, Alontaga AY, Yukl ET, Moënne-Loccoz P, and Rivera M (2010) Structural, NMR spectroscopic, and computational investigation of hemin loading in the hemophore HasAp from Pseudomonas aeruginosa. J. Am. Chem. Soc 132, 9857–9872. [PubMed: 20572666]

(34). Yukl ET, Jepkorir G, Alontaga AY, Pautsch L, Rodriguez JC, Rivera M, and Moënne-Loccoz P (2010) Kinetic and spectroscopic studies of hemin acquisition in the hemophore HasAp from Pseudomonas aeruginosa. Biochemistry 49, 6646–6654. [PubMed: 20586423]

(35). Kumar R, Matsumura H, Lovell S, Yao H, Rodriguez JC, Battaile KP, Moënne-Loccoz P, and Rivera M (2014) Replacing the axial ligand tyrosine 75 or its hydrogen bond partner histidine 83 minimally affects hemin acquisition by the Hemophore HasAp from Pseudomonas aeruginosa. Biochemistry 53, 2112–2125. [PubMed: 24625274]

(36). Dent AT, and Wilks A (2020) Contributions of the heme coordinating ligands of the Pseudomonas aeruginosa outer membrane receptor HasR to extracellular heme sensing and transport. J. Biol. Chem 295, 10456–10467. [PubMed: 32522817]

(37). Fuhrop JH, and Smith KM, Eds. (1975) Porphyrins and Metalloporphyrins, pp 804–807, Elsevier, Amsterdam.

(38). Centola G, Deredge DJ, Hom K, Ai Y, Dent AT, Xue F, and Wilks A (2020) Gallium(III)-Salophen as a Dual Inhibitor of Pseudomonas aeruginosa Heme Sensing and Iron Acquisition. ACS Infect. Dis 6, 2073–2085. [PubMed: 32551497]

(39). Fu Z-Q, Rose J, and Wang B-C (2005) SGXPro: a parallel workflow engine enabling optimization of program performance and automation of structure determination. Acta Crystallogr., Sect. D: Biol. Crystallogr 61, 951–959. [PubMed: 15983418]

(40). Adams PD, Afonine PV, Bunkoczi G, Chen VB, Davis IW, Echols N, Headd JJ, Hung LW, Kapral GJ, Grosse-Kunstleve RW, McCoy AJ, Moriarty NW, Oeffner R, Read RJ, Richardson DC, Richardson JS, Terwilliger TC, and Zwart PH (2010) PHENIX: a comprehensive Python-based system for macromolecular structure solution. Acta Crystallogr., Sect. D: Biol. Crystallogr 66, 213–221. [PubMed: 20124702]

(41). Emsley P, and Cowtan K (2004) Coot: model-building tools for molecular graphics. Acta Crystallogr., Sect. D: Biol. Crystallogr 60, 2126–3212. [PubMed: 15572765]

(42). Nicoletti FP, Bustamante JP, Droghetti E, Howes BD, Fittipaldi M, Bonamore A, Baiocco P, Feis A, Boffi A, Estrin DA, and Smulevich G (2014) Interplay of the H-bond donor-acceptor role of the distal residues in hydroxyl ligand stabilization of Thermobifida fusca truncated hemoglobin. Biochemistry 53, 8021–8030. [PubMed: 25437272]

(43). Kraus DW, and Wittenberg JB (1990) Hemoglobins of the Lucina pectinata/bacteria symbiosis. I. Molecular properties, kinetics and equilibria of reactions with ligands. J. Biol. Chem 265, 16043–16053. [PubMed: 2398044] Dent et al.Page 15Biochemistry. Author manuscript; available in PMC 2021 December 15.Author ManuscriptAuthor ManuscriptAuthor ManuscriptAuthor Manuscript

(44). Howes BD, Feis A, Indiani C, Marzocchi MP, and Smulevich G (2000) Formation of two types of low-spin heme in horseradish peroxidase isoenzyme A2 at low temperature. JBIC, J. Biol. Inorg. Chem 5, 227–235. [PubMed: 10819468]

(45). Ehrenberg A, and Poltarasky R (1967), Academic Press, New York.

(46). Watari H, Groudinsky O, and Labeyrie F (1967) Electron spin resonance of cytochrome b2 and of cytochrome b2 core. Biochim. Biophys. Acta, Bioenerg 131, 592–594.

(47). Brautigan DL, Feinberg BA, Hoffman BM, Margoliash E, Preisach J, and Blumberg WE (1977) Multiple low spin forms of the cytochrome c ferrihemochrome. EPR spectra of various eukaryotic and prokaryotic cytochromes c. J. Biol. Chem 252, 574–582. [PubMed: 13072]

(48). McGarvey BR (1998) Survey of ligand field parameters of strong d5 complexes obtained form the g matrix. Coord. Chem. Rev 170, 75–92.

(49). Blumberg WE, and Peisach J (1971) Low-spin compounds of heme proteins. Adv. Chem. Ser 100, 271–291.

(50). Alontaga AY, Rodriguez JC, Schonbrunn E, Becker A, Funke T, Yukl ET, Hayashi T, Stobaugh J, Moënne-Loccoz P, and Rivera M (2009) Structural characterization of the hemophore HasAp from Pseudomonas aeruginosa: NMR spectroscopy reveals protein-protein interactions between Holo-HasAp and hemoglobin. Biochemistry 48, 96–109. [PubMed: 19072037]

(51). Caillet-Saguy C, Piccioli M, Turano P, Lukat-Rodgers G, Wolff N, Rodgers KR, Izadi-Pruneyre N, Delepierre M, and Lecroisey A (2012) Role of the iron axial ligands of heme carrier HasA in heme uptake and release. J. Biol. Chem 287, 26932–26943. [PubMed: 22700962]

(52). Krieg S, Huche F, Diederichs K, Izadi-Pruneyre N, Lecroisey A, Wandersman C, Delepelaire P, and Welte W (2009) Heme uptake across the outer membrane as revealed by crystal structures of the receptor-hemophore complex. Proc. Natl. Acad. Sci. U. S. A 106, 1045–1050. [PubMed: 19144921]

(53). Kumar R, Lovell S, Matsumura H, Battaile KP, Moënne-Loccoz P, and Rivera M (2013) The hemophore HasA from Yersinia pestis (HasAyp) coordinates hemin with a single residue, Tyr75, and with minimal conformational change. Biochemistry 52, 2705–2707. [PubMed: 23578210]

(54). Kumar R, Qi Y, Matsumura H, Lovell S, Yao H, Battaile KP, Im W, Moënne-Loccoz P, and Rivera M (2016) Replacing Arginine 33 for Alanine in the Hemophore HasA from Pseudomonas aeruginosa Causes Closure of the H32 Loop in the Apo-Protein. Biochemistry 55, 2622–2631. [PubMed: 27074415]

(55). Gaudin CF, Grigg JC, Arrieta AL, and Murphy ME (2011) Unique heme-iron coordination by the hemoglobin receptor IsdB of Staphylococcus aureus. Biochemistry 50, 5443–5452. [PubMed: 21574663]

(56). Grigg JC, Mao CX, and Murphy ME (2011) Iron-coordinating tyrosine is a key determinant of NEAT domain heme transfer. J. Mol. Biol 413, 684–698. [PubMed: 21893067]

(57). Smith AD, Modi AR, Sun S, Dawson JH, and Wilks A (2015) Spectroscopic Determination of Distinct Heme Ligands in Outer-Membrane Receptors PhuR and HasR of Pseudomonas aeruginosa. Biochemistry 54, 2601–2612. [PubMed: 25849630]

Figure A.1

Steady-state analysis of binding of holo-HasAp Y75H to HasR by SPR. (A) Increasing concentrations of HasR (0–1000 nM) were injected over amine-coupled holo-HasAp Y75H in triplicate. (B) Plot of the response units at equilibrium (Req) vs HasR concentration. The data were fit to a 1:1 binding model using Biacore BIAeval version 4.1. The results represent one of three independent replicates.

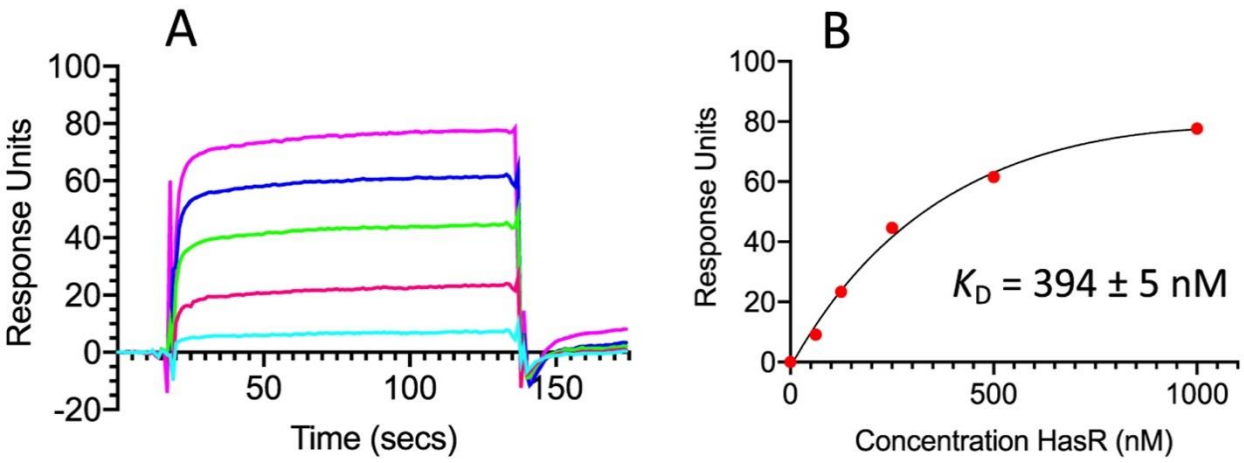
A
Response Units
100
80
60
40
20
0
-20
50
100
150
Time (secs)
B
Response Units
100
80
60
40
20
0
0
500
1000
Concentration HasR (nM)
K_D = 394 ± 5 nM

Figure A.2

Heme utilization by the ΔhasAp strain supplemented with [^{13}C]holo-HasAp **(A)** WT or **(B)** Y75H. LC-MS/MS analysis of the BVIX isomers supplemented with 1 μM [13C]holo-HasAp at 4 h. Biliverdin values represent the standard deviation of four biological replicates. The indicated p values for each strain compared back to PAO1 WT for the respective BVIX isomers were <0.005 (two asterisks) or <0.001 (three asterisks).

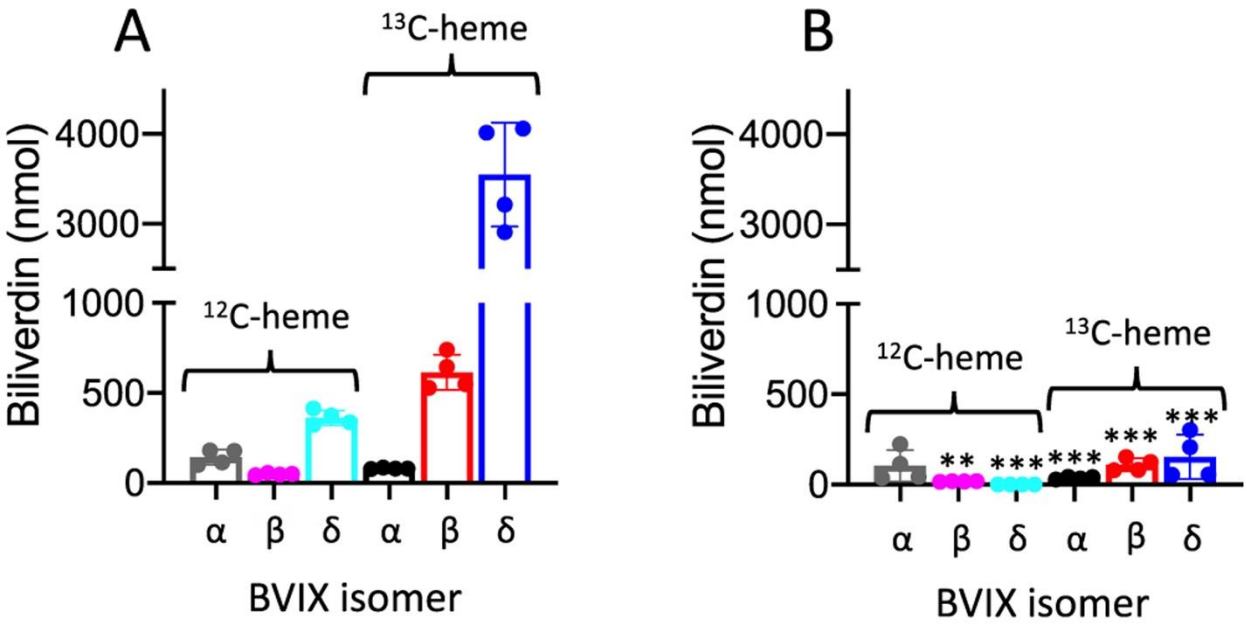
A
B
^{13}C-heme
^{12}C-heme
Biliverdin (nmol)
4000
3000
1000
500
0
α β δ α β δ
BVIX isomer
**
***
***
***
***

Figure A.3

Room-temperature **(A)** UV–vis and **(B and C)** RR spectra of WT and Y75H holo-HasAp. The UV–vis spectra were recorded directly from the Raman capillaries with ~150 μM protein in 100 mM HEPES (pH 7.5).

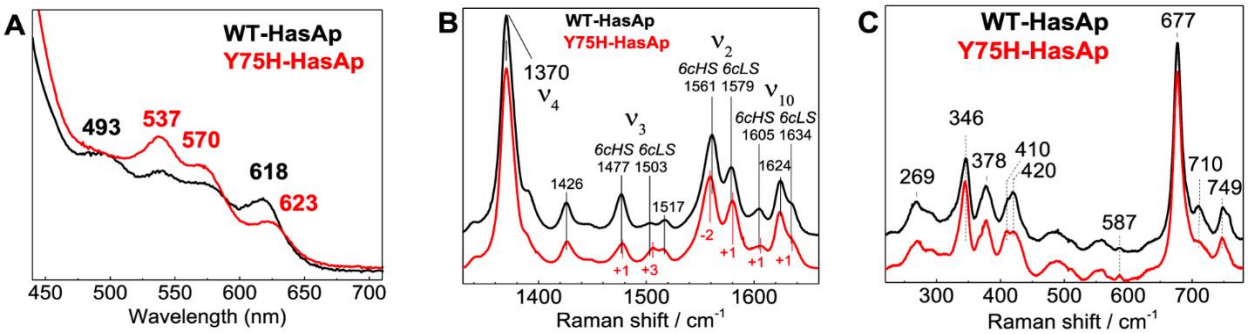
A
WT-HasAp
Y75H-HasAp
493
537
570
618
623
450 500 550 600 650 700
Wavelength (nm)
B
WT-HasAp
Y75H-HasAp
1370
ν4
ν3
6cHS 6cLS
1477 1503
1426
1517
ν2
6cHS 6cLS
1561 1579
ν10
6cHS 6cLS
1605 1634
1624
-2
+1
+3
+1
+1
+1
1400 1500 1600
Raman shift / cm-1
C
WT-HasAp
Y75H-HasAp
677
346
269
378
410
420
587
710
749
300 400 500 600 700
Raman shift / cm-1

Figure A.4

Low-temperature RR spectra of WT and Y75H holo-HasAp. The protein concentrations were ~200 μM in 100 mM HEPES (pH 7.5), and the level of H $^{18}_2$O or D_2O enrichment is >80%.

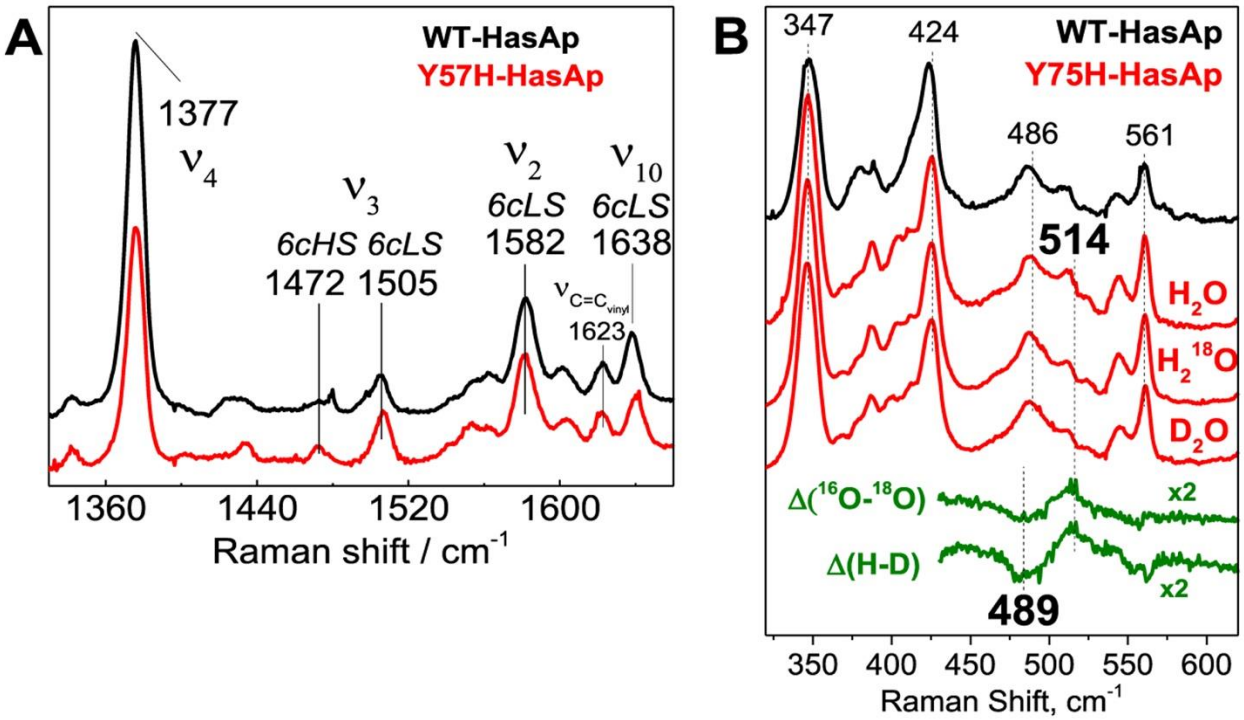
A
WT-HasAp
Y57H-HasAp
1377
ν4
ν3
6cHS 6cLS
1472 1505
ν2
6cLS
1582
ν10
6cLS
1638
νC=Cvinyl
1623
1360
1440
1520
1600
Raman shift / cm-1
B
347
424
WT-HasAp
Y75H-HasAp
486
561
514
H2O
H2 18O
D2O
Δ(16O-18O)
x2
Δ(H-D)
x2
489
350
400
450
500
550
600
Raman Shift, cm-1

Figure A.5

(A) EPR spectra (10 K) of WT and Y75H holo-HasAp and **(B)** correlation of axial and rhombic ligand-field parameters for HasAp low-spin heme complexes as well as representative bis-His and His-hydroxy heme proteins. The protein concentrations were ~200 μM in 100 mM HEPES (pH 7.5). Splitting parameters for Y75H HasAp (this work) and Y75A HasAp35 and for alkaline sperm whale myoglobin (alk. Mb),43 alkaline horseradish peroxidase (alk. HRP),44 liver microsomal cytochrome b5 (b5 and alk. b5),45 mitochondrial cytochrome b2 (cyt b2)46, and horse heart cytochrome c (cyt c).47 Bis-His entries are colored black, and His-hydroxy entries are colored red; the entry for WT HasAp with its His-Tyr axial ligands is colored blue.

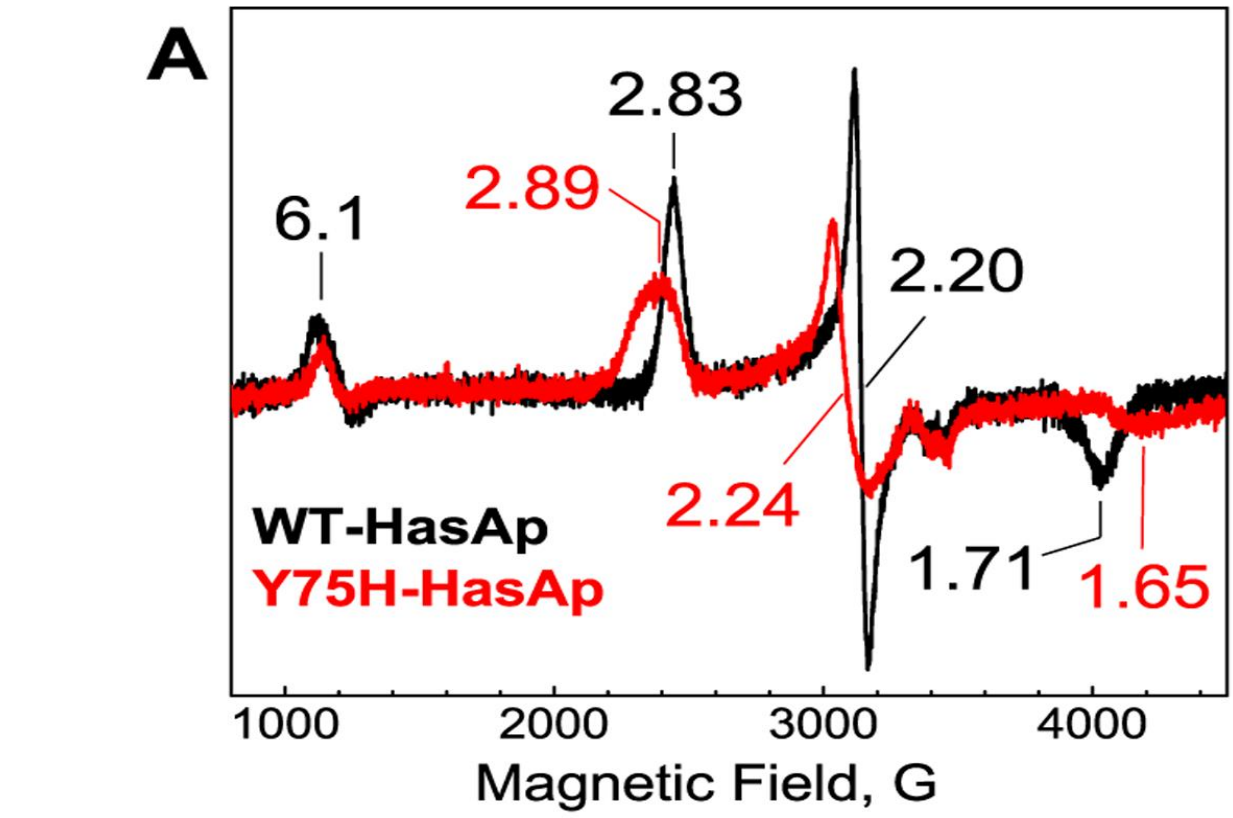
A
2.83
2.89
6.1
2.20
2.24
WT-HasAp
Y75H-HasAp
1.71
1.65
1000
2000
3000
4000
Magnetic Field, G

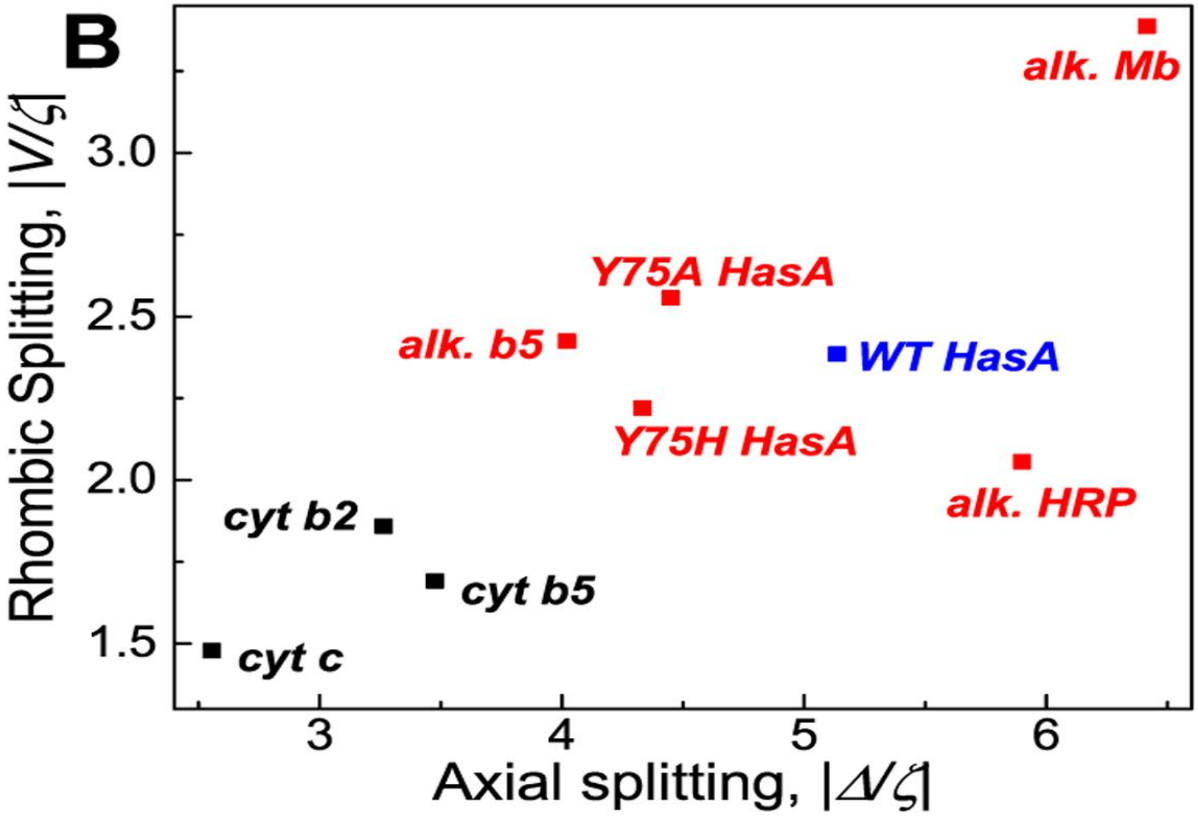
B
alk. Mb
Y75A HasA
alk. b5
WT HasA
Y75H HasA
alk. HRP
cyt b2
cyt b5
cyt c
Rhombic Splitting, |V/λ|
3.0
2.5
2.0
1.5
3
4
5
6
Axial splitting, |Δ/λ|

Figure A.6

Cartoon and stick representations of **(A)** Y75H holo-HasAp and comparison of the heme-bound wild-type HasAp model with the heme-bound forms of **(B)** the Y75H HasAp variant, **(C)** the Y75A HasAp variant, and **(D)** the H83A HasAp variant. In panel A, the H32 loop and Y75 loop are colored cyan and green, respectively, and heme-coordinating ligands in stick format are colored gold. The ligating water molecule is shown as a sphere, and hydrogen bonds to H75 and H83 are represented by dashed lines. Carbon, nitrogen, and oxygen atoms are colored tan, blue, and red, respectively. The 2Fo − Fc composite omit map, generated using the simulated annealing protocol, is shown as the blue cage and contoured at 2σ. In panels B–D, the wild-type model (PDB entry 3ELL) is colored cyan and the variant model is colored salmon. PDB entries for the Y75A, H83A, and Y75H models are 4O6Q, 4O6S, and 6U87, respectively. Key amino acid residues in the heme binding loops are labeled, and oxygen and nitrogen atoms are colored red and blue, respectively. For the heme-bound Y75H variant, a water molecule occupies the position of the phenolic oxygen in the WT protein.

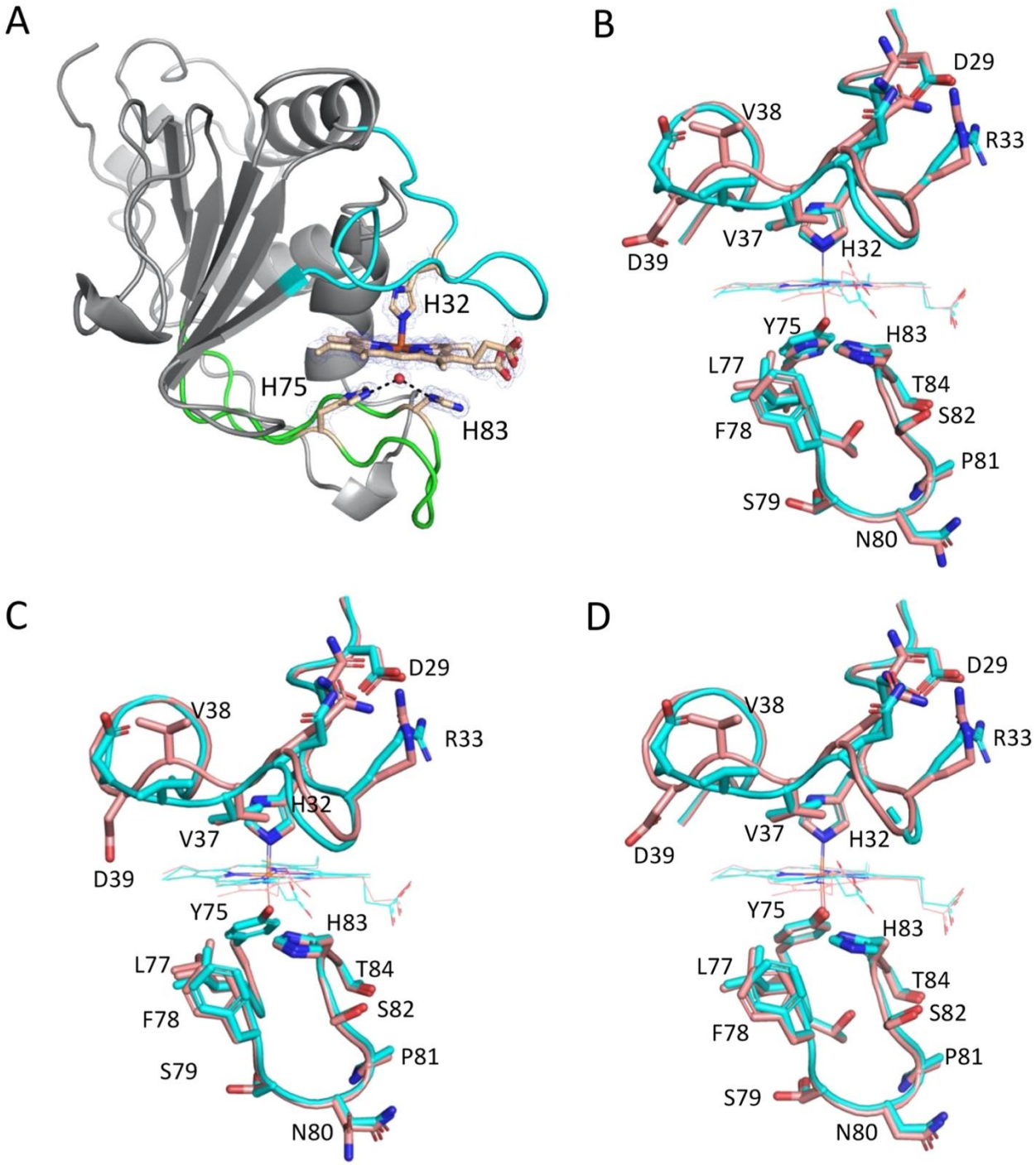
A
H32
H75
H83
B
D29
V38
R33
V37
H32
D39
Y75
H83
L77
T84
S82
F78
P81
S79
N80
C
D29
V38
R33
H32
V37
D39
Y75
H83
L77
T84
S82
F78
P81
S79
N80
D
D29
V38
R33
V37
H32
D39
Y75
H83
L77
T84
S82
F78
P81
S79
N80

Scheme A.1

Proposed Fe–OH2 Oscillator

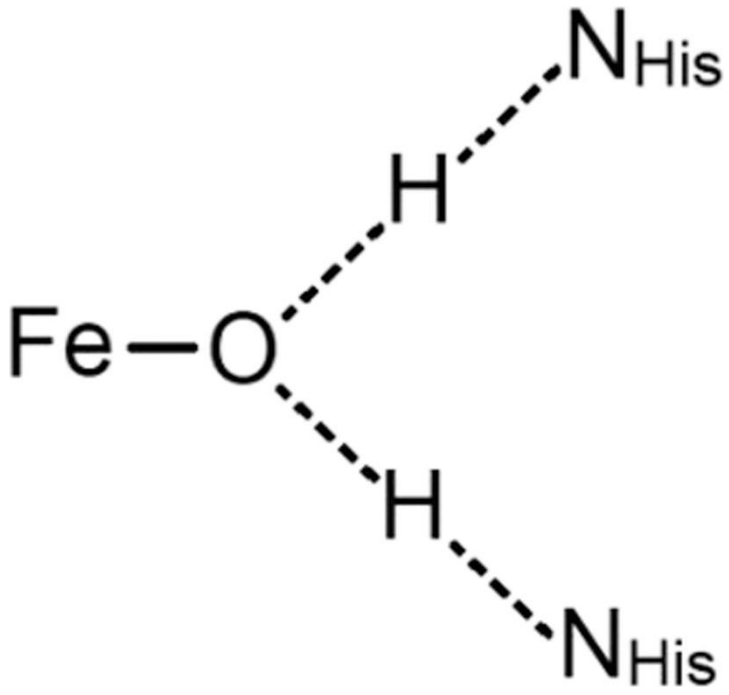
N His
H
Fe—O
H
N His